The properties of prompt emissions and afterglows of gamma-ray bursts observed by HETE-2 and BeppoSAX

Motoko Suzuki

Department of Physics. Graduated School of Science,
Tokyo Institute of Technology, Tokyo, Japan

February 25, 2005

Abstract

We present the study of correlation between properties of prompt gamma-ray emission and afterglows of gamma-ray bursts (GRBs).

Using 60 GRBs localized by the BeppoSAX satellite or the HETE-2 satellite, we analyze the light curves of optical afterglows. The analysis of light curves of optical afterglows reveals that more than three fourths of these afterglows become fainter than 20th magnitude within a day.
We divide the light curves spanning 0.0003 – 1000 days after the burst into 23 time intervals and estimate the magnitude of optical afterglows for these intervals.

Using the published fluences and the peak energies in the νF_ν spectrum ($E_{\rm peak}$) of the prompt emission, we study the correlation with magnitude of optical afterglow for 23 time intervals. As a result, we find a probable correlation between the magnitude of the optical afterglow and both the fluence and $E_{\rm peak}$. We also use 24 GRBs with known redshift to study the correlations of the redshift-corrected properties of GRBs. We find that the correlations of redshift corrected values are better than the correlations between the observer-frame properties. In particular the total radiated energy in prompt emission (under the assumption of isotropic emission) $E_{\rm iso}$ is well-correlated with the source-frame optical afterglow luminosity $L_{\rm ot}$. We performed the same correlation study using the total prompt energy — corrected for jet collimation — instead of $E_{\rm iso}$. We find that the collimation correction does not improve the correlation.

We evaluate the significance of correlations by three different statistical methods. The results are suggestive of time evolution of correlation strength. However detailed analysis shows that this apparent time evolution is due to the changing size of data samples, and that there is no significant difference in the correlation corresponding to different time intervals. The poor correlation of jet-corrected total energy may be also due to poor statistics.

We discuss the interpretation of this correlation in terms of the energy conversion efficiency of bursts. On the basis of this standard model, we can estimate the initial kinetic energy of the relativistic shells from the observation of afterglows. We found the efficiency of energy conversion is typically above 10%, which may present constraints on the mechanism of relativistic jet production.

Contents

Chapter 1

Introduction

The Gamma-ray burst (GRB) phenomenon is among the most extraordinary known to astrophysics. It was discovered as an extremely bright flash of gamma rays in 1960's. GRBs occur at random positions in the sky. Their durations span from a fraction of a second to hundreds of seconds. There appears to be no standard value for their intensities. There is a huge variety in their time profile: some are only short single spikes, some have long smooth light curves, and some exhibit complex, sometimes intermittent, series of spikes. For thirty years after the discovery, despite of various attempts, the origin of gamma-ray burst was elusive. Even their typical distance from the earth or the solar system was uncertain by many orders of magnitude.

Their origin at cosmological distance was first suggested by the isotropic distribution in the sky found in 1990's, and was convincingly confirmed by various observations led by the discovery of X-ray afterglows with the BeppoSAX satellite in 1997. The distance and energy scale of GRBs are now firmly established by means of measurements of redshifts of the optical afterglows or detection of host galaxies. BeppoSAX was capable of providing locations of GRBs with sufficient accuracy (a few arcmin or better) and short time delay (several hours), to permit observations of afterglows in X-ray, optical, near infrared, and radio bands. (see Chapter 2)

The afterglow of GRBs is well understood as a synchrotron emission of the external shock in the framework of the relativistic fireball model. A simple model can explain most of the characteristics of afterglows successfully. Observations of afterglows, in particular with multi-wavelength coverage and well-sampled light curves, can provide important physical parameters, such as the explosion energy, magnetic field, ambient density, and the Lorentz factor of the relativistic jets, which are supposed to be the driving engine of the shocks.

On the other hand, we do not have good description of the physical process of the "prompt emission" — the initial intense burst emission of gamma rays and X rays. In the framework of the relativistic fireball model, the prompt emission is often attributed to the collision of relativistic shells with nonzero relative velocities (internal shocks). Complicated and diverse properties of the prompt emission, however, create difficulties for this simple interpretation. Naturally, observations of afterglows are expected to provide valuable information for understanding the nature of the prompt emission. However, the correlation between the properties of afterglows and those of prompt GRB emission has not been studied well, partly due to small number of GRB afterglow detections, and partly due to uncontrolled diverse observing instruments and conditions.

Since the first detection, optical afterglows have been detected for more than 60 GRBs. However, those are only 40% of well-localized GRBs. There are more bursts without optical counterparts — the so-called "optically dark bursts". In addition, optical afterglows of soft bursts, the so-called "X-ray rich GRBs (XRRs)" or "X-ray flashes (XRFs)", tend to be fainter than those of hard GRBs.

Amati et al. (2002) found that hard GRBs radiate more energy in prompt gamma-ray emission than soft bursts (see section 2.1.1). If the radiated energy in the prompt emission is related to the brightness of the optical afterglow, the dimness of soft bursts can be naturally explained. However no such study has been performed until now, because no afterglows of XRFs had been detected.

HETE-2 has changed the situation. Two thirds of the bursts localized by HETE-2 are XRRs or XRFs, and an optical transient has been found for the extremely soft XRF 020903 (Sakamoto et al., 2004b), (Soderberg et al., 2004).

The first goal of this work, therefore, is to study the relation between the prompt emission and the afterglow of gamma-ray bursts. We examine the existence or lack of correlations between properties of the prompt emission (such as fluence, radiated energy or spectral peak energy), and the properties of the optical afterglow (flux, isotropic luminosity, or jet-corrected luminosity). For this purpose, we develop a procedure to analyze many optical afterglow observations taken at various epochs. With this study, we hope to find the properties of the prompt emission that control the darkness/brightness of optical afterglows.

The second goal of this work is to determine the efficiency of energy conversion in the prompt emission. According to the standard "fireball" model of GRBs, the energy of GRB source is initially in the form of the kinetic energy of relativistic shells. Some part of kinetic energy is converted into radiation of prompt emission and the rest of the energy is converted into afterglow emission slowly through the interaction with the surrounding medium. On the basis of this standard model, we can estimate the initial kinetic energy of the relativistic shells from the observation of afterglows. The energy conversion efficiency, which is the ratio of radiated energy in the prompt emissions to the initial kinetic energy, will provide an insight on the emission mechanism of the prompt emission, and is an excellent test for the internal shock scenario. Furthermore, if the efficiency for GRBs, XRRs and XRFs are different from each other, it may also give a hint on the nature of XRRs and XRFs.

In this thesis, we report the correlations between the properties of prompt emission and brightness of optical afterglows. In order to study the correlations, we used the GRBs whose prompt emission is detected and localized by BeppoSAX or HETE-2. We gathered data on optical afterglows from circulars of the GRB Coordinates Network (GCN), as well as from published papers. We plotted the light curves of optical afterglows for 60 bursts. We estimated the afterglow magnitude or luminosity based on these data and compared the brightness of optical afterglow with the fluence (time integrated flux), $E_{\rm peak}$ (characteristic energy of the spectrum) and radiated energy of prompt emission.

In chapter 2, we review the observations and standard theories of GRBs related to this study. Chapter 3 and Chapter 4 contain method of observation and data analysis of prompt emission and afterglows respectively. The results of correlation studies are summarized in chapter 5. Chapter 6 is a discussion in two parts: the first part comprises the evaluation of reliability and interpretation of correlation, while the second part is the discussion of the efficiency of energy conversion in prompt emission. The conclusions are given in chapter 7.

The statistical method used in our correlation study is described in appendix A. A study of localization accuracy of HETE-2 is summarized in appendix B. Appendix C contains details of definition of the burst durations. In Appendix D, we show all the scatter plots of properties of prompt emissions vs. brightness or luminosity of optical afterglows.

Chapter 2

Review of GRB

2.1 Observational properties of GRBs

History and overview

In 1960's, the Vela satellites, which were launched for surveillance of nuclear tests in the space, detected gamma-rays from outer space. The phenomenon lasted for several seconds. This observation was reported in 1973 by Klebesadel et al. (1973) as a "Gamma-ray Burst (GRB)".

Since then a large number of GRBs have been observed. The largest contribution to the number of observed GRBs was made by the BATSE (Burst And Transient Source Experiment) on the Compton Gamma-Ray Observatory (CGRO) satellite. BATSE consisted of eight scintillation counters, placed at the eight corners of the Compton Gamma-ray Observatory. The observations are compiled into a large catalog of GRBs Paciesas et al. (1999)[1]. The BATSE catalog contains 2704 GRBs. Large number of events revealed a highly isotropic angular distribution in the sky (fig.2.1[2]). The log N - log P distribution (the cumulative distribution of GRBs as a function of the peak flux) shows a deviation from the power-law with a index of $-3/2$, the value expected for a uniform Euclidean space (fig.2.2) (Stern et al., 2002). The isotropic and non-Euclidean space distribution favored their cosmological origin rather than an origin in the Galactic plane or in the Galactic halo.

The direct evidence that GRB sources (or at least the long/soft class of GRBs, see section 2.1.1) are at cosmological distances was provided in 1997. The BeppoSAX satellite found an X-ray counterpart to the GRB observed on February 28, 1997 (GRB970228) (Costa et al., 1997). This X-ray source was also observed at optical wavelengths (van Paradijs et al., 1997; Guarnieri et al., 1997; Fruchter et al., 1999). This was the first detection of X-ray and optical afterglows. There is an extended emission under the optical afterglow, corresponding to the host galaxy of GRB970228 (Bloom et al., 2001). The galaxy was later found to have a redshift z=0.695.

The second detection of an optical transient (OT) associated with a GRB was made for GRB970508. Intensive observations revealed the power-law decline of the optical flux from two to 300 days after the burst (Garcia et al., 1998). For GRB970508 a radio afterglow was also found (Frail and Kulkarni, 1997). The first redshift measurement of a GRB was made for this GRB with z =0.835. It firmly established the cosmological origin of GRBs.

[1] http://www.batse.msfc.nasa.gov/batse/grb/catalog/current/
[2] http://www.batse.msfc.nasa.gov/batse/grb/skymap/

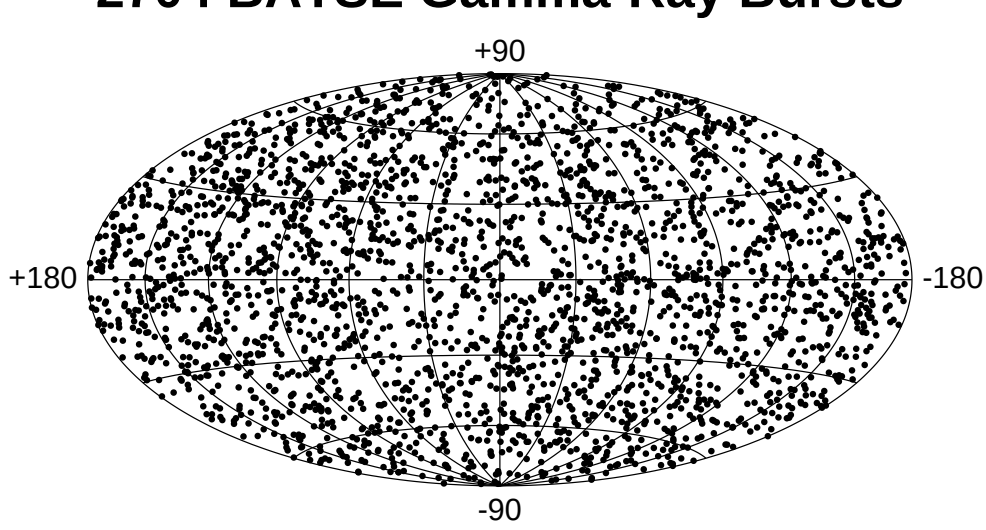

Figure 2.1: This map shows the locations of a total of 2704 Gamma-Ray Bursts recorded with the Burst and Transient Source Experiment on board NASA's Compton Gamma-Ray Observatory during the nine-year mission.

2.1.1 Prompt emissions

Bimodal distribution in duration/hardness

There are 2 sub-classes of GRBs. The first report of sub-classes is given by Kouveliotou et al. (1993); one is the long/soft class and the other is the short/hard class. Long/soft GRBs have duration T_{90} (see section C.1.1) longer than ~ 2 seconds (Fig. 2.3). All the burst with afterglow emissions belong to the long/soft class. No successful observation has been made of the afterglow of a short/hard burst.

Spectra of GRBs and Distribution of $E_{\rm peak}$

The spectra of GRBs are known to be well-fitted with an empirical model: a smoothly joined broken power law function:

$$N_E(E) = \begin{cases} AE^{\alpha}\exp\left(-\frac{E}{E_0}\right) & (\alpha-\beta)E_0 \geq E\,, \\ A\left[(\alpha-\beta)E_0\right]^{\alpha-\beta}\exp\left(\beta-\alpha\right)E^{\beta} & (\alpha-\beta)E_0 \leq E\,. \end{cases} \tag{2.1}$$

The model is called Band function (Band et al., 1993) (hereafter BAND). The model parameters of BAND are A (amplitude in the unit of [photons s^{-1} cm^{-2} keV^{-1}]), α (low energy spectral index), β (high energy spectral index) and E_0 (break energy). Sometimes the observed energy region is not sufficient to determine the high-energy power-law index β. In these cases, we fit a power-law with a high-energy cut off (CPL):

$$N_E(E) = AE^{\alpha}\exp\left(-\frac{E}{E_0}\right)\,, \tag{2.2}$$

or a simple power-law function (PL):

$$N_E(E) = AE^{\alpha}\,. \tag{2.3}$$

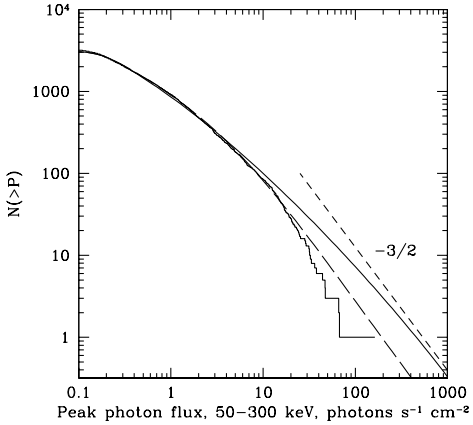

Figure 2.2: Peak count rate distribution of 3255 BATSE bursts. $N(> P)$ is the number of bursts with peak flux larger than P. (Stern et al., 2002)

One of the important spectral parameters of GRBs is the "peak energy" $E_{\rm peak}$, defined as the energy of the peak of the νF_ν spectrum. For the case of BAND and CPL, $E_{\rm peak}$ is given by

$$E_{\rm peak} = E_0(2+\alpha)\,. \tag{2.4}$$

Preece et al. (2000) studied the spectra of 156 bright BATSE bursts. The distribution of $E_{\rm peak}$ is shown in figure 2.4. From this figure, we can see $E_{\rm peak}$ is clustered strongly around 250 keV.

XRRs and XRFs

There are categories of GRBs that are spectrally distinct from those sampled by BATSE. These bursts have relatively soft spectra compared to the BATSE sample. These bursts are called X-ray rich Gamma-ray bursts (XRRs) or X-ray flashes (XRFs).

Strohmayer et al. (1998) reported the results of the analysis of 22 XRRs or XRFs observed by the Ginga satellite. Ginga (1987 – 1991) had a spectral bandpass of 2 – 400 keV. They found that the distribution of E_0 extends below 10 keV (fig. 2.5 left). They also noted that there are some examples of equal energy in the X-rays (2 – 10 keV) and gamma-rays (50 – 300 keV) (fig. 2.5 right).

Another detailed investigation of XRRs and XRFs was carried out with the bursts observed by the BeppoSAX satellite. The BeppoSAX satellite had two type of instruments which could observe prompt emission from GRBs. One is the Gamma-Ray Burst Monitor (GRBM) which covers the 40 – 700 keV energy range. The other is the Wide Field Camera (WFC) which covers the 2 – 25 keV energy range. Heise et al. (2001) selected 17 events out of 39 X-ray transient events detected by the WFC, which last less than 1000 sec and not were detected by GRBM. They compared the properties of these events with properties of the X-ray counterparts of GRBs observed with WFC. The results are shown in fig. 2.6.

The WXM and the FREGATE on-board HETE-2 also have a sufficiently wide energy range to observe XRRs and XRFs. Sakamoto et al. (2004a) analyzed 45 Bursts observed by both the

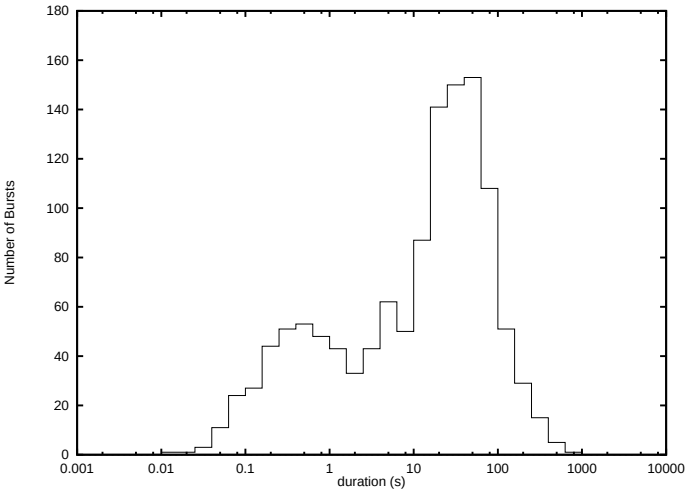

Figure 2.3: The distribution of duration T_{90}. (Kouveliotou et al., 1993)

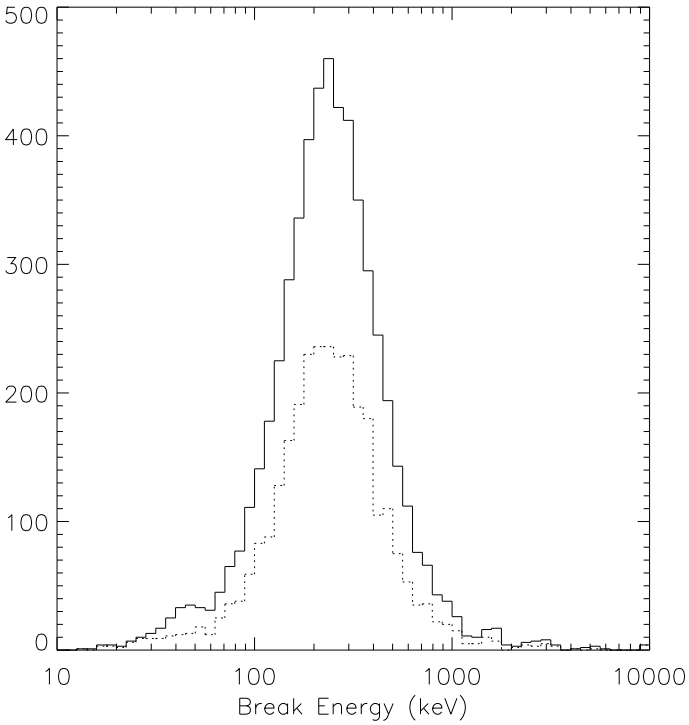

Figure 2.4: Break energy ($E_{\rm peak}$) distribution for the entire sample (solid line). The subset of bursts not fit with the GRB model is also shown (dotted line). (Preece et al., 2000)

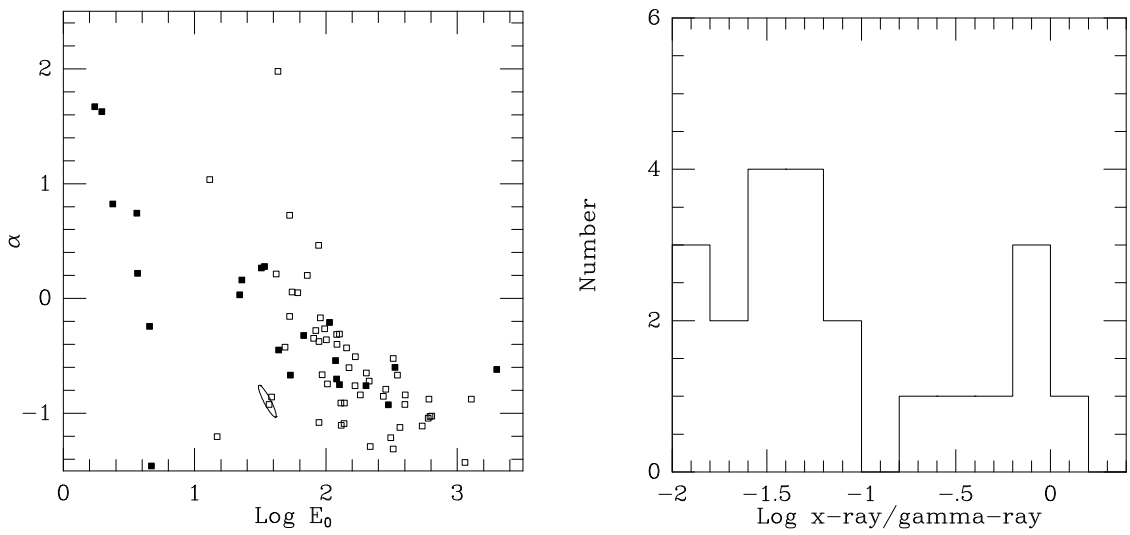

Figure 2.5: Left: Low energy index α and break energy E_0 for Ginga and BATSE events. Open squares are 54 BATSE events by Band et al. (1993), and the solid squares are the 22 Ginga events reported in Strohmayer et al. (1998). Right: Distribution of the ratio of the energy emitted in the X-rays (2 – 10 keV) to that emitted in gamma-rays (50 – 300 keV). (Strohmayer et al., 1998)

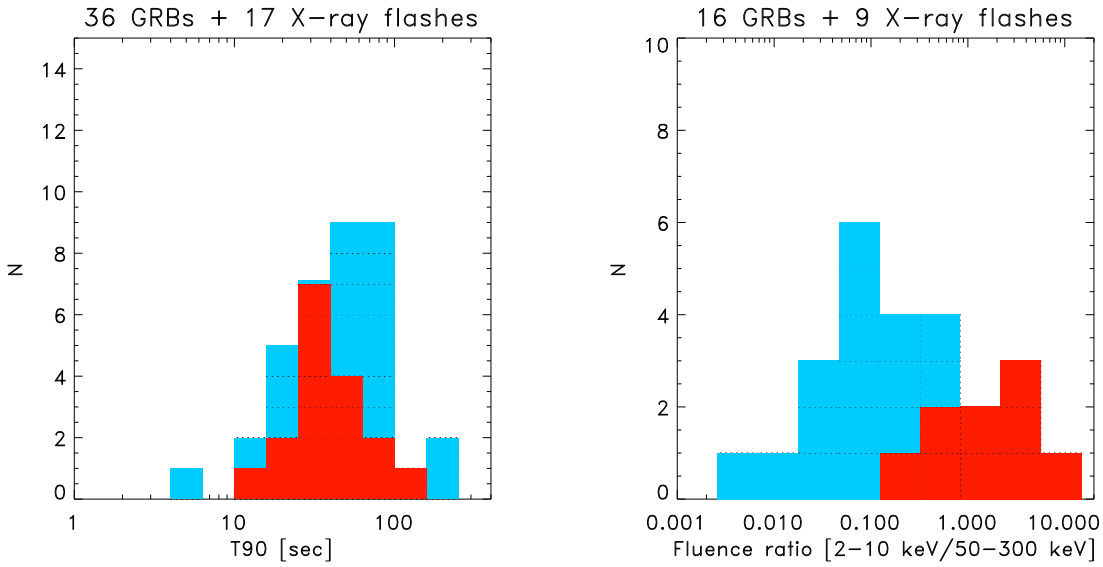

Figure 2.6: Histogram of X-ray counterpart of GRBs (blue) and X-ray flashes (red). Left: Histogram of T_{90} Right: Histogram of ratio of fluence in X-ray to gamma-ray (Heise et al., 2001)

FREGATE and the WXM and studied their global characteristics. They adopted the definition of GRBs, XRRs and XRFs using ratio of fluence in X-rays $S_{\rm X}$ (2 – 30 keV) to fluence in gamma-rays S_γ (30 – 400 keV). They set the boundary between XRRs and GRBs to $\log(S_{\rm X}/S_\gamma) = -0.5$ and the boundary between XRRs and XRFs to $\log(S_{\rm X}/S_\gamma) = 0$ (fig. 2.7) They found that the

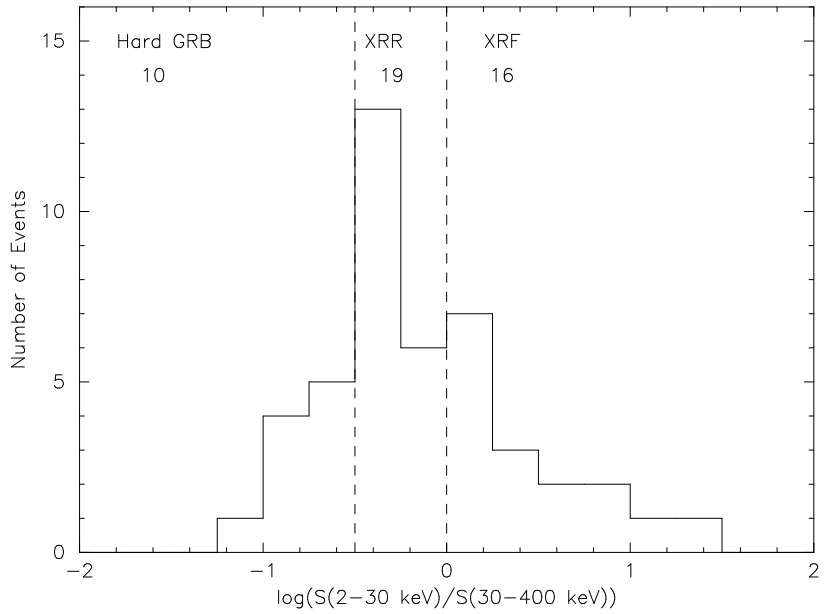

Figure 2.7: Distribution of the fluence ratio $S_{\rm X}/S_\gamma$. The dashed lines correspond to the borders between hard GRBs and XRRs, and between XRRs and XRFs. (Sakamoto et al., 2004a)

distribution of the X-ray to gamma-ray fluence ratio is a continuum from hard GRBs to XRFs.

Amati's relation on $E^{\rm src}_{\rm peak}$ and $E_{\rm iso}$

Amati et al. (2002) studied the spectral properties of BeppoSAX bursts with known redshifts. They investigated the spectral parameters of time-averaged spectra in the GRB source frame (i.e. the redshift corrected spectra) and found a tight correlation between the source-frame $E_{\rm peak}$ and the isotropic equivalent energy radiated in the 1 – 10000 keV range (fig. 2.8 left). Sakamoto et al. (2004b) confirmed this relation using the samples detected with HETE-2 and found the relation extends to extremely soft XRF (fig. 2.8 right).

2.1.2 Afterglows

Afterglows are the phenomena subsequent to the prompt emission of GRBs. They are observed at X-ray, optical, infrared and radio frequencies. Once the counterparts are found, we can determine sufficiently accurate positions of the bursts to point large telescopes, to carry out spectroscopy or find underlying host galaxies. Afterglows are known to decay as power-law functions of time. However, there are often breaks or bumps in the light curves of afterglows. These structures provide information about the burst progenitors and their environments. In this section, we introduce observational properties of afterglows.

Discovery

On 1997 February 28, a GRB was detected by the Gamma-Ray Burst Monitor (GRBM) on BeppoSAX and was localized with the Wide Field Cameras (WFCs). At 8 hours after the

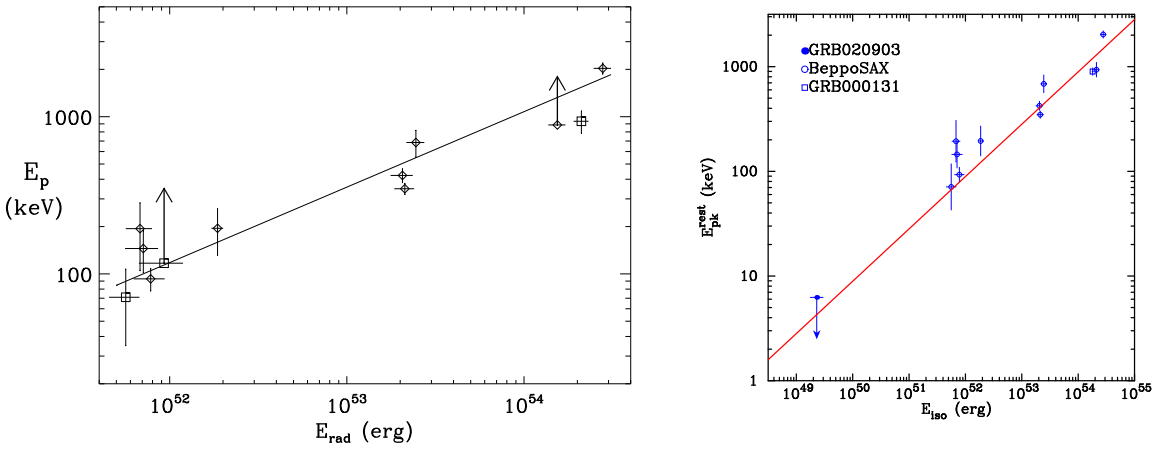

Figure 2.8: The correlation between the isotropic equivalent energy and $E_{\rm peak}$ at the GRB source frame. Left: Original (Amati et al., 2002) Right: Extended to XRF (Sakamoto et al., 2004b)

burst, Target of Opportunity (TOO) observation of BeppoSAX narrow field instruments (NFIs) started. There was only one source in the 3 arcmin WFC error circle (Costa et al., 1997). This was the first detection of an X-ray afterglow. The source had a power law spectrum in the 0.1–10 keV range, with photon index of -2.1 $\pm$ 0.3. The intensity decayed as a power-law function of time, with time dependence $t^{-1.32}$.

There was also an optical transient (OT) at a position consistent with that of the X-ray source. The OT was detected in the B- and R-bands 16.5 hours after the burst, with magnitudes of 22.3(B) and 21.1(R) (Guarnieri et al., 1997), and in the V- and I-bands 20.8 hours after the burst, with magnitudes of 21.3(V) and 20.6(I) (van Paradijs et al., 1997).

Power-law behavior of afterglows

The optical afterglow of GRB 970228 decayed with time as a power-law (Sahu et al., 1997; Galama et al., 1997; Masetti et al., 1998) The time dependence of the decline was $t^{-1.1}$ (Fruchter et al., 1999). A power-law decline was also observed for the next optical afterglow GRB 970508 (Garcia et al., 1998), although the OT behaved differently in the first 2 days after the burst (Pedersen et al., 1998). The spectrum of X-ray and optical afterglow of GRB 970228 was adequately fit by power law. This power-law behavior of light curves and spectra are consistent with the prediction of fireball model (Wijers et al., 1997). The fireball model succeeds in explaining afterglow phenomena. Panaitescu and Kumar (2001) fit X-ray, optical and radio light curves of eight GRB afterglows with a fireball model and determined the physical parameters, such as the explosion energy, magnetic field, ambient density, etc. (figure 2.9).

Redshift measurement

The first measurement of a GRB redshift was made for GRB 970508. Metzger et al. (1997) found absorption lines of Fe II, Mg II and Mg I in the spectrum of OT. These lines were identified with an absorption system at redshift $z = 0.835$. Bloom et al. (1998) observed the host galaxy of GRB 970508 and found emission lines that were identified with [O II] and [Ne III] at $z = 0.835$, consistent with the result of the absorbing system. So far, redshifts have been measured for more than 40 GRBs.

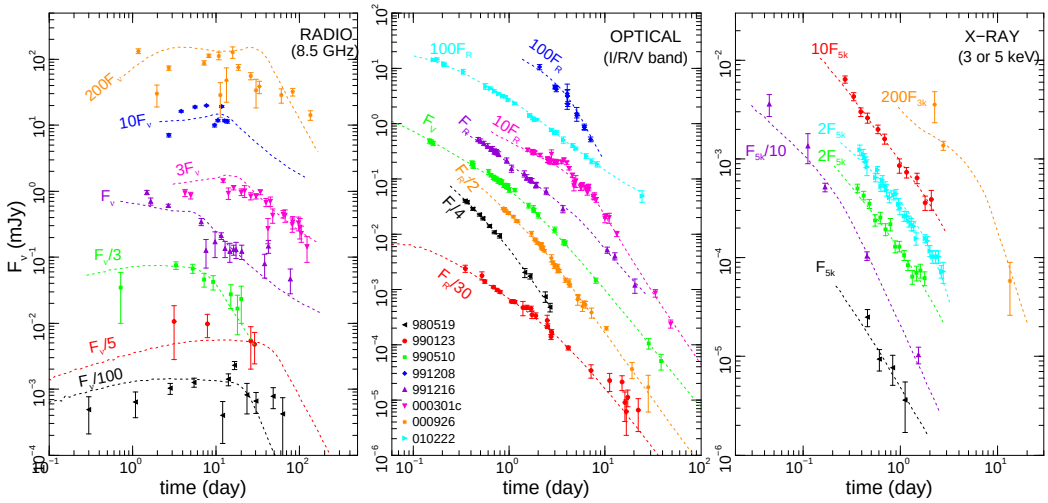

Figure 2.9: Radio optical and X-ray emission and model light curves for the GRB afterglows. (Panaitescu and Kumar, 2001)

SN connection

There is evidence that supports the association of long/soft GRBs with core-collapse supernovae.

Supernova Bump

A significant deviation from the pure power-low decay was found in the light curve of the optical afterglow of GRB970228 (fig 2.10 top), about 1 – 2 weeks after the burst (Galama et al., 2000). This was interpreted as evidence of a possible supernova component in the light curve.

Since the first suggestion of a supernova bump in GRB afterglows by Bloom et al. (1999) (fig 2.10 bottom), there have been several observations of afterglow light curves with possible supernova bumps; for example, 990712 (Björnsson et al., 2001), 011121 (Bloom et al., 2002), 020405 (Price et al., 2003), etc.

SN1998bw/GRB980425

The most suggestive evidence for the supernova and GRB connection before the HETE-2 era was the SN1998bw/GRB980425 association. The WFC on-board BeppoSAX localized the position of GRB 980425 to an error box containing an unusual supernova, SN1998bw. This GRB is peculiar in several ways: the radiated total energy of prompt emission was unusually small (1.6×10^{48} erg) compared to that of other bursts (typically above 10^{51} erg). The "usual" afterglow was not observed. The redshift measured from the observation of SN is 0.0085 is in contrast to more typical GRB redshifts around $z = 1$. These circumstances create some doubt as to whether GRB 980425 is due to the same phenomenon as other GRBs.

SN2003dh/GRB030329

HETE-2 detected and localized GRB 030329, the brightest GRB HETE-2 had ever detected. The optical observations started $\sim$ 1 hour after the burst proceeded and continuously for > 10 days. The redshift of GRB 030329 was determined to be 0.1685 (Greiner et al., 2003). Hjorth et al. (2003) reported that the spectrum of the optical transient was well fitted with a power-law at first, but started to deviate gradually from a power-law $\sim$ 10 days after the burst. By 33 days after the burst, the spectrum was dominated by the supernova component SN 2003dh.

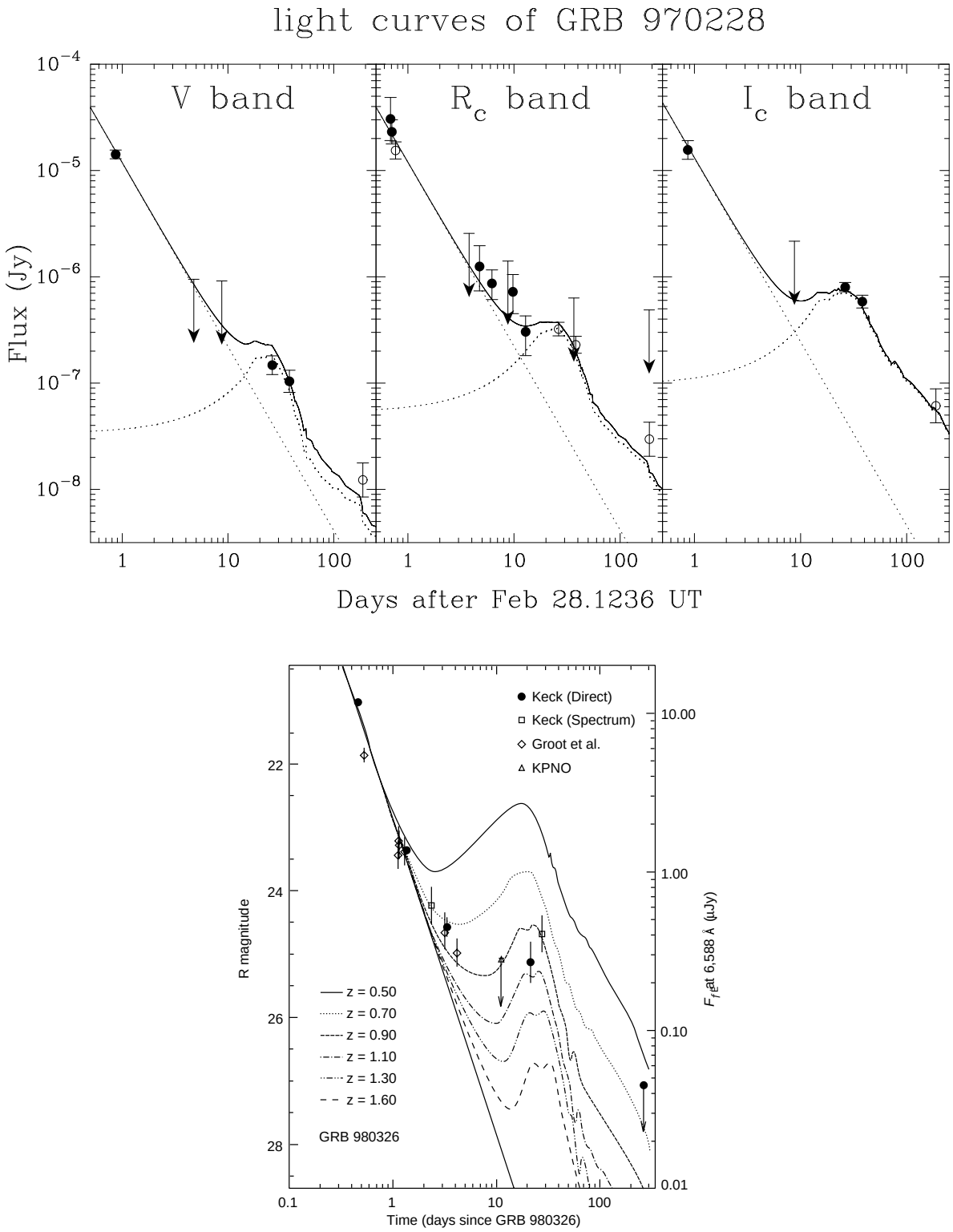

Figure 2.10: Top: V, R_c, I_c band light curves of GRB970228. The dotted curves indicate power-law decays with -1.51 and redshifted SN 1998bw light curves (Galama et al., 2000) Bottom: the R band right curve of GRB980326. Overlaid curves are the power-law afterglow decline summed with the bright supernova light curve at different redshift Bloom et al. (1999).

The spectrum of SN 2003dh 33 days after the burst was similar to the spectrum of SN 1998bw after 33 days (figure 2.11). This is conclusive evidence that at least some of long/soft GRBs are associated with energetic supernova.

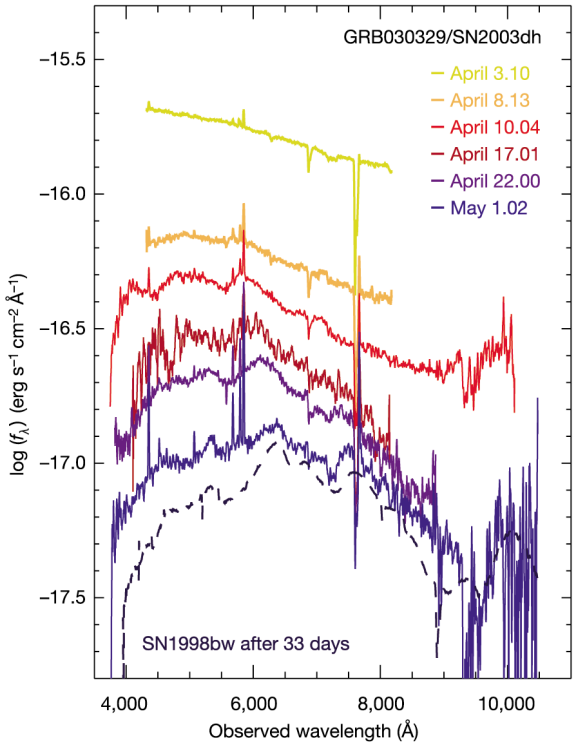

Figure 2.11: Spectral evolution of GRB 030329/SN 2003dh. For comparison, the spectrum of SN 1998bw after 33 days shifted to the GRB 030329 redshift is shown (dashed line). (Hjorth et al., 2003)

Hosts

After optical afterglows decay, the host galaxies can be observed. We can measure redshift from the observations of host galaxies even if the redshift has not been measured from the observations of afterglows. The observations of host galaxies also provide us with the information on the environments of GRB progenitors. From analyses of the broad-band spectral energy distributions (SEDs) of host galaxies, we can estimate star-formation rates. For example, Christensen et al. (2004) derived ultraviolet star-formation rate for 10 GRB hosts and found that these host galaxies have large SFRs but they are not significantly younger than the other starburst galaxies.

Optically dark GRBs

About 90% of GRBs well-localized by BeppoSAX had X-ray afterglows. On the other hand, only about 40% of them had optical afterglows. The GRBs with no optical candidates or dim optical transients are called "optically dark GRBs".

Some of them may not be intrinsically dark but may only be the results of poor observations. Actually, 13 of 14 GRBs well-localized by SXC (soft X-ray camera) on board HETE-2 had an optical afterglow.

Fynbo et al. (2001) plotted the limiting R-band magnitude of 41 GRBs and compared them to the light curve of dim OT GRB 000630. They concluded that in the case of $\gtrsim 75\%$ of GRBs without detected OTs, an OT as dim as or dimmer than the OT corresponding to GRB 000630 might have been present despite the lack of detection. They also investigated the distribution of R-band magnitude 1 day after the burst, and remarked that an OT of $R = 24$ 1 day after the burst would almost certainly not be detected with current search strategies.

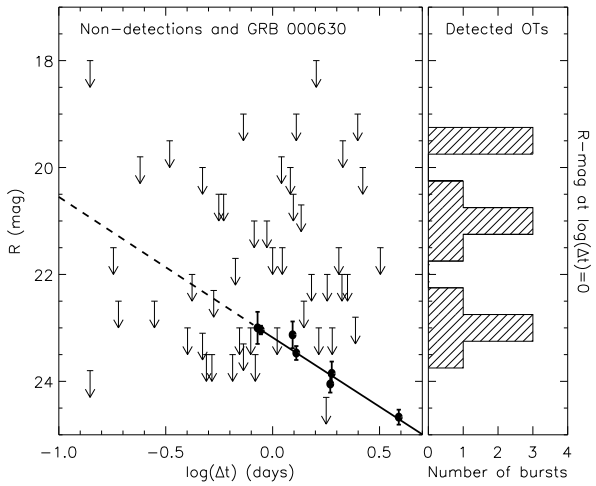

Figure 2.12: Left: the limiting magnitude in R-band vs. the time after the burst (Δt) in day. The light curve of GRB 000630 is plotted with filled circles. The extrapolation to earlier times than the first data is shown as a dashed line. Right: a histogram of R-band magnitude at 1 day after the burst for GRBs with detected OTs. (Fynbo et al., 2001)

De Pasquale et al. (2003) show the comparison of flux of X-ray afterglows with the magnitude of optical afterglows (fig 2.13). They found that the X-ray flux of afterglows of optically dark GRBs are typically about 5 times lower than that of other afterglows. This number is consistent with the results of optical observations suggesting that optically dark GRBs have R-band magnitudes 2 lower than typical GRBs, if the flux ratios of X-ray to optical are identical. The result suggests that optically dark GRBs may be interpreted as GRBs at high (>5) redshift, or as GRBs with afterglows subjected to high absorption. Convincing evidence of dust extinction in an optical afterglow comes from GRB030115. The early follow-up observation at optical, near-infrared (NIR) and radio wavelengths reveals that the optical afterglow is much fainter than the NIR and radio afterglow. (fig 2.14) The SED in the optical and NIR bands can be well fitted by a dust extinction model.

There are also some bursts featuring rapid decay in the early light curve (fig 2.15). These bursts would be certainly classified as optically dark GRBs without early follow-up observations.

2.1.3 Relation between prompt emissions and afterglows

Recently, there are some interesting studies combining the properties of prompt emissions and afterglows. These studies are important to our understanding of the nature of GRB jets.

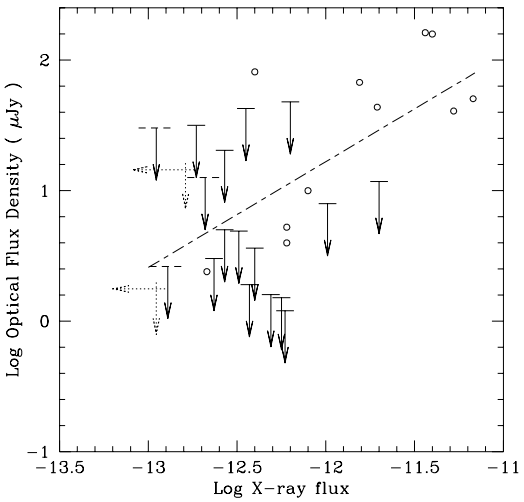

Figure 2.13: Flux of optical afterglows and X-ray afterglows. Open circles are events with both X-ray and optical afterglows. Upper limits of optical afterglows are shown with solid (confirmed X-ray afterglow) and dashed (candidate X-ray afterglow) arrows. Upper limits in both X-ray and optical band are shown with dotted arrows. Short-long dashed line is best fit of open circles. (De Pasquale et al., 2003)

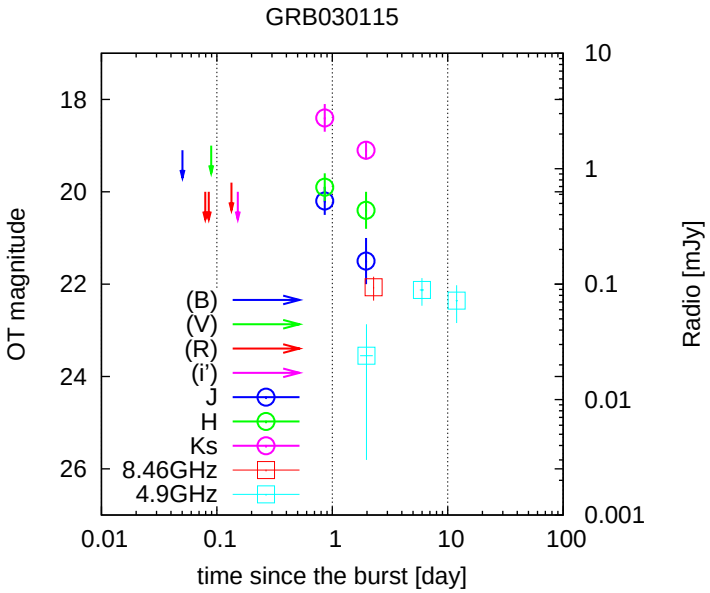

Figure 2.14: An example of the light curve of afterglow which is detected in near-infrared (circles) and radio wavelength (squares) but not in optical (arrows), which suggests dust extinction.

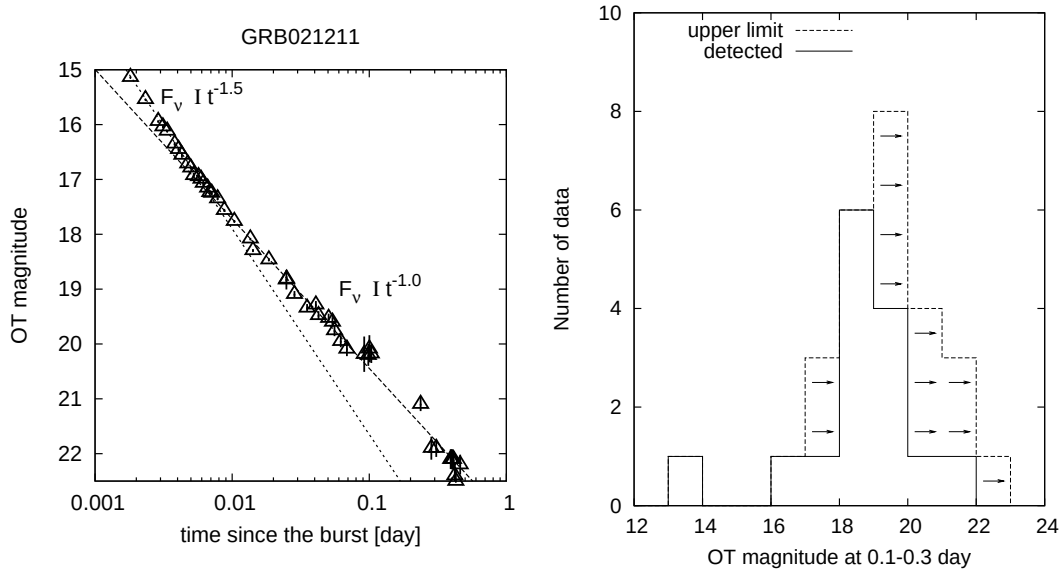

Figure 2.15: An examples of optical transients with rapid decay (left) and histogram of OT magnitude at 0.1-0.3 day after the burst (right).

Standard Energy Reserve

From the theory of GRB jet, we expect a simultaneous break in the light curves of the afterglow at all wavelengths, when the bulk Lorentz factor of GRB jet (Γ) decreases to the inverse of the geometrical opening angle of the jet ($1/\theta_j$) (see section 2.2.3). Conversely, we can estimate jet opening angle from the break time (t_j) in the light curves of afterglows as

$$\theta_j \propto \left(\frac{t_j}{1\mathrm{day}}\right)^{3/8} \left(\frac{1+z}{2}\right)^{-3/8} \left(\frac{E_{\mathrm{iso}}}{10^{53}\mathrm{ergs}}\right)^{-1/8} \left(\frac{\eta_\gamma}{0.2}\right)^{1/8} \left(\frac{n}{0.1\mathrm{cm}^{-3}}\right)^{1/8}, \qquad (2.5)$$

where η_γ is the efficiency of the fireball in converting the energy in the ejecta into gamma rays and n is the mean circumburst density.

Frail et al. (2001) used this relation to calculate the prompt energy emitted, corrected for the jet opening angle (E_{jet}), for 17 GRBs with known redshift. They found that E_{jet} clustered around 5×10^{50} erg, despite the 3 order-of-magnitude variation in E_{iso} (the energy emitted at the prompt emission under the assumption of isotropic emission) (figure 2.16). Bloom et al. (2003b) revised this distribution for larger samples.

Jet opening angle correction in Amati's relation

Ghirlanda et al. (2004) took into account the jet collimation and revised the Amati relation. Figure 2.17 shows the revised correlation of E_{jet} and $E^{\mathrm{src}}_{\mathrm{peak}}$. They found that the correlation between E_{jet} and $E^{\mathrm{src}}_{\mathrm{peak}}$ is very tight, and that the scatter of each GRB from the correlation is confined to a narrow region (fig 2.17 right).

Kinetic energy of fireball and energy conversion efficiency in prompt emissions

Freedman and Waxman (2001) derived the internal energy of a fireball per unit solid angle from the observation of an X-ray afterglow. They compared the energy of the fireball with the energy radiated in prompt emission and found that the ratio of observed prompt gamma-ray emission

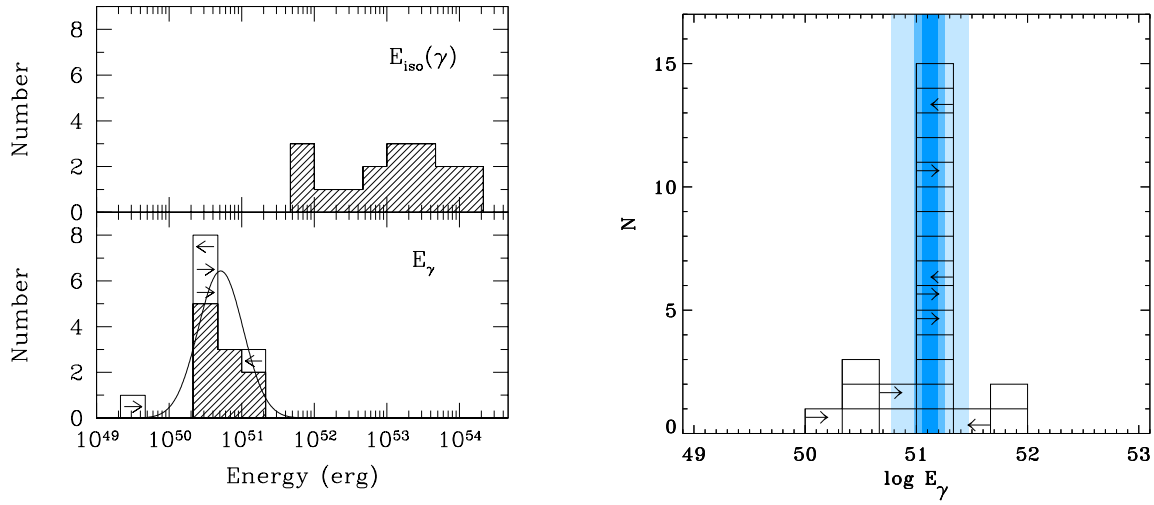

Figure 2.16: Left: Distribution of the isotropic total energy (top panel) vs. the geometry-corrected energy (bottom panel). Arrows indicate upper or lower limits to the geometry-corrected energy. (Frail et al., 2001) Right: Revised distribution of the geometry-corrected energy. (Bloom et al., 2003b)

to fireball energy per unit solid angle, ϵ_γ/ϵ, is of order unity, satisfying $|\log_{10}(\epsilon_\gamma/\epsilon)| \lesssim 0.5$ (figure 2.18).

Lloyd-Ronning and Zhang (2004) studied the correlation between kinetic energy of GRB ejecta ($E_{\rm kinetic}$), which is estimated from the observations of X-ray afterglows, and properties of GRBs such as radiated energy in prompt emission $E_{\rm iso}$, total energy ($E_{\rm tot} \equiv E_{\rm iso} + E_{\rm kinetic}$), jet opening angle θ_j, and $E^{\rm src}_{\rm peak}$. They define the GRB efficiency ζ as

$$\zeta \equiv E_{\rm iso}/(E_{\rm kinetic} + E_{\rm iso}) \tag{2.6}$$

and also studied the correlation between ζ and $E_{\rm iso}$, $E_{\rm tot}$, θ_j and $E^{\rm src}_{\rm peak}$. They found correlations between these quantities. In addition, they argued that the softest burst XRF 020903 follows the same trends.

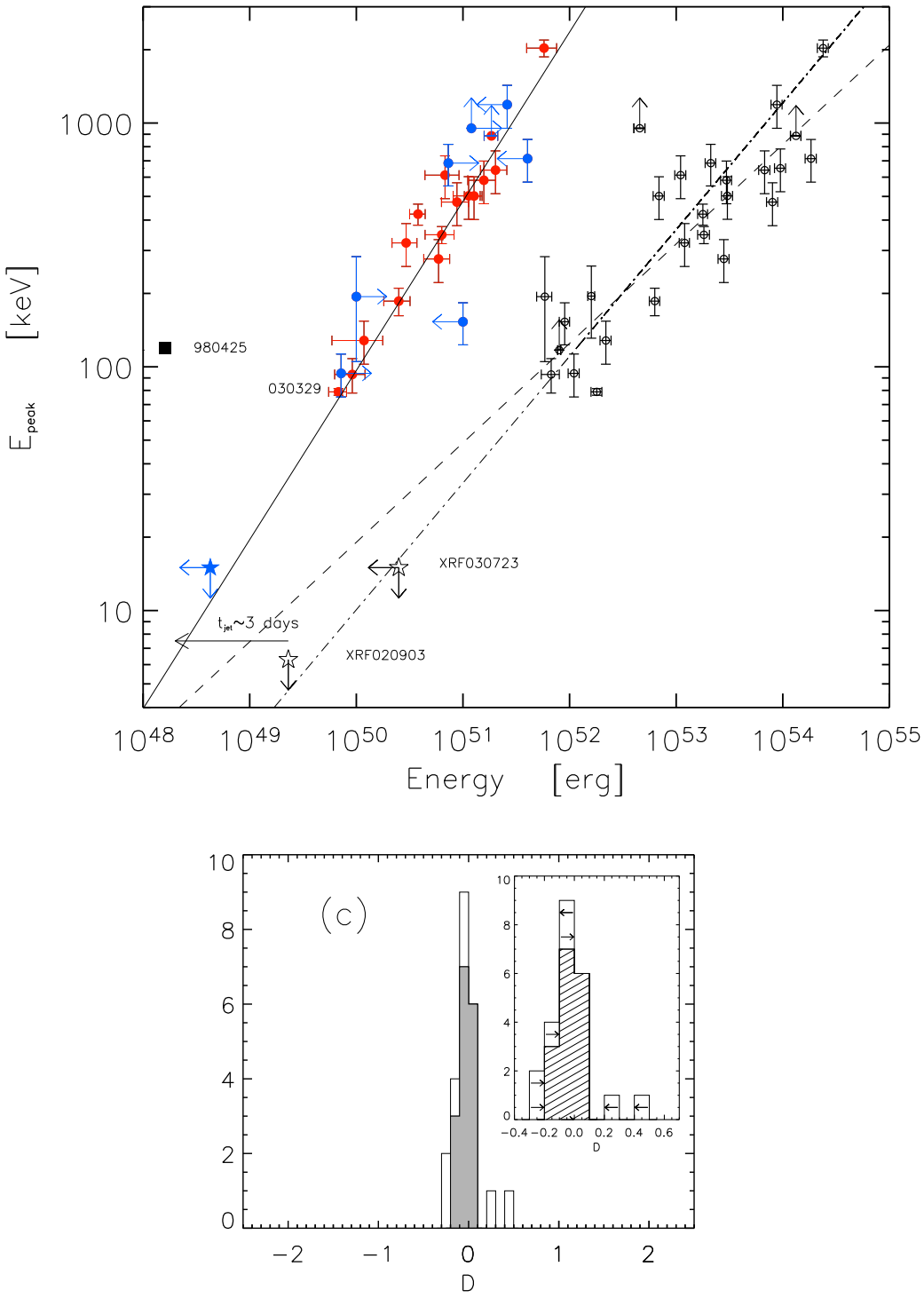

Figure 2.17: Top: The correlation between $E^{\rm src}_{\rm peak}$ and total energy of prompt emission assuming isotropic emission (open circles) or jet (filled circles). The solid line represents the best fit to filled circles. The dashed line represents the best fit to open circles and the dash-dotted line is the correlation reported by Amati et al. (2002). Bottom: distribution of the distance of each GRB from the correlation between $E^{\rm src}_{\rm peak}$ and total energy with jet correction. Insert: distribution of the distance from the correlation with upper and lower limits indicated. (Ghirlanda et al., 2004)

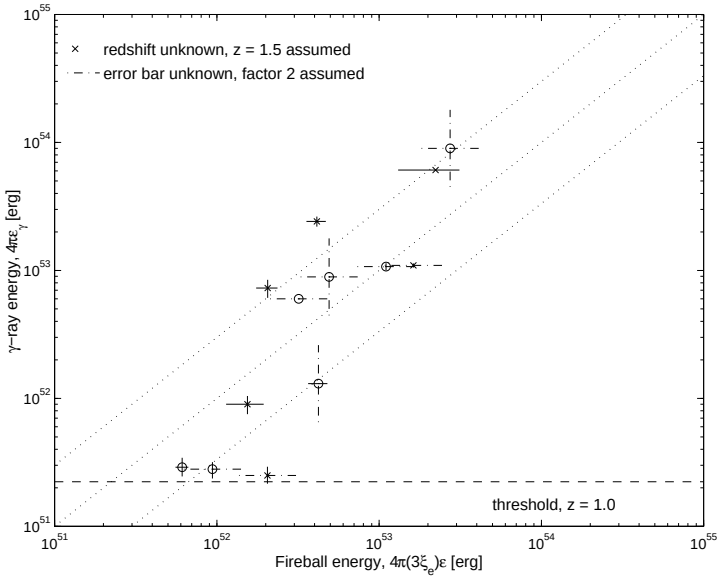

Figure 2.18: Relation between observed gamma-ray energy of prompt emission per unit solid angle (ϵ_γ) and fireball energy oer unit solid angle (ϵ). Dotted lines correspond to $\epsilon_\gamma/\epsilon = \frac{1}{3}$, 1 and 3. (Freedman and Waxman, 2001)

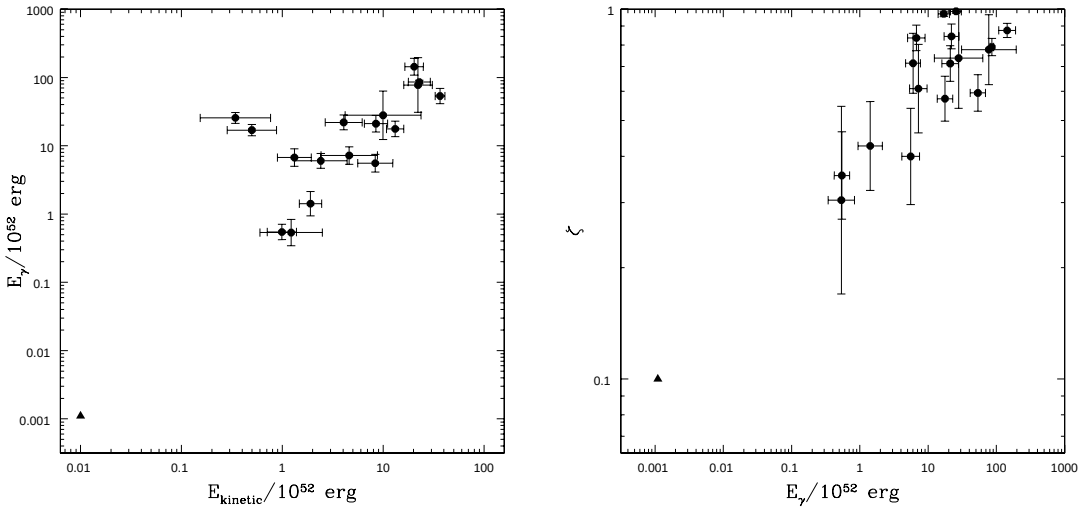

Figure 2.19: The correlation between $E_{\rm iso}$ and $E_{\rm kinetic}$ (left) and efficiency ζ and $E_{\rm iso}$ (right). The triangular point in the bottom is XRF 020903. (Lloyd-Ronning and Zhang, 2004)

2.2 Theory of GRB

In this section, we introduce standard scenario of the fireball model of GRBs. The fireball model is introduced in order to avoid the compactness problem (see below). The basic idea of the fireball model is that the radiating medium (so-called shells) is moving towards the observers with ultra-relativistic velocity and therefore we are observing blue-shifted and Lorentz contracted emission. The fireball model substantially succeed in explaining the observed phenomena, although several modifications are applied to fit individual observations.

2.2.1 Compactness problem and fireball model

Compactness problem

Until 1990s', GRB sources were considered to be located in our galaxy. This is mainly due to large amount of observed energy and short time variability of prompt emission. The time scale of the variability of the prompt emission provides an estimate of (or at least an upper limit to) the size of the emission region, $r = c\,\delta t$, where δt is the shortest time scale of the variability. High energy photons confined within small region interact each other, creating electron - positron pairs. The optical depth of pair creation $\tau_{\gamma\gamma}$ is written as

$$\tau_{\gamma\gamma} = \frac{f_p \sigma_T F D^2}{r^2 m_e c^2} \sim 10^{13} f_p \left(\frac{F}{10^{-7}\mathrm{erg/cm^2}}\right)\left(\frac{D}{1\mathrm{G\,ly}}\right)^2\left(\frac{\delta t}{1\mathrm{ms}}\right)^{-2}, \tag{2.7}$$

where f_p is a fraction of photon pairs which satisfy $\sqrt{E_1 E_2} > m_e c^2$ (E_1, E_2 are the energy of photons), σ_T is the Thomson cross section, F is the observed fluence, d is the distance to the source and $m_e c^2$ is the rest mass energy of electron. From equation (2.7), the optical depth is much grater than 1. The expected spectrum emitted from such a region must be thermal, which is inconsistent with the observed spectra of GRBs. This is the "compactness problem".

Fireball model

In order to reduce the optical depth, we consider the relativistic motion of the emission region toward observer. If an emission region moves with Lorentz factor Γ, the size of the region becomes $\Gamma^2 r$ and f_p becomes f_p/Γ^2. Therefore,

$$\tau_{\gamma\gamma} = \frac{10^{13}}{\Gamma^6} f_p \left(\frac{F}{10^{-7}\mathrm{erg/cm^2}}\right)\left(\frac{D}{1\mathrm{G\,ly}}\right)^2\left(\frac{\delta t}{1\mathrm{ms}}\right)^{-2}, \tag{2.8}$$

with $\Gamma \approx 10^{13/6} \approx 100$.

This is fundamental idea of "fireball model". The fireball model assume a relativistic motion of emission region with $\Gamma \sim 100$. Initially, almost all the energy of the source is kinetic energy. Then kinetic energy is converted into radiation through some process.

2.2.2 Energy conversion — Synchrotron emission from relativistic shell

The fireball model usually considers shock acceleration of electrons through the interaction between the "shell" moving toward observer and inter-stellar medium (ISM). The accelerated electrons emit radiation by synchrotron emission.

Sari et al. (1998) calculated energy spectrum of synchrotron emission from the shocked region.

emission from one electron

The characteristic synchrotron frequency of an electron with Lorentz factor γ_e in a magnetic field B is

$$\nu(\gamma_e) = \Gamma\gamma_e^2 \frac{q_e B}{2\pi m_e c}\,. \tag{2.9}$$

Assuming that the magnetic energy density behind the shock is a constant fraction (ϵ_B) of the shock energy, we find the magnetic field strength in the comoving frame as

$$B = (32\pi m_p \epsilon_B n)^{1/2}\Gamma c\,, \tag{2.10}$$

where n is a number density of particles in ISM. The form of the single-electron emission spectrum depends on whether the electron Lorentz factor is above or below the critical Lorentz factor, which is written as

$$\gamma_c = \frac{6\pi m_e c}{\sigma_T \Gamma B^2 t} = \frac{3m_e}{16\epsilon_B \sigma_T m_p c}\frac{1}{t\Gamma^3 n}\,. \tag{2.11}$$

Then we determine $\nu_c \equiv \nu(\gamma_c)$. The high-energy electrons, that is those with Lorentz factors larger than γ_c, lose a significant fraction of their energy to radiation and cool down quickly.

The case of high energy electrons: $\nu_c < \nu_e$

$$P(\nu)d\nu \;\propto\; \begin{cases} \nu^{1/3} & (\nu < \nu_c) \\ \nu^{-1/2} & (\nu_c < \nu) \end{cases} \tag{2.12}$$

The case of low energy electrons: $\nu_e < \nu_c$

$$P(\nu)d\nu \;\propto\; \begin{cases} \nu^{1/3} & (\nu < \nu_e) \\ \exp\left[-\nu/\nu_c\right] & (\nu_e < \nu) \end{cases} \tag{2.13}$$

The net energy spectrum

We assume that energy spectrum of electrons is

$$N(\gamma_e)d\gamma_e \propto \gamma_e^{-p} d\gamma_e \qquad (\gamma_e \leq \gamma_m)\,, \tag{2.14}$$

and that a constant fraction (ϵ_e) of the shock energy goes into the electrons. Then the minimum Lorentz factor γ_m is written as

$$\gamma_m = \epsilon_e \left(\frac{p-2}{p-1}\right)\frac{m_p}{m_e}\Gamma\,. \tag{2.15}$$

The net spectrum of radiation from electrons is written as

$$F_\nu = \begin{cases} (\nu/\nu_c)^{1/3} F_{\nu,max}, & (\nu_c > \nu)\,, \\ (\nu/\nu_c)^{-1/2} F_{\nu,max}, & (\nu_m > \nu > \nu_c)\,, \\ (\nu_m/\nu_c)^{-1/2}(\nu/\nu_m)^{-p/2} F_{\nu,max}, & (\nu > \nu_m)\,, \end{cases} \tag{2.16}$$

for the case of fast cooling ($\nu_m > \nu_c$), and

$$F_\nu = \begin{cases} (\nu/\nu_m)^{1/3} F_{\nu,max}, & (\nu_c > \nu)\,, \\ (\nu/\nu_m)^{-(p-1)/2} F_{\nu,max}, & (\nu_c > \nu > \nu_m)\,, \\ (\nu_c/\nu_m)^{-(p-1)/2}(\nu/\nu_c)^{-p/2} F_{\nu,max}, & (\nu > \nu_c)\,, \end{cases} \tag{2.17}$$

for the case of slow cooling ($\nu_c > \nu_m$), where $\nu_m \equiv \nu(\gamma_m)$ and

$$F_{\nu,max} \equiv \frac{4\pi R^3}{3} n \times \frac{m_e c^2 \sigma_T}{3q_e} \Gamma B \times \frac{1}{4\pi D^2}\,, \tag{2.18}$$

which is the observed peak flux at distance D from the source.

Hydrodynamic evolution of shell

To find the time evolution of relativistic shell, we begin with the equation of conservation of energy and momentum of the shell,

$$M\Gamma + dm = (M + dm + dE)(\Gamma + d\Gamma) \tag{2.19}$$

and

$$M\Gamma\beta = (M + dm + dE)(\Gamma + d\Gamma)(\beta + d\beta)\,, \tag{2.20}$$

where M is the rest frame energy of the shell and m is the mass of ISM that has already collided with the shell and dE is the internal energy of the shell produced by the shock heating. From equation (2.19) and (2.20), we find

$$\begin{aligned} M\beta\Gamma &= (M\Gamma + dm)(\beta + d\beta) \\ -\frac{dm}{M} &= \Gamma\frac{d\beta}{\beta}\,. \end{aligned} \tag{2.21}$$

Using

$$\frac{d\beta}{\beta} = \frac{d\Gamma}{\Gamma^3}\left(1 - \frac{1}{\Gamma^2}\right)^{-1}\,, \tag{2.22}$$

equation (2.21) is written as

$$-\frac{dm}{M} = \frac{d\Gamma}{\Gamma^2 - 1}\,. \tag{2.23}$$

From equation (2.19) and (2.23),

$$\Gamma(1-\Gamma)\frac{dm}{d\Gamma} + dm = \left((1-\Gamma^2)\frac{dm}{d\Gamma} + dm\,, + dE\right)(\Gamma + d\Gamma) \tag{2.24}$$

and therefore

$$(\Gamma - 1)dm = dE\,. \tag{2.25}$$

Assuming a part of the energy ϵdE is converted into radiation and escapes from the system, the increment of the mass dM is written as

$$\begin{aligned} dM &= (1-\epsilon)dE + dm \\ &= [(1-\epsilon)\Gamma + \epsilon]dm \end{aligned} \tag{2.26}$$

and from (2.23)

$$-\frac{dM}{M} = \frac{(1-\epsilon)\Gamma + \epsilon}{\Gamma^2 - 1}d\Gamma\,. \tag{2.27}$$

Integrating equation (2.27), we get

$$\left(\frac{M}{M_0}\right)^{-2} = \frac{\Gamma - 1}{\Gamma_0 - 1}\frac{(\Gamma+1)^{1-2\epsilon}}{(\Gamma_0+1)^{1-2\epsilon}}\,. \tag{2.28}$$

From equation (2.28) and (2.23),

$$-\frac{m(R)}{M_0} = (\Gamma_0 - 1)^{1/2}(\Gamma_0 + 1)^{1/2-\epsilon} \int_{\Gamma_0}^{\Gamma} (\Gamma' - 1)^{3/2}(\Gamma' + 1)^{3/2-\epsilon} d\Gamma' \,. \tag{2.29}$$

In the limit $\Gamma_0 \gg \Gamma \gg 1$,

$$m(R) = \frac{M_0}{(2-\epsilon)\Gamma_0} \left(\frac{\Gamma}{\Gamma_0}\right)^{-2+\epsilon} \,. \tag{2.30}$$

$m(R)$ is also expressed as

$$m(R) = \frac{4\pi}{3} R^3 n m_p \tag{2.31}$$

and $E_0 = M_0 c^2 \Gamma_0$,

$$R^3 \Gamma^{2-\epsilon} = \frac{E_0}{\frac{4\pi}{3} n m_p c^2} (2-\epsilon)^{-1} \Gamma_0^{-\epsilon} \,. \tag{2.32}$$

Kinetic energy of fireball

Now, in order to estimate the kinetic energy of the fireball from observations of afterglows, we assume the following:

1. The fireball expands adiabatically and the internal energy of the relativistic shell is quickly radiated away.
2. the time of the observation is late enough that slow cooling ($\nu_m < \nu_c$) dominates.
3. the frequency of the observation ν_1 is high enough to satisfy $\nu_1 > \nu_c$.

Under these assumptions, we can write the flux at frequency ν_1 and time t_1 as

$$F(\nu_1, t_1) = \nu_1^{-p/2} \nu_m^{(p-1)/2} \nu_c^{1/2} F_{\nu,max} \tag{2.33}$$

In the case of adiabatic expansion of the relativistic shell, that is $\epsilon = 0$ in Eq. (2.32), we can write the Lorentz factor of the shell and the radius of the shell R as functions of the kinetic energy E_k and time t (which satisfies $t = R/2c\Gamma$), by

$$\Gamma(t) \propto (E_k/t^3)^{1/8} \,, \tag{2.34}$$

and

$$R(t) \propto (E_k t)^{1/4} \,. \tag{2.35}$$

Using equation 2.9, 2.15, 2.10 and 2.34,

$$\nu_m \propto \epsilon_e^2 \epsilon_B^{1/2} t^{-3/2} E_k^{1/2} \,, \tag{2.36}$$

from equation 2.9, 2.11, 2.10 and 2.34,

$$\nu_c \propto \epsilon_B^{-3/2} n^{-1} t^{-1/2} E_k^{-1/2} \,, \tag{2.37}$$

and from equation 2.18, 2.10 and 2.32,

$$F_{\nu,max} \propto \epsilon_B^{-3/2} n^{1/2} E_k D^{-2} \,. \tag{2.38}$$

If the source is at redshift z, these values are corrected as follows:

$$\nu_m \propto \epsilon_e^2 \epsilon_B^{1/2} t^{-3/2} E_k^{1/2} (1+z)^{1/2} , \tag{2.39}$$

$$\nu_c \propto \epsilon_B^{-3/2} n^{-1} t^{-1/2} E_k^{-1/2} (1+z)^{-1/2} , \tag{2.40}$$

$$F_{\nu,max} \propto \epsilon_B^{-3/2} n^{1/2} E_k (1+z) D^{-2} . \tag{2.41}$$

Using (2.33), (2.39), (2.40) and (2.41), observed flux is written as

$$F(\nu_1, t_1) \propto \epsilon_B^{(p-2)/4} \epsilon_e^{(p-1)} E_k^{(p+2)/4} (1+z)^{(p+2)/4} t_1^{(-3p+2)/4} \nu_1^{-p/2} D^{-2} . \tag{2.42}$$

The luminosity of the afterglow is defined by $L(\nu_1, t_1) \equiv 4\pi D^2 \nu_1 F(\nu_1, t_1)$, and is therefore

$$L(\nu_1, t_1) \propto \epsilon_B^{(p-2)/4} \epsilon_e^{(p-1)} E_k^{(p+2)/4} (1+z)^{(p+2)/4} t_1^{(-3p+2)/4} \nu_1^{(2-p)/2} ,$$

so we obtain the following expression for E_k:

$$E_k \propto L(\nu_1, t_1)^{4/(2+p)} \epsilon_B^{(2-p)/(2+p)} \epsilon_e^{4(1-p)/(2+p)} (1+z)^{-1} t_1^{(3p-2)/(p+2)} \nu_1^{2(p-2)/(p+2)} . \tag{2.43}$$

Inserting constants, we get

$$\begin{aligned} E_{k,3\mathrm{day}} &= 4.17 \times 10^{52} \mathrm{erg} \left(\frac{L_{\mathrm{R},3\mathrm{d}}}{10^{46} \mathrm{erg/s}} \right)^{4/(2+p)} \\ &\quad \times \epsilon_{B,-2}^{(2-p)/(2+p)} \epsilon_{e,-1}^{4(1-p)/(2+p)} (\frac{1+z}{2})^{-1} t_{3\mathrm{day}}^{(3p-2)/(p+2)} \nu_{\mathrm{R}}^{2(p-2)/(p+2)} , \end{aligned} \tag{2.44}$$

where $\epsilon_{B,-2} = \epsilon_B/0.01$, $\epsilon_{e,-1} = \epsilon_e/0.1$, $t_{3\mathrm{day}} = t/3$ day and $\nu_{\mathrm{R}} = \nu/(4.6 \times 10^{14})$ Hz (effective frequency of R band). In order to find the kinetic energy of the shell just after the prompt emission (we take the time 50 sec), we consider the radiative loss, which is described by Sari (1997) as

$$\frac{dE}{dt} = -\frac{17}{16} \epsilon_e \frac{E}{t} . \tag{2.45}$$

Therefore the kinetic energy just after the prompt emission E_{kinetic} is

$$E_{\mathrm{kinetic}} = E_{k,3\mathrm{day}} \left[\frac{t(3\mathrm{day})}{t(50\mathrm{sec})} \right]^{17\epsilon_e/16} . \tag{2.46}$$

Light curves of GRB afterglow

Sari et al. (1998) also calculated the light curves of GRBs. Since the hydrodynamic evolution of a relativistic shell varies with efficiency of energy conversion, there are two extreme limits: the fully radiative case and the fully adiabatic case.

For a fixed frequency, there are three characteristic times: t_0 (the time of transition from fast cooling to slow cooling), t_c (the time when ν_c crosses the frequency) and t_m (the time when ν_m crosses the frequency). There are two possible orderings of these times: $t_0 > t_m > t_c$ expected at high frequency and $t_m > t_c > t_0$ expected at low frequency. The light curves in each case are shown in figure 2.20.

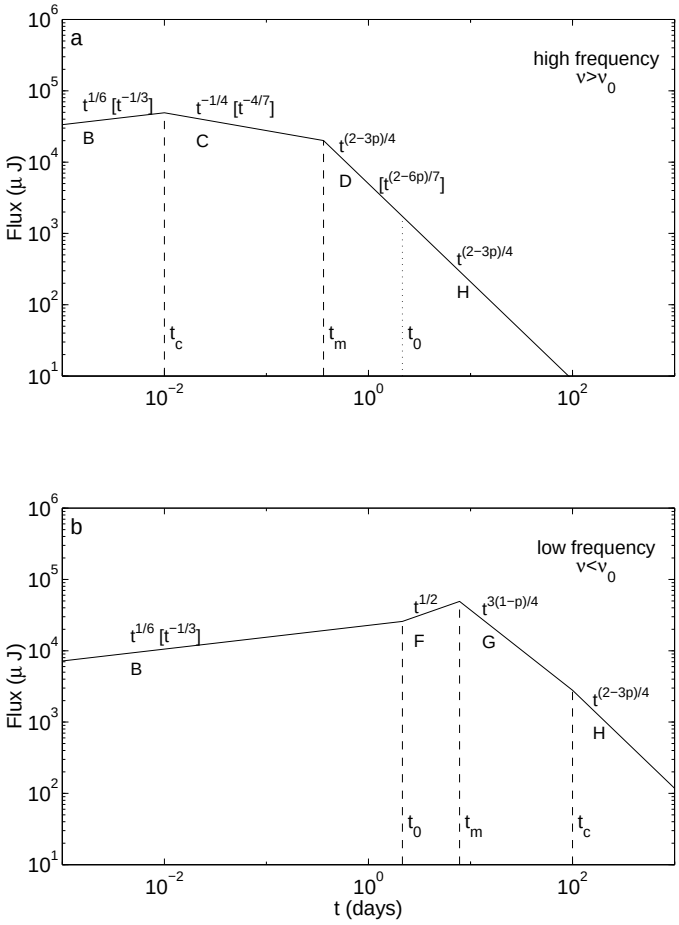

Figure 2.20: The light curve of afterglows predicted by synchrotron model. The observed flux varies as the power-low function of the time. The time dependence given in square brackets are the case of radiative evolution of relativistic shell. The others are the case of adiabatic evolution. (Sari et al., 1998)

2.2.3 Internal - external scenario

The above model succeeds in explaining the behavior of afterglows. However there is difficulty in producing the short time variability observed in the prompt emission of GRBs.

If there are multiple shells with different Lorentz factors, the time variability can be explained. These shells collide with each other and produce the observed peaks (Sari and Piran, 1997). The shock produced by the collision between shells is called "internal shock". On the other hand the shock produced by the collision between the shell and external medium is called "external shock" and this shock produce afterglow.

This "internal - external scenario" is shown in figure 2.21 schematically.

2.2.4 Jet break in the afterglow light curve

In order to estimate the total energy radiated by a GRB, it is necessary to know the geometry of emission region. The emission from a jet cannot be distinguished from the emission from a spherical shell due to relativistic beaming. However, when the Lorentz factor of jet drops below the inverse of the jet opening angle, we expect a break in the light curve of the afterglow.

Assuming the evolution of jet Lorentz factor Γ, we can estimate the jet opening angle θ_j

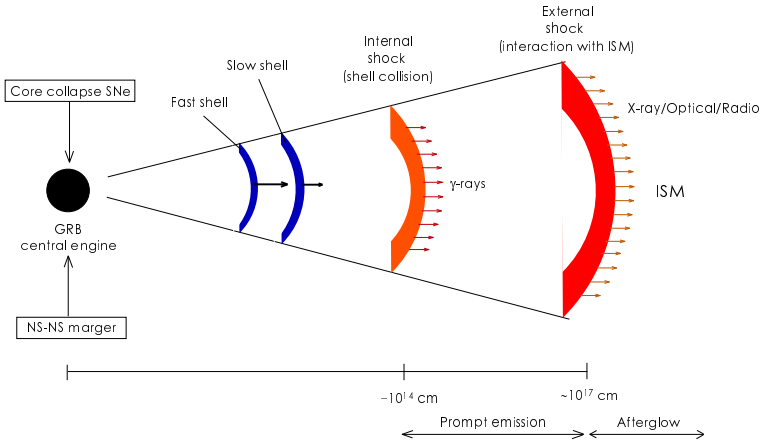

Figure 2.21: The schematic picture of internal-external scenario. The central engine of GRB produce ultra-relativistic shells. These shells collide each other and cause internal shock. Then shells collide with ISM and cause external shock. The prompt emission is emitted by the particles accelerated through the internal shock and afterglow is emitted by the particles accelerated through the external shock.

from jet break time t_j by

$$\theta_j = 0.057 \left(\frac{t_j}{1\mathrm{day}}\right)^{3/8} \left(\frac{1+z}{2}\right)^{-3/8} \left(\frac{E_{\mathrm{iso}}}{10^{53}\mathrm{erg}}\right)^{-1/8} \left(\frac{\eta_\gamma}{0.2}\right)^{1/8} \left(\frac{n}{0.1\mathrm{cm}^{-3}}\right)^{1/8}, \tag{2.47}$$

where η_γ is the efficiency of the fireball in converting the energy in the ejecta into gamma-rays and n is the mean circumburst density (Frail et al., 2001).

Chapter 3

The properties of prompt emissions

In this section, the observing instruments and the observational properties of the prompt emission of GRBs are described.

3.1 Instrumentation and operation

3.1.1 The BeppoSAX satellite

Overview of BeppoSAX

The Italian-Dutch X-ray satellite BeppoSAX, Satellite italiano per Astronomica X, is an X-ray mission with wide spectral coverage from 0.1 to 300 keV (Boella et al., 1997). BeppoSAX was launched on April 30 1996. BeppoSAX mission operations ended at the end of April 2002: 55 GRB locations were reported in the six-year mission.

Science instruments

The scientific payload of BeppoSAX consisted of four different types of Narrow Field Instruments (NFI) and two Wide Field Cameras (WFC). The NFI consisted of three MECS (Medium Energy Concentrator Spectrometers) (Boella et al., 1997), the LECS (the Low-Energy Concentrator Spectrometer) (Parmar et al., 1997), the HPGSPC (the High Pressure Gas Scintillation Proportional Counter) (Manzo et al., 1997), and the PDS (Phoswich Detector System). In addition, the GRBM (Gamma-Ray Burst Monitor) (Feroci et al., 1997) uses the four lateral active shields of the PDS to detect the prompt emission from gamma-ray bursts together with WFCs.

Figure 3.1 shows the composition and layout of the science instruments on-board BeppoSAX. More detailed descriptions of the instruments are given below.

GRBM

The GRBM consists of the four anti-coincidence (AC) detectors of the PDS. Each AC detector is 1 cm thick and has dimensions 27.5 x 41.3 cm, for a geometric area of about 1136 cm^2. The GRBM has open field of view and is sensitive to photons in the 40-700 keV band. The GRBM is able to detect GRBs with a peak flux of 10^{-8} ergs cm^{-2} s^{-1} and provides burst triggers, spectra and light curves with a temporal resolution of $\sim$1 ms.

WFC

The WFCs monitor large fields of view and can be used to determine the direction of GRBs. Each of the WFCs is a coded-mask proportional counter and has a field of view of $20^\circ \times 20^\circ$

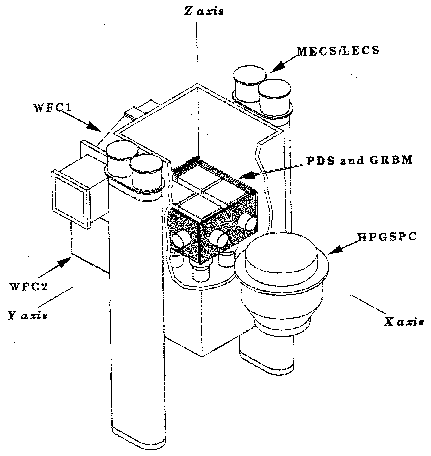

Figure 3.1: The layout of science instruments of BeppoSAX. (Feroci et al., 1997)

(FWHM) with a resolution of 5′. Two WFCs are aligned anti-parallel to each other in the direction of the Y and $-Y$ axes of the satellite, which are orthogonal both to the normal vector of the solar cell panels and to the optical axis of the NFIs. Therefore, a transient source found in the WFC field of view generally lies within the sun-angle constraint of the NFIs and can be followed-up by the NFIs.

MECS and LECS

BeppoSAX has four mirror units (MUs). Three of them provide focusing for MECS and the other one for LECS. The detectors of MECS and LECS are position-sensitive Gas Scintillation Proportional Counters. The performance of MECS and LECS are summarized in Table 3.1. The

	MECS	LECS
Energy range [keV]	1.3 – 10	0.1 – 10
FOV (diameter) [arcmin]	56	37
Angular Resolution [arcmin]	1.2@6 keV	3.5@0.25 keV
Energy Resolution FWHM [%]	$8\times(E_{\rm keV}/6)^{-0.5}$	$8\times(E_{\rm keV}/6)^{-0.5}$
Energy binning [channels]	256	1024
Image size [pixels]	256 × 256	256 × 255
Pixel size [arcsec]	14 × 14	20 × 20

Table 3.1: The performance of MECS and LECS.

MECS and LECS, thanks to their high sensitivity, have been used to observe X-ray afterglows of GRBs, which are much fainter than the prompt emission. Their good angular resolution provides precise positions (∼arcsecond) of GRBs, which are often useful for pointing large ground-based telescopes.

Operation of the BeppoSAX satellite

BeppoSAX was launched into an equatorial low-earth orbit, which has the advantage of a low charged particle background rate. It has also offers the benefit of having a contact with the ground station (Malindi in Kenya) once every orbit, when the data from the previous orbit is downlinked and inspected for triggers in the GRBM. If a trigger in GRBM is found, the

WFC data is examined for a transient source in the field of view. If a new source is found, its coordinates are calculated, and are sent to the community by methods such as e-mails. This process of observing, downlink, ground analysis, and notification took at least a few hours after the burst trigger. In many cases, where various constraints allowed, the entire spacecraft was reoriented to observe the X-ray afterglow of the GRB with the MECS and LECS. Since it requires another contact at the ground station, this procedure took even more time. Follow-up observations of GRBs detected by BeppoSAX were made six or more hours after the burst trigger.

3.1.2 The HETE-2 satellite

Overview of HETE-2 satellite

The High Energy Transient Explorer 2 (HETE-2) (Ricker et al., 2003) is the first astronomical satellite dedicated for observing GRBs. The HETE-2 satellite was launched into equatorial orbit on 9 October 2000. HETE-2 has two unique features: 1) prompt localization of GRBs (within a few tens of seconds of the trigger) with good precision (a few tens of arcminutes), 2) X-ray and gamma-ray spectroscopy of the prompt emission in a wide energy range (2-400 keV). The former feature is essential for early follow-up observations.

Science instruments

There are three scientific instruments on-board HETE-2: the French Gamma Telescope (FREGATE) (Atteia et al., 2003), the Wide-field X-ray Monitor (WXM) (Kawai et al., 2003) and the Soft X-ray Camera (SXC) (Villasenor et al., 2003).

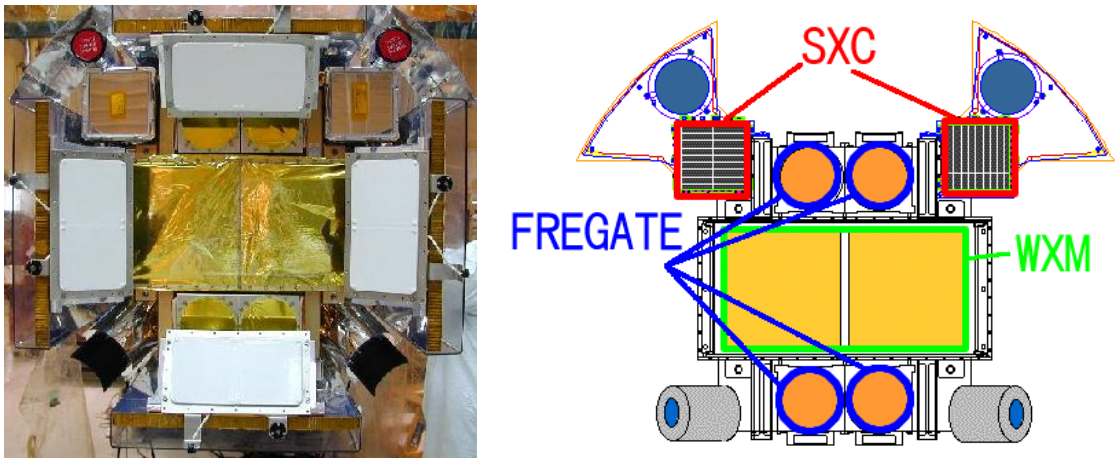

Figure 3.2: The front end of HETE with the solar panels folded. The large rectangular instrument in the center covered by gold foil is the coded aperture of the WXM. Part of the four circular detectors of FREGATE are seen below the S-band antennas at the ends of panels above and below the WXM. The two SXCs (squares) and two optical cameras (small circles) are located upper left and upper right corners of WXM.

FREGATE

The French gamma telescope (FREGATE) is a set of four detectors, each consisting of a cleaved NaI crystal and a photomultiplier. FREGATE is sensitive to photons in the 6-400 keV energy range. The performance of FREGATE is summarized in Table 3.2 The FREGATE

Energy range	6–400 keV
Effective area (4 detectors, on axis)	600 cm^2
Field of view	70°
Energy resolution	$\sim$ 12 % @122 keV

Table 3.2: FREGATE performance

Energy range	2–25 keV
Effective area (1 counter, without coded mask, on axis)	$\sim$ 80 cm^2 keV
Field of view	$\sim 40° \times 40°$
Energy resolution (FWHM)	$\sim$ 20 % @8 keV
Angular Resolution	*sim* $10'$

Table 3.3: WXM performance

provides burst triggers and spectra in a wide energy band.

WXM

The WXM is the main instrument for the localization of GRBs. The WXM consists of two units, each a one-dimensional position sensitive proportional counter covered with a coded mask. The two units are called the X-camera and Y-camera. The orientation of the X-camera is perpendicular to that of the Y-camera, and the X- and Y-locations of GRBs (one-dimensional incidence angle projected to the satellite X- and Y-axes) are determined separately. The onboard computer uses the WXM and FREGATE data for triggering, and uses WXM data to obtain the "flight location" of GRBs (flight localization). The flight location is broadcasted to the network of the Burst Alert Stations on the ground. The performance of WXM is summarized in Table 3.3

SXC

The Soft X-ray Camera (SXC) was designed to provide fine localization and the spectroscopy in the soft X-ray band. Similar to WXM, there are two SXC cameras for providing one-dimensional localization in X and Y axes, each consisting of an X-ray CCD and fine one-dimensional coded mask. SXC can provide the location of burst with an error of $\sim 1'$.

Operation of the HETE-2 satellite

There are 17 Burst Alert Stations within 15 degrees latitude of the equator to provide nearly permanent contact with HETE-2 (fig 3.3).

Each of these is a receive-only stations equipped with omnidirectional VHF antenna and an amateur-class receiver connected to a personal computer for decoding the signal and relaying it to the internet. When a burst trigger occurs, the coordinates of the GRBs are broadcasted to the ground with other essential pieces of information such as trigger time, trigger criterion, trigger significance, signal-to-noise ratios in the light curve, goodness of the localization. These onboard processed data are transmitted from the BAS to the Mission Operations Center at MIT. The raw GRB coordinates are converted to calibrated celestial coordinates and immediately relayed to the GRB Coordinate Network (GCN) for distribution to registered follow-up observers. This entire procedure, from the spacecraft to the observer, takes only a few seconds. The accuracy of these flight locations is usually $\sim$ 30 arcmin (diameter).

The raw data in the form of time-tagged photons are downlinked at one of the three primary

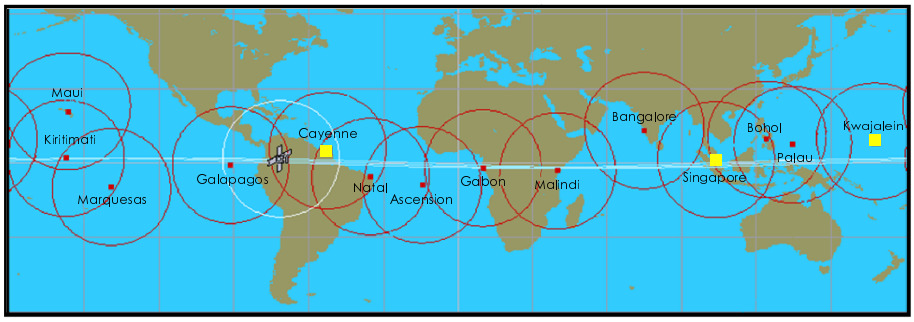

Figure 3.3: HETE-2's Burst Alert Stations.

stations located at Singapore, Kwajalein, and Cayenne, and immediately transferred to the Mission Operation Center at MIT, where the scientists on duty make detailed analysis. The refined burst location obtained with the ground analysis are sent as *HETE_Gnd_Analysis* notice manually. It usually takes 20–30 minutes for the data to come down to MIT, and the ground analyses usually take a comparable time. Therefore, if flight localization fails for some reason, it usually takes an hour or longer since the GRB trigger for the first localization notice to be made available to the community.

3.2 The properties of prompt emissions

In this section, we introduce the properties of GRB prompt emission which we used for the study of the correlation with afterglows. We chose the following five parameters for the correlation study:

1. the observed spectral peak energy ($E_{\rm peak}$)
2. the redshift corrected spectral peak energy ($E^{\rm src}_{\rm peak}$)
3. the energy fluence in 2-30, 30-400 and 2-400 keV ($S_{\rm X}$, S_γ and $S_{\rm total}$)
4. the isotropic total energy emitted at prompt emission ($E_{\rm iso}$)
5. the jet corrected total energy emitted at prompt emission ($E_{\rm jet}$)

Among the above properties, we can estimate 2, 4 and 5 only for bursts with known redshift.

First, we describe the definition of these parameters in section 3.2.1 and then detail the data of parameters for individual bursts in section 3.2.2.

3.2.1 The definitions of properties of prompt emissions

The observed spectral peak energy: $E_{\rm peak}$

The spectral models of GRBs were introduced in section 2.1.1 (see equation 2.1 – 2.3). The parameters for each spectral model are summarized in table 3.4. $E_{\rm peak}$ is peak energy of νF_ν spectrum and related with E_0 and α as

$$E_{\rm peak} = E_0(2+\alpha)\,.$$

Model	number of parameters	parameters
BAND	4	A, α, β, E_0
CPL	3	A, α, E_0
PL	2	A, α

Table 3.4: The model parameters of fitting function for the spectrum of GRBs. A is amplitude in the unit of [photons s^{-1} cm^{-2} keV^{-1}], α is low energy spectral index, β is high energy spectral index and E_0 is break energy in [keV].

The redshift corrected spectral peak energy: $E^{\rm src}_{\rm peak}$

For the bursts with known redshift z, we can calculate the peak energy at the source frame $E^{\rm src}_{\rm peak}$ as

$$E^{\rm src}_{\rm peak} = E_{\rm peak}(1+z)\,. \tag{3.1}$$

The energy fluence: $S_{\rm X}$, S_γ and $S_{\rm total}$

The energy fluence is the energy flux integrated over the burst duration in a finite energy range in the observer frame and expressed in units of [erg cm^{-2}]. $S_{\rm X}$, S_γ and $S_{\rm total}$ are the fluence in the 2–30 keV, 30–400 keV and 2–400 keV respectively. $S_{\rm total}$ is calculated as the sum of $S_{\rm X}$ and S_γ.

The isotropic total energy emitted in prompt emission: $E_{\rm iso}$

It is easy to calculate the total energy directly from the observed fluence as $E = S_{\rm total} \times 4\pi D_L^2$, where D_L is luminosity distance to the source. However, the total energy derived from the above equation corresponds to the total energy in different energy range for the bursts with different redshift, because we use finite energy range in the observer frame for calculating fluence. In order to avoid an influence of finite bandpass of observation, Amati et al. (2002) propose the procedure for calculating the total energy to be 1) blue-shift the GRB spectra to their cosmological rest frame and then 2) integrate the spectra in 1–10000 keV energy range. The total energy is given by:

$$E_{\rm iso} = \frac{\int_1^{10000} EN(E,\alpha,E_0,\beta,A)dE \;\times\; 4\pi D_L^2}{(1+z)^2}\,, \tag{3.2}$$

where N is redshift-corrected photon spectrum of the best-fit model for the burst.

The jet corrected total energy emitted at prompt emission: $E_{\rm jet}$

Geometry of GRBs are considered to be a jet of certain opening angle θ_j. Therefore total energy should be corrected as

$$E_{\rm jet} = f_b E_{\rm iso}\,, \tag{3.3}$$

where f_b is given as

$$\begin{aligned} f_b &= (1-\cos\theta_j) \\ &\simeq \theta_j^2/2\,, \end{aligned} \tag{3.4}$$

(Frail et al., 2001). θ_j can be measured by the observations of afterglows (see 2.2.4).

3.2.2 The data of prompt emissions

Most of the data of the parameters of prompt emission we used were taken from published papers. For the parameters of the bursts detected by BeppoSAX, we referred to Amati et al. (2002); for the parameters of the bursts detected by HETE-2, we referred to Sakamoto et al. (2004a). The properties of prompt emission from these GRBs is summarized in table 3.5 and 3.6.

GRB name	$S_{\rm X}$	S_γ	$E_{\rm peak}$
GRB010213	$7.88^{+0.25}_{-0.54}$	$0.69^{+0.58}_{-0.32}$	3.41
GRB010629B	$25.41^{+1.67}_{-1.66}$	$28.56^{+2.69}_{-2.47}$	45.57
GRB011019	$3.03^{+0.58}_{-0.58}$	$1.10^{+1.39}_{-0.74}$	18.71
GRB011130	$5.85^{+0.98}_{-0.96}$	$0.98^{+1.17}_{-0.62}$	4.9
GRB011212	$4.24^{+0.64}_{-0.64}$	$3.37^{+2.53}_{-1.68}$	—
GRB020127	$6.73^{+0.51}_{-0.5}$	$20.49^{+4.48}_{-3.65}$	104.00
GRB020331	$16.07^{+1.04}_{-1.03}$	$53.32^{+8.52}_{-7.39}$	91.57
GRB020625	$2.37^{+0.55}_{-0.5}$	$0.12^{+0.35}_{-0.11}$	8.52
GRB020801	$25.66^{+2.83}_{-2.72}$	$95.23^{+10.67}_{-10.54}$	53.35
GRB020812	$7.91^{+1.09}_{-1.09}$	$19.15^{+8.18}_{-5.86}$	87.62
GRB020819	$25.20^{+1.1}_{-1.11}$	$62.53^{+8.33}_{-9.27}$	49.90
GRB021104	$10.32^{+2.06}_{-1.8}$	$6.13^{+4.4}_{-2.67}$	28.21
GRB021112	$1.31^{+0.25}_{-0.25}$	$2.14^{+1.08}_{-0.9}$	57.15
GRB030115	$7.89^{+0.61}_{-0.61}$	$15.17^{+4.02}_{-3.2}$	82.79
GRB030324	$5.49^{+0.44}_{-0.44}$	$12.75^{+3.35}_{-3.01}$	146.80
GRB030418	$17.11^{+1.09}_{-1.1}$	$17.34^{+7.27}_{-5.22}$	46.10
GRB030528	$62.54^{+2.8}_{-2.79}$	$56.34^{+7.13}_{-7.32}$	31.84
GRB030723	$2.43^{+0.33}_{-0.33}$	$2.79^{+1.64}_{-1.18}$	—
GRB030725	$94.12^{+2.27}_{-2.25}$	$166.70^{+10.3}_{-10.1}$	102.80
GRB030823	$23.05^{+1.56}_{-1.55}$	$12.74^{+4.43}_{-3.53}$	26.57
GRB030824	$8.90^{+1.07}_{-1.07}$	$5.83^{+2.38}_{-1.89}$	8.7
GRB031026	$4.73^{+0.81}_{-0.82}$	$27.84^{+6.29}_{-6.06}$	148.3
GRB031111A	$14.88^{+0.6}_{-0.67}$	$178.57^{+4.83}_{-4.86}$	404.4
GRB031111B	$5.73^{+0.87}_{-0.86}$	$6.01^{+2.85}_{-2.34}$	—
GRB031220	$5.53^{+0.56}_{-0.55}$	$5.64^{+2.86}_{-1.96}$	46.98
GRB040228B	$2.99^{+0.73}_{-0.73}$	$0.13^{+1.9}_{-0.1}$	11.92
GRB040511	$31.74^{+2.98}_{-2.86}$	$96.57^{+9.57}_{-8.79}$	93.91
GRB040916B	$3.80^{+1.14}_{-0.99}$	$0.52^{+1.44}_{-0.43}$	—

Table 3.5: The summary of $S_{\rm X}$, S_γ and $E_{\rm peak}$ for the bursts without known redshifts. $S_{\rm X}$ and S_γ are in the unit of [10^{-7} erg cm^{-2}]. $E_{\rm peak}$ is in the unit of [keV].

GRB name	$S_{\rm X}$	S_γ	$E_{\rm peak}$	$E^{\rm src}_{\rm peak}$	$E_{\rm iso}$	$E_{\rm jet}$	z
GRB970228	45.58	102.77	195.04	330.59	1.86 ± 0.14	—	0.695
GRB970508	15.30	23.84	145.58	267.14	0.71 ± 0.15	0.049	0.835
GRB971214	7.27	124.27	684.48	3025.40	24.5 ± 2.8	0.116	3.42
GRB980326	9.85	19.16	70.84	141.68	0.56 ± 0.11	0.003	1
GRB980329	29.57	732.81	934.32	—	—	—	<3.9
GRB980613	7.69	20.99	194.94	408.59	0.68 ± 0.11	0.016	1.096
GRB990123	79.57	1253.56	2029.1	5275.66	278.3 ± 31.5	1.088	1.60
GRB990510	62.88	331.95	422.73	1107.13	20.6 ± 2.9	0.045	1.619
GRB990705	76.46	541.55	347.70	646.72	21.2 ± 2.7	0.094	0.86
GRB990712	70.40	77.89	93.48	134.05	0.78 ± 0.15	0.016	0.434
GRB010222	340.64	1040.37	94.90	235.07	154.2 ± 17	0.252	1.477
GRB010921	$71.60^{+3.42}_{-3.2}$	$112.60^{+8.6}_{-8.4}$	88.63	128.60	0.954 ± 0.3	0.156	0.451
GRB020124	$19.74^{+1.4}_{-1.41}$	$61.33^{+8.79}_{-7.63}$	86.93	365.11	36.85 ± 12	0.518	3.2
GRB020813	$138.50^{+2.7}_{-2.3}$	$839.60^{+12.3}_{-12.5}$	142.10	319.72	153.5 ± 10	0.245	1.25
GRB020903	$0.83^{+0.28}_{-0.24}$	$0.16^{+0.44}_{-0.14}$	5.0	6.25	1.4E-3 ±1.2E-3	—	0.25
GRB021004	$7.65^{+0.69}_{-0.69}$	$17.79^{+7.01}_{-5}$	79.79	265.54	4.395 ± 3.5	0.117	2.328
GRB021211	$11.60^{+0.29}_{-0.29}$	$23.71^{+2.03}_{-2.01}$	45.56	91.39	1.684 ± 0.3	0.020	1.006
GRB030226	$13.20^{+1.18}_{-1.18}$	$42.92^{+6.85}_{-6.02}$	97.12	290.00	6.766 ± 2.5	0.028	1.986
GRB030323	$3.40^{+1.29}_{-1.21}$	$8.91^{+3.84}_{-3.48}$	—	—	7.239	0.036	3.37
GRB030328	$81.86^{+1.31}_{-1.29}$	$287.40^{+13.9}_{-14.1}$	126.30	318.28	33.1 ± 9	0.096	1.52
GRB030329	$553.10^{+3.10}_{-3.20}$	$1076.00^{+13.0}_{-14.0}$	67.86	79.26	1.795 ± 0.07	0.012	0.168
GRB030429	$4.74^{+0.49}_{-0.49}$	$3.80^{+1.4}_{-1.17}$	35.04	127.90	3.084 ± 0.7	0.032	2.65
GRB040924	$1.96^{+0.04}_{-0.04}$	$1.96^{+0.06}_{-0.12}$	40.63	75.53	—	—	0.856
GRB041006	$52.61^{+1.38}_{-0.93}$	$83.86^{+9.06}_{-2.97}$	50.76	87.10	2.105 ± 0.071	—	0.716

Table 3.6: The summary of $S_{\rm X}$, S_γ, $E_{\rm peak}$, $E^{\rm src}_{\rm peak}$, $E_{\rm iso}$, $E_{\rm jet}$ and z for the bursts with known redshifts. $S_{\rm X}$ and S_γ are in the unit of [10^{-7} erg cm^{-2}]. $E_{\rm peak}$ and $E^{\rm src}_{\rm peak}$ are in the unit of [keV]. $E_{\rm iso}$ and $E_{\rm jet}$ are in the unit of [10^{52} erg].

Chapter 4

Data analysis of afterglows

In the first two sections of this chapter, the general properties and the methods used in the analysis of the afterglow emission of GRBs were described. The rest of this chapter is the summary of our analysis of optical afterglows for individual bursts.

4.1 Data of optical observations

4.1.1 Choice of color band

The most commonly used color band for studying light curves of GRB optical afterglows is the red band of the Johnson-Morgan-Cousins system (the R_c band). We therefore selected the photometric measurements in the R_c band in the present work. The effective wavelength of R_c band is 0.66 μm and width is 0.14 μm (Fukugita et al., 1996).

In addition to these filtered observations, we also include the unfiltered observations in our analysis. Small telescopes are preferred in observing the early phase of optical afterglows, because of need to slew a telescope promptly to the direction of the bursts, or to cover a large imaging field to accommodate the initial error circles which often have large uncertainties. These small telescopes tend to be used with unfiltered CCD camera in order to collect as much photons as possible. The measurements taken with such system are usually presented by the magnitude in the R_c band, and we adopt these values. It can be justified because sensitivity of CCD cameras usually peaks in the passband of the R_c filter, and the error in the conversion of magnitude expected to be small.

4.1.2 flux density and magnitude

The radiation flux density of a source can be estimated from the measured magnitude if the spectrum of the source and the band-pass function of the filter is completely known. In the present work, we assume the standard "Vega"-like spectrum and and estimate the flux with the procedure given as follows. Although neither of these conditions are likely to be met with the collection of the GRB afterglow observations conducted with variety of telescopes, the error in conversion is not likely to affect the validity of our analysis and discussion, given the large dynamic range of the data values used.

The flux density is related to the magnitude m as

$$m = -2.5 \log_{10}(f_\nu / f_{\nu 0}) \,. \tag{4.1}$$

where $f_{\nu 0}$ is the flux density of Vega in the bandpass.

Oke and Gunn (1983) defined the AB magnitude by

$$AB_\nu = -2.5 \log f_\nu - 48.60\,, \tag{4.2}$$

where f_ν is in the unit of [erg s^{-1} cm^{-2} Hz^{-1}]. Fukugita et al. (1996) reported that R_c magnitude of Vega is related to the AB magnitude by

$$AB = R + 0.212\,. \tag{4.3}$$

Therefore R_c magnitude is calculated by

$$\begin{aligned} R + 0.212 &= -2.5 \log f_\nu - 48.60 & (4.4)\\ R &= -2.5 \log(f_\nu / 2.987 \times 10^{-20})\,. & (4.5) \end{aligned}$$

4.1.3 Data selection

BeppoSAX reported 55 GRBs locations and HETE-2 reported 61 (as of mid-October 2004). We collected information on observations of the optical, infra-red and radio afterglows of these GRBs from papers published in journals and GCN circulars. The collected data include both positive detections and upper limits (U.L. hereafter). With the examination of these results, we found only 1/3 of the well-localized GRBs have confirmed optical afterglows. Details are shown in table 4.1 and figure 4.1.

Source of localization	BeppoSAX	HETE-2
Number of well-localized GRBs	55	61
Detected optical afterglows	16	22
Number of events used for this study	17	43

Table 4.1: Statistics of the detection of optical afterglows

The aim of this study is to investigate how the brightness of optical afterglows is related to the properties of the prompt emission, such as fluence or $E_{\rm peak}$. Each piece of the optical afterglow data consists of the observed epoch and the observed magnitudes (or upper limits in some cases). The sensitivities and epochs of follow-up (with respect to the burst time) of observations in this data set vary over a very broad range. This inhomogeneity is a source of biases, as is the wide range source distances. We therefore attempt to homogenize the data by applying various corrections as described later in this section, and try to compare the afterglow brightness at similar epochs.

We used 43 events of HETE-2 in this study. Almost all the events which have magnitude of optical transient (OT) or U.L. of optical afterglows are included in those 43 events. Thirteen of them have known redshifts. In order to the study correlations between properties of optical afterglows and prompt emissions in the source frame, the samples of GRBs with known redshift are essential. Therefore we also included 17 events localized by BeppoSAX for which redshifts are known.

Figure 4.1 shows the fraction of GRB events associated with optical afterglows. It also shows the selection for this study. The colors of the outer rings indicate the fraction of events associated with optical transients (OTs). The fraction of the events used for this study is shown by the colored region of the inner ring.

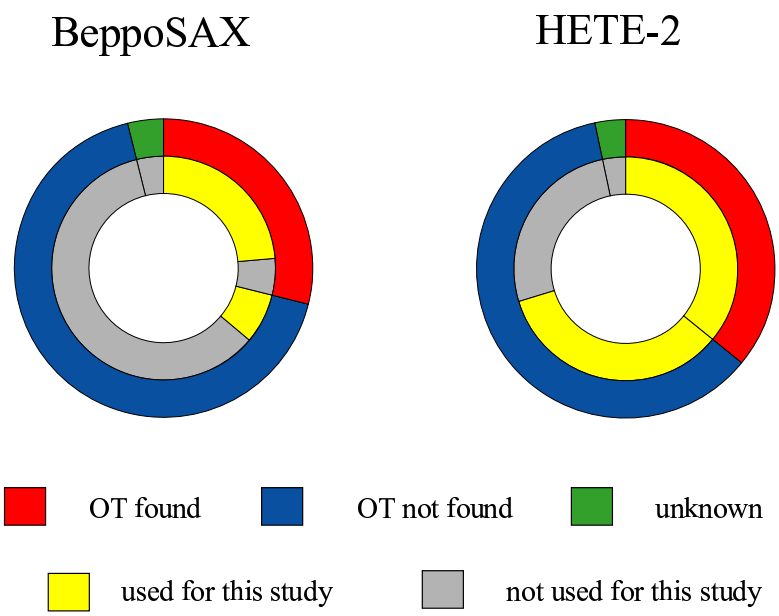

Figure 4.1: Fraction of GRB events associated with optical transients (OT) is indicated by the colors of the outer rings. The colors of the inner rings shows the fraction of the events used for the present work.

4.1.4 Classification of optical afterglows

We classified these events into 4 classes according to the apparent magnitude of the optical afterglow and observation sensitivity. Both of these quantities are compared to the magnitude expected at the epoch of observations for the "standard" light curve, which is a power-law decay curve ($f_\nu \propto t^{-1}$) with the fiducial magnitude of $R = 20$ at the epoch of $t = 1$day. The definitions of classes are shown in figure 4.2 schematically. An optical transient detected above the standard light curve is classified as a "bright OT" (class B). If the detection is below the this line, it is classified as a "dim OT" (class M). If no OT was detected and all upper limits are above the boundary, the event is classified as an "insufficient observation" (class N). The events with no OT detection and upper limits below the boundary are classified as "dark GRBs" (class D). The events we analyzed are classified as the figure 4.3.

4.2 Homogenizing afterglow measurements

The next step is to determine the brightness of each afterglow sample. But "How should we define the brightness of optical afterglow?" is not a trivial question. The situations and observing conditions of optical afterglow may differ from one burst to another, and also from one measurement to another for a single GRB. One event has an observed data point at a certain epoch, but another event may not have data point at the same epoch. In order to compare the measurements of afterglows from different sources at different epochs, we need to establish a procedure to homogenizing the data by applying a few corrections based on reasonable physical assumptions.

In this section, we introduce the procedure of obtaining a fair sample of homogeneous data from various observations of optical afterglows.

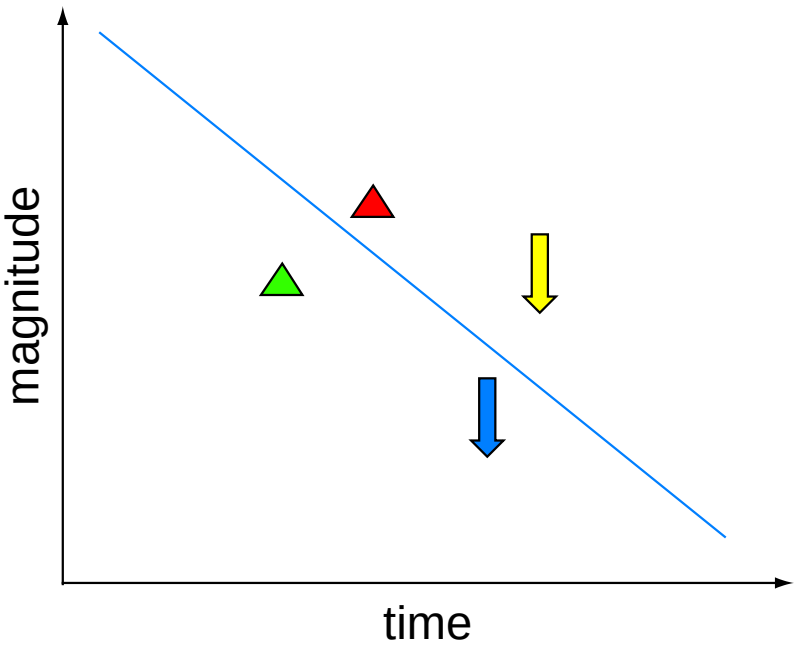

Figure 4.2: The definition of the OT classification is shown schematically with the "standard" light curve of optical afterglow. The solid line is the "standard" afterglow light curve, which follows a power-law decay ($f_\nu \propto t^{-1}$) with the fiducial magnitude of $R = 20$ at the epoch of $t = 1$day, and it defines the boundary between the classes. If an OT is detected above the line, the event is classified as a bright GRB (red triangle). If an OT is detected and all the measured points lie below the line, the event is classified as a dim OT (green triangle). Those events that have upper limits below the boundary are classified as dark GRBs (blue arrow). If no associated OT was detected and all the upper limits are above the boundary, the event is classified as an insufficient observation (yellow).

4.2.1 Time-resolved magnitude of afterglow

In order to evaluate the measurements of the time-variable light curve, we estimated time-resolved magnitude of each afterglow.

First, we subdivided time elapsed since the burst into logarithmic intervals one order of magnitude or half an order of magnitude wide. Almost all of the afterglow observations are covered by the time interval from 0.001 day to 1000 days after the burst. Therefore, we took 23 time intervals: 12 intervals logarithmically spaced by an order of magnitude (0.0003–0.003, 0.001–0.01, $\cdots$, 30–300, 100–1000 days) and 11 intervals logarithmically spaced by a half order of magnitude (0.001–0.003, 0.003–0.01, $\cdots$, 30–100, 100–300 days). Then we determined the representative magnitude of OT for each time interval with the following procedure (see figure 4.4).

Time interval with multiple upper limits: adopt the dimmest upper limit as the limit for the time interval,

Time interval with a single upper limit: adopt the upper limit as the limit of the time interval,

Time interval with upper limit(s) and a single detected point: adopt the detected point as the brightness of the time interval and ignore limits,

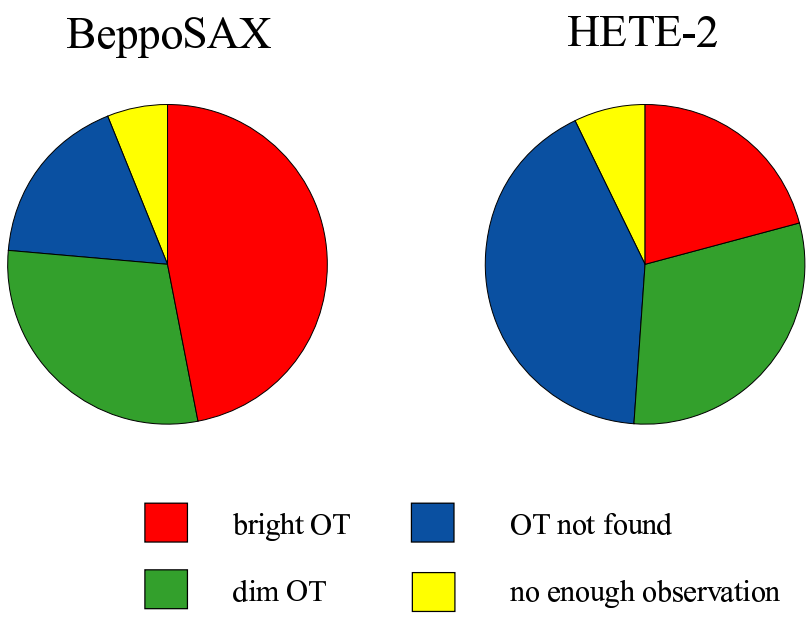

Figure 4.3: The classification of OTs according to their apparent brightness relative to the standard decay light curve. Note that the results are affected by selection of the samples.

Time interval with single detected point: adopt the detected point as the brightness of the time interval,

Time interval with upper limit(s) and detected points: fit the detected points to a power-law function (with the power-law index fixed to -1 if data are not sufficient) and estimate the brightness at the middle of the time interval where upper limits are ignored,

Time interval with multiple detected points: fit the detected points to a power-law function (with the power-law index fixed to -1 if data are not sufficient) and estimate the brightness at the middle of the time interval.

4.2.2 Corrections of optical afterglows

In order to estimate the luminosity of optical afterglows in the GRB source frame, we apply several corrections based on reasonable assumptions.

(i) Cosmological time dilation

We observe optical afterglows at arbitrary time. We usually measure the time of observation in observer frame and the origin of the time is defined as the time of prompt emission.

First, we have to take into account the effect of cosmological time dilation. The time in the GRB source frame ($t^{\rm src}$) is written as

$$t^{\rm src} = t^{\rm obs} / (1+z)\,, \tag{4.6}$$

where z is the cosmological redshift of the GRB source.

(ii) Cosmological redshift of observing frequency

The frequency in the GRB source frame ($\nu^{\rm src}$) is find as follows:

$$\nu^{\rm src} = \nu^{\rm obs} / (1+z)\,. \tag{4.7}$$

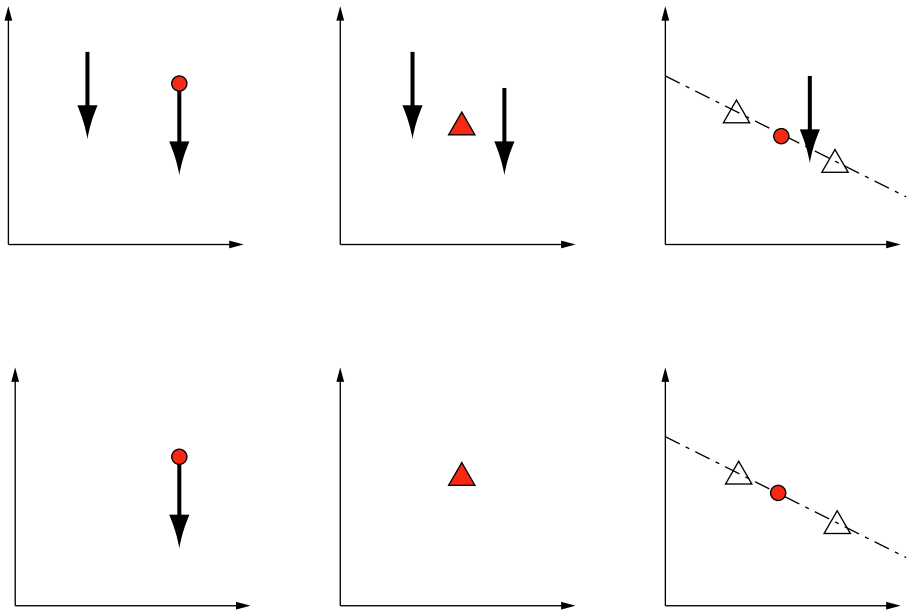

Figure 4.4: The definition of the data in each time interval (see text).

(iii) Extrapolation of flux density in time and frequency

We estimate the spectral flux density at the fiducial epoch and frequency by extrapolating the observed spectral flux density assuming a canonical relativistic synchrotron-shock spectrum. Assuming the frequency of observation (i.e. R-band) is above the cooling frequency (ν_c) at the epoch $t^{\rm src} \geq 1$, we expect the light curve to have an decay index

$$\alpha_l = \frac{2-3p}{4}, \tag{4.8}$$

where p is the electron energy index (see equation 2.43).

Then, we can estimate flux density at the source frame in the energy band $\nu^{\rm src}(1+z)$ at the source frame epoch $t^{\rm src}$ by extrapolating from the nearest data point along the light curve with $\alpha_l = -1$, where we assume $p = 2$.

To estimate the flux of certain energy band, we have to assume some spectral energy distributions at the source frame. Since we assume the energy band we observed is above the critical frequency ν_c and synchrotron peak frequency ν_m, an expected spectral index β above observing frequency is $-p/2$ i.e. $\beta = -1$.

(iv) Conversion from magnitude to luminosity

The source-frame luminosity at a specified band is determined from the observed R magnitude by the following procedure. Here, we denote the luminosity of the source which emits radiation in frequency range $[\nu_1, \nu_2]$ at time t is as $L^{\rm src}(\nu_1, \nu_2, t^{\rm src})$, and the apparent R-band magnitude of the source at time t' as $m(R, t')$. We can convert magnitude to observed flux density $f^{\rm obs}$ by definition as follows,

$$m(R, t') = -2.5 \log \left\{ f^{\rm obs}(R, t') / f_{\rm V}(R) \right\}. \tag{4.9}$$

where $f_{\rm V}(R)$ is the flux density of Vega in R-band and

$$f_{\rm V}(R) = 2.15 \times 10^{-5} \qquad [\mathrm{erg\,s^{-1}\,cm^{-2}\,\mu m^{-1}}]. \tag{4.10}$$

Therefore,

$$f^{\rm obs}(R,t) = 10^{-\frac{m(R,t')}{2.5}} \times f_{\rm V}(R) \tag{4.11}$$

We write observed flux in energy range $[\nu_1, \nu_2]$ at time t' as $F^{\rm obs}(\nu_1, \nu_2, t')$. Now we consider a source at a redshift z with a luminosity $L^{\rm src}(\nu_1, \nu_2, t^{\rm src})$. Using energy conservation, we can derive

$$L^{\rm src}(\nu_1, \nu_2, t^{\rm src}) = F^{\rm obs}(\nu_1(1+z), \nu_2(1+z), t^{\rm src}(1+z)) \times (1+z) \times 4\pi D_L^2, \tag{4.12}$$

where D_L is the luminosity distance for redshift z.

Adopting the decay index $\alpha_l = -1$ and spectral index $\beta = -1$, we can write

$$f^{\rm obs}(R,t) \times t = const \tag{4.13}$$

and

$$\begin{aligned} F^{\rm obs}(\nu_1, \nu_2, t) &= \int_{\nu_1}^{\nu_2} C\nu^{-1} d\nu \\ &= \int_{\nu_1(1+z)}^{\nu_2(1+z)} C \left(\frac{\nu}{1+z}\right)^{-1} \frac{d\nu}{1+z} \\ &= \int_{\nu_1(1+z)}^{\nu_2(1+z)} C\nu^{-1} d\nu \\ &= F^{\rm obs}(\nu_1(1+z), \nu_2(1+z), t). \end{aligned} \tag{4.14}$$

Using $f^{\rm obs}(R,t) \times d\nu_R \approx F^{\rm obs}(\nu_{R1}, \nu_{R2}, t)$, finally we obtain

$$\begin{aligned} L^{\rm src}(\nu_{R1}, \nu_{R2}, t_{\rm src}) &= F^{\rm obs}(\nu_{R1}(1+z), \nu_{R2}(1+z), t^{\rm src}(1+z)) \times (1+z) \times 4\pi D_L^2 \\ &= F^{\rm obs}(\nu_{R1}, \nu_{R2}, t^{\rm src}(1+z)) \times (1+z) \times 4\pi D_L^2 \\ &= f^{\rm obs}(R, t^{\rm src}(1+z)) \times (1+z) \times 4\pi D_L^2 \\ &= f^{\rm obs}(R, t') \frac{t'}{t^{\rm src}(1+z)} \times (1+z) \times 4\pi D_L^2 \\ &= 10^{-\frac{m(R,t')}{2.5}} \times f_{\rm V}(R) \frac{t'}{t^{\rm src}} \times 4\pi D_L^2 \end{aligned} \tag{4.15}$$

(vi) Correction for the collimation

For early afterglows before the jet break time, we view the the emission which is relativistically beamed. $L^{\rm src}$ defined above is derived for isotropic emission, and would be an overestimation for collimated emission. We therefore define the luminosity with jet correction $L_{\rm jet}^{\rm src}$ as

$$L_{\rm jet}^{\rm src} = f_b L^{\rm src}\,, \tag{4.16}$$

where f_b is the same as equation 3.4.

4.3 Data

This section contains tables of the magnitudes of the optical afterglow for each burst at each time interval. We adopted the fitting function $m(t) = m_0 + \alpha \log(t/1{\rm day})$, where $m(t)$ is the OT magnitude at time t. The best-fit parameters of α and m_0 are listed in the table. The data# in the tables corresponds to the data# in the table of each burst in the Appendix E.

GRB970228

The prompt emission of this burst is XRR. This is the first event with afterglow, which is detected in X-ray, optical and Radio wavelength. Optical afterglow of this event is dim. Measured redshift of the burst is 0.695.

Time interval [day]	Detect/U.L.	α	m_0	$m(t)$	data#
0.1:1	Detect	-1.59 ± 2.06	21.1 ± 0.37	19.2 ± 2.23	1-2
0.3:1	Detect	-1.59 ± 2.06	21.1 ± 0.37	20.1 ± 0.95	1-2
0.3:3	Detect	-1.11 ± 0.15	21.1 ± 0.04	21.1 ± 0.04	1-3
1:3	Detect	—	—	22.3 ± 0.9	3
1:10	Detect	-2.14 ± 0.74	19.9 ± 1.35	22.6 ± 0.54	3-5
3:10	Detect	-1 (fixed)	22.6 ± 0.25	24.4 ± 0.25	4-5
3:30	Detect	-0.58 ± 0.56	23.2 ± 1.99	24.7 ± 0.60	4-8
10:30	Detect	-2.68 ± 2.38	15.7 ± 8.54	24.1 ± 1.10	6-8
10:100	Detect	-2.68 ± 2.38	15.7 ± 8.54	25.8 ± 0.41	6-8
100:300	Detect	—	—	27.0 ± 0.35	9

Table 4.2: Time resolved magnitude of GRB970228.

GRB970508

The prompt emission of this burst is XRR. The optical afterglow of this GRB is bright. Measured redshift of the burst is 0.835.

Time interval [day]	Detect/U.L.	α	m_0	$m(t)$	data#
0.03:0.3	Detect	-0.13 ± 0.39	21.4 ± 0.54	21.1 ± 0.44	1-3
0.1:0.3	Detect	-0.13 ± 0.39	21.4 ± 0.54	21.2 ± 0.20	1-3
0.1:1	Detect	+0.28 ± 0.10	20.8 ± 0.12	21.2 ± 0.06	1-6
0.3:1	Detect	+0.32 ± 0.13	20.8 ± 0.14	21.0 ± 0.08	3-6
0.3:3	Detect	+0.43 ± 0.18	20.3 ± 0.12	20.3 ± 0.12	4-20
1:3	Detect	+0.38 ± 0.20	20.2 ± 0.13	20.0 ± 0.07	7-20
1:10	Detect	-0.15 ± 0.15	20.0 ± 0.14	20.2 ± 0.10	7-26
3:10	Detect	-1.25 ± 0.22	18.6 ± 0.32	21.0 ± 0.12	21-26
3:30	Detect	-1.30 ± 0.04	18.5 ± 0.09	21.8 ± 0.05	21-35
10:30	Detect	-1.68 ± 0.09	17.3 ± 0.28	22.6 ± 0.04	27-35
10:100	Detect	-1.17 ± 0.08	18.9 ± 0.30	23.3 ± 0.06	27-45
30:100	Detect	-0.77 ± 0.09	20.5 ± 0.38	23.8 ± 0.04	36-45
30:300	Detect	-0.71 ± 0.06	20.8 ± 0.29	24.4 ± 0.04	36-52
100:300	Detect	-0.54 ± 0.18	21.8 ± 1.00	24.8 ± 0.07	46-52
100:1000	Detect	-0.53 ± 0.15	21.8 ± 0.84	25.1 ± 0.13	46-53
300:1000	Detect	—	—	25.2 ± 0.25	53

Table 4.3: Time resolved magnitude of GRB970508.

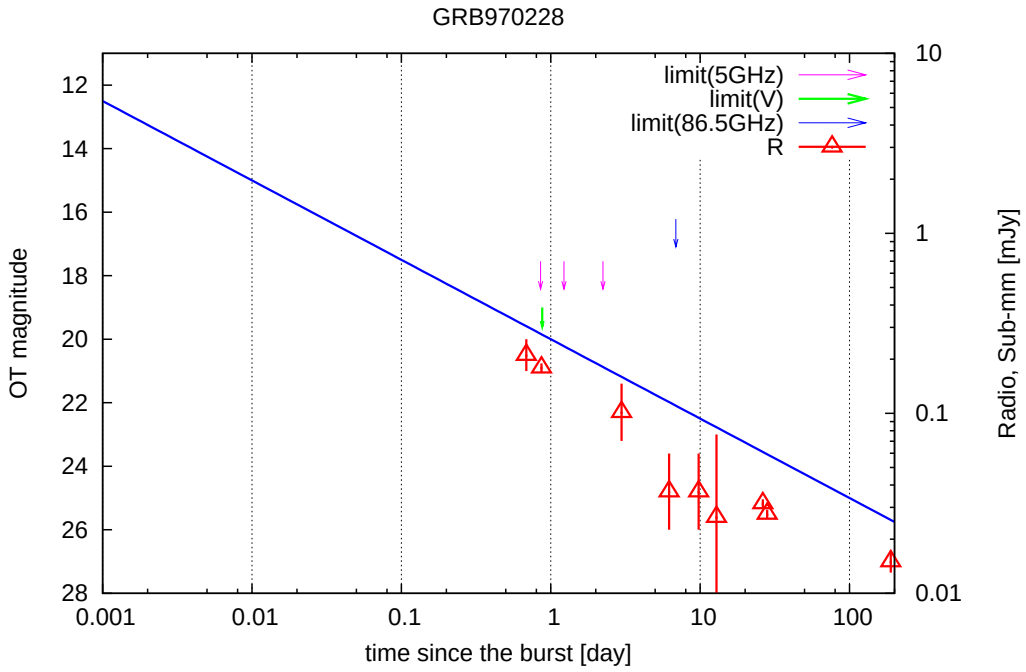

Figure 4.5: Optical afterglow of GRB970228.

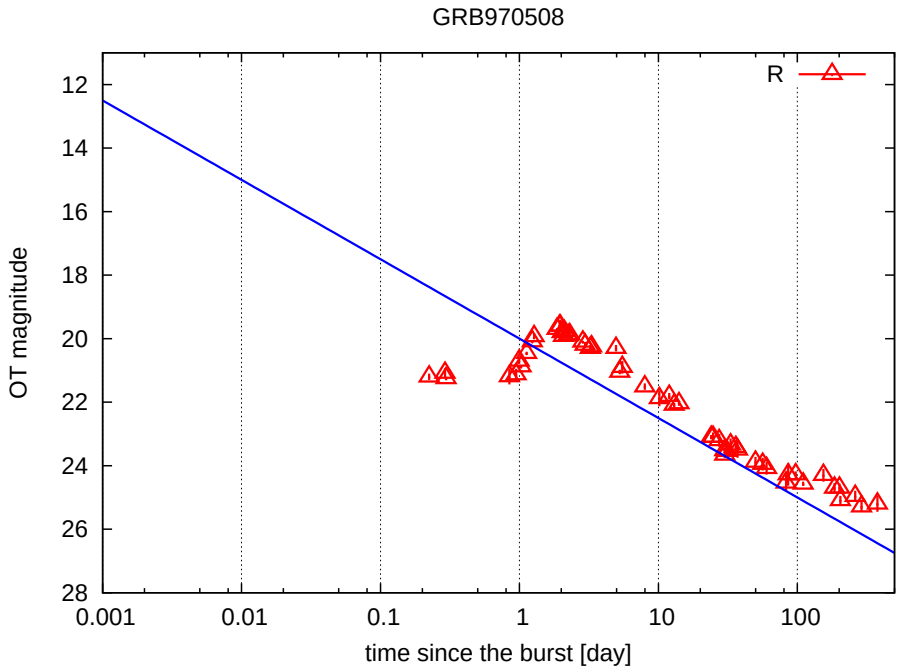

Figure 4.6: Optical afterglow of GRB970508.

GRB971214

The prompt emission of this burst is GRB. Optical afterglow of this event is dim. Measured redshift of the burst is 3.42.

Time interval [day]	Detect/U.L.	α	m_0	$m(t)$	data#
0.1:1	Detect	-1 (fixed)	22.6 ± 0.17	21.4 ± 0.17	1-2
0.3:1	Detect	-1 (fixed)	22.6 ± 0.17	22.0 ± 0.17	1-2
0.3:3	Detect	-1.26 ± 0.15	22.8 ± 0.11	22.8 ± 0.11	1-5
1:3	Detect	-1.43 ± 0.23	22.7 ± 0.17	23.6 ± 0.06	3-5
1:10	Detect	-1.41 ± 0.11	22.7 ± 0.10	24.4 ± 0.06	3-6
3:10	Detect	—	—	24.6 ± 0.22	6
3:30	Detect	—	—	24.6 ± 0.22	6

Table 4.4: Time resolved magnitude of GRB971214.

GRB980326

The prompt emission of this burst is XRR. Optical afterglow of this event is dim. The redshift of the burst is measured to be 1.0 ± 0.1.

Time interval [day]	Detect/U.L.	α	m_0	$m(t)$	data#
0.1:1	Detect	-2.65 ± 0.22	23.5 ± 0.18	20.2 ± 0.10	1-3
0.3:1	Detect	-2.65 ± 0.22	23.5 ± 0.18	21.8 ± 0.05	1-3
0.3:3	Detect	-1.84 ± 0.07	22.9 ± 0.04	22.9 ± 0.04	1-9
1:3	Detect	-1.67 ± 0.21	22.9 ± 0.10	24.0 ± 0.08	4-9
1:10	Detect	-1.30 ± 0.13	23.0 ± 0.10	24.7 ± 0.11	4-11
3:10	Detect	-1 (fixed)	23.3 ± 0.14	25.2 ± 0.14	10-11
3:30	Detect	-0.13 ± 0.13	24.6 ± 0.29	25.0 ± 0.15	11-13
10:30	Detect	-1 (fixed)	21.6 ± 0.35	24.8 ± 0.35	12-13
10:100	Detect	-1 (fixed)	21.6 ± 0.35	25.4 ± 0.35	12-13
30:300	U.L.	—	—	27.3	14
100:300	U.L.	—	—	27.3	14
100:1000	U.L.	—	—	27.3	14

Table 4.5: Time resolved magnitude of GRB980326.

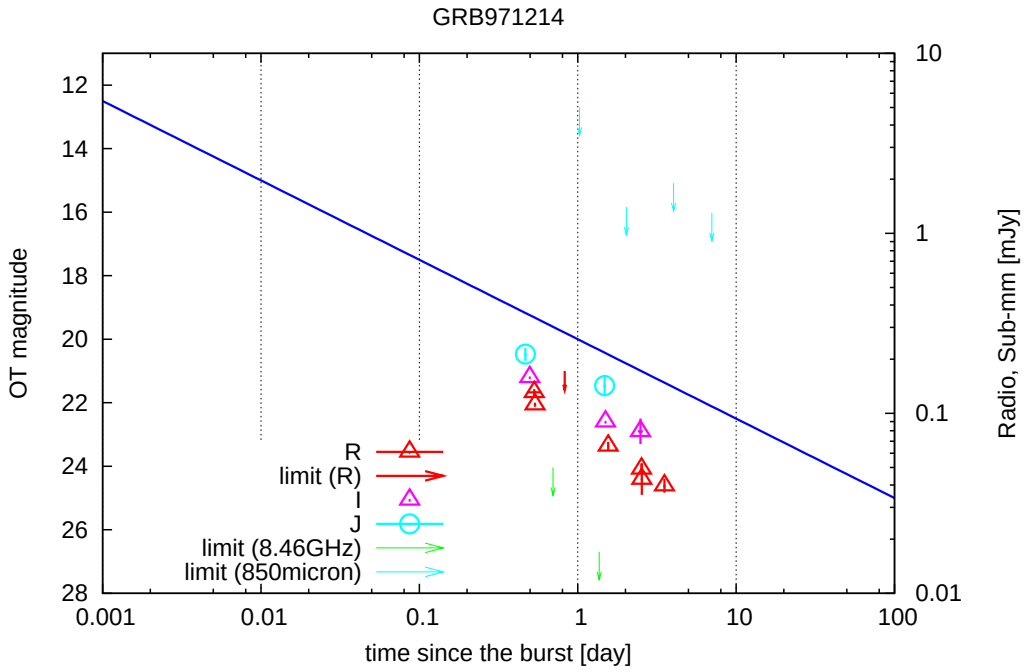

Figure 4.7: Optical afterglow of GRB971214.

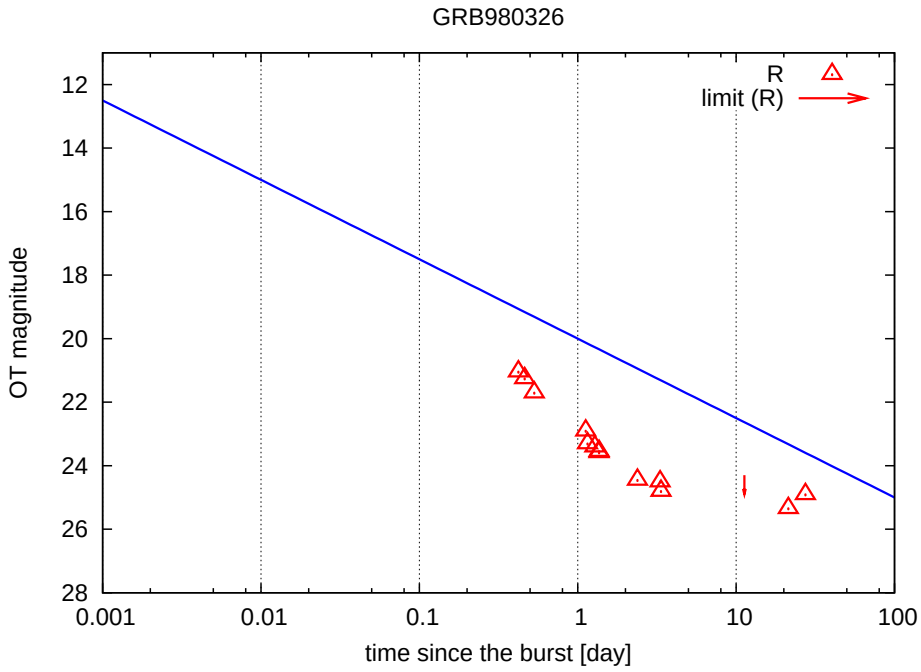

Figure 4.8: Optical afterglow of GRB980326.

GRB980329

The prompt emission of this burst is GRB. Optical afterglow of this event is dim. The redshift of the burst is measured to be < 3.9.

Time interval [day]	Detect/U.L.	α	m_0	$m(t)$	data#
0.1:1	Detect	—	—	23.5 ± 0.2	1
0.3:1	Detect	—	—	23.5 ± 0.2	1
0.3:3	Detect	-1.05 ± 0.43	23.7 ± 0.19	23.7 ± 0.19	1-2
1:3	Detect	—	—	24.8 ± 0.5	2
1:10	Detect	-2.16 ± 1.40	22.5 ± 1.91	25.2 ± 0.29	2-3
3:10	Detect	—	—	25.7 ± 0.3	3
3:30	Detect	—	—	25.7 ± 0.3	3

Table 4.6: Time resolved magnitude of GRB980329.

GRB980613

The prompt emission of this burst is XRR. Optical afterglow of this event is dim. The redshift of the burst is measured to be 1.096.

Time interval [day]	Detect/U.L.	α	m_0	$m(t)$	data#
0.1:1	Detect	—	—	22.9 ± 0.2	1
0.3:1	Detect	—	—	22.9 ± 0.2	1
0.3:3	Detect	-0.13 ± 0.49	23.0 ± 0.08	23.0 ± 0.08	1-2
1:3	Detect	-1.30 ± 0.43	22.9 ± 0.09	23.7 ± 0.25	2-3
1:10	Detect	-0.10 ± 0.16	23.0 ± 0.26	23.1 ± 0.17	2-4
3:10	Detect	+1.35 ± 0.52	26.2 ± 1.13	23.6 ± 0.18	3-4
3:30	Detect	-1 (fixed)	21.0 ± 0.36	23.5 ± 0.36	3-4

Table 4.7: Time resolved magnitude of GRB980613.

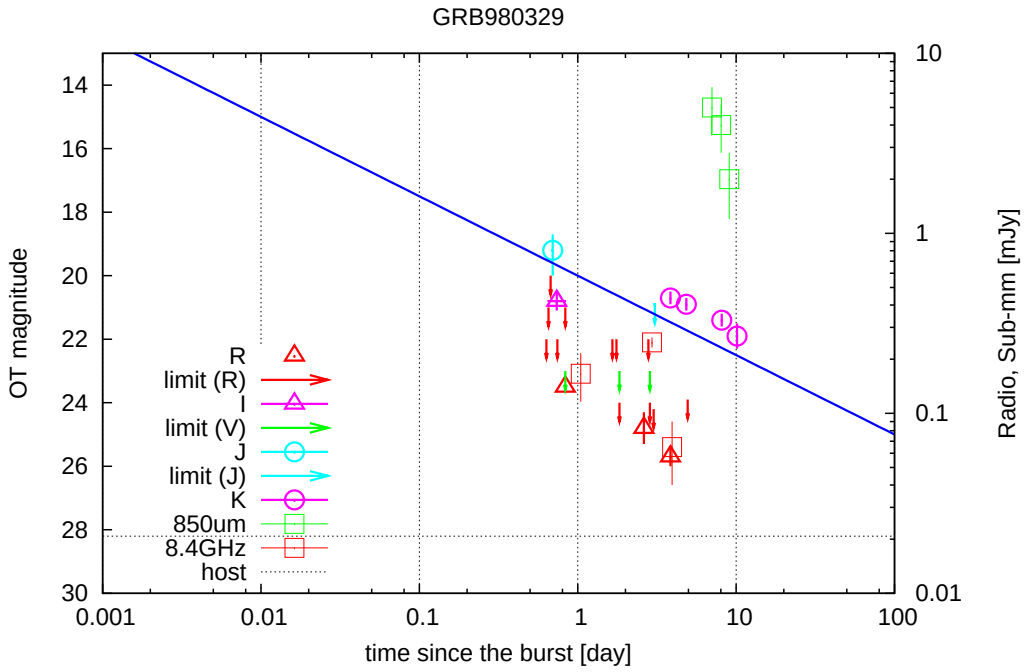

Figure 4.9: Optical afterglow of GRB980329.

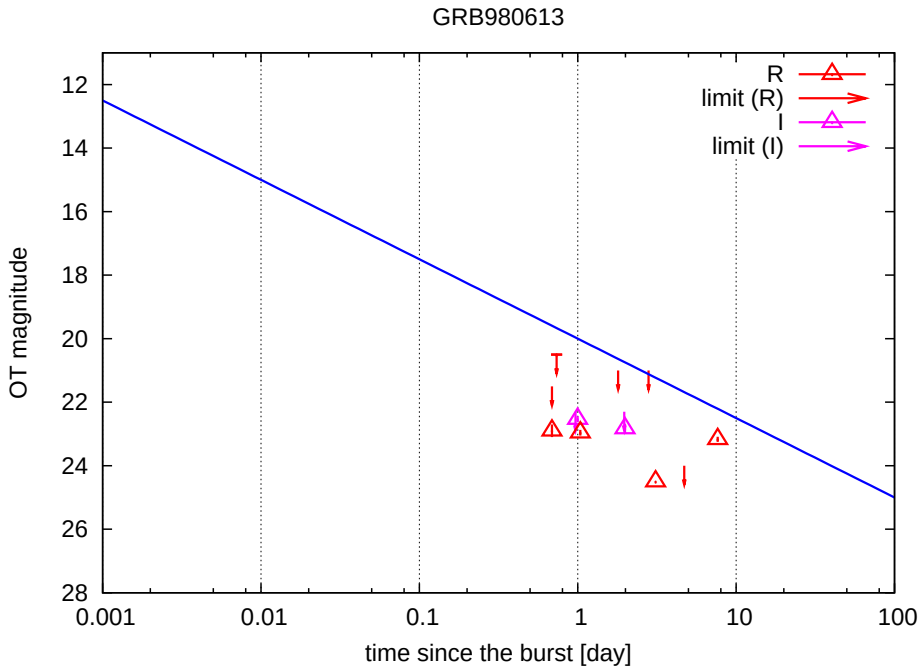

Figure 4.10: Optical afterglow of GRB980613.

GRB990123

The prompt emission of this burst is GRB. The optical afterglow of this GRB is bright. The redshift of the burst is measured to be 1.60.

Time interval [day]	Detect/U.L.	α	m_0	$m(t)$	data#
0.0003:0.001	Detect	+1.69 ± 2.13	-3.6 ± 17.62	10.0 ± 0.97	1-3
0.0003:0.003	Detect	-2.07 ± 0.03	26.1 ± 0.26	10.5 ± 0.03	2-4
0.001:0.01	Detect	-1.58 ± 0.03	23.0 ± 0.02	13.1 ± 0.002	4-6
0.003:0.01	Detect	-1.58 ± 0.03	23.0 ± 0.02	14.1 ± 0.001	4-6
0.003:0.03	Detect	-1.58 ± 0.03	23.0 ± 0.02	15.1 ± 0.002	4-6
0.03:0.3	Detect	-0.79 ± 0.33	20.1 ± 0.61	18.2 ± 0.26	7-11
0.1 0.3	Detect	-0.79 ± 0.33	20.1 ± 0.61	18.7 ± 0.11	7-11
0.1:1	Detect	-0.79 ± 0.07	20.1 ± 0.10	19.2 ± 0.06	7-15
0.3:1	Detect	-0.65 ± 0.27	20.1 ± 0.09	19.7 ± 0.09	11-15
0.3:3	Detect	-1.19 ± 0.16	20.3 ± 0.10	20.3 ± 0.10	12-19
1:3	Detect	-0.79 ± 0.67	20.6 ± 0.49	21.1 ± 0.17	16-19
1:10	Detect	-1.09 ± 0.38	20.6 ± 0.49	21.7 ± 0.24	16-20
3:10	Detect	—	—	23.0 ± 0.24	20
3:30	Detect	-0.57 ± 0.13	21.8 ± 0.39	23.3 ± 0.08	20-24
10:30	Detect	-0.56 ± 0.29	21.8 ± 0.90	23.6 ± 0.07	21-24
10:100	Detect	-0.56 ± 0.29	21.8 ± 0.90	23.9 ± 0.21	21-24

Table 4.8: Time resolved magnitude of GRB990123.

GRB990510

The prompt emission of this burst is GRB. The optical afterglow of this GRB is bright. The redshift of the burst is measured to be 1.619.

Time interval [day]	Detect/U.L.	α	m_0	$m(t)$	data#
0.03:0.3	Detect	-0.59 ± 0.41	19.5 ± 0.83	18.0 ± 0.19	1-3
0.1:0.3	Detect	-0.59 ± 0.41	19.5 ± 0.83	18.4 ± 0.06	1-3
0.1:1	Detect	-0.70 ± 0.11	19.8 ± 0.13	18.9 ± 0.07	1-13
0.3:1	Detect	-0.29 ± 0.31	19.5 ± 0.22	19.4 ± 0.08	4-13
0.3:3	Detect	-0.31 ± 0.24	19.6 ± 0.17	19.6 ± 0.17	4-17
1:3	Detect	-1.52 ± 0.12	19.5 ± 0.03	20.4 ± 0.05	14-17
1:10	Detect	-1.92 ± 0.03	19.4 ± 0.04	21.8 ± 0.03	14-20
3:10	Detect	-2.14 ± 0.10	18.9 ± 0.21	23.0 ± 0.02	18-20
3:30	Detect	-2.14 ± 0.10	18.9 ± 0.21	24.3 ± 0.05	18-20

Table 4.9: Time resolved magnitude of GRB990510.

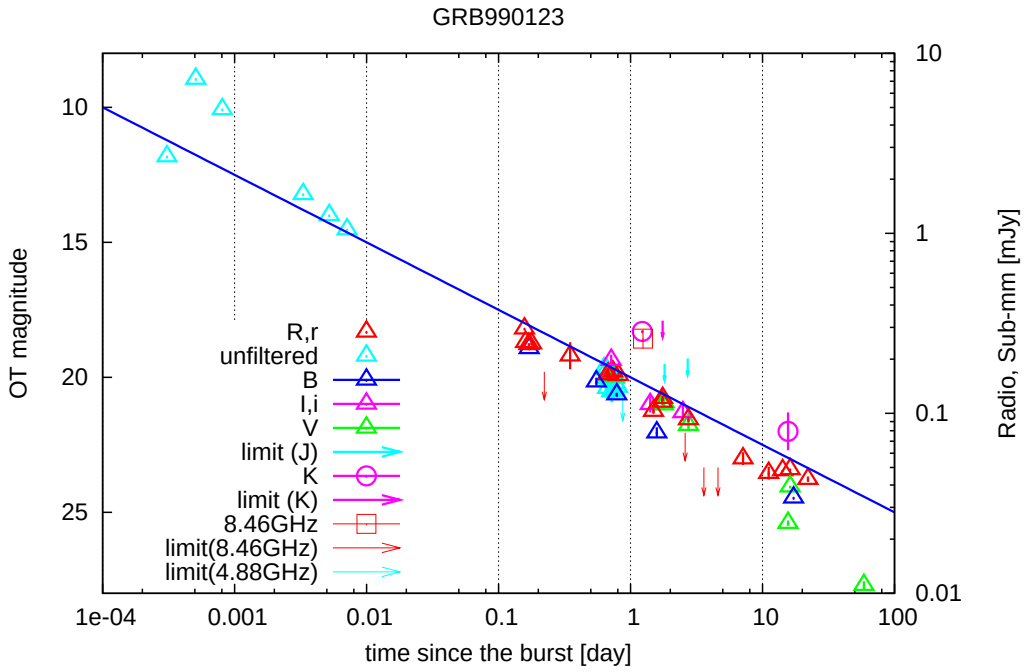

Figure 4.11: Optical afterglow of GRB990123.

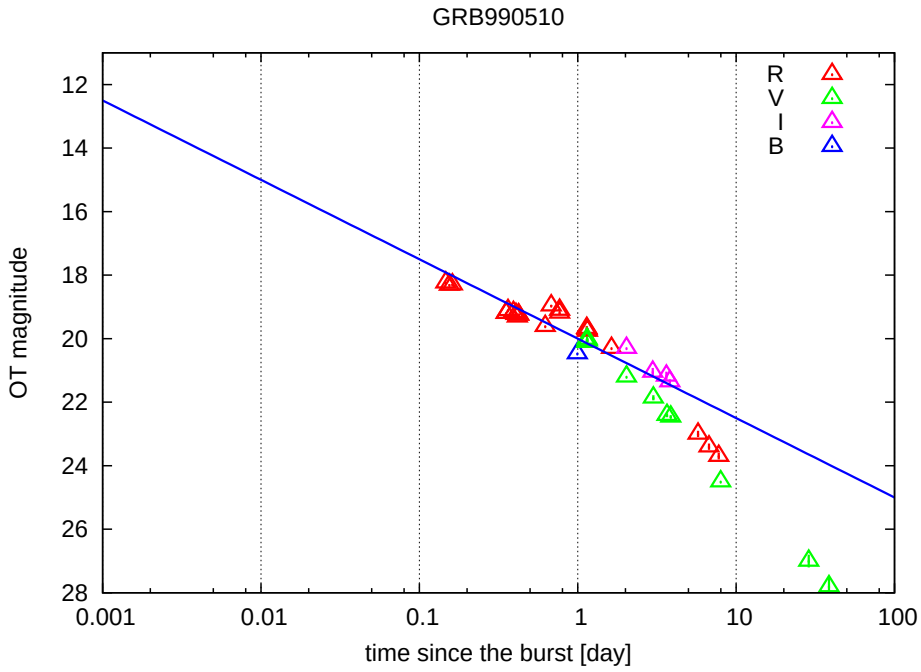

Figure 4.12: Optical afterglow of GRB990510.

GRB990705

The prompt emission of this burst is GRB. Optical afterglow for this burst is searched sufficiently. However no detection has reported. The redshift of the burst is measured to be 0.86.

Time interval [day]	Detect/U.L.	α	m_0	$m(t)$	data#
0.3:3	U.L.	—	—	22.3	2
1:3	U.L.	—	—	22.3	2
1:10	U.L.	—	—	22.3	2

Table 4.10: Time resolved magnitude of GRB990705.

GRB990712

The prompt emission of this burst is XRR. The optical afterglow of this GRB is bright. The redshift of the burst is measured to be 0.434.

Time interval [day]	Detect/U.L.	α	m_0	$m(t)$	data#
0.03:0.3	Detect	—	—	19.5 ± 0.02	1
0.1:0.3	Detect	—	—	19.5 ± 0.02	1
0.1:1	Detect	-1.00 ± 0.03	21.4 ± 0.03	20.1 ± 0.02	1-7
0.3:1	Detect	-1.03 ± 0.08	21.4 ± 0.06	20.8 ± 0.02	2-7
0.3:3	Detect	-0.95 ± 0.04	21.3 ± 0.03	21.3 ± 0.03	2-12
1:3	Detect	-0.85 ± 0.53	21.4 ± 0.23	21.9 ± 0.13	8-12
1:10	Detect	-1.02 ± 0.08	21.3 ± 0.08	22.6 ± 0.06	8-14
3:10	Detect	-0.75 ± 0.09	21.8 ± 0.17	23.2 ± 0.04	13-14
3:30	Detect	-0.39 ± 0.14	22.4 ± 0.37	23.4 ± 0.11	13-15
10:30	Detect	—	—	23.7 ± 0.04	15
10:100	Detect	-1.25 ± 0.40	19.6 ± 1.41	24.3 ± 0.11	15-17
30:100	Detect	-0.10 ± 0.31	23.9 ± 1.16	24.4 ± 0.20	16-17

Table 4.11: Time resolved magnitude of GRB990712.

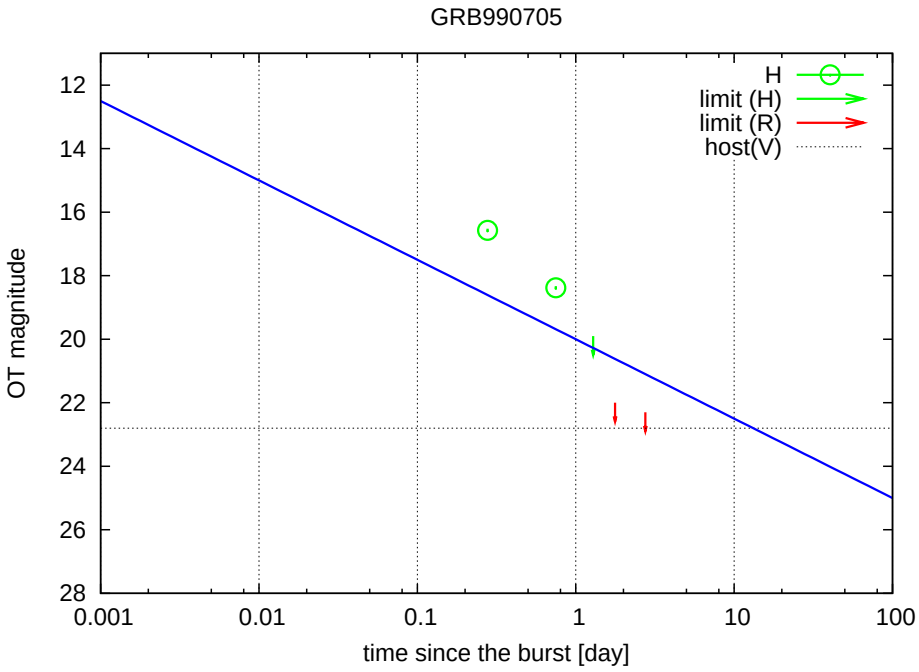

Figure 4.13: Optical afterglow of GRB990705.

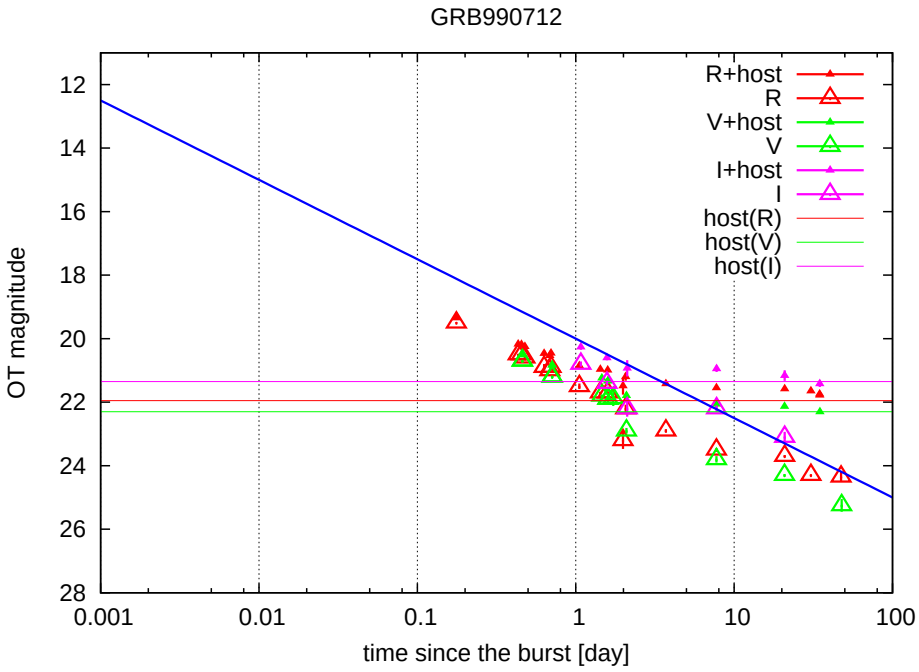

Figure 4.14: Optical afterglow of GRB990712.

GRB000210

The prompt emission of this burst is GRB (Piro et al., 2002). Optical afterglow for this burst is searched sufficiently. However no detection has reported. The redshift of the burst is measured to be 0.846.

Time interval [day]	Detect/U.L.	α	m_0	$m(t)$	data#
0.03:0.3	U.L.	—	—	18.0	1
0.1:0.3	U.L.	—	—	18.0	1
0.1:1	U.L.	—	—	23.3	2
0.3:1	U.L.	—	—	23.3	2
0.3:3	U.L.	—	—	23.3	2

Table 4.12: Time resolved magnitude of GRB000210.

GRB000214

The prompt emission of this burst is XRR. Optical afterglow for this burst is not searched sufficiently. The redshift of the burst is between 0.37 and 0.47.

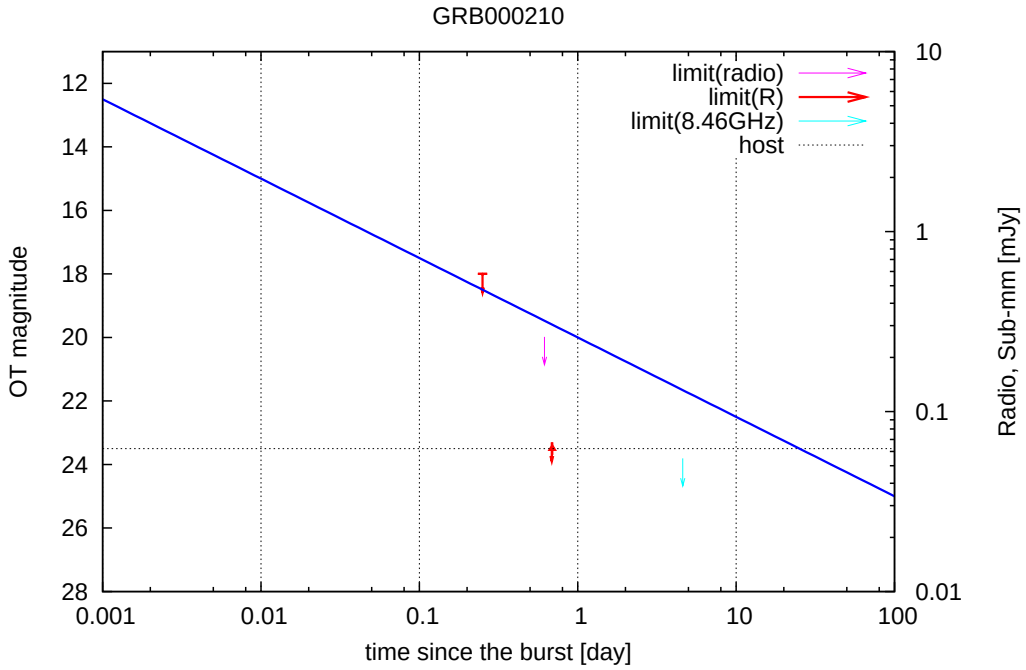

Figure 4.15: Optical afterglow of GRB000210. (upper limit)

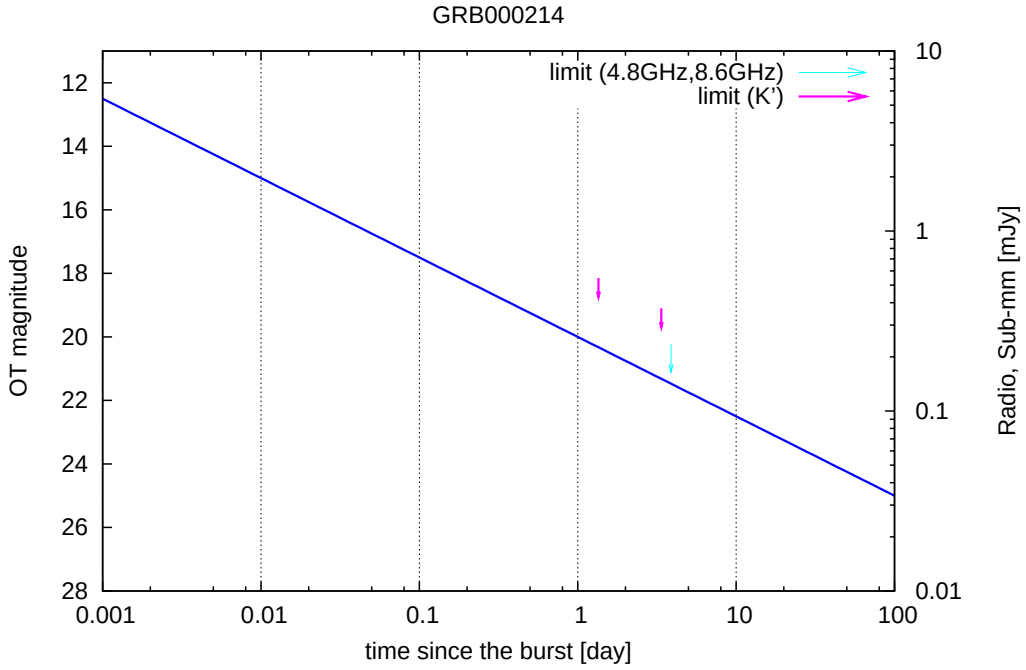

Figure 4.16: Optical afterglow of GRB000214. (upper limit)

GRB010213

The prompt emission of this burst is bright XRF. Optical afterglow for this burst is searched sufficiently. However no detection has reported.

Time interval [day]	Detect/U.L.	α	m_0	$m(t)$	data#
0.3:3	U.L.	—	—	22	1
1:3	U.L.	—	—	22	1
1:10	U.L.	—	—	22	1

Table 4.13: Time resolved magnitude of GRB010213.

GRB010222

The prompt emission of this burst is XRR. The optical afterglow of this GRB is bright. The redshift of the burst is measured to be 1.477.

Time interval [day]	Detect/U.L.	α	m_0	$m(t)$	data#
0.03:0.3	Detect	-0.89 ± 0.19	20.0 ± 0.35	17.7 ± 0.12	1-8
0.03:0.3	Detect	-0.89 ± 0.19	20.0 ± 0.35	18.3 ± 0.03	1-8
0.1:1	Detect	-0.95 ± 0.02	20.1 ± 0.02	18.9 ± 0.02	1-19
0.3:1	Detect	-1.21 ± 0.18	20.1 ± 0.05	19.4 ± 0.07	9-19
0.3:3	Detect	-1.25 ± 0.04	20.1 ± 0.02	20.1 ± 0.02	9-28
1:3	Detect	-1.08 ± 0.17	20.3 ± 0.13	21.0 ± 0.04	20-28
1:10	Detect	-1.25 ± 0.08	20.2 ± 0.07	21.7 ± 0.04	20-32
3:10	Detect	-1.27 ± 0.04	20.2 ± 0.08	22.6 ± 0.01	29-32
3:30	Detect	-1.25 ± 0.02	20.2 ± 0.05	23.4 ± 0.01	29-33
10:30	Detect	—	—	24.5 ± 0.25	33
10:100	Detect	—	—	24.5 ± 0.25	33

Table 4.14: Time resolved magnitude of GRB010222.

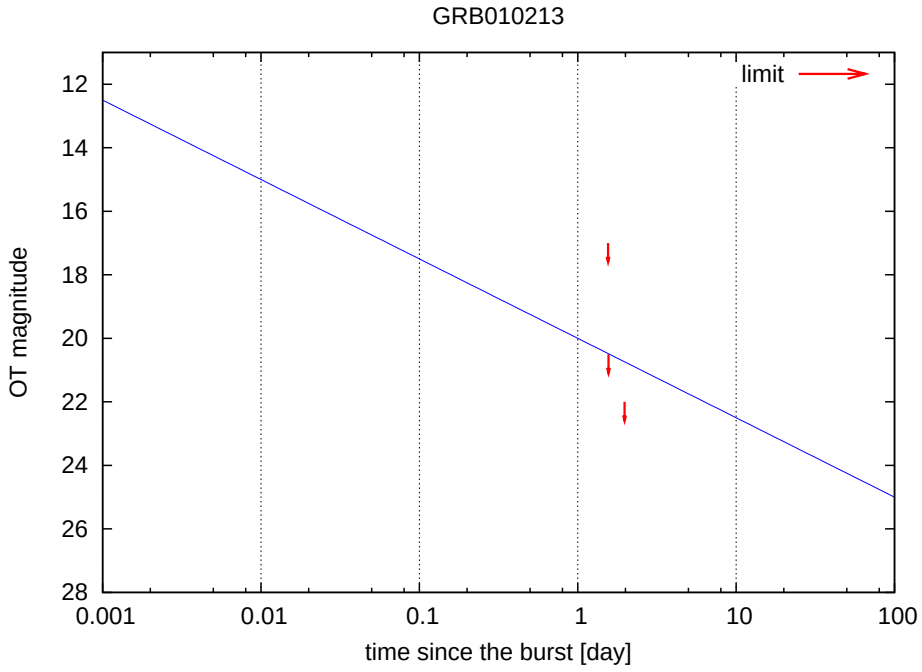

Figure 4.17: Optical afterglow of GRB010213. (upper limit)

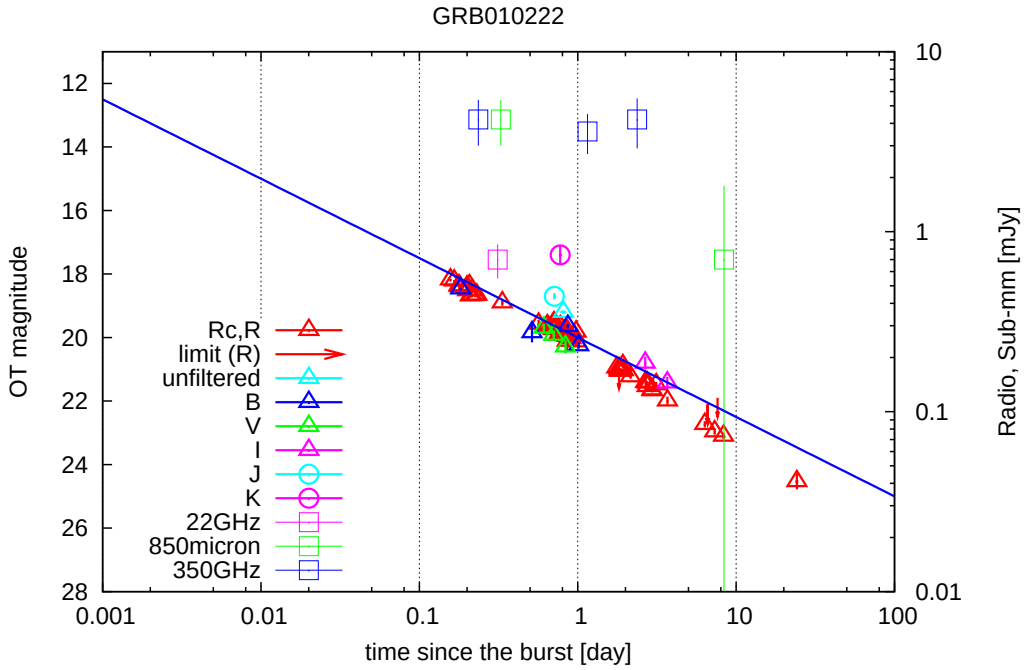

Figure 4.18: Optical afterglow of GRB010222.

GRB010629B

Optical afterglow for this burst is searched sufficiently. However no detection has reported.

Time interval [day]	Detect/U.L.	α	m_0	$m(t)$	data#
0.1:1	U.L.	—	—	20	1
0.3:1	U.L.	—	—	20	1
0.3:3	U.L.	—	—	20	1

Table 4.15: Time resolved magnitude of GRB010629B.

GRB010921

The first event detected by HETE-2 which have observed optical afterglow. The optical afterglow of this GRB is bright.

Time interval [day]	Detect/U.L.	α	m_0	$m(t)$	data#
0.01:0.1	U.L.	—	—	15.3	1
0.03:0.1	U.L.	—	—	15.3	1
0.03:0.3	U.L.	—	—	15.3	1
0.1:1	Detect	-1 (fixed)	19.6 $\pm$ 0.11	18.4 $\pm$ 0.11	2-3
0.3:1	Detect	-1 (fixed)	19.6 $\pm$ 0.11	19.0 $\pm$ 0.11	2-3
0.3:3	Detect	-2.24 $\pm$ 1.32	19.8 $\pm$ 0.13	19.8 $\pm$ 0.13	2-4
1:3	Detect	—	—	19.9 $\pm$ 0.2	4
1:10	Detect	—	—	19.9 $\pm$ 0.2	4

Table 4.16: Time resolved magnitude of GRB010921.

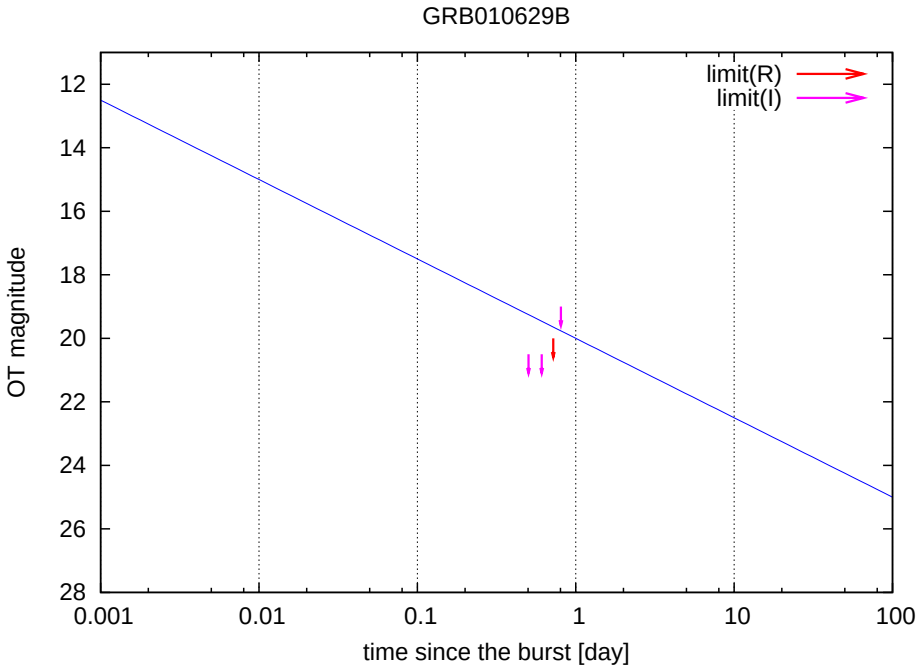

Figure 4.19: Optical afterglow of GRB010629B. (upper limit)

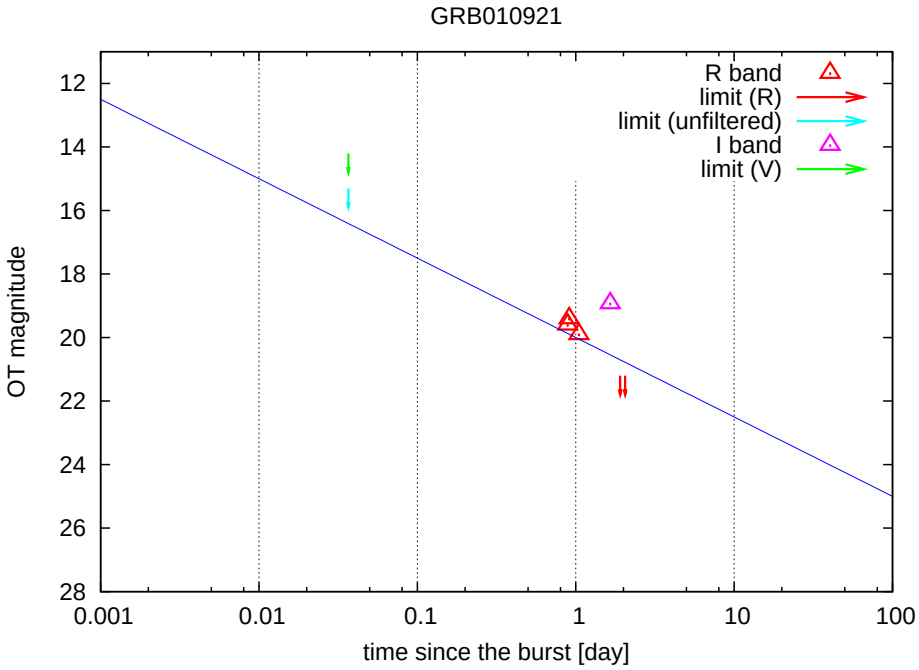

Figure 4.20: Optical afterglow of GRB010921.

GRB011019

Optical afterglow for this burst is searched sufficiently. However no detection has reported.

Time interval [day]	Detect/U.L.	α	m_0	$m(t)$	data#
0.1:1	U.L.	—	—	19	1
0.3:1	U.L.	—	—	19	1
0.3:3	U.L.	—	—	25	2
1:3	U.L.	—	—	25	2
1:10	U.L.	—	—	25	2

Table 4.17: Time resolved magnitude of GRB011019.

GRB011030

Optical afterglow for this burst is searched sufficiently. However no detection has reported. The redshift of the burst is between 0.6 and 3 (Fruchter et al., 2002; Bloom et al., 2003a).

Time interval [day]	Detect/U.L.	α	m_0	$m(t)$	data#
0.03:0.3	U.L.	—	—	21	1
0.1:0.3	U.L.	—	—	21	1
0.1:1	U.L.	—	—	21	1
0.3:3	U.L.	—	—	23.6	2
1:3	U.L.	—	—	23.6	2
1:10	U.L.	—	—	23.6	2
3:10	U.L.	—	—	23.3	3
3:30	U.L.	—	—	23.3	3

Table 4.18: Time resolved magnitude of GRB011030.

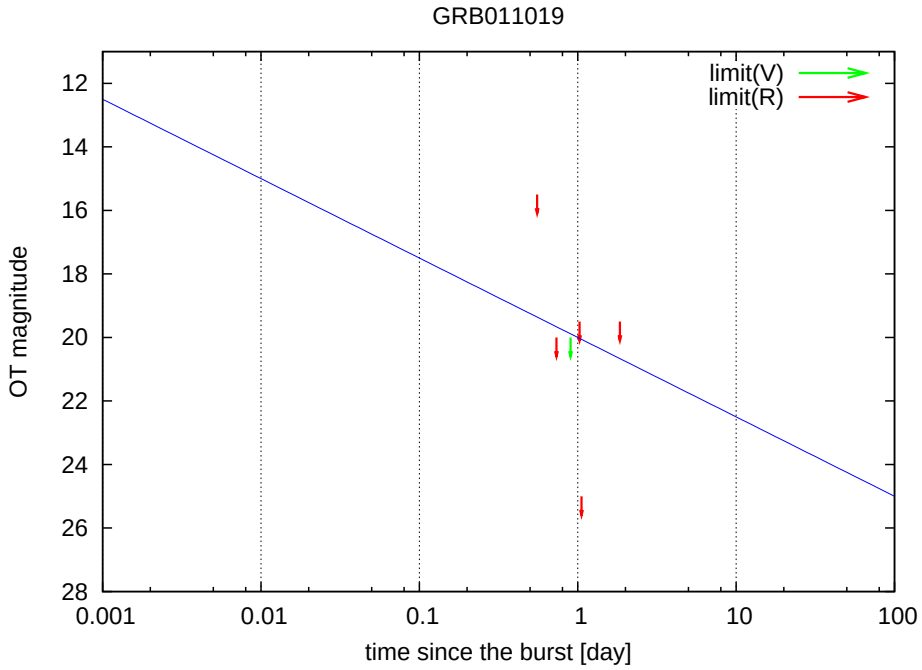

Figure 4.21: Optical afterglow of GRB011019. (upper limit)

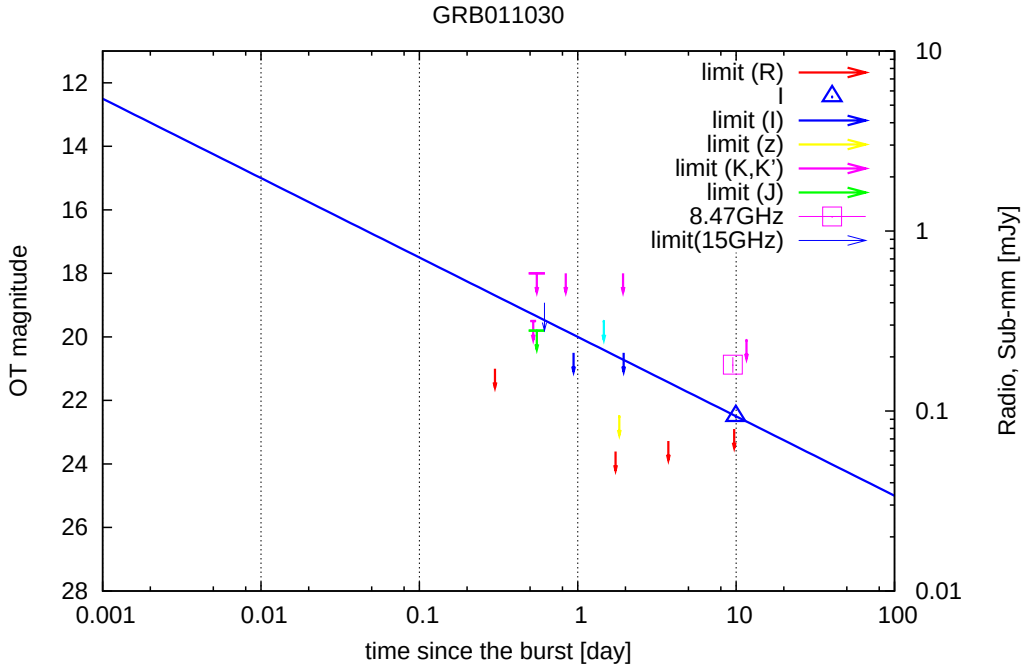

Figure 4.22: Optical afterglow of GRB011030. (upper limit)

GRB011121

The optical afterglow of this GRB is bright. The redshift of the burst is measured to be 0.36.

Time interval [day]	Detect/U.L.	α	m_0	$m(t)$	data#
0.1:1	Detect	-1.73 ± 0.14	20.6 ± 0.10	18.5 ± 0.07	1-4
0.3:1	Detect	-1.73 ± 0.14	20.6 ± 0.10	19.6 ± 0.02	1-4
0.3:3	Detect	-1.51 ± 0.04	20.5 ± 0.03	20.5 ± 0.03	1-7
1:3	Detect	-1.38 ± 0.19	20.6 ± 0.14	21.4 ± 0.06	5-7
1:10	Detect	-1.38 ± 0.19	20.6 ± 0.14	22.3 ± 0.13	5-7

Table 4.19: Time resolved magnitude of GRB011121.

GRB011130

Optical afterglow for this burst is not searched sufficiently.

Time interval [day]	Detect/U.L.	α	m_0	$m(t)$	data#
0.1:1	U.L.	—	—	18.5	1
0.3:1	U.L.	—	—	18.5	1
0.3:3	U.L.	—	—	18.5	1

Table 4.20: Time resolved magnitude of GRB011130.

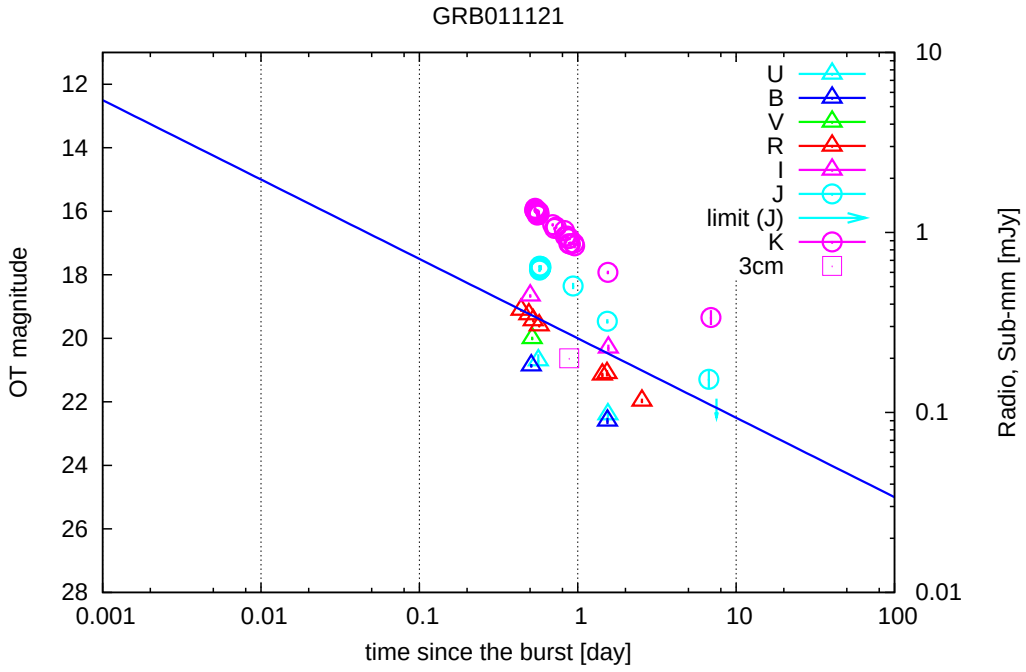

Figure 4.23: Optical afterglow of GRB011121.

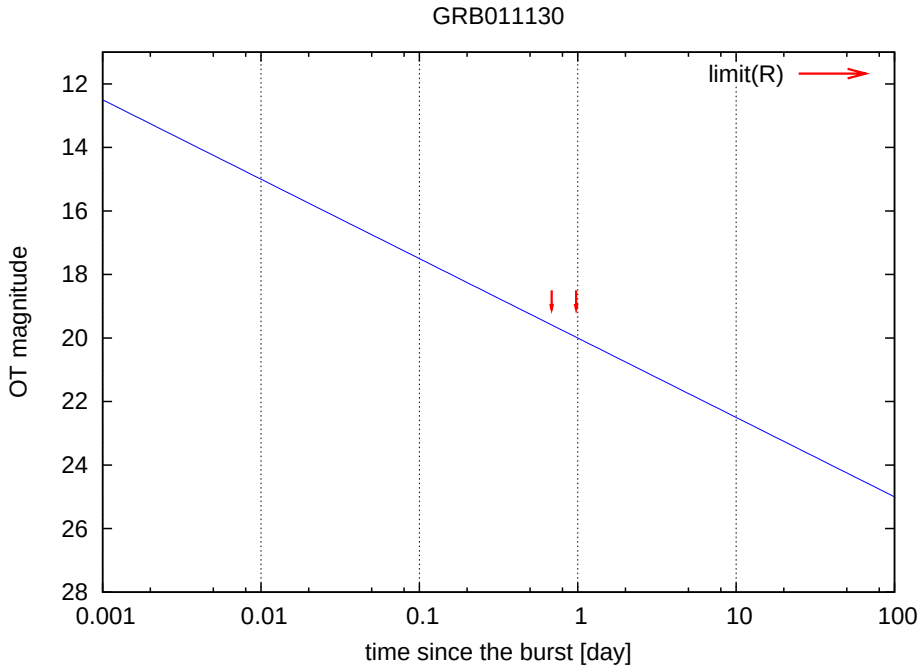

Figure 4.24: Optical afterglow of GRB011130. (upper limit)

GRB011211

The optical afterglow of this GRB is bright. The redshift of the burst is measured to be 2.14.

Time interval [day]	Detect/U.L.	α	m_0	$m(t)$	data#
0.1:1	Detect	-1.38 ± 0.27	21.5 ± 0.21	19.7 ± 0.13	1-9
0.3:1	Detect	-1.38 ± 0.27	21.5 ± 0.21	20.6 ± 0.05	1-9
0.3:3	Detect	-0.81 ± 0.06	21.0 ± 0.05	21.0 ± 0.05	1-16
1:3	Detect	-1.77 ± 0.17	20.7 ± 0.06	21.8 ± 0.06	10-16
1:10	Detect	-1.77 ± 0.06	20.7 ± 0.03	22.9 ± 0.06	10-21
3:10	Detect	-2.28 ± 0.31	19.6 ± 0.70	23.8 ± 0.14	17-21
3:30	Detect	-2.36 ± 0.25	19.5 ± 0.66	25.4 ± 0.15	17-23
10:30	Detect	-1.11 ± 0.39	23.5 ± 1.23	27.0 ± 0.13	22-23
10:100	Detect	-1.33 ± 0.44	22.9 ± 1.40	27.9 ± 0.30	22-24
30:100	Detect	—	—	28.4 ± 0.48	24

Table 4.21: Time resolved magnitude of GRB011211.

GRB011212

The prompt emission of this burst is XRF. Optical afterglow for this burst is searched sufficiently. However no detection has reported.

Time interval [day]	Detect/U.L.	α	m_0	$m(t)$	data#
0.1:1	U.L.	—	—	22.7	1
0.3:1	U.L.	—	—	22.7	1
0.3:3	U.L.	—	—	22.7	1
1:3	U.L.	—	—	20.5	2
1:10	U.L.	—	—	20.5	2

Table 4.22: Time resolved magnitude of GRB011212.

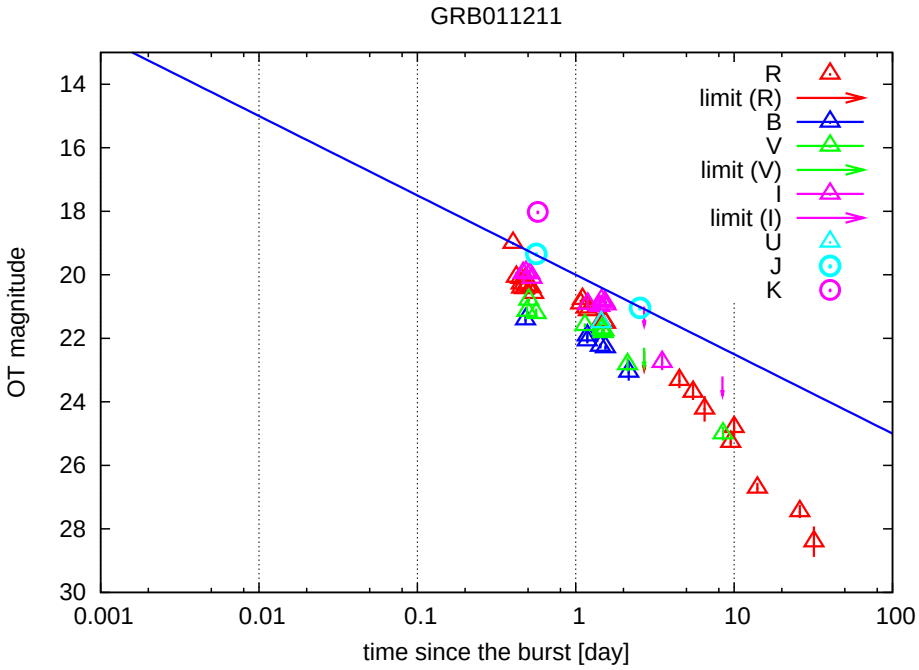

Figure 4.25: Optical afterglow of GRB011211.

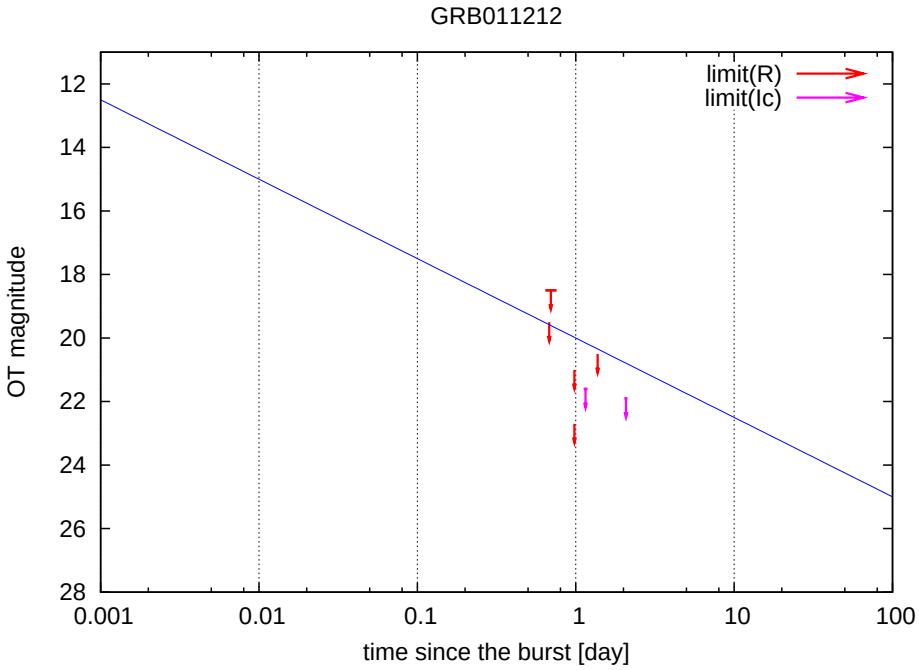

Figure 4.26: Optical afterglow of GRB011212. (upper limit)

GRB020124

The prompt emission of this burst is XRR. Optical afterglow of this event is dim. Measured redshift of the burst is 3.2.

Time interval [day]	Detect/U.L.	α	m_0	$m(t)$	data#
0.01:0.1	Detect	-1.76 ± 1.08	23.1 ± 3.09	16.5 ± 0.96	1-6
0.03:0.1	Detect	-1.76 ± 1.08	23.1 ± 3.09	17.6 ± 0.29	1-6
0.03:0.3	Detect	-1.36 ± 0.12	22.0 ± 0.33	18.6 ± 0.04	1-10
0.1:0.3	Detect	-1.66 ± 1.20	22.7 ± 2.79	19.6 ± 0.54	7-10
0.1:1	Detect	-1.66 ± 1.20	22.7 ± 2.79	20.6 ± 1.29	7-10
0.3:1	U.L.	—	—	19.1	16
0.3:3	Detect	-3.14 ± 1.60	22.2 ± 0.94	22.2 ± 0.94	11-12
1:3	Detect	-3.14 ± 1.60	22.2 ± 0.94	24.2 ± 0.15	11-12
1:10	Detect	-3.14 ± 1.60	22.2 ± 0.94	26.1 ± 1.08	11-12
3:30	Detect	-1.80 ± 1.50	23.1 ± 4.80	27.6 ± 1.06	13-14
10:30	Detect	-1.80 ± 1.50	23.1 ± 4.80	28.7 ± 0.24	13-14
10:100	Detect	-1.47 ± 0.24	24.1 ± 0.81	29.6 ± 0.13	13-15
30:100	Detect	—	—	29.6 ± 0.6	15
30:300	Detect	—	—	29.6 ± 0.6	15

Table 4.23: Time resolved magnitude of GRB020124.

GRB020127

The prompt emission of this burst is XRR. Optical afterglow for this burst is searched sufficiently. However no detection has reported.

Time interval [day]	Detect/U.L.	α	m_0	$m(t)$	data#
0.03:0.3	U.L.	—	—	21.5	1
0.1:0.3	U.L.	—	—	21.5	1
0.1:1	U.L.	—	—	21.5	1

Table 4.24: Time resolved magnitude of GRB020127.

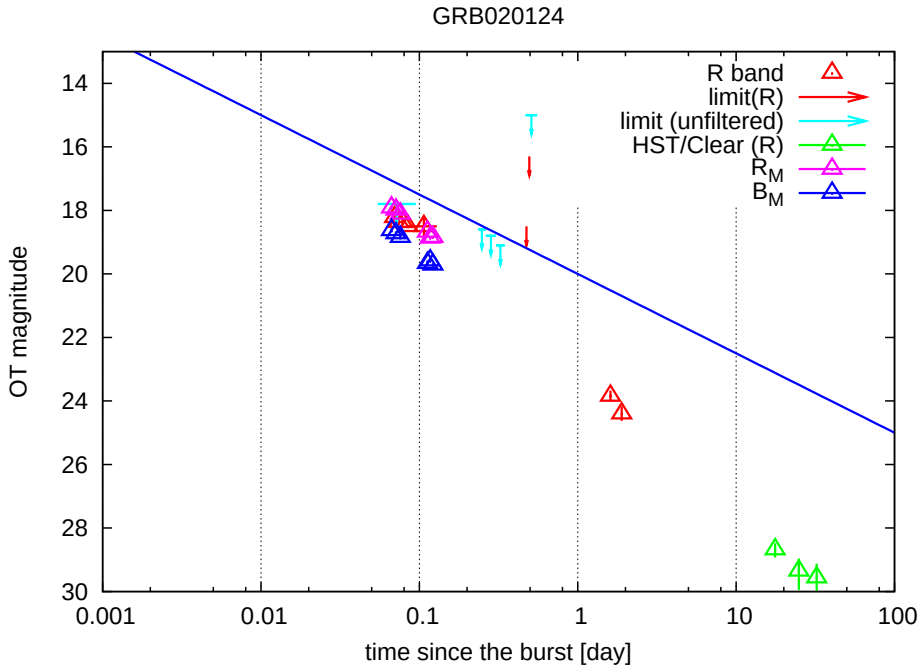

Figure 4.27: Optical afterglow of GRB020124. (detection)

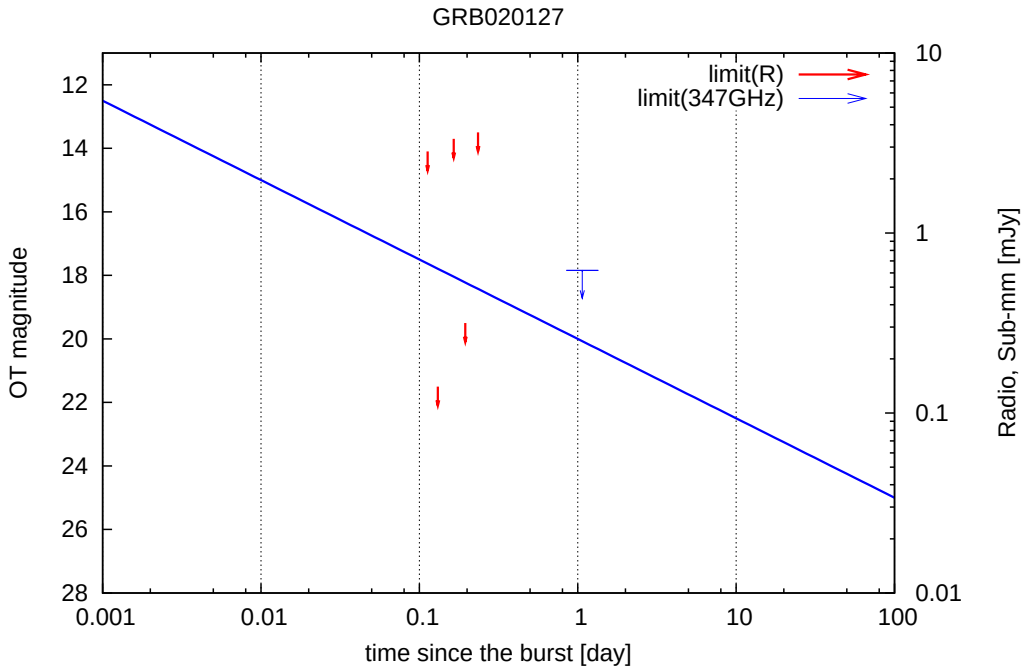

Figure 4.28: Optical afterglow of GRB020127. (upper limit)

GRB020305

The prompt emission of this event is detected just before the scheduled shutdown of the science instruments. Thus little information of prompt emission can be obtained. Optical afterglow of this event is bright.

Time interval [day]	Detect/U.L.	α	m_0	$m(t)$	data#
0.1:1	Detect	—	—	20.1 ± 0.5	1
0.3:1	Detect	—	—	20.1 ± 0.5	1
0.3:3	Detect	—	—	20.1 ± 0.5	1
1:3	Detect	—	—	22.6	2
1:10	Detect	—	—	22.6	2
3:30	Detect	—	—	22.6	2
10:100	Detect	—	—	24.7 ± 0.01	3
30:100	Detect	—	—	24.7 ± 0.01	3
30:300	Detect	-1.40 ± 0.03	19.1 ± 0.11	26.2 ± 0.03	3-4
100:300	Detect	—	—	26.2 ± 0.03	4
100:1000	Detect	—	—	26.2 ± 0.03	4

Table 4.25: Time resolved magnitude of GRB020305.

GRB020331

The prompt emission of this burst is GRB. Optical afterglow of this event is dim.

Time interval [day]	Detect/U.L.	α	m_0	$m(t)$	data#
0.01:0.1	Detect	—	—	17.9 ± 0.6	1
0.03:0.1	Detect	—	—	17.9 ± 0.6	1
0.03:0.3	Detect	—	—	17.9 ± 0.6	1
0.1:0.3	U.L.	—	—	19.3	9
0.1:1	Detect	-1 (fixed)	21.6 ± 0.18	20.3 ± 0.18	2-3
0.3:1	Detect	-1 (fixed)	21.6 ± 0.18	20.9 ± 0.18	2-3
0.3:3	Detect	-1 (fixed)	21.6 ± 0.18	21.6 ± 0.18	2-3
1:10	Detect	—	—	22.9 ± 0.14	4
3:10	Detect	—	—	22.9 ± 0.14	4
3:30	Detect	-1.48 ± 0.14	19.5 ± 0.46	23.2 ± 0.12	4-5
10:30	Detect	—	—	24.5 ± 0.07	5
10:100	Detect	-0.49 ± 0.23	22.9 ± 0.89	24.7 ± 0.08	5-8
30:100	Detect	+0.24 ± 0.78	25.9 ± 3.15	24.8 ± 0.27	6-8
30:300	Detect	+0.24 ± 0.78	25.9 ± 3.15	24.7 ± 0.75	6-8

Table 4.26: Time resolved magnitude of GRB020331.

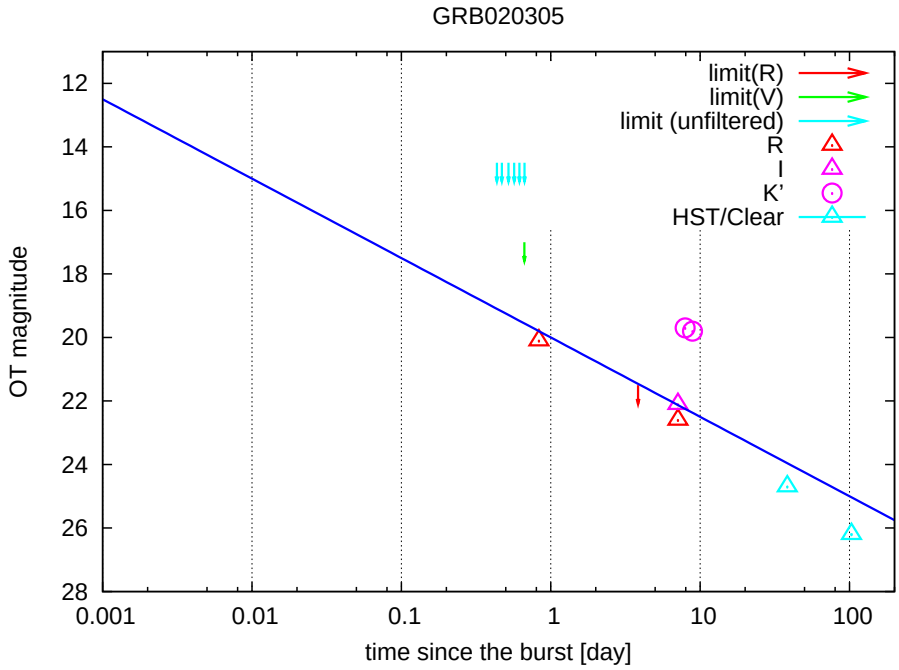

Figure 4.29: Optical afterglow of GRB020305. (detection)

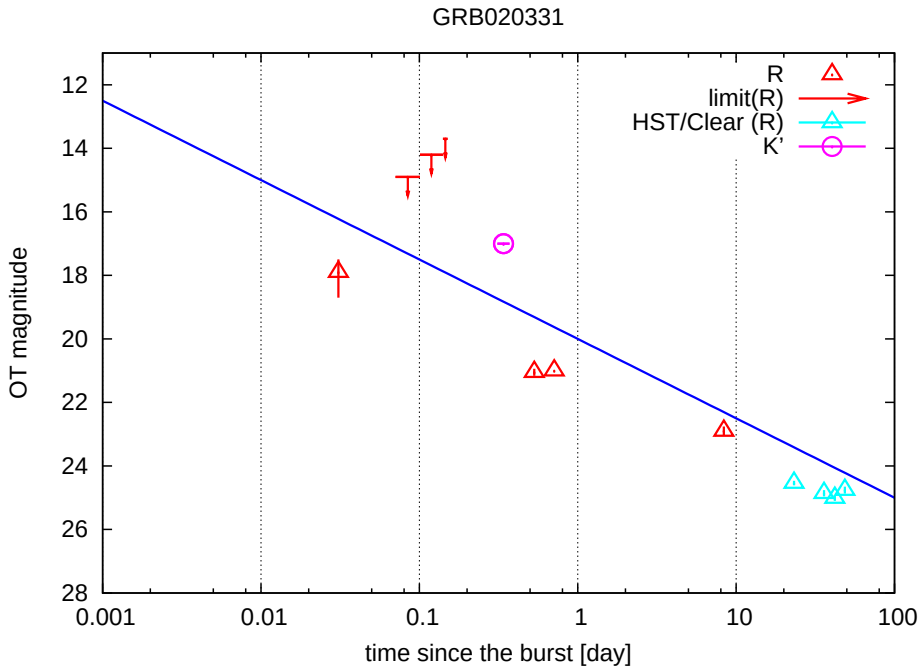

Figure 4.30: Optical afterglow of GRB020331. (detection)

GRB020405

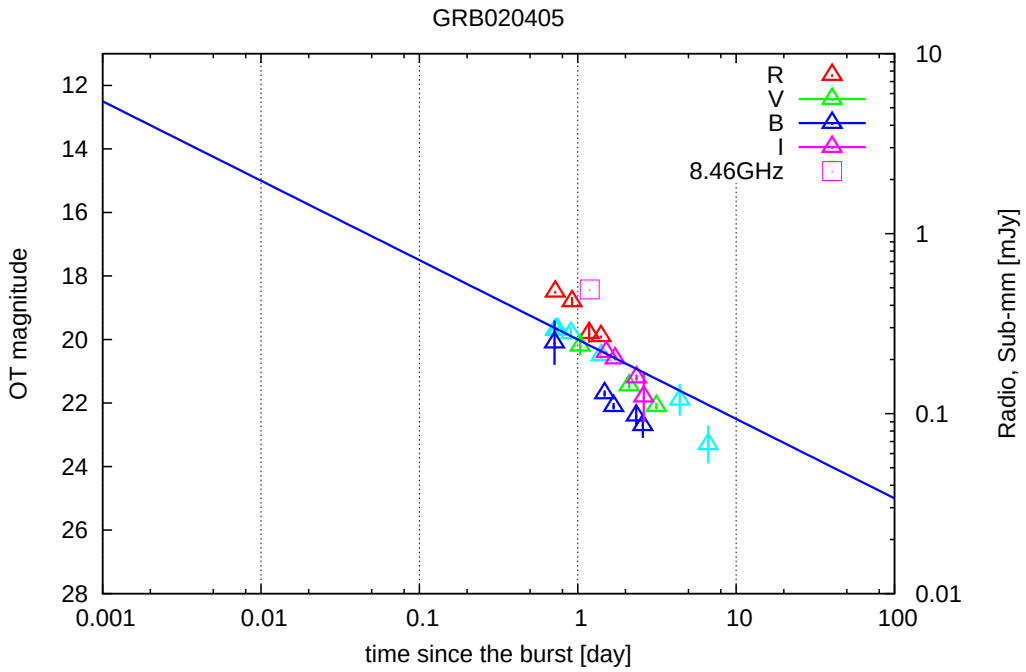

Figure 4.31: Optical afterglow of GRB020405.

The optical afterglow of this GRB is bright. The redshift of the burst is measured to be 0.69.

Time interval [day]	Detect/U.L.	α	m_0	$m(t)$	data#
0.1:1	Detect	-0.84 $\pm$ 0.13	19.9 $\pm$ 0.04	18.8 $\pm$ 0.04	1-4
0.3:1	Detect	-0.84 $\pm$ 0.13	19.9 $\pm$ 0.04	19.4 $\pm$ 0.04	1-4
0.3:3	Detect	-1.28 $\pm$ 0.05	20.0 $\pm$ 0.01	20.0 $\pm$ 0.01	1-5
1:3	Detect	—	—	20.5 $\pm$ 0.08	5
1:10	Detect	-1.37 $\pm$ 0.23	20.0 $\pm$ 0.13	21.7 $\pm$ 0.21	5-7
3:10	Detect	-2.89 $\pm$ 1.68	17.2 $\pm$ 3.01	22.7 $\pm$ 0.40	6-7
3:30	Detect	-2.89 $\pm$ 1.68	17.2 $\pm$ 3.01	24.5 $\pm$ 1.27	6-7

Table 4.27: Time resolved magnitude of GRB020405.

GRB020531

This event is the first short/hard burst that is localized. Despite the extended search of optical and X-ray afterglow, the source is not identified. There are two candidate of the afterglows.

GRB020625

The prompt emission of this burst is XRF. Optical afterglow for this burst is searched sufficiently. However no detection has reported.

Time interval [day]	Detect/U.L.	α	m_0	$m(t)$	data#
0.03:0.3	U.L.	—	—	19.5	1
0.1:0.3	U.L.	—	—	19.5	1
0.1:1	U.L.	—	—	19.5	1
0.3:1	U.L.	—	—	18.2	2
0.3:3	U.L.	—	—	18.2	2

Table 4.28: Time resolved magnitude of GRB020625.

GRB020801

The prompt emission of this burst is GRB. Optical afterglow for this burst is searched sufficiently. However no detection has reported.

Time interval [day]	Detect/U.L.	α	m_0	$m(t)$	data#
0.1:1	U.L.	—	—	20	1
0.3:1	U.L.	—	—	20	1
0.3:3	U.L.	—	—	20	1

Table 4.29: Time resolved magnitude of GRB020801.

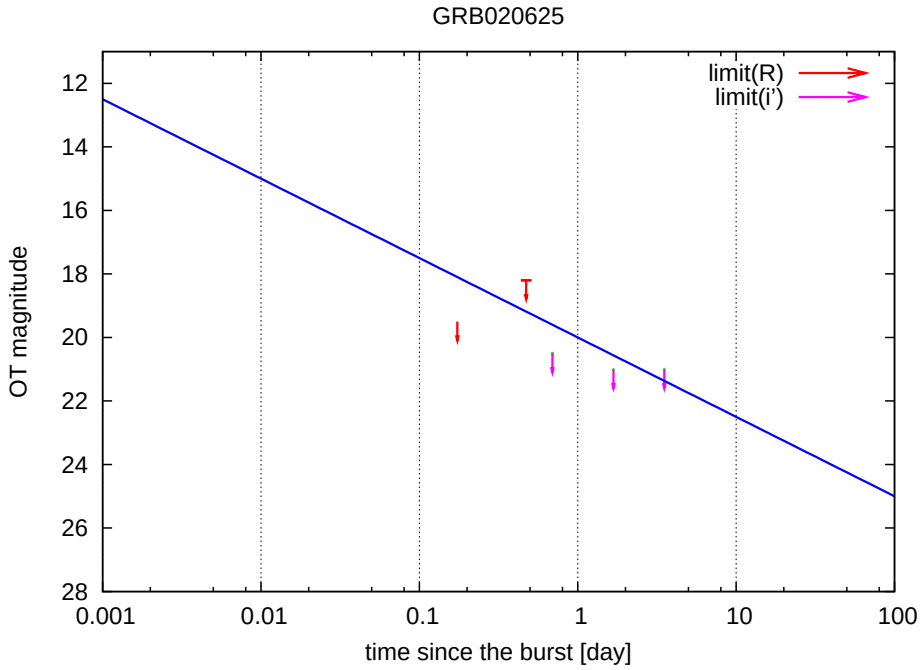

Figure 4.32: Optical afterglow of GRB020625. (upper limit)

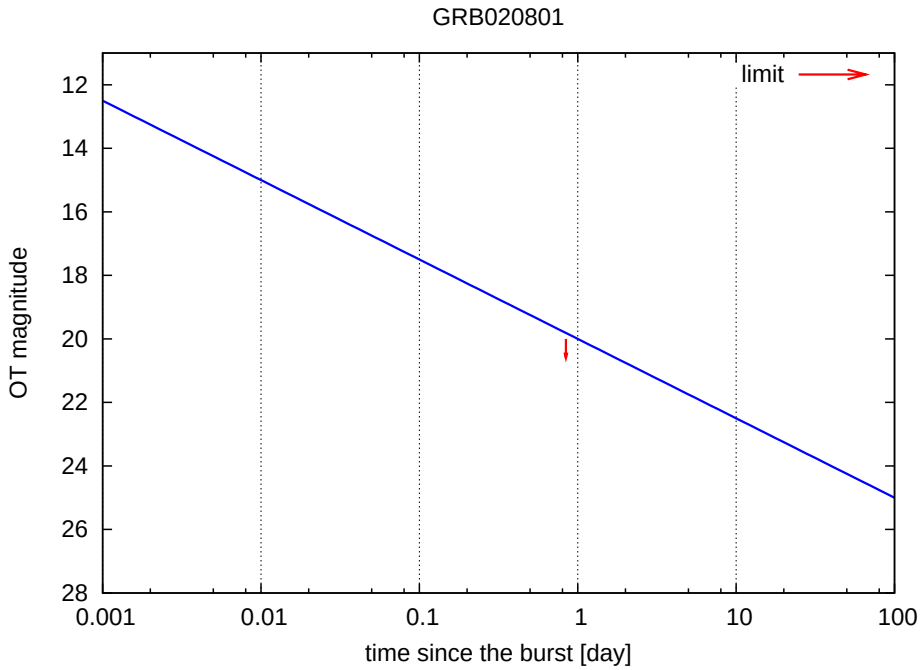

Figure 4.33: Optical afterglow of GRB020801. (upper limit)

GRB020812

The prompt emission of this burst is XRR. Optical afterglow for this burst is searched sufficiently. However no detection has reported.

Time interval [day]	Detect/U.L.	α	m_0	$m(t)$	data#
0.03:0.3	U.L.	—	—	19.1	2
0.1:0.3	U.L.	—	—	19.1	2
0.1:1	U.L.	—	—	20	1
0.3:1	U.L.	—	—	20	1
0.3:3	U.L.	—	—	20	1
1:3	U.L.	—	—	19.1	3
1:10	U.L.	—	—	19.1	3

Table 4.30: Time resolved magnitude of GRB020812.

GRB020813

The prompt emission of this burst is GRB. Optical afterglow of this event is bright. Measured redshift of the burst is 1.25.

Time interval [day]	Detect/U.L.	α	m_0	$m(t)$	data#
0.003:0.03	U.L.	—	—	16.0	10
0.01:0.03	U.L.	—	—	16.0	10
0.01:0.1	Detect	—	—	18.4 ± 0.38	1
0.03:0.1	Detect	—	—	18.4 ± 0.38	1
0.03:0.3	Detect	-0.53 ± 0.22	19.6 ± 0.40	18.2 ± 0.14	1-4
0.1:0.3	Detect	-0.81 ± 0.06	20.1 ± 0.11	18.6 ± 0.01	2-4
0.1:1	Detect	-1.03 ± 0.04	20.5 ± 0.06	19.2 ± 0.03	2-7
0.3:1	Detect	-1.37 ± 0.06	20.5 ± 0.02	19.7 ± 0.03	5-7
0.3:3	Detect	-1.39 ± 0.10	20.5 ± 0.03	20.5 ± 0.04	5-9
1:3	Detect	-1 (fixed)	20.6 ± 0.21	21.3 ± 0.21	8-9
1:10	Detect	-1 (fixed)	20.6 ± 0.21	21.9 ± 0.21	8-9

Table 4.31: Time resolved magnitude of GRB020813.

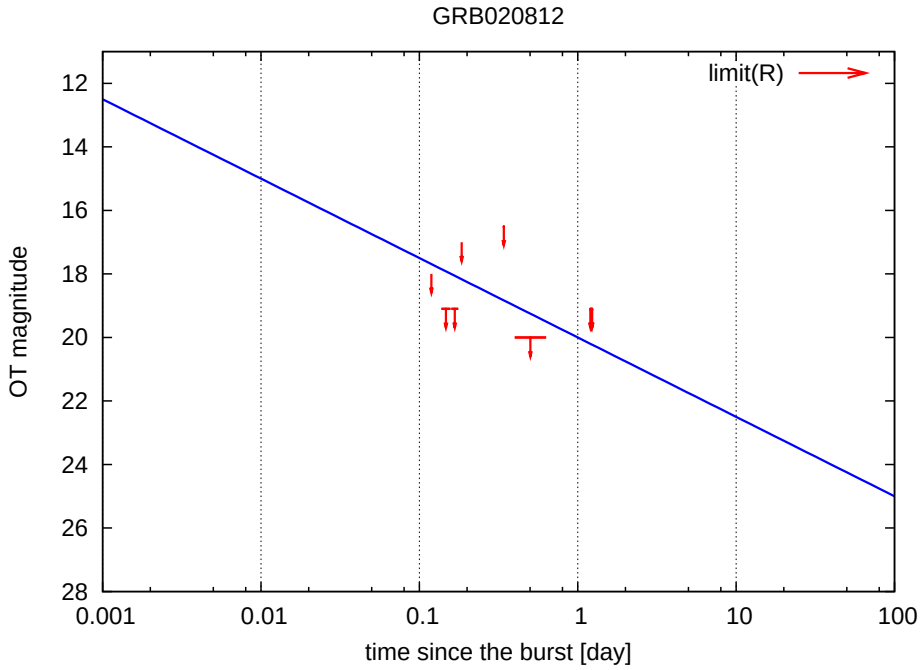

Figure 4.34: Optical afterglow of GRB020812. (upper limit)

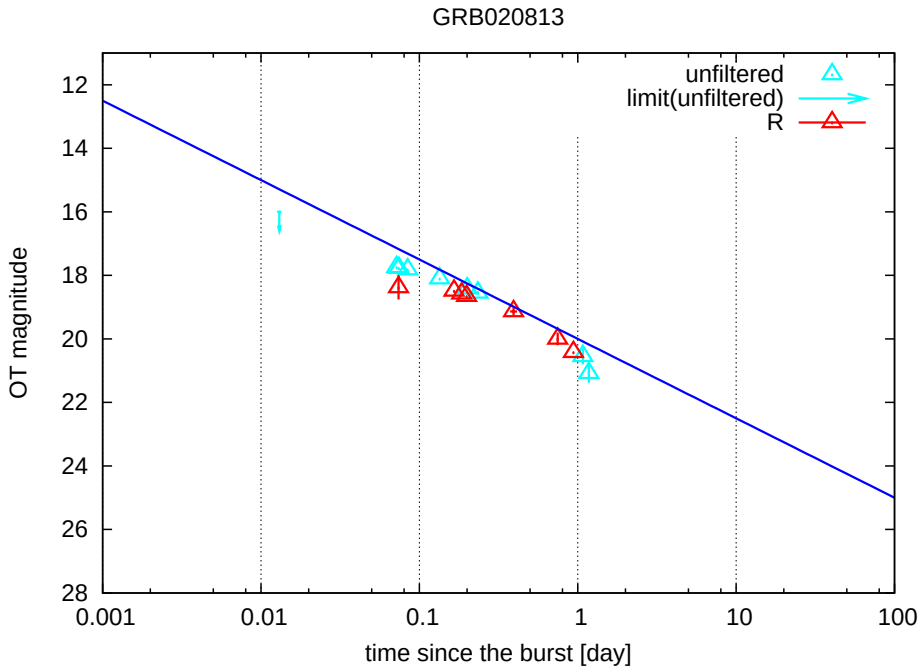

Figure 4.35: Optical afterglow of GRB020813. (detection)

GRB020819

The prompt emission of this burst is XRR. Optical afterglow for this burst is searched sufficiently. However no detection has reported. Radio afterglow was detected. The host galaxy of the burst is bright.

Time interval [day]	Detect/U.L.	α	m_0	$m(t)$	data#
0.03:0.3	U.L.	—	—	20.6	1
0.1:0.3	U.L.	—	—	20.6	1
0.1:1	U.L.	—	—	22.3	2
0.3:1	U.L.	—	—	22.3	2
0.3:3	U.L.	—	—	22.3	2

Table 4.32: Time resolved magnitude of GRB020819.

GRB020903

The prompt emission of this burst is XRF. Optical afterglow of this event is bright. This is the first detection of the afterglow of XRF. Measured redshift of the burst is 0.25.

Time interval [day]	Detect/U.L.	α	m_0	$m(t)$	data#
0.03:0.3	U.L.	—	—	17.5	3
0.1:0.3	U.L.	—	—	17.5	3
0.1:1	Detect	—	—	19.5	1
0.3:1	Detect	—	—	19.5	1
0.3:3	Detect	—	—	19.5	1
1:10	Detect	—	—	22.5	2
3:10	Detect	—	—	22.5	2
3:30	Detect	—	—	22.5	2

Table 4.33: Time resolved magnitude of GRB020903.

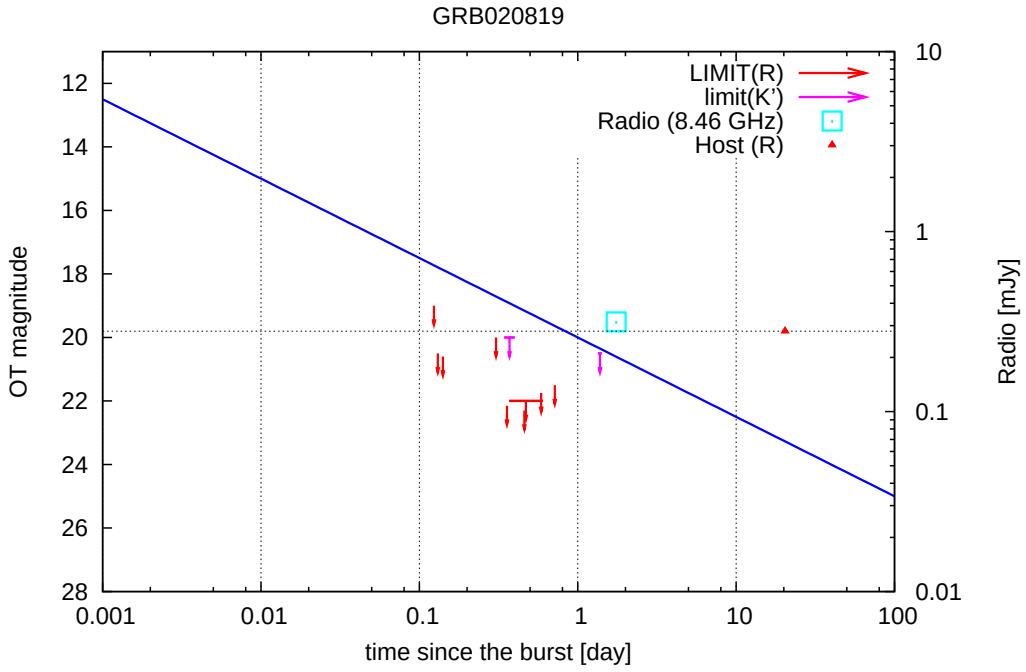

Figure 4.36: Optical and radio afterglow of GRB020819. (upper limit)

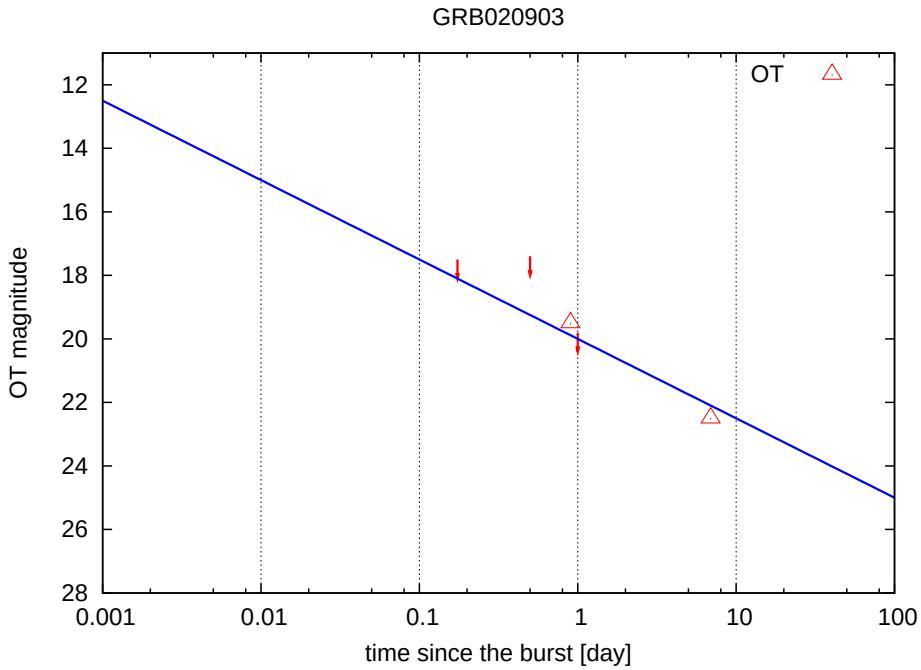

Figure 4.37: Optical afterglow of GRB020903. (detection)

GRB021004

The prompt emission of this burst is XRR. Optical afterglow of this event is bright. Measured redshift of the burst is 2.328.

Time interval [day]	Detect/U.L.	α	m_0	$m(t)$	data#
0.001:0.01	Detect	-0.57	18.5	14.9	1-2
0.003:0.01	Detect	-0.57	18.5	15.2	1-2
0.003:0.03	Detect	-0.89 ± 0.15	20.1 ± 0.70	15.7 ± 0.10	1-5
0.01:0.03	Detect	-1.03 ± 0.48	20.7 ± 2.06	16.2 ± 0.19	3-5
0.01:0.1	Detect	-0.29 ± 0.10	17.4 ± 0.37	16.3 ± 0.07	3-10
0.03:0.1	Detect	-0.01 ± 0.12	16.5 ± 0.40	16.5 ± 0.05	6-10
0.03:0.3	Detect	-0.34 ± 0.08	17.6 ± 0.20	16.7 ± 0.05	6-16
0.1:0.3	Detect	-0.76 ± 0.14	18.4 ± 0.29	17.0 ± 0.05	11-16
0.1:1	Detect	-1.31 ± 0.05	19.6 ± 0.06	17.9 ± 0.04	11-31
0.3:1	Detect	-1.40 ± 0.09	19.6 ± 0.07	18.7 ± 0.04	17-31
0.3:3	Detect	-0.96 ± 0.06	19.3 ± 0.04	19.3 ± 0.04	17-41
1:3	Detect	-0.83 ± 0.07	19.3 ± 0.07	19.8 ± 0.02	32-41
1:10	Detect	-1.03 ± 0.04	19.1 ± 0.05	20.4 ± 0.02	32-49
3:10	Detect	-1.41 ± 0.06	18.4 ± 0.12	21.1 ± 0.02	42-49
3:30	Detect	-1.44 ± 0.04	18.4 ± 0.08	22.0 ± 0.03	42-55
10:30	Detect	-1.42 ± 0.15	18.5 ± 0.45	22.9 ± 0.06	50-55
10:100	Detect	-1.34 ± 0.12	18.7 ± 0.37	23.7 ± 0.10	50-56

Table 4.34: Time resolved magnitude of GRB021004.

GRB021104

The prompt emission of this burst is XRF. Optical afterglow for this burst is searched sufficiently. However no detection has reported.

Time interval [day]	Detect/U.L.	α	m_0	$m(t)$	data#
0.03:0.3	U.L.	—	—	21	1
0.1:0.3	U.L.	—	—	21	1
0.1 1	U.L.	—	—	21	1

Table 4.35: Time resolved magnitude of GRB021104.

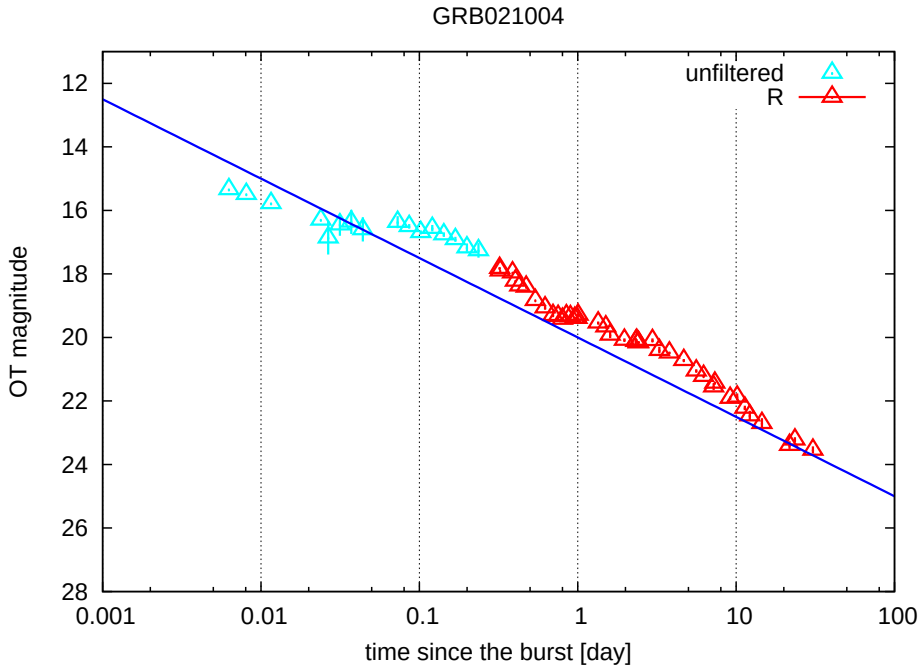

Figure 4.38: Optical afterglow of GRB021004. (detection)

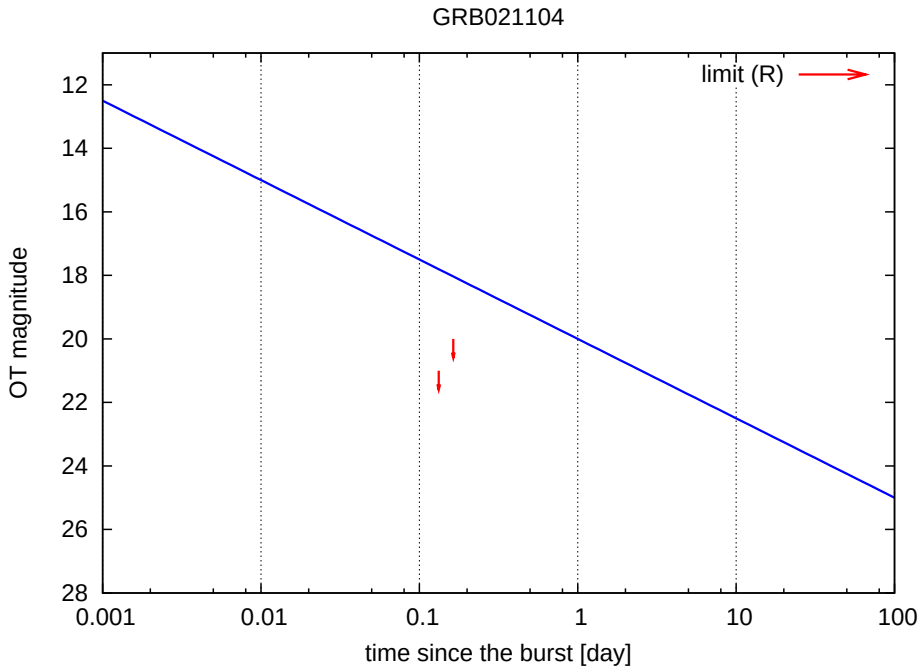

Figure 4.39: Optical afterglow of GRB021104. (upper limit)

GRB021112

The prompt emission of this burst is XRR. Optical afterglow for this burst is searched sufficiently. However no detection has reported.

Time interval [day]	Detect/U.L.	α	m_0	$m(t)$	data#
0.0003:0.003	U.L.	—	—	11.4	1
0.001:0.003	U.L.	—	—	11.4	1
0.001:0.01	U.L.	—	—	11.7	2
0.003:0.01	U.L.	—	—	11.7	2
0.003:0.03	U.L.	—	—	11.7	2
0.01:0.1	U.L.	—	—	21.8	3
0.03:0.1	U.L.	—	—	21.8	3
0.03:0.3	U.L.	—	—	21.8	3
0.1:0.3	U.L.	—	—	20	4
0.1:1	U.L.	—	—	20	4

Table 4.36: Time resolved magnitude of GRB021112.

GRB021113

Little information of prompt emission can be obtained due to incomplete downlink data for this burst. Optical afterglow for this burst is searched sufficiently. However no detection has reported.

Time interval [day]	Detect/U.L.	α	m_0	$m(t)$	data#
0.03:0.3	U.L.	—	—	22.1	1
0.1:0.3	U.L.	—	—	22.1	1
0.1:1	U.L.	—	—	22.1	1
0.3:1	U.L.	—	—	20.3	2
0.3:3	U.L.	—	—	20.3	2

Table 4.37: Time resolved magnitude of GRB021113.

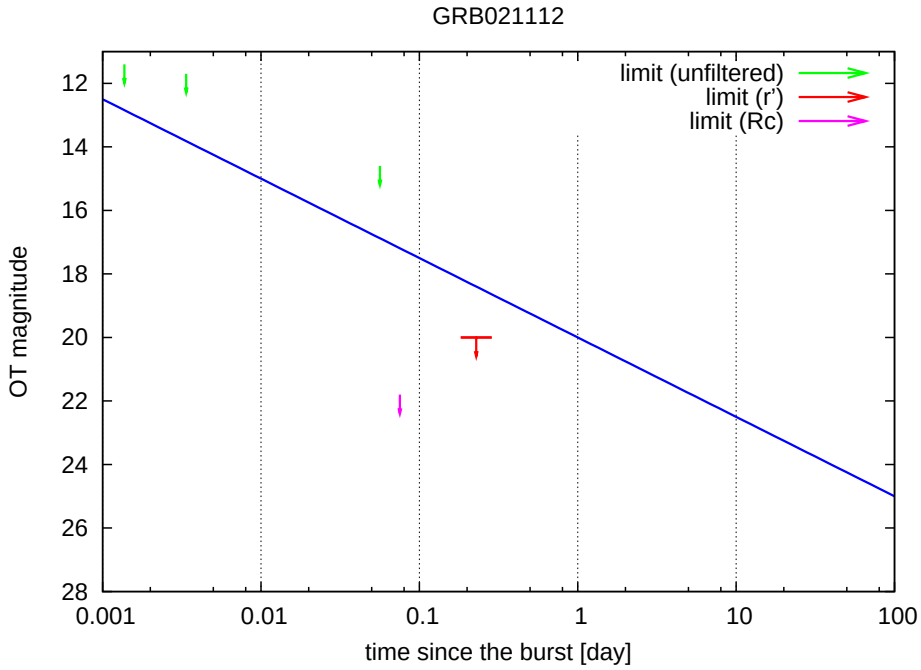

Figure 4.40: Optical afterglow of GRB021112. (upper limit)

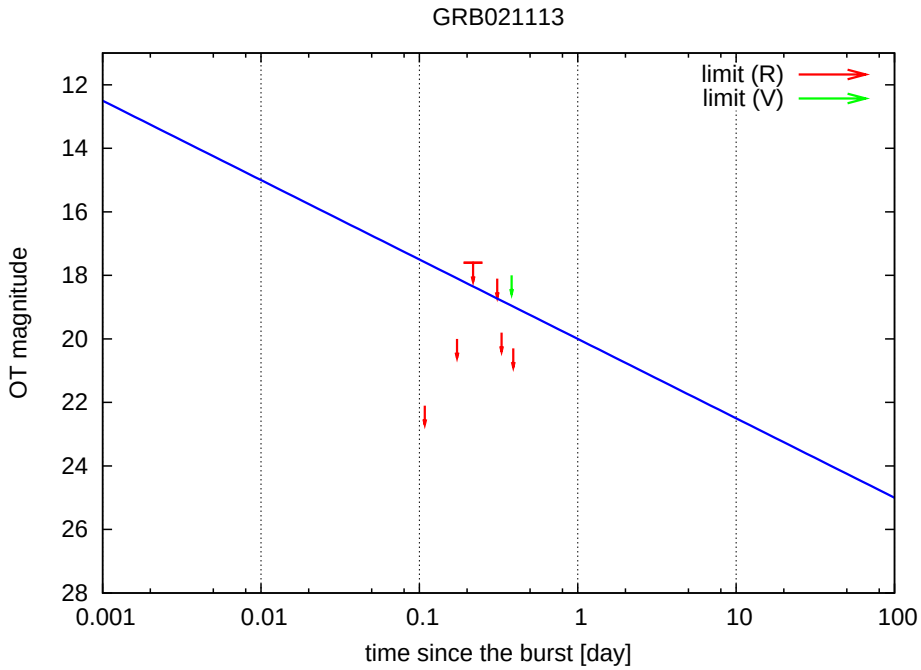

Figure 4.41: Optical afterglow of GRB021113. (upper limit)

GRB021211

The prompt emission of this burst is XRR. Optical afterglow of this event is dim. The light curve before 0.1 day has steep decay index.

Time interval [day]	Detect/U.L.	α	m_0	$m(t)$	data#
0.0003:0.003	Detect	-1.49 ± 0.07	25.2 ± 0.45	14.0 ± 0.05	1-3
0.001:0.003	Detect	-1.49 ± 0.07	25.2 ± 0.45	14.9 ± 0.02	1-3
0.001:0.01	Detect	-1.52 ± 0.02	25.4 ± 0.11	15.9 ± 0.01	1-20
0.003:0.01	Detect	-1.42 ± 0.02	24.8 ± 0.13	16.8 ± 0.01	4-20
0.003:0.03	Detect	-1.33 ± 0.02	24.3 ± 0.10	17.7 ± 0.02	4-27
0.01:0.03	Detect	-1.16 ± 0.10	23.5 ± 0.46	18.4 ± 0.04	21-27
0.01:0.1	Detect	-1.09 ± 0.04	23.2 ± 0.17	19.1 ± 0.03	21-37
0.03:0.1	Detect	-0.94 ± 0.13	22.7 ± 0.44	19.7 ± 0.04	28-37
0.03:0.3	Detect	-0.96 ± 0.07	22.7 ± 0.21	20.3 ± 0.06	28-41
0.1:0.3	Detect	-1.27 ± 0.29	23.3 ± 0.57	20.9 ± 0.14	38-41
0.1:1	Detect	-1.38 ± 0.09	23.5 ± 0.12	21.8 ± 0.05	38-49
0.3:1	Detect	-1.24 ± 0.16	23.4 ± 0.16	22.6 ± 0.07	42-49
0.3:3	Detect	-1.21 ± 0.07	23.4 ± 0.05	23.4 ± 0.05	42-50
1:3	Detect	-1 (fixed)	22.9 ± 0.46	23.5 ± 0.46	50-51
1:10	Detect	-1 (fixed)	22.9 ± 0.46	24.2 ± 0.46	50-51
3:30	Detect	—	—	24.5 ± 0.18	52
10:30	Detect	—	—	24.5 ± 0.18	52
10:100	Detect	-0.42 ± 0.25	23.2 ± 1.09	24.8 ± 0.19	52-55
30:100	Detect	-0.17 ± 0.19	24.4 ± 0.85	25.1 ± 0.08	53-55
30:300	Detect	-0.17 ± 0.19	24.4 ± 0.85	25.2 ± 0.12	53-55

Table 4.38: Time resolved magnitude of GRB021211.

GRB030115

The prompt emission of this burst is XRR. Optical afterglow of this event is dim. Radio and IR afterglow were detected.

Time interval [day]	Detect/U.L.	α	m_0	$m(t)$	data#
0.0003:0.003	U.L.	—	—	10	1
0.001:0.003	U.L.	—	—	10	1
0.001:0.01	U.L.	—	—	10	1
0.01:0.1	U.L.	—	—	20	2
0.03:0.1	U.L.	—	—	20	2
0.03:0.3	U.L.	—	—	20	2
0.1:0.3	U.L.	—	—	20	3
0.1:1	U.L.	—	—	20	3

Table 4.39: Time resolved magnitude of GRB030115.

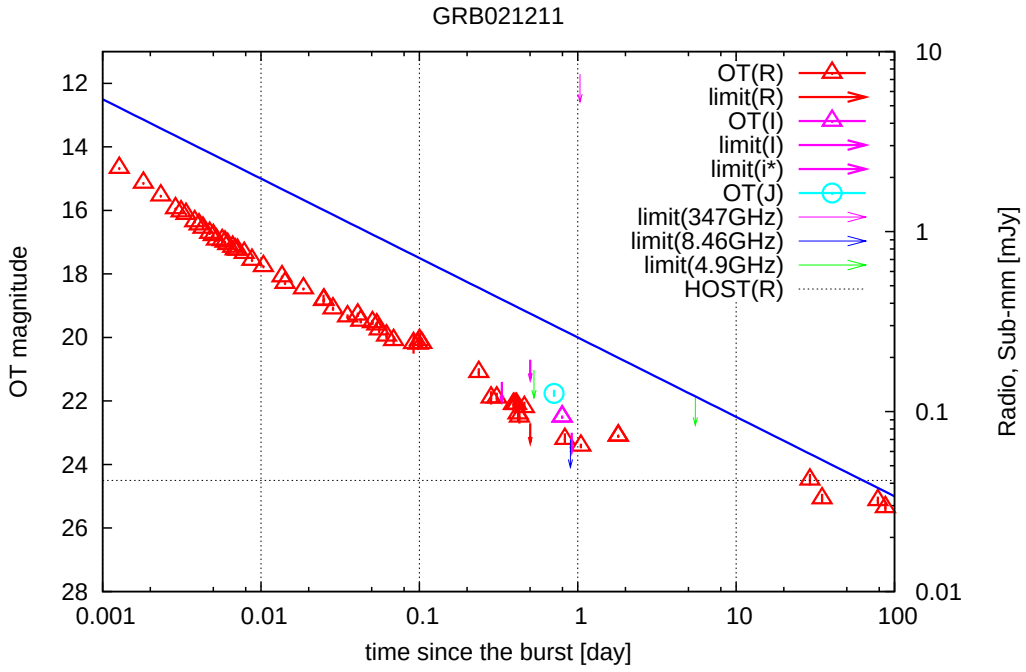

Figure 4.42: Optical afterglow of GRB021211. (detection)

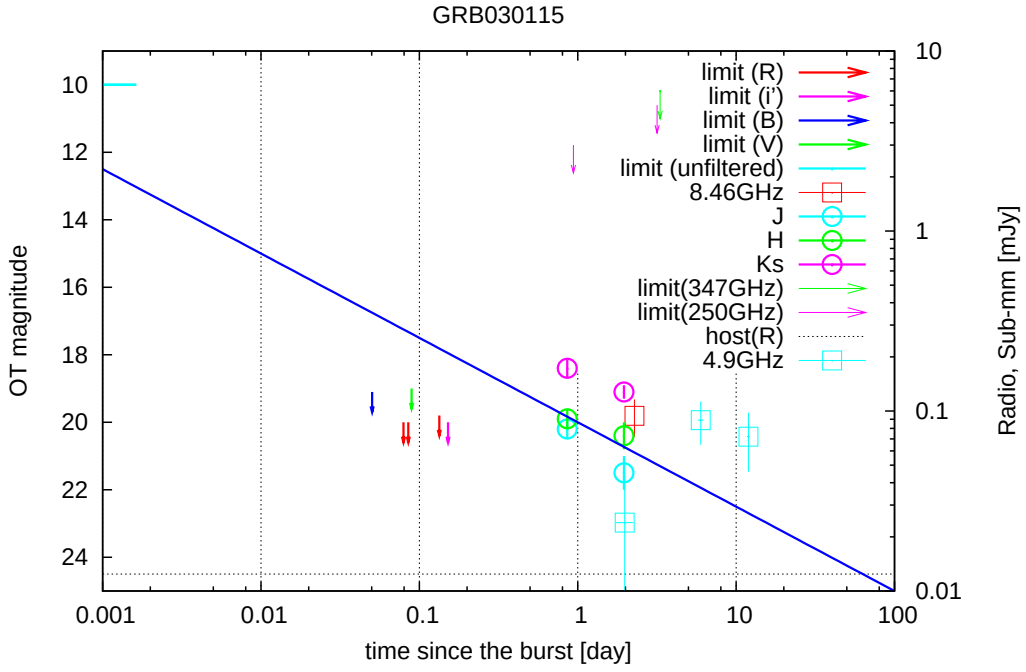

Figure 4.43: Optical, IR and radio afterglow of GRB030115. (detection)

GRB030226

The prompt emission of this burst is GRB. Optical afterglow of this event is bright.

Time interval [day]	Detect/U.L.	α	m_0	$m(t)$	data#
0.0003:0.003	U.L.	—	—	11.5	1
0.001:0.003	U.L.	—	—	11.5	1
0.001:0.01	U.L.	—	—	11.5	1
0.003:0.01	U.L.	—	—	11.5	1
0.003:0.03	U.L.	—	—	11.5	1
0.03:0.3	Detect	-2.18 ± 0.53	22.7 ± 1.10	17.3 ± 0.26	2-5
0.1:0.3	Detect	-2.18 ± 0.53	22.7 ± 1.10	18.6 ± 0.13	2-5
0.1:1	Detect	-1.13 ± 0.10	20.5 ± 0.12	19.1 ± 0.09	2-12
0.3:1	Detect	-1.17 ± 0.11	20.7 ± 0.02	19.6 ± 0.05	6-12
0.3:3	Detect	-1.59 ± 0.08	20.6 ± 0.01	20.6 ± 0.01	6-20
1:3	Detect	-1.95 ± 0.02	20.6 ± 0.04	21.8 ± 0.12	13-20
1:10	Detect	-2.31 ± 0.08	20.5 ± 0.03	23.4 ± 0.09	13-22
3:10	Detect	-1.76 ± 0.29	21.5 ± 0.48	24.8 ± 0.09	21-22
3:30	Detect	-1.76 ± 0.29	21.5 ± 0.48	25.9 ± 0.25	21-22

Table 4.40: Time resolved magnitude of GRB030226.

GRB030323

The prompt emission of this burst is XRR. Optical afterglow of this event is bright.

Time interval [day]	Detect/U.L.	α	m_0	$m(t)$	data#
0.03:0.3	U.L.	—	—	16.6	16
0.1:0.3	U.L.	—	—	16.6	16
0.1:1	Detect	-2.25 ± 0.24	21.1 ± 0.20	18.3 ± 0.14	1-7
0.3:1	Detect	-2.25 ± 0.24	21.1 ± 0.20	19.7 ± 0.08	1-7
0.3:3	Detect	-1.37 ± 0.13	20.3 ± 0.09	20.4 ± 0.09	1-12
1:3	Detect	-1.15 ± 0.17	20.3 ± 0.07	21.1 ± 0.07	8-12
1:10	Detect	-1.45 ± 0.16	20.2 ± 0.14	22.1 ± 0.12	8-15
3:10	Detect	-2.26 ± 1.95	19.3 ± 2.52	23.6 ± 1.14	13-15
3:30	Detect	-2.26 ± 1.95	19.3 ± 2.52	25.0 ± 2.36	13-15

Table 4.41: Time resolved magnitude of GRB030323.

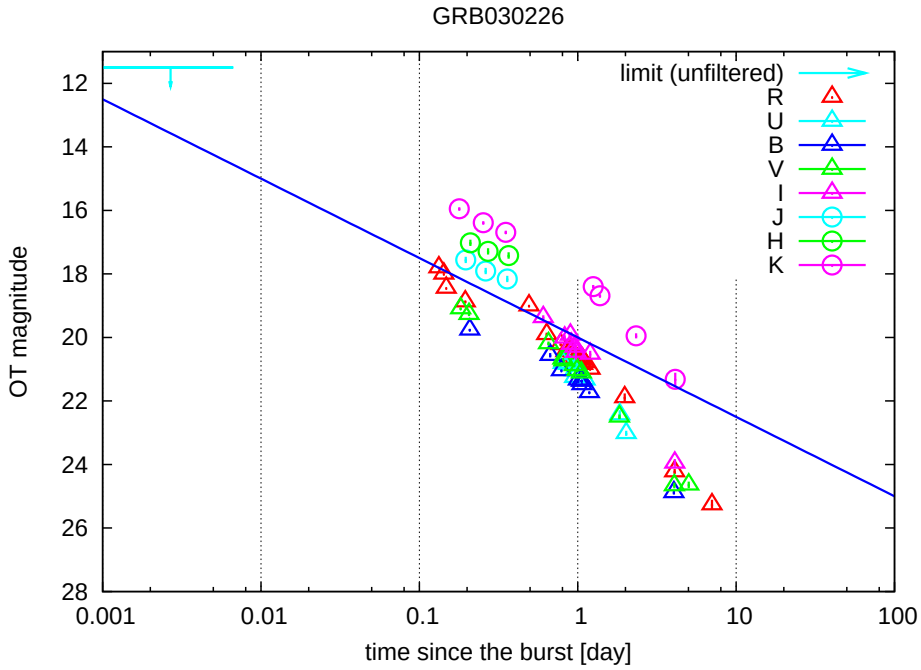

Figure 4.44: Optical afterglow of GRB030226. (detection)

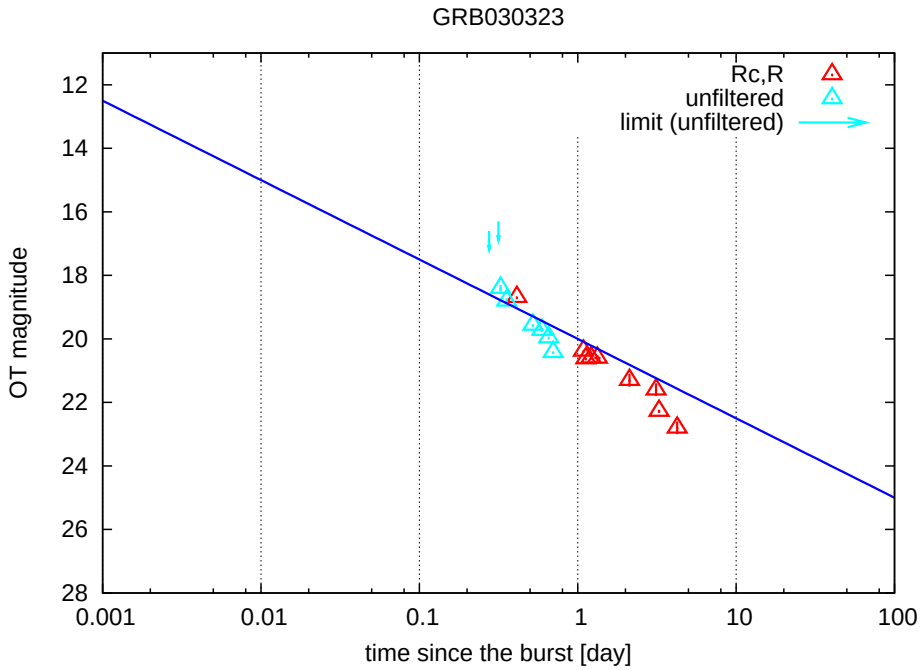

Figure 4.45: Optical afterglow of GRB030323. (detection)

GRB030324

The prompt emission of this burst is XRR. Optical afterglow of this event is dim.

Time interval [day]	Detect/U.L.	α	m_0	$m(t)$	data#
0.0001:0.001	U.L.	—	—	14.8	1
0.0003:0.001	U.L.	—	—	14.8	1
0.0003:0.003	U.L.	—	—	15.2	2
0.001:0.003	U.L.	—	—	15.2	2
0.01:0.1	U.L.	—	—	20	3
0.03:0.1	U.L.	—	—	20	3
0.03:0.3	U.L.	—	—	22.4	4
0.1:0.3	U.L.	—	—	22.4	4
0.1:1	U.L.	—	—	22.5	5
0.3:1	U.L.	—	—	22.5	5
0.3:3	U.L.	—	—	22.7	6
1:3	U.L.	—	—	22.7	6
1:10	U.L.	—	—	22.7	6

Table 4.42: Time resolved magnitude of GRB030324.

GRB030328

The prompt emission of this burst is GRB. Optical afterglow of this event is dim.

Time interval [day]	Detect/U.L.	α	m_0	$m(t)$	data#
0.1:1	Detect	-1.22 $\pm$ 0.16	21.5 $\pm$ 0.09	19.9 $\pm$ 0.12	1-10
0.3:1	Detect	-1.22 $\pm$ 0.16	21.5 $\pm$ 0.09	20.7 $\pm$ 0.03	1-10
0.3:3	Detect	-1.27 $\pm$ 0.10	21.5 $\pm$ 0.06	21.5 $\pm$ 0.06	1-12
1:3	Detect	-1 (fixed)	21.6 $\pm$ 0.18	22.2 $\pm$ 0.18	11-12
1:10	Detect	-1 (fixed)	21.6 $\pm$ 0.18	22.9 $\pm$ 0.18	11-12

Table 4.43: Time resolved magnitude of GRB030328.

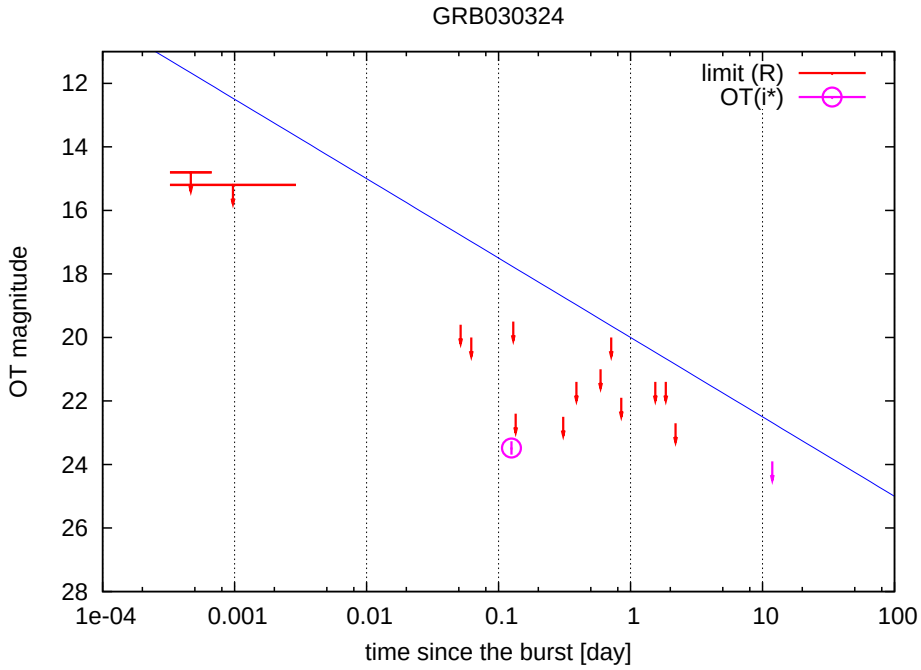

Figure 4.46: Optical afterglow of GRB030324. (detection in i*)

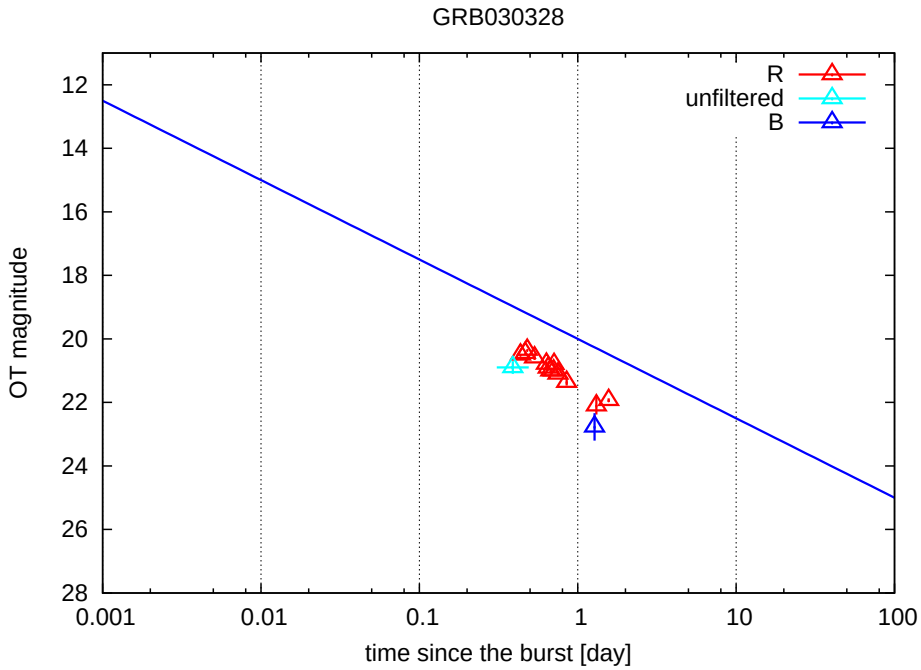

Figure 4.47: Optical afterglow of GRB030328. (detection)

GRB030329

The prompt emission of this burst is XRR. Optical afterglow of this event is bright. Measured redshift of the burst is 0.168.

Time interval [day]	Detect/U.L.	α	m_0	$m(t)$	data#
0.01:0.1	Detect	—	—	12.6 ± 0.02	1
0.03:0.1	Detect	—	—	12.6 ± 0.02	1
0.03:0.3	Detect	-0.87 ± 0.02	15.2 ± 0.06	13.0 ± 0.02	1-5
0.1:0.3	Detect	-0.93 ± 0.10	15.3 ± 0.18	13.5 ± 0.02	2-5
0.1:1	Detect	-1.41 ± 0.05	16.0 ± 0.03	14.3 ± 0.03	2-11
0.3:1	Detect	-1.41 ± 0.05	16.0 ± 0.03	15.1 ± 0.02	6-11
0.3:3	Detect	-1.26 ± 0.09	16.0 ± 0.05	16.0 ± 0.05	6-16
1:3	Detect	-0.66 ± 0.27	16.3 ± 0.14	16.7 ± 0.09	12-16
1:10	Detect	-1.18 ± 0.14	16.0 ± 0.18	17.5 ± 0.11	12-20
3:10	Detect	-2.31 ± 0.21	13.9 ± 0.34	18.3 ± 0.09	17-20
3:30	Detect	-1.63 ± 0.22	15.0 ± 0.38	19.3 ± 0.21	17-23
10:30	Detect	-1.30 ± 0.07	15.5 ± 0.25	19.6 ± 0.03	21-23
10:100	Detect	-1.39 ± 0.08	15.2 ± 0.33	20.5 ± 0.05	21-30
30:100	Detect	-1.37 ± 0.19	15.3 ± 0.84	21.3 ± 0.07	24-30

Table 4.44: Time resolved magnitude of GRB030329.

GRB030418

The prompt emission of this burst is XRR. Optical afterglow of this event is dim.

Time interval [day]	Detect/U.L.	α	m_0	$m(t)$	data#
0.003:0.03	Detect	—	—	18.1 ± 0.4	1
0.01:0.03	Detect	—	—	18.1 ± 0.4	1
0.01:0.1	Detect	-0.68 ± 0.39	21.0 ± 1.25	18.4 ± 0.21	1-2
0.03:0.1	Detect	—	—	18.8	2
0.03:0.3	Detect	-0.86	21.6	19.4	2-3
0.1:0.3	Detect	—	—	19.8	3
0.1:1	Detect	-0.66 ± 0.28	21.2 ± 0.58	20.3 ± 0.23	3-4
0.3:1	Detect	—	—	20.5 ± 0.3	4
0.3:3	Detect	-1.38 ± 0.16	21.9 ± 0.16	21.9 ± 0.16	4-5
1:3	Detect	—	—	23.3 ± 0.1	5
1:10	Detect	-1.59 ± 0.41	21.7 ± 0.46	23.6 ± 0.12	5-6
3:10	Detect	—	—	24.9 ± 0.4	6
3:10	Detect	—	—	24.9 ± 0.4	6

Table 4.45: Time resolved magnitude of GRB030418.

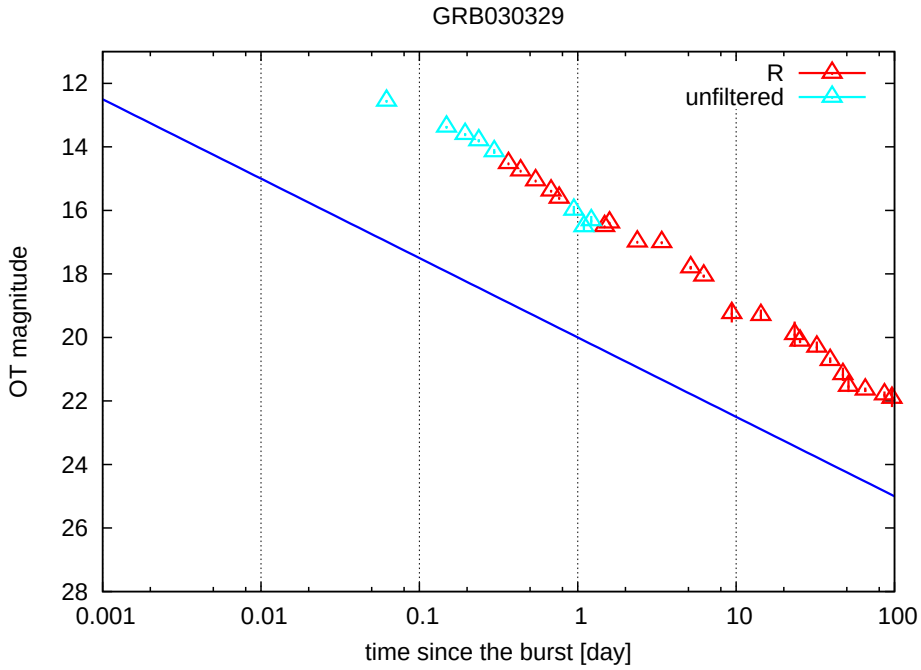

Figure 4.48: Optical afterglow of GRB030329. (detection)

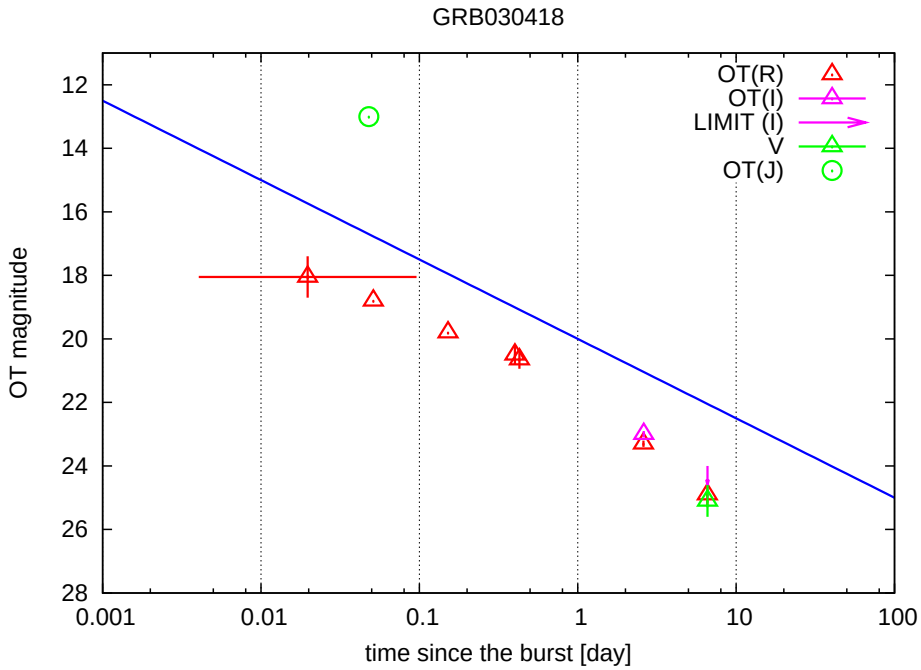

Figure 4.49: Optical afterglow of GRB030418. (detection)

GRB030429

The prompt emission of this burst is XRF. Optical afterglow of this event is dim.

Time interval [day]	Detect/U.L.	α	m_0	$m(t)$	data#
0.01:0.1	U.L.	—	—	18.2	1
0.03:0.1	U.L.	—	—	18.2	1
0.03:0.3	Detect	-0.11 ± 0.55	19.8 ± 1.08	19.5 ± 0.32	2-5
0.1:0.3	Detect	-0.11 ± 0.55	19.8 ± 1.08	19.5 ± 0.09	2-5
0.1:1	Detect	-0.96 ± 0.07	21.4 ± 0.07	20.2 ± 0.05	2-8
0.3:1	Detect	-0.87 ± 0.26	21.4 ± 0.14	20.8 ± 0.07	6-8
0.3:3	Detect	-0.98 ± 0.08	21.4 ± 0.05	21.4 ± 0.05	6-12
1:3	Detect	-2.39 ± 0.54	20.0 ± 0.55	21.5 ± 0.22	9-12
1:10	Detect	-2.76 ± 0.27	19.7 ± 0.29	23.1 ± 0.08	9-14
3:10	Detect	-2.27 ± 0.49	20.5 ± 0.74	24.8 ± 0.22	13-14
3:30	Detect	-2.27 ± 0.49	20.5 ± 0.74	26.2 ± 0.51	13-14
10:100	U.L.	—	—	26.3	15
30:100	U.L.	—	—	26.3	15
30:300	U.L.	—	—	26.3	15

Table 4.46: Time resolved magnitude of GRB030429.

GRB030528

The prompt emission of this burst is XRF. Optical afterglow for this burst is searched sufficiently. However no detection has reported.

Time interval [day]	Detect/U.L.	α	m_0	$m(t)$	data#
0.0003:0.003	U.L.	—	—	16.0	1
0.001:0.003	U.L.	—	—	16.0	1
0.001:0.01	U.L.	—	—	16.0	1
0.01:0.1	U.L.	—	—	18.7	2
0.03:0.1	U.L.	—	—	18.7	2
0.03:0.3	U.L.	—	—	18.7	2
0.1:1	U.L.	—	—	20.5	3
0.3:1	U.L.	—	—	20.5	3
0.3:3	U.L.	—	—	20.5	3
100:1000	Detect	—	—	22.0 ± 0.2	4

Table 4.47: Time resolved magnitude of GRB030528.

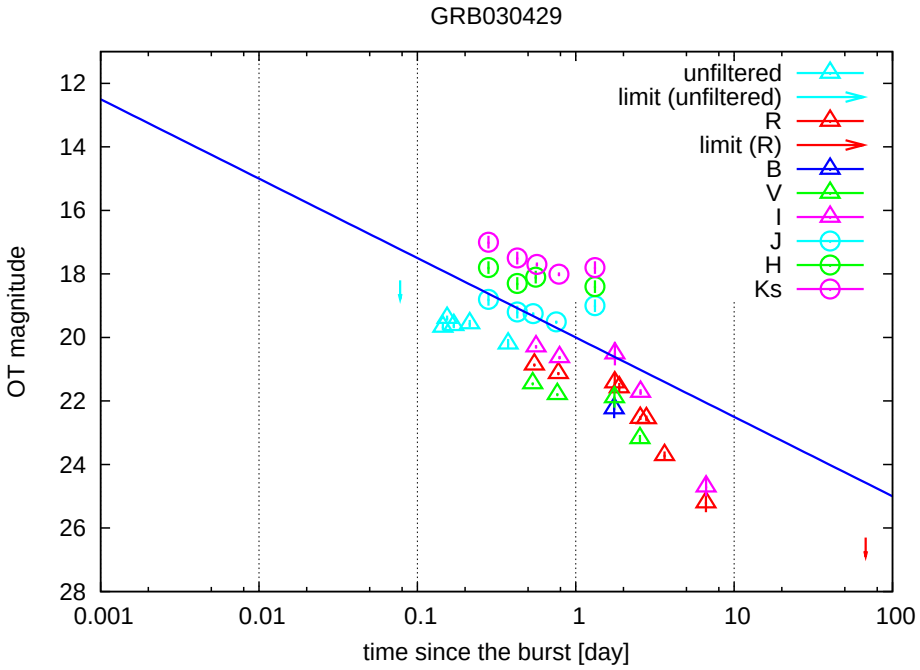

Figure 4.50: Optical afterglow of GRB030429. (detection)

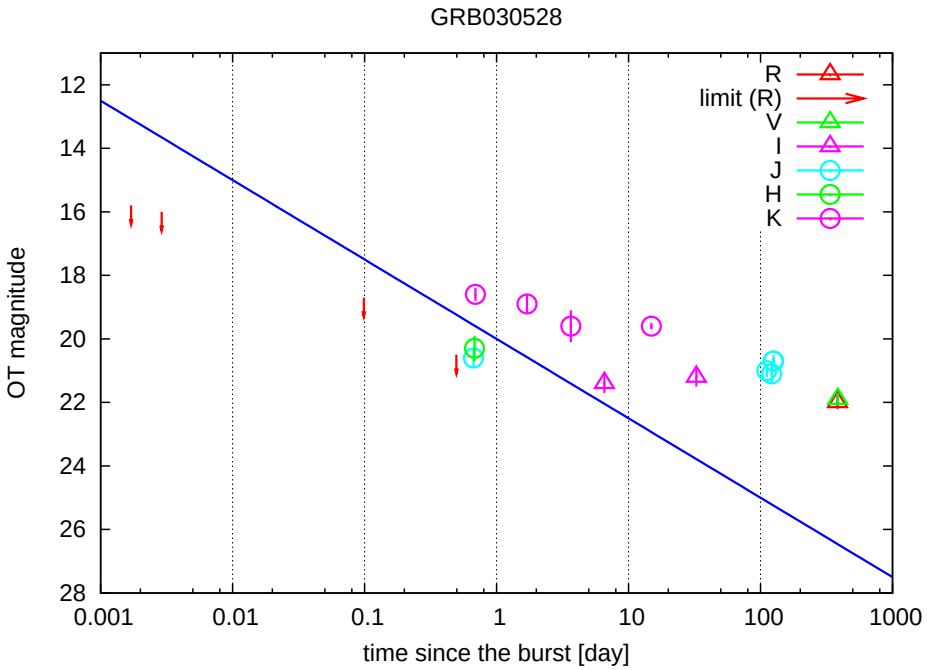

Figure 4.51: Optical afterglow of GRB030528. (limit)

GRB030723

The prompt emission of this burst is XRR. Optical afterglow of this event is dim.

Time interval [day]	Detect/U.L.	α	m_0	$m(t)$	data#
0.0003:0.001	U.L.	—	—	19.0	1
0.0003:0.003	U.L.	—	—	19.7	2
0.001:0.003	U.L.	—	—	19.7	2
0.001:0.01	U.L.	—	—	19.7	2
0.003:0.01	U.L.	—	—	19.1	3
0.003:0.03	Detect	$+0.58 \pm 1.64$	17.1 ± 6.55	20.0 ± 1.69	4-5
0.01:0.03	Detect	$+0.58 \pm 1.64$	17.1 ± 6.55	19.6 ± 0.70	4-5
0.01:0.1	Detect	$+0.58 \pm 1.64$	17.1 ± 6.55	19.3 ± 0.48	4-5
0.1:1	Detect	—	—	21.0	6
0.3:1	Detect	—	—	21.0	6
0.3:3	Detect	-1.58 ± 0.14	21.0 ± 0.07	21.0 ± 0.07	7-9
1:3	Detect	-1.58 ± 0.14	21.0 ± 0.07	22.0 ± 0.06	7-9
1:10	Detect	-1.80 ± 0.09	20.9 ± 0.09	23.2 ± 0.08	7-10
3:10	Detect	—	—	24.2 ± 0.3	10
3:30	Detect	—	—	24.2 ± 0.3	10

Table 4.48: Time resolved magnitude of GRB030723.

GRB030725

The prompt emission of this burst is XRR. Optical afterglow of this event is bright.

Time interval [day]	Detect/U.L.	α	m_0	$m(t)$	data#
0.03:0.3	Detect	—	—	18.8	1
0.1:0.3	Detect	—	—	18.8	1
0.1:1	Detect	-1.83 ± 0.42	21.1 ± 0.46	18.9 ± 0.10	1-3
0.3:1	Detect	-1 (fixed)	20.3 ± 0.18	19.7 ± 0.18	2-3
0.3:3	Detect	-1 (fixed)	20.3 ± 0.18	20.3 ± 0.18	2-3
1:10	Detect	-1.91 ± 0.23	18.3 ± 0.49	20.7 ± 0.20	4-6
3:10	Detect	-1.91 ± 0.23	18.3 ± 0.49	21.9 ± 0.07	4-6
3:30	Detect	-1.91 ± 0.23	18.3 ± 0.49	23.1 ± 0.10	4-6

Table 4.49: Time resolved magnitude of GRB030725.

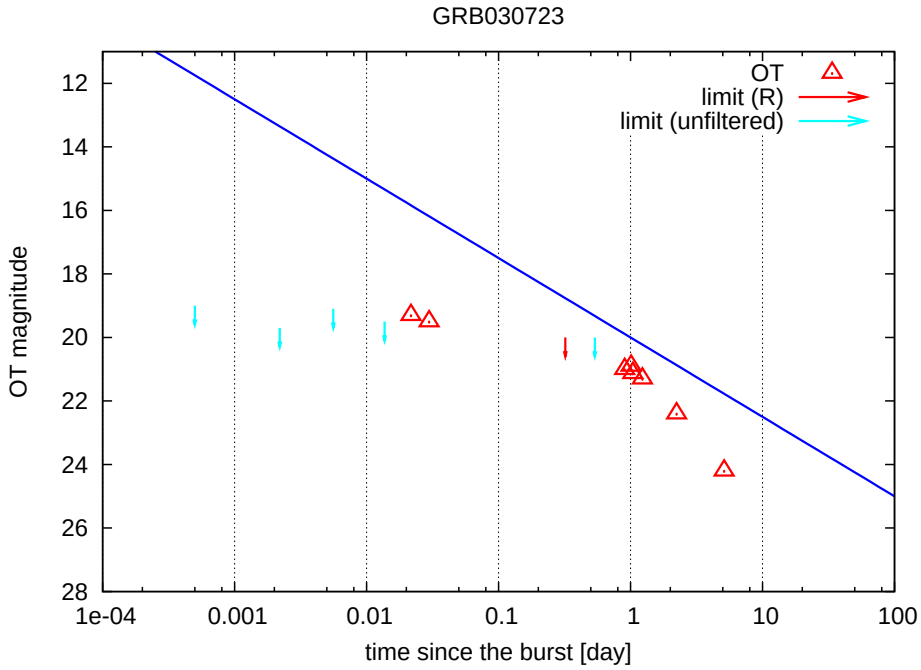

Figure 4.52: Optical afterglow of GRB030723. (detection)

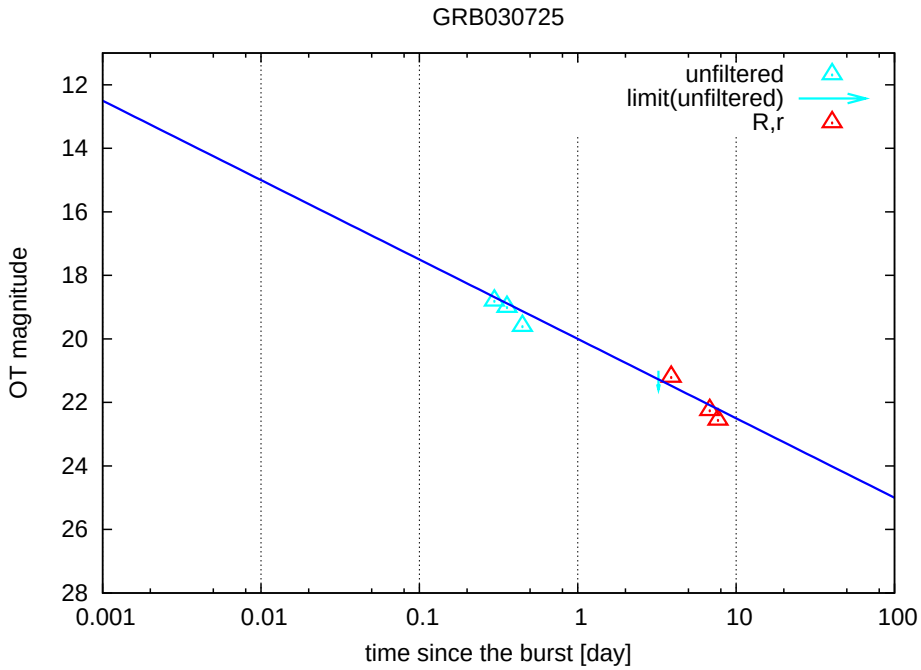

Figure 4.53: Optical afterglow of GRB030725. (detection)

GRB030823

The prompt emission of this burst is XRF. Optical afterglow for this burst is searched sufficiently. However no detection has reported.

Time interval [day]	Detect/U.L.	α	m_0	$m(t)$	data#
0.01:0.1	U.L.	—	—	16.5	1
0.03:0.1	U.L.	—	—	16.5	1
0.03:0.3	U.L.	—	—	19.5	2
0.1:0.3	U.L.	—	—	19.5	2
0.1:1	U.L.	—	—	20.5	3
0.3:1	U.L.	—	—	20.5	3
0.3:3	U.L.	—	—	20.5	3

Table 4.50: Time resolved magnitude of GRB030823.

GRB030824

The prompt emission of this burst is XRF. Optical afterglow for this burst is searched sufficiently. However no detection has reported.

Time interval [day]	Detect/U.L.	α	m_0	$m(t)$	data#
0.03:0.3	U.L.	—	—	17.5	1
0.1:0.3	U.L.	—	—	17.5	1
0.1:1	U.L.	—	—	22.5	2
0.3:1	U.L.	—	—	22.5	2
0.3:3	U.L.	—	—	22.5	2

Table 4.51: Time resolved magnitude of GRB030824.

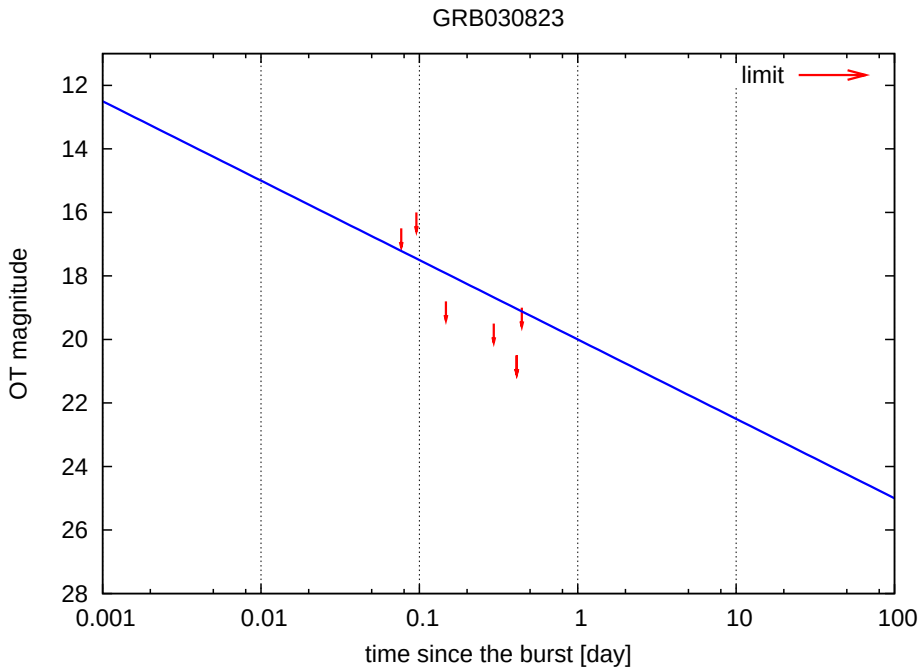

Figure 4.54: Optical afterglow of GRB030823. (limit)

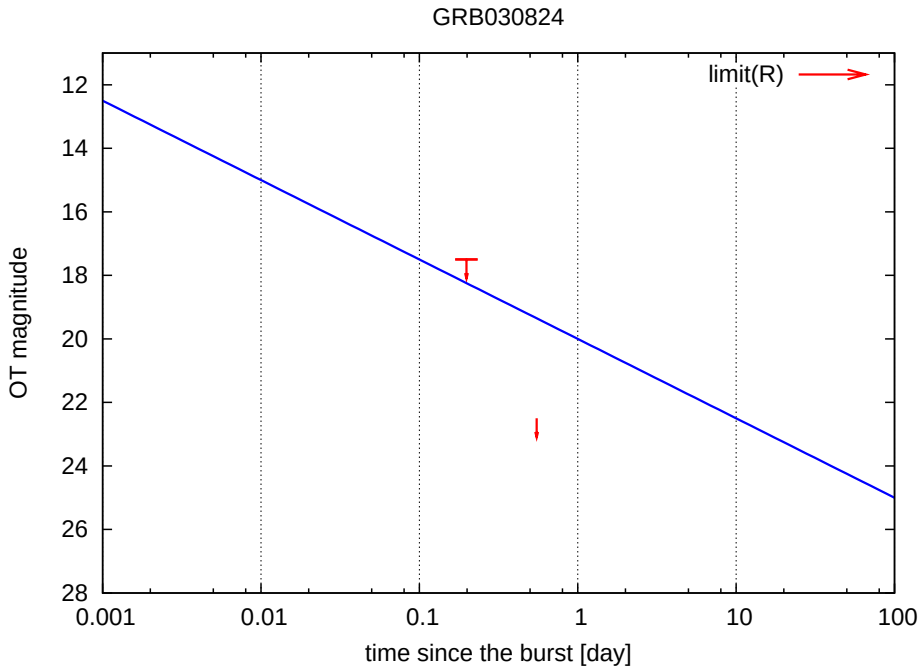

Figure 4.55: Optical afterglow of GRB030824. (limit)

GRB031026

The prompt emission of this burst is GRB. Optical afterglow for this burst is searched sufficiently. However no detection has reported.

Time interval [day]	Detect/U.L.	α	m_0	$m(t)$	data#
0.03:0.3	U.L.	—	—	18	1
0.1:0.3	U.L.	—	—	18	1
0.1:1	U.L.	—	—	20.9	2
0.3:1	U.L.	—	—	20.9	2
0.3:3	U.L.	—	—	20.9	2

Table 4.52: Time resolved magnitude of GRB031026.

GRB031111

The prompt emission of this burst is GRB. Optical afterglow for this burst is not searched sufficiently.

Time interval [day]	Detect/U.L.	α	m_0	$m(t)$	data#
0.3:3	U.L.	—	—	18.5	1
1:3	U.L.	—	—	18.5	1
1:10	U.L.	—	—	18.5	1

Table 4.53: Time resolved magnitude of GRB031111.

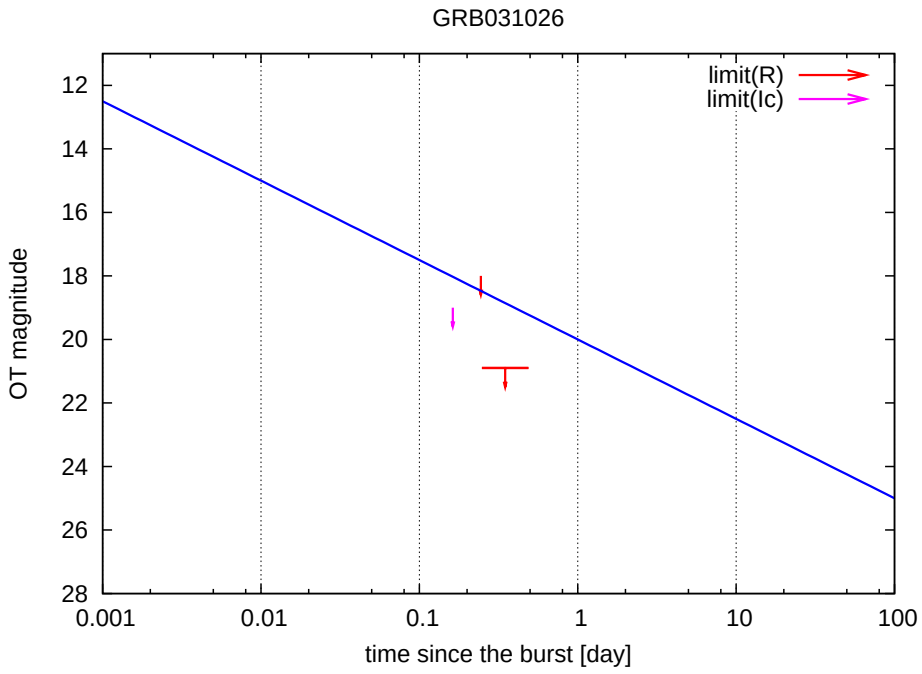

Figure 4.56: Optical afterglow of GRB031026. (limit)

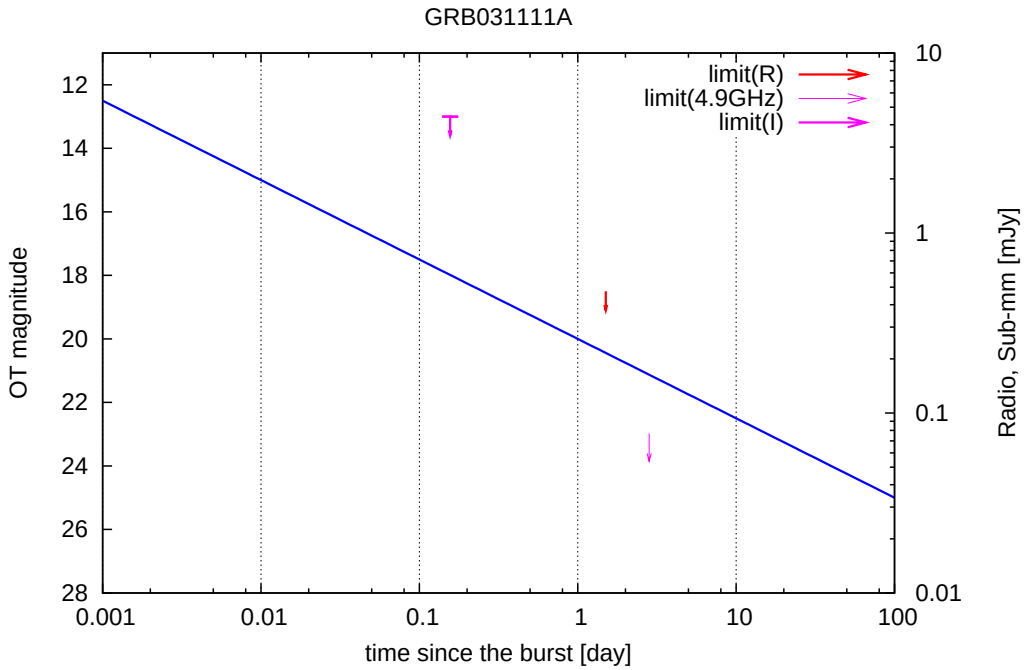

Figure 4.57: Optical afterglow of GRB031111. (limit)

GRB031111B

The prompt emission of this burst is XRR. Optical afterglow for this burst is not searched sufficiently.

Time interval [day]	Detect/U.L.	α	m_0	$m(t)$	data#
0.1:1	U.L.	—	—	17.2	1
0.3:1	U.L.	—	—	17.2	1
0.3:3	U.L.	—	—	17.2	1

Table 4.54: Time resolved magnitude of GRB031111B.

GRB031220

The prompt emission of this burst is XRR. Optical afterglow of this event is dim.

Time interval [day]	Detect/U.L.	α	m_0	$m(t)$	data#
0.01:0.1	U.L.	—	—	19.2	1
0.03:0.1	U.L.	—	—	19.2	1
0.03:0.3	U.L.	—	—	23	2
0.1:0.3	U.L.	—	—	23	2
0.1:1	U.L.	—	—	23	2
0.3:1	U.L.	—	—	20.9	3
0.3:3	Detect	—	—	24.4 ± 0.18	4
1:3	Detect	—	—	24.4 ± 0.18	4
1:10	Detect	—	—	24.4 ± 0.18	4
3:10	U.L.	—	—	24	5
3:30	U.L.	—	—	24	5

Table 4.55: Time resolved magnitude of GRB031220.

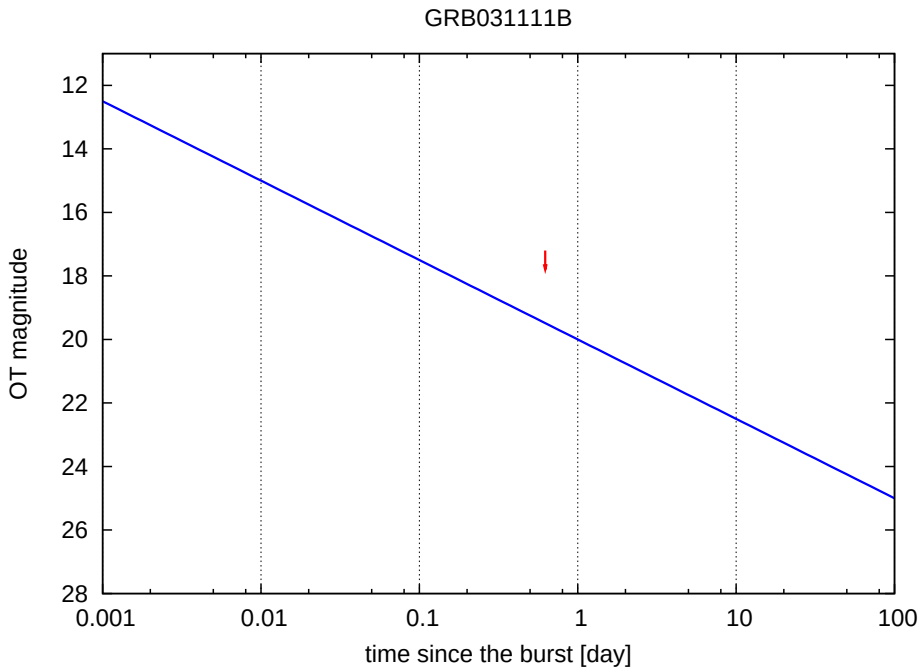

Figure 4.58: Optical afterglow of GRB031111B. (limit)

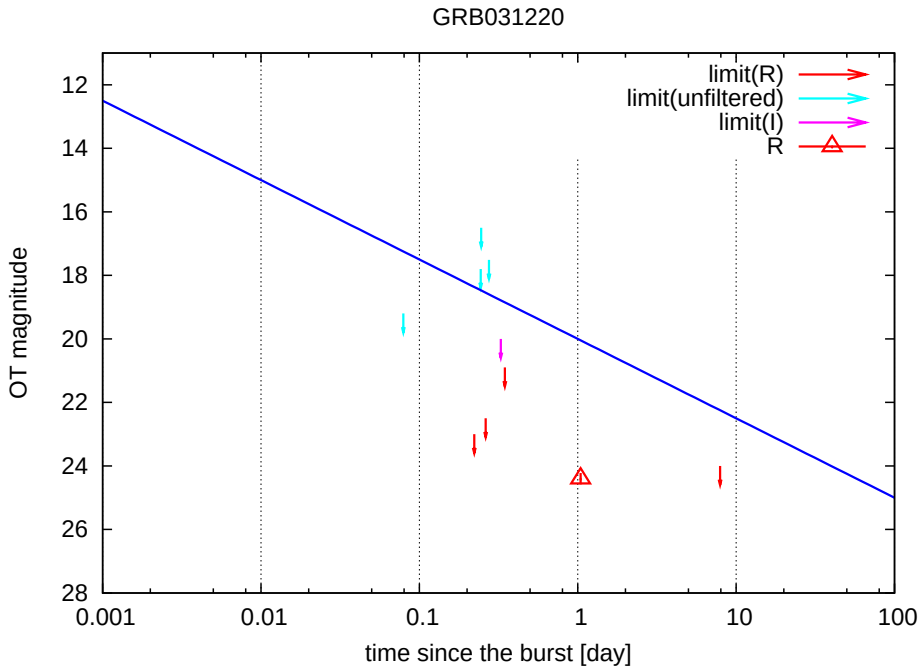

Figure 4.59: Optical afterglow of GRB031220. (detection)

GRB040228B

The prompt emission of this burst is XRF. Optical afterglow for this burst is searched sufficiently. However no detection has reported.

Time interval [day]	Detect/U.L.	α	m_0	$m(t)$	data#
0.01:0.1	U.L.	—	—	10.5	1
0.03:0.1	U.L.	—	—	10.5	1
0.03:0.3	U.L.	—	—	10.5	1
0.1:1	U.L.	—	—	19.5	2
0.3:1	U.L.	—	—	19.5	2
0.3:3	U.L.	—	—	19.5	2

Table 4.56: Time resolved magnitude of GRB040228B.

GRB040511

The prompt emission of this burst is XRR. Optical afterglow for this burst is searched sufficiently. However no detection has reported.

Time interval [day]	Detect/U.L.	α	m_0	$m(t)$	data#
0.01:0.1	U.L.	—	—	17.5	1
0.03:0.1	U.L.	—	—	17.5	1
0.03:0.3	U.L.	—	—	17.6	2
0.1:0.3	U.L.	—	—	17.6	2
0.1:1	U.L.	—	—	21	3
0.3:1	U.L.	—	—	21	3
0.3:3	U.L.	—	—	21	3

Table 4.57: Time resolved magnitude of GRB040511.

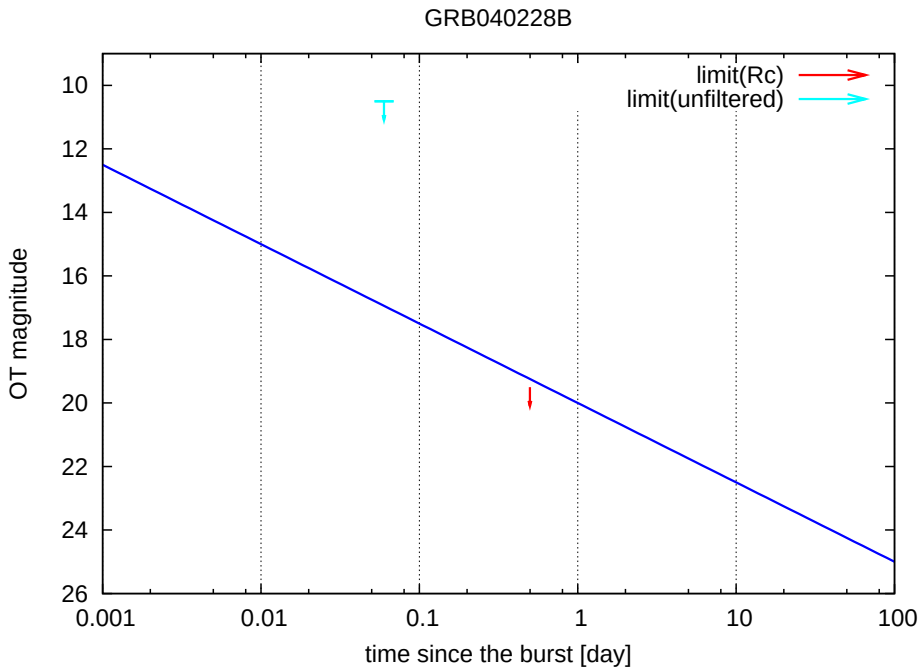

Figure 4.60: Optical afterglow of GRB040228B. (limit)

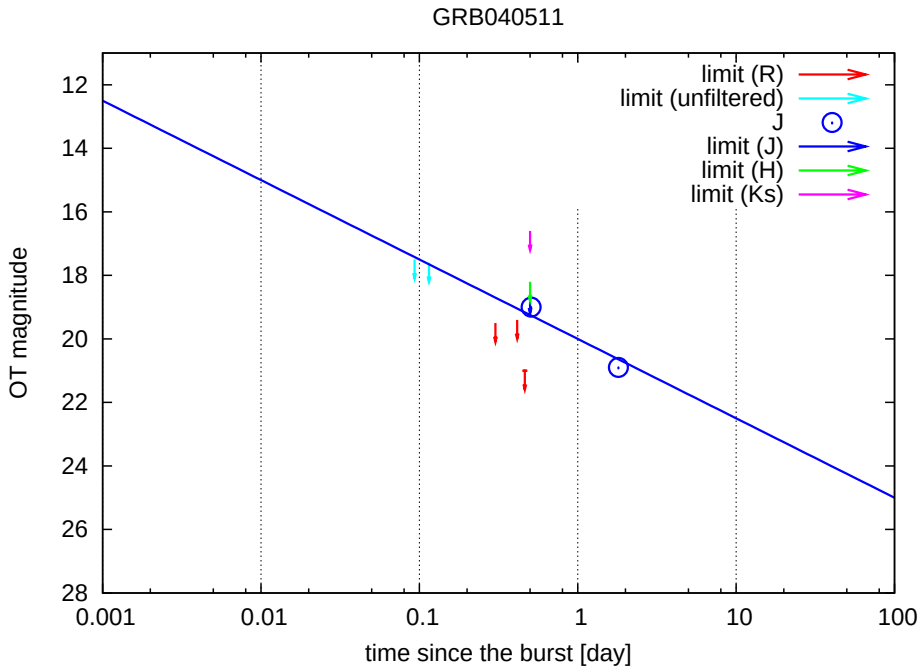

Figure 4.61: Optical afterglow of GRB040511. (detection)

GRB040916B

Optical afterglow for this burst is dim.

Time interval [day]	Detect/U.L.	α	m_0	$m(t)$	data#
0.01:0.1	U.L.	—	—	13.0	1
0.03:0.1	U.L.	—	—	13.0	5
0.03:0.3	Detect	—	—	22.3 ± 0.2	1
0.1:0.3	Detect	—	—	22.3 ± 0.2	1
0.1:1	Detect	-0.81 ± 0.73	23.6 ± 1.06	22.6 ± 0.22	1-2
0.3:1	Detect	—	—	22.7 ± 0.3	2
0.3:3	Detect	-1.01 ± 0.20	23.8 ± 0.21	23.8 ± 0.21	2-3
1:3	Detect	—	—	24.8 ± 0.3	3
1:10	Detect	-0.32 ± 0.48	24.5 ± 0.78	24.9 ± 0.18	3-4
3:10	Detect	—	—	25	4
3:30	Detect	—	—	25	4

Table 4.58: Time resolved magnitude of GRB040916B.

GRB040924

Optical afterglow for this burst is dim.

Time interval [day]	Detect/U.L.	α	m_0	$m(t)$	data#
0.003:0.03	Detect	-0.51	20.5	18.0	1-2
0.003:0.03	Detect	-0.51	20.5	18.3	1-2
0.01:0.1	Detect	-0.78 ± 0.08	21.8 ± 0.35	18.8 ± 0.05	1-4
0.03:0.1	Detect	-1.22	23.3	19.5	3-4
0.03:0.3	Detect	-1.10 ± 0.01	22.9 ± 0.04	20.2 ± 0.01	3-5
0.1:0.3	Detect	—	—	21.4	5
0.1:1	Detect	-0.56 ± 0.53	22.4 ± 0.54	21.7 ± 0.28	5-7
0.3:1	Detect	0.00	22.1	22.1	6-7
0.3:3	Detect	-1.06 ± 0.55	23.0 ± 0.39	23.0 ± 0.39	6-8
1:3	Detect	—	—	23.7 ± 0.2	8
1:10	Detect	—	—	23.7 ± 0.2	8

Table 4.59: Time resolved magnitude of GRB040924.

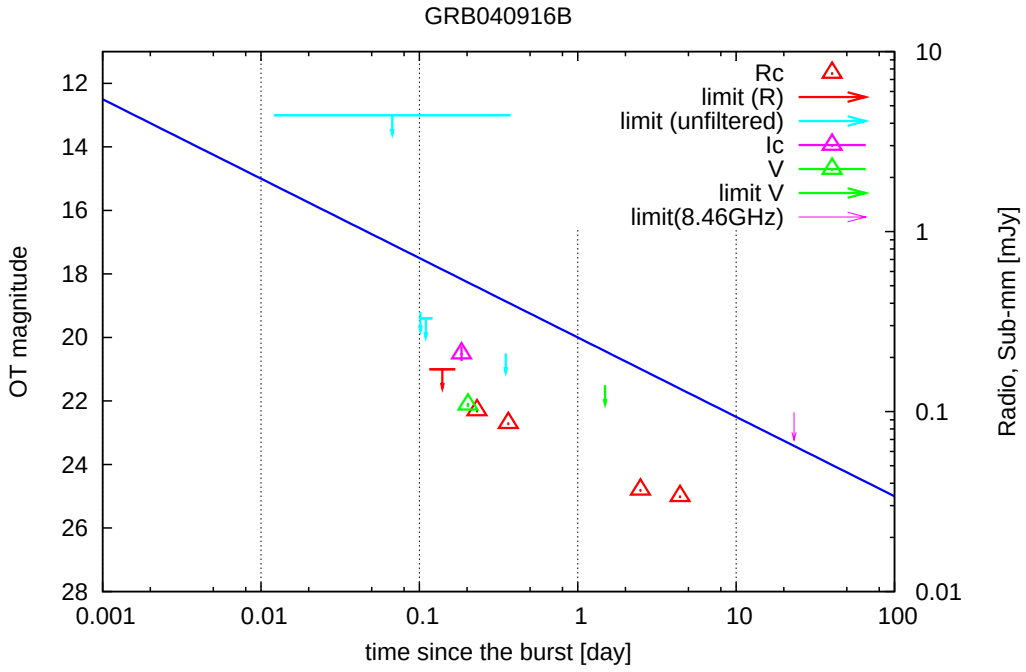

Figure 4.62: Optical afterglow of GRB040916B. (detection)

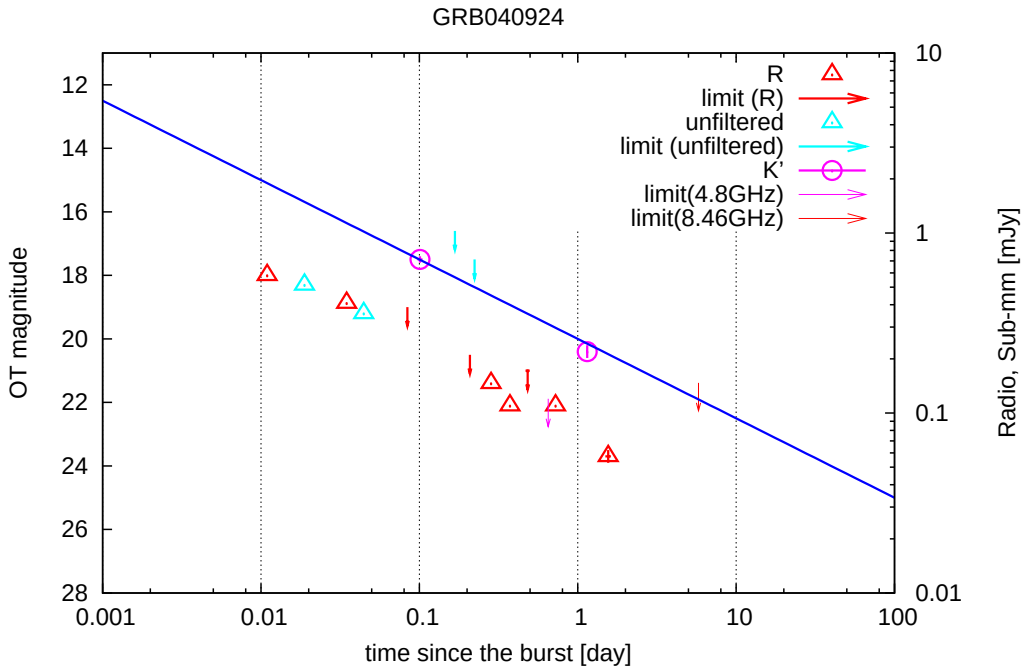

Figure 4.63: Optical afterglow of GRB040924. (detection)

GRB041006

Optical afterglow for this burst is dim.

Time interval [day]	Detect/U.L.	α	m_0	$m(t)$	data#
0.0003:0.003	Detect	—	—	16.8	1
0.001:0.003	Detect	—	—	16.8	1
0.001:0.01	Detect	—	—	16.8	1
0.003:0.03	Detect	—	—	17.1 ± 0.4	2
0.01:0.03	Detect	—	—	17.1 ± 0.4	2
0.01:0.1	Detect	-0.62 ± 0.36	19.9 ± 1.30	17.6 ± 0.29	2-5
0.03:0.1	Detect	-1.99 ± 0.21	24.1 ± 0.65	17.9 ± 0.07	3-5
0.03:0.3	Detect	-1.14 ± 0.17	21.3 ± 0.43	18.5 ± 0.12	3-8
0.1:0.3	Detect	-1.77 ± 0.10	22.4 ± 0.16	19.0 ± 0.03	6-8
0.1:1	Detect	-1.35 ± 0.07	21.7 ± 0.08	20.0 ± 0.02	6-14
0.3:1	Detect	-1.25 ± 0.05	21.6 ± 0.05	20.8 ± 0.02	9-14
0.3:3	Detect	-1.24 ± 0.02	21.6 ± 0.01	21.6 ± 0.01	9-16
1:3	Detect	-1.93 ± 0.96	21.2 ± 0.55	22.4 ± 0.07	15-16
1:10	Detect	-1.18 ± 0.10	21.6 ± 0.11	23.1 ± 0.07	15-18
3:10	Detect	-0.32 ± 0.55	23.1 ± 0.66	23.7 ± 0.09	17-18
3:30	Detect	-0.37 ± 0.03	23.0 ± 0.05	23.9 ± 0.02	17-19
10:30	Detect	—	—	24.0 ± 0.2	19
10:100	Detect	—	—	24.0 ± 0.2	19

Table 4.60: Time resolved magnitude of GRB041006.

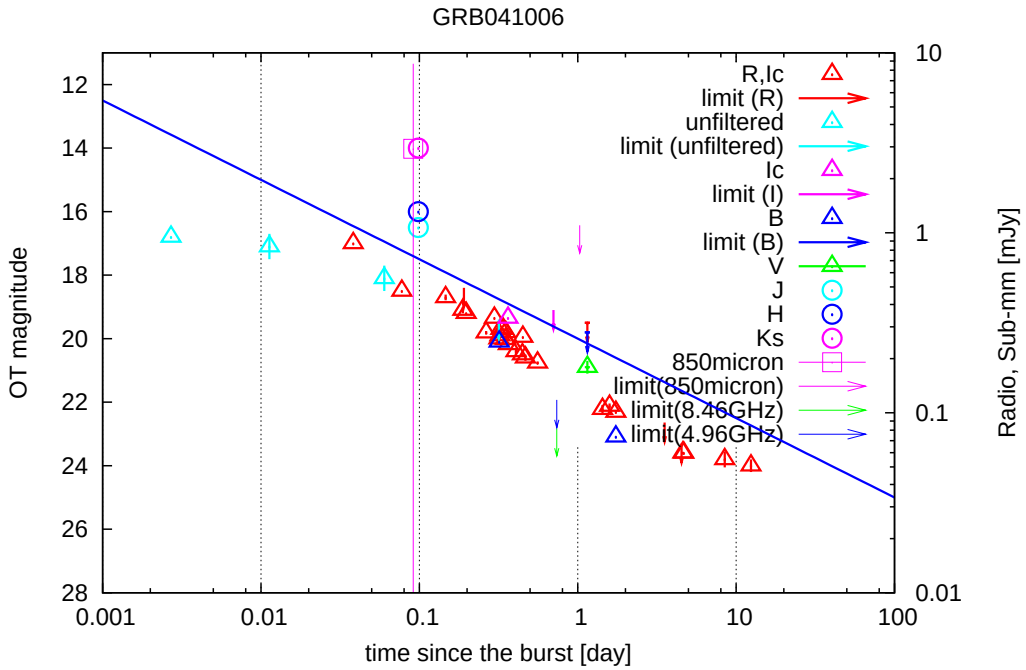

Figure 4.64: Optical afterglow of GRB041006. (detection)

Chapter 5

Correlation between prompt emissions and Afterglows

Using the bursts listed in tables 3.5 (28 bursts) and 3.6 (23 bursts), we examined the correlation between properties of prompt emission and brightness of afterglows.

For the properties of prompt emissions, we used both the properties in the observer frame (which are $E_{\rm peak}$, fluence in 2-30 keV (S_x), fluence in 30-400 keV (S_γ) and fluence in 2-400 keV (S_a)) and the properties in the source frame (which are $E^{\rm src}_{\rm peak}$, $E_{\rm iso}$ are $E_{\rm jet}$). For the optical afterglow, we used both magnitude and luminosity for all 23 time intervals (which is defined in section 4.2.1). We also used luminosity of optical afterglow with jet correction (see equation 4.16). The properties of prompt emission in the observer frame are compared with magnitudes of OTs. The properties of prompt emission in the source frame are compared with luminosities of OTs.

First, we plotted all the combinations of properties of prompt emission and brightness of afterglows (see appendix D.1). An observer-frame example of such scatter plots is shown in figure 5.1. Then we plotted all the combinations of properties in the source frame (appendix D.2). figure 5.2 is an example of a scatter plot of source-frame properties.

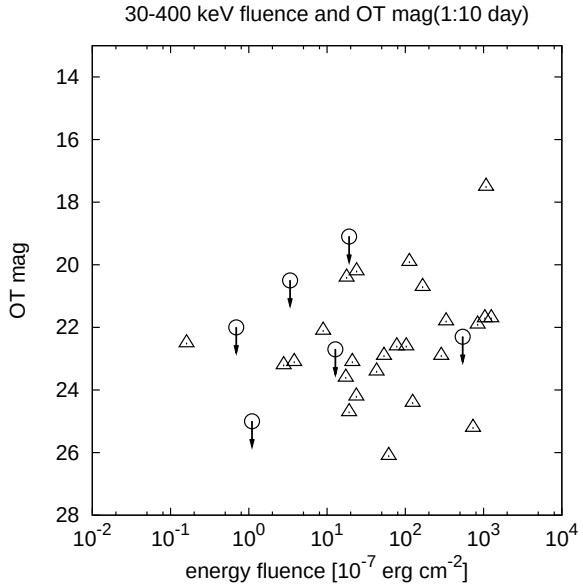

Figure 5.1: An example of scatter plot of the properties in the observer frame.

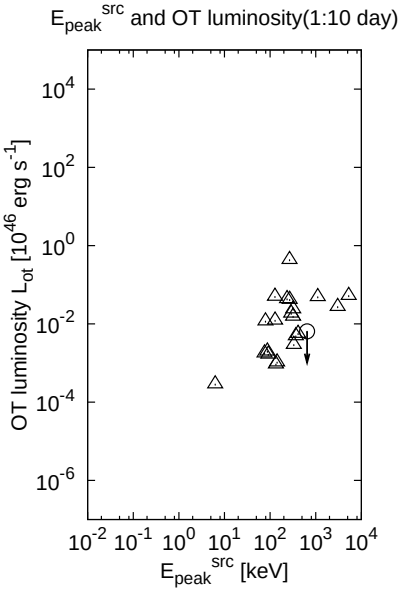

Figure 5.2: An example of scatter plot of the properties in the source frame.

5.1 Evaluation method of the significance of correlations

5.1.1 Sample correlation coefficient: r

To evaluate the significance of correlation, we calculated the sample correlation coefficient r (hereafter SCC). The SCC is defined by

$$r = \frac{\sum_{i=1}^{n}(x_i - \bar{x})(y_i - \bar{y})}{n s_x s_y}, \tag{5.1}$$

where $\bar{x}$ and $\bar{y}$ are sample mean values and s_x and s_y are the sample standard deviations of X and Y.

The SCC must be a number between -1 and 1. The closer the absolute value of the SCC is to 1, the better the correlation.

5.1.2 Cox's method and BHK method

We also calculated significance levels for independence of properties (i.e. no correlation) of prompt emissions and afterglows. We used Cox's method (see appendix A.2) and the BHK method (appendix A.3) to calculate null hypothesis probabilities; i.e. the probability of seeing a correlation when there is no real correlation. These two methods have an advantage over the SCC, because these methods can make use of upper limit data.

5.2 Results

In this section, we show the results of evaluating correlation significances. The significance of correlations is sensitive to the number of samples. Therefore, we plotted both significance of correlation and number of data in a figure.

5.2.1 The properties in the observer frame

Figure 5.3 – 5.5 show the significance of correlation for the properties in the observer frame.

From figure 5.4 and 5.5, fluence of prompt emission is significantly correlated with OT magnitude 0.01–0.1 days after the GRB. This feature is common to both Cox's method and BHK method. It is interesting to know the correlation in the earlier time interval. There are, however, far fewer samples observed earlier than 0.01 day. We need more early-time observations, especially earlier than 0.01 day after the burst.

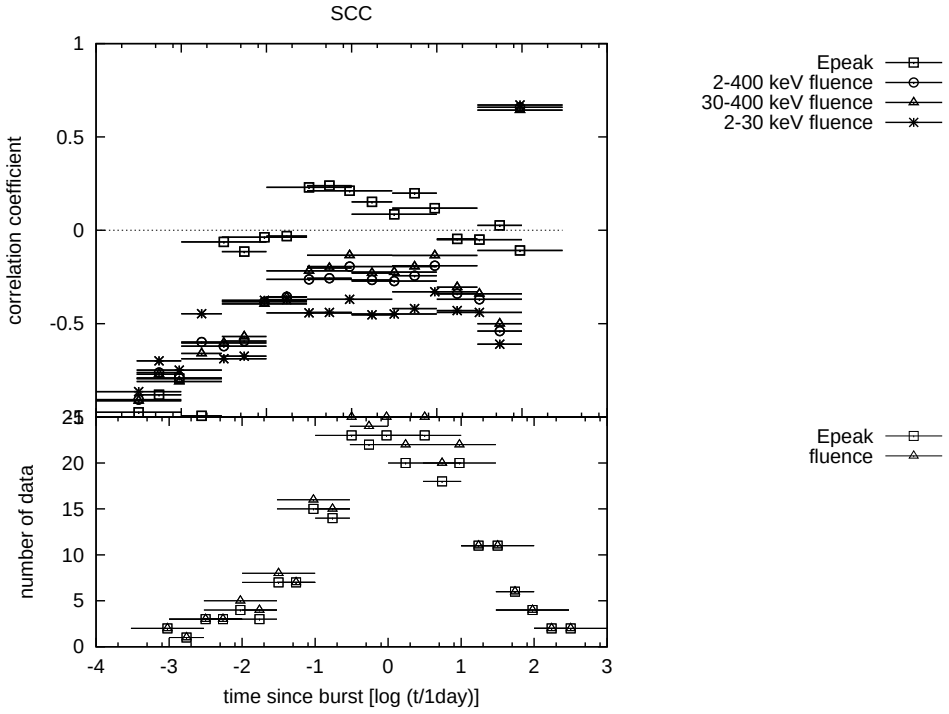

Figure 5.3: The summary of the significance of correlation in the observer frame. Top: The significance evaluated with sample correlation coefficient r. Bottom: The number of data in each time interval.

5.2.2 The properties in the source frame

Figure 5.6 – 5.8 show the significance of correlation for the properties in the source frame.

As shown in these figures, we found a tight correlation between $E_{\rm iso}$ and $L_{\rm ot}$ in the time intervals around 0.1–10 days. The significances of the correlations between $E_{\rm iso}$ in these time intervals are greater than 99%. There is also a probable correlation between $E^{\rm src}_{\rm peak}$ or $E_{\rm iso}$ and $L_{\rm ot}$ in the same time intervals. The significance of the correlation for these time intervals between $E^{\rm src}_{\rm peak}$ and $L_{\rm ot}$, and between $E_{\rm iso}$ and $L_{\rm ot}$, are greater than 95%. We will discuss these relations in the next chapter.

5.2.3 The difference between Cox's method and BHK method

From figure 5.8 (BHK method), $E_{\rm iso}$ and $L_{\rm ot}$ are significantly correlated in the 0.3–3 day time interval. In contrast, null hypothesis probability of Cox's method (figure 5.7) for these combinations is not small. The difference between these methods is that Cox's method uses

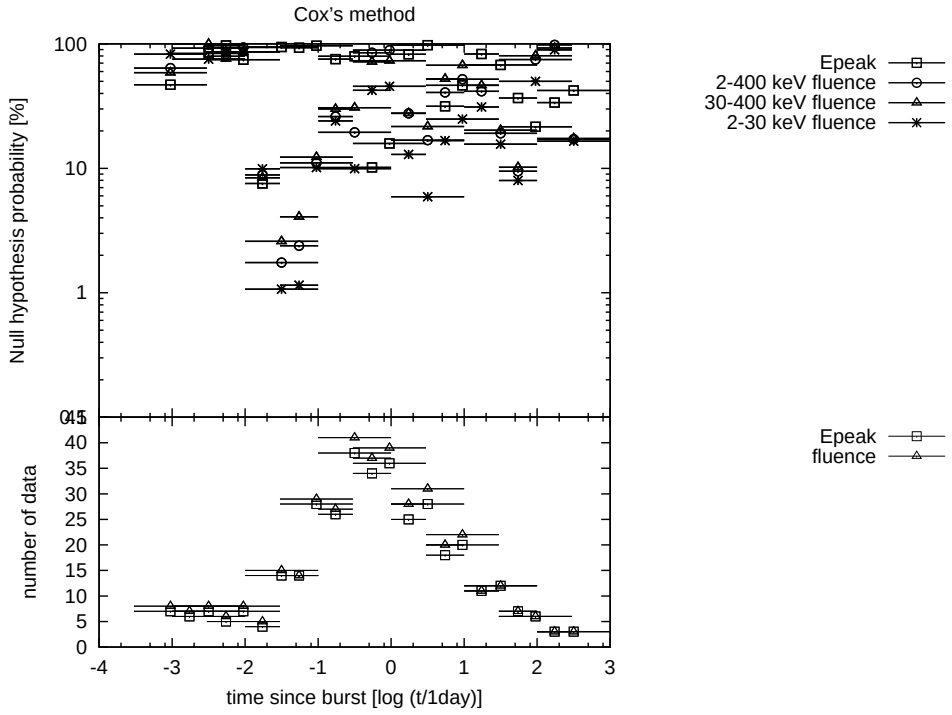

Figure 5.4: The summary of the significance of correlation in the observer frame. Top: The significance evaluated with Cox's method. Bottom: The number of data in each time interval.

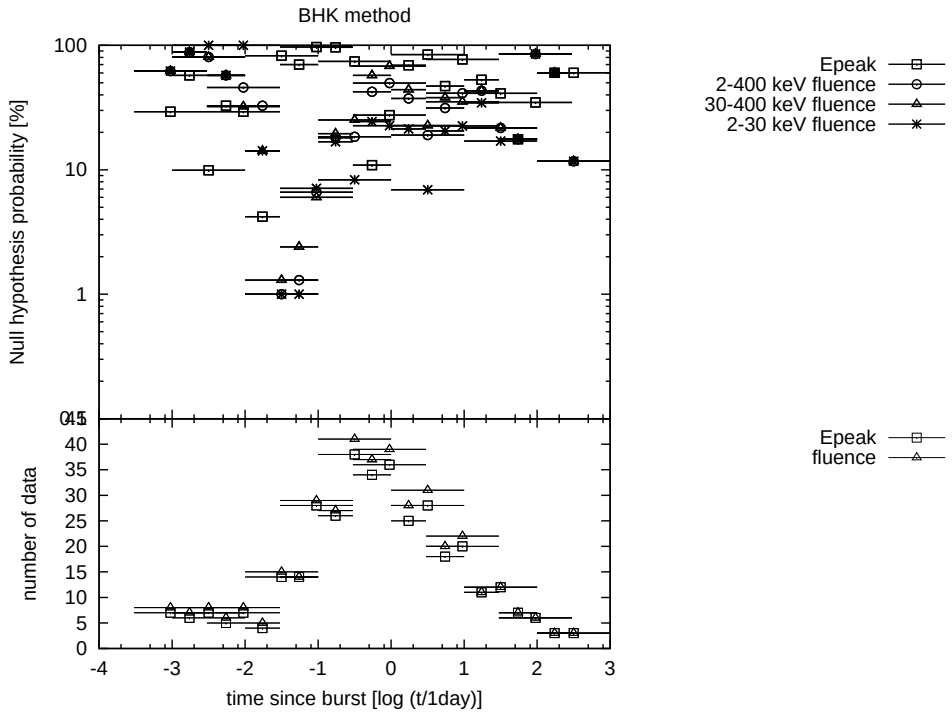

Figure 5.5: The summary of the significance of correlation in the observer frame. Top: The significance is evaluated with BHK method. Bottom: The number of data in each time interval.

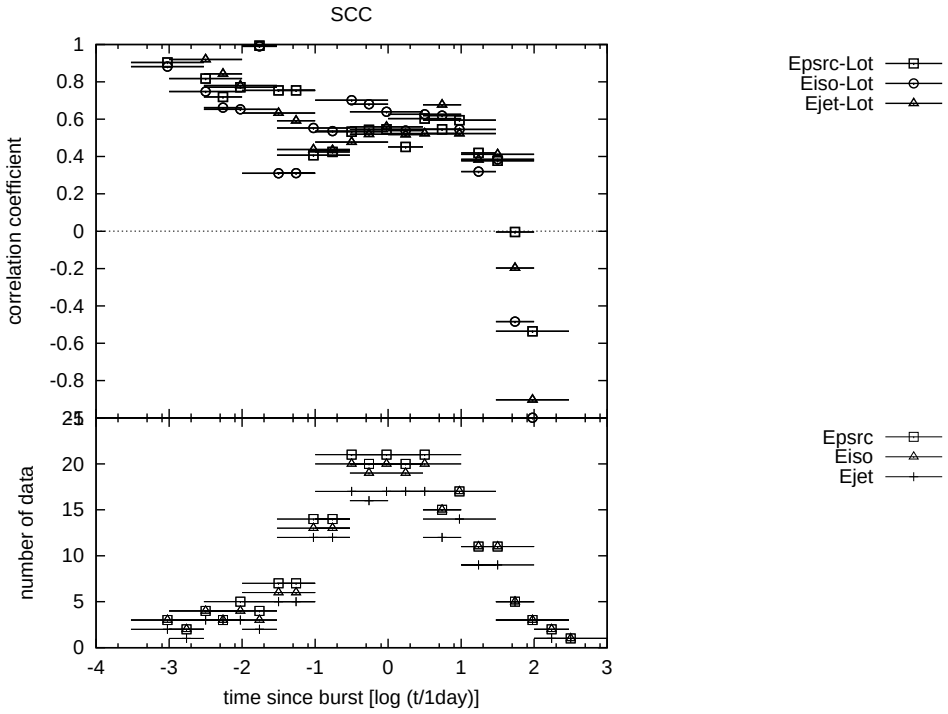

Figure 5.6: The summary of the significance of correlation in the source frame. Top: The significance evaluated with sample correlation coefficient r. Bottom: The number of data in each time interval.

the data value directly for the calculation. Therefore, the probability from Cox's method is strongly affected by points that lie outside of the cluster of other data points. On the other hand, BHK method does not use data values, but rather counts only the rank order of values of the data points. The scatter plot of OT luminosity vs. $E_{\rm iso}$ (top left panel of figure D.23) contains such a point.

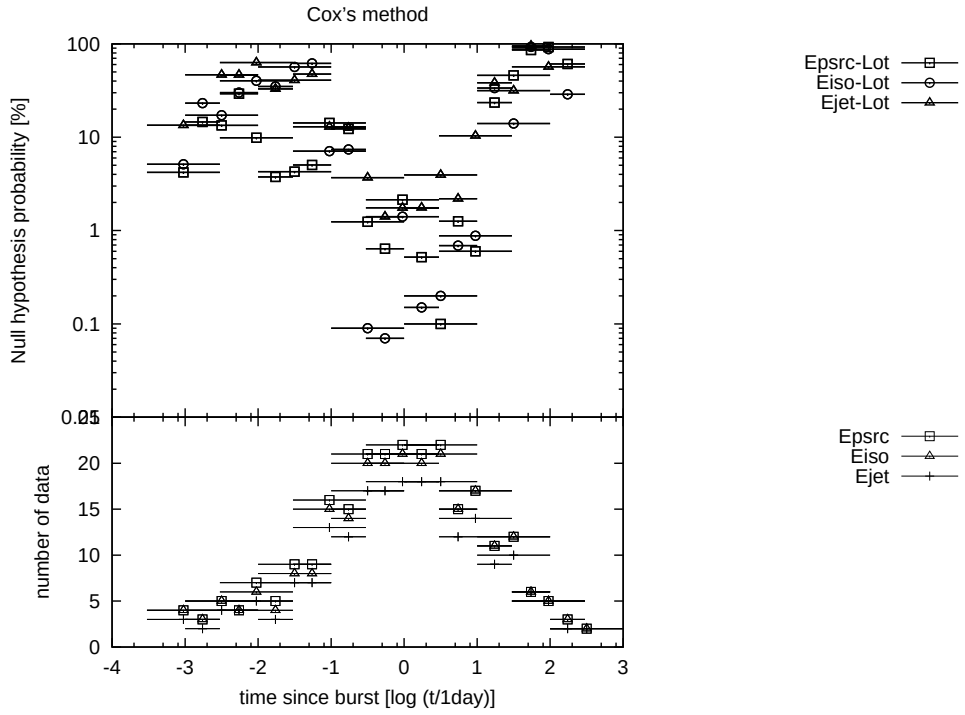

Figure 5.7: The summary of the significance of correlation in the source frame. Top: The significance evaluated with Cox's method. Bottom: The number of data in each time interval.

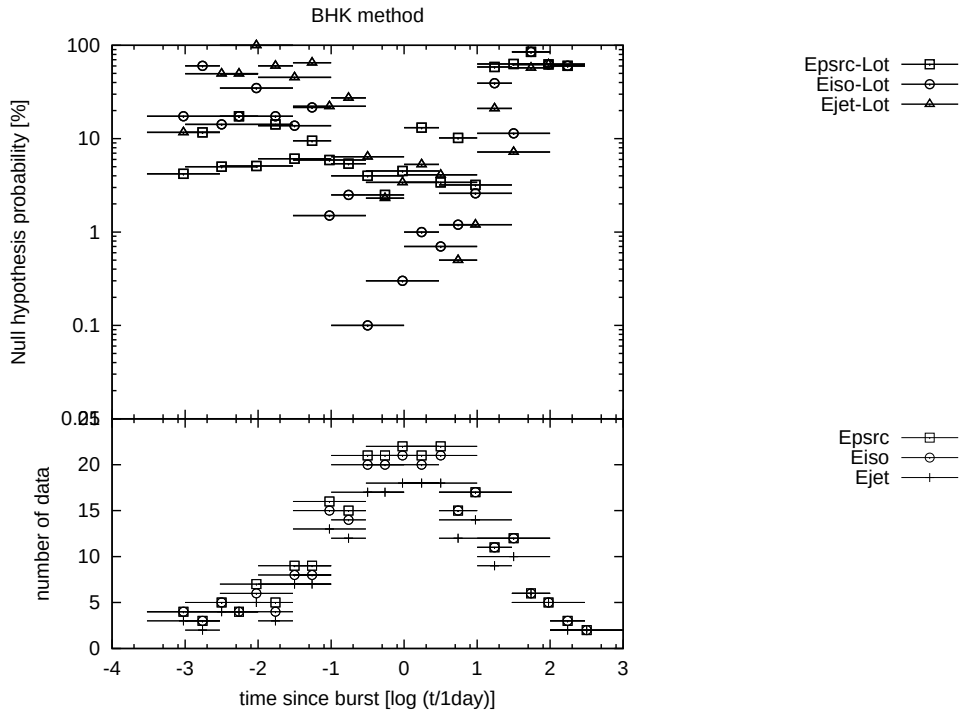

Figure 5.8: The summary of the significance of correlation in the source frame. Top: The significance is evaluated with BHK method. Bottom: The number of data in each time interval.

Chapter 6

Discussions

We have shown in the previous chapter that there are significant correlations between some properties of the prompt emission and the afterglow emission at certain epochs. In particular, we found a tight correlation between the isotropic-equivalent radiated energy in the prompt emission ($E_{\rm iso}$) and the luminosity of the optical afterglow in the time interval around 0.1–10 days after the burst, where both quantities are determined in the GRB source frame. In this chapter, we discuss the apparent dependence of the correlation significance on the elapsed time from the burst, and show that the lack of significant correlation at early and late epochs can arise from the small size of the measurement samples. Then, we present a physical interpretation for the newly found correlation between the radiated energy in the prompt emission and the luminosity of the optical afterglow. The kinetic energy of a relativistic shell is derived on the basis of the external shock model, and the energy conversion efficiency of the prompt emission is derived for the present sample of GRBs.

6.1 Influence of number of data upon the significance of the correlations

We find in figures 5.7 and 5.8, that the time intervals in which we obtain significant correlations correspond to the time intervals containing more copious data. In order to clarify the nature of the evolution of correlation, we studied the dependence of null hypothesis probability on the number of data samples. For this test, we took a real data set which shows a strong correlation, and we examined how the significance decreases as we reduce the number of data samples by randomly taking out samples.

We use the data of $E_{\rm iso}$ vs. luminosity of OTs. The number of data samples and null hypothesis probabilities for all time intervals are summarized in table 6.1. As examples of data sets with high significance and moderately high significance, we take the data in the time interval of 0.1–1 days and 0.3–3 days as the original sets of data. These data sets contain 20 and 21 data samples, respectively. The null hypothesis probability for existence of a correlation between $E_{\rm iso}$ and OT luminosity is 0.09% in the time interval of 0.1–1 days, and 1.41% in the 0.3–3 days.

Then we take away data points randomly from the original data set to form a reduced data subset and calculate the null hypothesis probability for lack of correlation. We repeat this calculation for all the subsets if the total number is smaller than 1000, and 1000 randomly picked different subsets if the number is larger. The null hypothesis probabilities thus calculated are plotted in figure 6.1 against the size of the subset (i.e. number of data samples in the subset). Comparison of this plot with the null hypothesis probabilities for the data sets with intrinsically

Time interval (days after the burst)		$E_{\rm iso}$ and $L_{\rm ot}$ Number of data	$E_{\rm iso}$ and $L_{\rm ot}$ Null hypothesis probability (%)	$E_{\rm jet}$ and $L_{\rm ot}$ Number of data	$E_{\rm jet}$ and $L_{\rm ot}$ Null hypothesis probability (%)
0.0003	0.003	4	5.14	3	13.45
0.001	0.003	3	23.19	2	NA
0.001	0.01	5	17.18	4	46.72
0.003	0.01	4	30.02	4	46.72
0.003	0.03	6	40.30	5	63.17
0.01	0.03	4	35.01	3	32.93
0.01	0.1	8	56.62	7	40.87
0.03	0.1	8	61.87	7	47.43
0.03	0.3	15	7.09	13	12.95
0.1	0.3	14	7.40	12	12.57
0.1	1	20	0.09	17	3.69
0.3	1	20	0.07	17	1.41
0.3	3	21	1.41	18	1.75
1	3	20	0.15	18	1.76
1	10	21	0.20	18	3.95
3	10	15	0.69	12	2.19
3	30	17	0.88	14	10.38
10	30	11	33.63	9	38.29
10	100	12	14.02	10	31.63
30	100	6	92.96	6	95.15
30	300	5	87.71	5	56.74
100	300	3	28.86	2	NA

Table 6.1: Number of data samples and null hypothesis probability for existence of correlation between $E_{\rm iso}$ or $E_{\rm jet}$ and luminosity of OTs. Cox's method is used for this calculation.

small sample size can help us understand the true "significance" for data sets with different number of data. For example, the time interval 0.03–0.3 day contains 15 $E_{\rm iso}$ vs. $L_{\rm ot}$ data points and the null hypothesis probability for lack of correlation in this time interval is 7.09%. None of the subsets with 15 samples taken from the data of 0.1–1 days produce such a large probability. So, the correlation in the 0.03–0.3 day time interval is likely to be weaker than in 0.1–1 day interval. On the other hand, 10.6% of the 15-sample subsets of 0.3–3 day produce a null hypothesis probability larger than 7.09%. therefore it is not certain whether the correlation is weaker in 0.03–0.3 day than 0.3–3 day. By comparing figure 6.1 and table 6.1, we find that the large null hypothesis probability of 10% or larger found for the time intervals with sample numbers of 14 or less, is actually possible for the subset of the sample of the 0.3–3 day interval if the size is reduced to the same number. This result shows that the lack of significance for the $E_{\rm jet}$-$L_{\rm ot}$ correlation at early (< 0.1 days) and later (> 10 days) may be due to the small sample size of the data.

6.2 Relation between $E_{\rm iso}$ or $E_{\rm jet}$ and $L_{\rm ot}$

As shown in the previous chapter, we found significant correlation between the isotropic radiated energy $E_{\rm iso}$ and the afterglow luminosity $L_{\rm ot}$, evaluated in the GRB source frame. In the

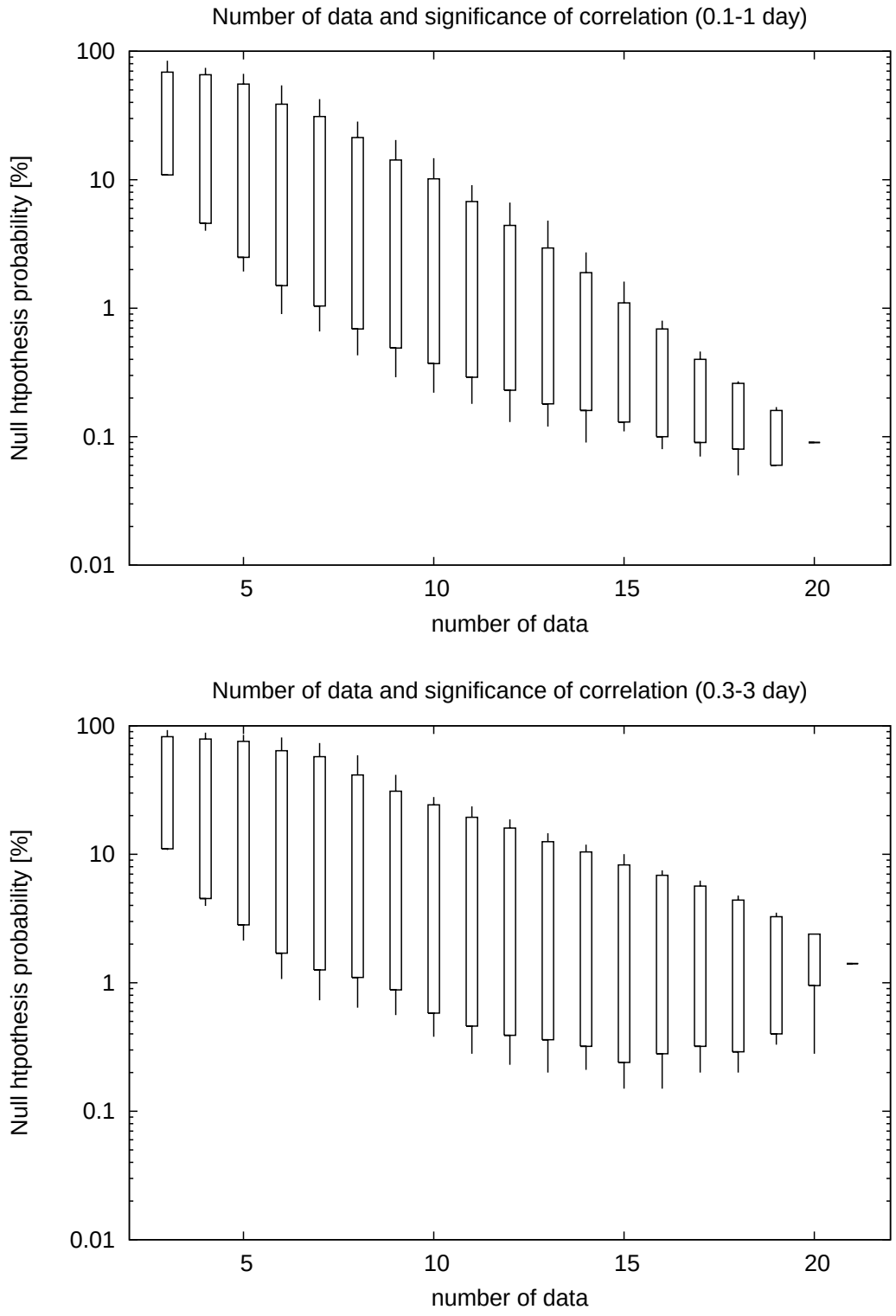

Figure 6.1: The null hypothesis probabilities of data set which was randomly picked up from the data set of $E_{\rm iso}$–$L_{\rm ot}$ of 0.1–1 day (top) and 0.3–3 day (bottom). The boxes and thin lines in the plots indicate the range of probability which contain 90% and 95% of the subsets, respectively.

previous section, we also found that the correlation between $E_{\rm jet}$ and $L_{\rm ot}$ ia as significant as the $E_{\rm iso}$–$L_{\rm ot}$ correlation, and that apparent difference of significance may be due to the difference of the number of samples.

We fit the data of $E_{\rm iso}$ and $L_{\rm ot}$ to the following formula, which assumes a power-law relation between the two quantities:

$$\log(L_{\rm ot}) = a \times \log(E_{\rm iso}) + b\,. \tag{6.1}$$

Here, $E_{\rm iso}$ is measured in units of 10^{52}ergs, and $L_{\rm ot}$ is normalized by $L0 = 10^{46}{\rm ergs\,s^{-1}}$. The results for the data sets which have a small value (less than 5%) of the null hypothesis probabilities of Cox's method are listed in table 6.2. If the luminosities of OTs are proportional to

Time interval		Number of data		Null hypothesis	a	b
		Detected	U. L.	probability (Cox)		
0.1	1	20	0	0.09	0.50 ± 0.12	-1.19 ± 0.16
0.3	1	19	1	0.07	0.47 ± 0.12	-1.42 ± 0.16
0.3	3	20	1	1.41	0.43 ± 0.12	-1.63 ± 0.16
1	3	19	1	0.15	0.47 ± 0.18	-1.98 ± 0.21
1	10	20	1	0.20	0.41 ± 0.12	-2.23 ± 0.16
3	10	15	0	0.69	0.40 ± 0.14	-2.47 ± 0.18
3	30	17	0	0.88	0.31 ± 0.12	-2.71 ± 0.15

Table 6.2: Results of fitting for the relation between $E_{\rm iso}$ and $L_{\rm ot}$. For the meaning of the parameters, see text.

Time interval		Number of data		Null hypothesis	a	b
		Detected	U. L.	probability (Cox)		
0.1	1	17	0	0.4	0.60 ± 0.28	-0.03 ± 0.39
0.3	1	16	1	0.3	0.67 ± 0.29	-0.18 ± 0.41
0.3	3	17	1	1.1	0.66 ± 0.25	-0.44 ± 0.35
1	3	17	1	1.9	0.60 ± 0.25	-0.79 ± 0.35
1	10	17	1	0.9	0.55 ± 0.23	-1.15 ± 0.32
3	10	12	0	1.4	0.71 ± 0.24	-1.10 ± 0.37

Table 6.3: Results of fitting for the relation between $E_{\rm jet}$ and $L_{\rm ot}$. For the meaning of the parameters, see text.

the radiated energy of prompt emissions, the coefficient a should be unity. All the values of a listed in table 6.2 are significantly smaller than unity (most of them are clustered around 0.4), which seems to indicate a non-linear relation between $L_{\rm ot}$ and $E_{\rm iso}$.

However, the radiation of the optical afterglow at these time intervals may not be collimated by relativistic beaming. Therefore, we should also compare the $L_{\rm ot}$ with $E_{\rm jet}$. We fit the $E_{\rm jet}$ and $L_{\rm ot}$ data with the same function. The results are listed in table 6.3. As we can see in 6.2 and 6.3, the coefficients a for the case of $E_{\rm jet}$ are larger than the case of $E_{\rm iso}$. This result can be naturally understood, because $E_{\rm jet}$ is clustered strongly around 10^{51} erg (Frail et al., 2001; Bloom et al., 2003b). For the case of $E_{\rm jet}$, the values of a are still smaller than unity. We note, however, that the small coefficient may be due to selection effects. In fact, there is only one data point at the low end of the $E_{\rm jet}$ distribution in figure 6.2 This same point is also the datum with the lowest OT luminosity. Considering that the luminosities of OTs for events with high

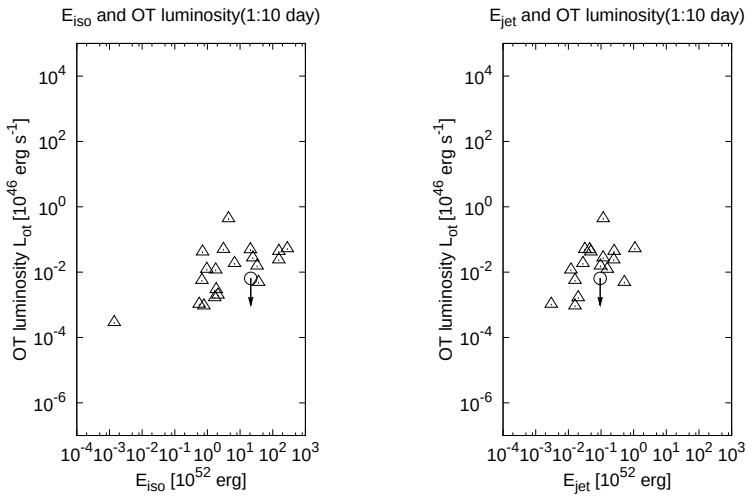

Figure 6.2: An example of scatter plot of $E_{\rm iso}$ and $L_{\rm ot}$ and $E_{\rm jet}$ and $L_{\rm ot}$.

$E_{\rm jet}$ are distributed over two orders of magnitude, it is quite possible that there are events with much dimmer OTs and low $E_{\rm iso}$, which do not appear in this plot because their redshift cannot be measured due to the faintness of their optical afterglows.

6.3 The efficiency of energy conversion

In this section, we further investigate the physical interpretation of the correlation between the radiated energy in the prompt emission ($E_{\rm iso}$ or $E_{\rm jet}$) and the luminosity of the optical afterglow ($L_{\rm ot}$).

From the results of the previous chapter, the time interval which corresponds to the most significant correlation is 0.1–1 day. However, we use the time interval of 1–10 days for this study for the following reasons. First, most of events of our sample have a jet break in the time interval of 1–10 days. Therefore we can compare $L_{\rm ot}$ with $E_{\rm jet}$ without worrying about relativistic beaming corrections for the data at late times. Second, in the following study, we assume the observing band (R-band) is lower than cooling frequency of synchrotron emission model. This assumption may not be applicable at < 1 day.

According to the fireball model with internal-external shock scenario, we can estimate kinetic energy of the fireball immediately after the prompt emission from the luminosity of the afterglow emission. The kinetic energy of fireball is given by equation (2.44) and (2.46).

The formula shows that the kinetic energy of a relativistic shell is related to the luminosity of the afterglow by

$$E_{\rm kinetic} \propto L^{4/(p+2)} \,. \tag{6.2}$$

On the other hand, we found a correlation between the luminosity of the optical afterglow $L_{\rm ot}$ and the total energy of prompt emission $E_{\rm iso}$ or $E_{\rm jet}$. Therefore there must be some correlation between $E_{\rm kinetic}$ and $E_{\rm iso}$ or $E_{\rm jet}$.

We use the luminosity at the time interval 1–10 days, which has the most significant correlation, and calculate the kinetic energy of the shell. We take $\epsilon_B = 0.01$, $\epsilon_e = 0.1$ and $p = 2.2$, as Lloyd-Ronning and Zhang (2004), $\nu = 4.6 \times 10^{14}$ (the center of R-band) and $t = 3$ day (the center of the time interval). Then we compare the kinetic energy with $E_{\rm iso}$ and $E_{\rm jet}$. Figure 6.3 shows the comparison of $E_{\rm kinetic}$ with $E_{\rm iso}$. There is only one event (XRF 020903) that

has $E_{\rm iso} < E_{\rm kinetic}$. However, most of the events have a jet break before 3 days. Therefore we

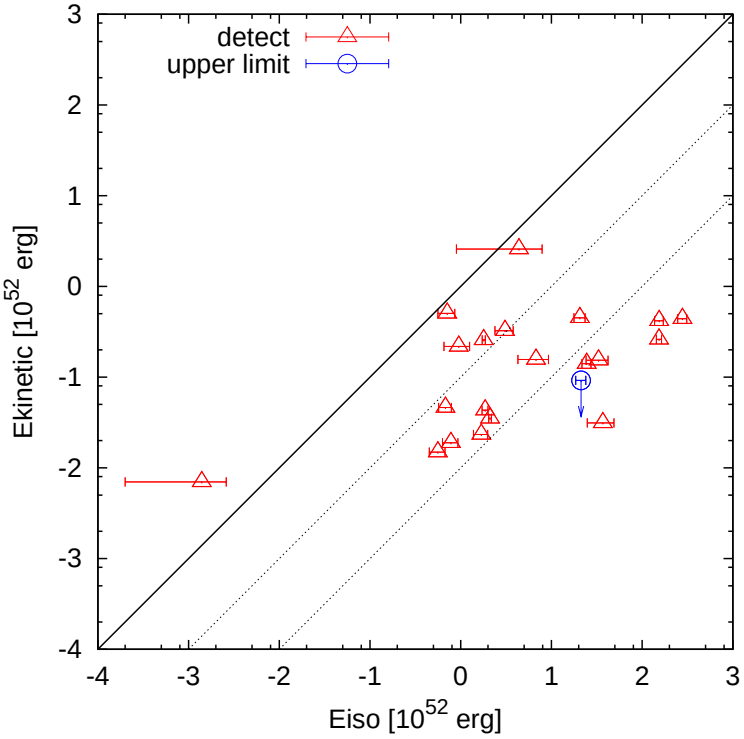

Figure 6.3: Isotropic total energy of prompt emission $E_{\rm iso}$ and kinetic energy of relativistic shell $E_{\rm kinetic}$. The solid black line represents $E_{\rm iso} = E_{\rm kinetic}$.

observed entire jet at 3 days and the kinetic energy of entire jet should be compared with $E_{\rm jet}$. Figure 6.4 shows the comparison of $E_{\rm kinetic}$ with $E_{\rm jet}$. From the figure, $E_{\rm jet}$ is comparable to the $E_{\rm kinetic}$ or at least 10% of $E_{\rm kinetic}$. We also plotted the $E_{\rm jet}$ and energy conversion efficiency ζ, which is $\zeta \equiv E_{\rm jet}/(E_{\rm kinetic} + E_{\rm jet})$.

Figure 6.5 shows the comparison of ζ from X-ray afterglows and optical afterglows. We summarize the values of $E_{\rm iso}$, $E_{\rm jet}$ and ζ in table 6.4.

Events with low efficiency

In the right panel of figure 6.5, there are several events which have low efficiencies while $E_{\rm jet}$ is moderately large (GRB990510, GRB021004, GRB030429, GRB970508 and GRB030329). We fid that these event have re-brightening or flat part in the light curve of optical afterglow (figure 6.6).

GRB 021004, which has the lowest efficiency, is known to have temporal variation from power-law decay of the light curve of its optical afterglow. There are plateaus around 0.5 day and 1 day (figure 6.6, left middle). These variations from power-law decay are interpreted as energy injection from the central engine at the afterglow phase (Fox et al., 2003b), which is referred to as a "refreshed shock" (Rees and Meszaros, 1998).

GRB 990510 has a re-brightening at $\sim$ 0.7 day (figure 6.6, left top) and GRB 030429 is almost flat from 0.7 day to 1.7 day (figure 6.6, right top). OT of GRB970508 was almost same magnitude from 0.2 to 0.9 day and then brightened by 1.6 magnitude until 2 days (figure 6.6, right middle). GRB 030329 was almost flat around 1 day and 10 days (figure 6.6, bottom).

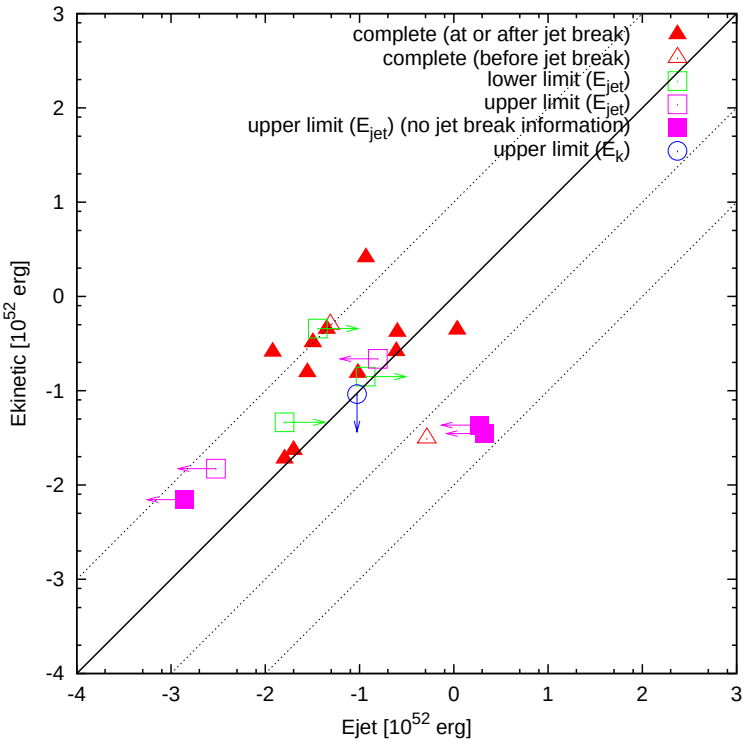

Figure 6.4: Jet corrected total energy of prompt emission $E_{\rm jet}$ and kinetic energy of relativistic shell $E_{\rm kinetic}$. The solid black line represents $E_{\rm jet} = E_{\rm kinetic}$. The red filled triangles are the events which have jet break before 10 days. The red open triangles are the events which have jet break after 10 days. The green and magenta open square represents the event which only have lower limit or upper limit of jet break time. The lower limit and upper limit of jet break time gives the lower limit and upper limit of $E_{\rm jet}$. For the events without jet break information, we plotted $E_{\rm iso}$ with magenta filled square, which also give the upper limit of total energy of prompt emission.

GRB name	$E_{\rm iso}$ [10^{52}erg]		$m_{\rm OT}$ [mag]	$L_{\rm ot}$ [10^{46}erg/s]	$E_{\rm kinetic}$ [10^{52}erg]	$E_{\rm jet}$ [10^{52}erg]	$t_{\rm jet}$ [day]	ζ
complete (at or after jet break)								
GRB990123	278.3	± 31.5	21.8	0.048	0.441	1.088	2.04	0.712
GRB990510	20.6	± 2.9	21.8	0.049	0.450	0.045	1.57	0.091
GRB990712	0.78	± 0.15	22.6	0.001	0.019	0.016	1.60	0.458
GRB010222	154.2	± 17	21.7	0.043	0.418	0.252	0.93	0.376
GRB020813	153.5	± 10	21.9	0.024	0.261	0.245	0.43	0.484
GRB021004	4.395	± 3.5	20.5	0.398	2.583	0.117	7.60	0.043
GRB021211	1.684	± 0.3	24.2	0.002	0.023	0.020	1.4	0.462
GRB030226	6.766	± 2.5	23.4	0.019	0.156	0.028	1.04	0.152
GRB030328	33.1	± 9	22.9	0.015	0.154	0.096	0.80	0.385
GRB030329	1.795	± 0.07	17.5	0.012	0.257	0.012	0.48	0.046
GRB030429	3.084	± 0.7	23.1	0.050	0.325	0.032	2.00	0.090
complete (before jet break)								
GRB970508	0.71	± 0.15	20.3	0.038	0.503	0.049	25.0	0.089
GRB020124	36.85	± 12	26.1	0.005	0.031	0.518	15.0	0.943
$E_{\rm jet}$ lower limit								
GRB971214	24.5	± 2.8	24.5	0.025	0.141	0.116	>2.50	>0.452
GRB980613	0.68	± 0.11	23.6	0.004	0.046	0.016	>3.10	>0.257
GRB030323	7.239	—	22.1	0.223	0.456	0.036	>1.40	>0.073
$E_{\rm jet}$ upper limit								
GRB980326	0.56	± 0.11	24.7	0.001	0.015	0.003	<0.40	<0.168
GRB010921	0.954	± 0.3	19.9	0.012	0.218	0.156	<33.0	<0.417
$E_{\rm jet}$ upper limit (no jet-break report)								
GRB970228	1.86	± 0.14	22.7	0.003	0.043	—	—	<0.977
GRB020903	1.4E-3	±1.2E-3	22.5	0.0003	0.007	—	—	<0.167
GRB041006	2.105	± 0.071	23	0.002	0.035	—	—	<0.984
$E_{\rm kinetic}$ upper limit								
GRB990705	21.2	± 2.7	>22.3	0.007	<0.092	0.094	1.00	>0.505

Table 6.4: The summary of $E_{\rm iso}$, $E_{\rm jet}$ and ζ. OT magnitude and $L_{\rm ot}$ are the value of the time interval 1–10 days. $t_{\rm jet}$ is the observed jet break time.

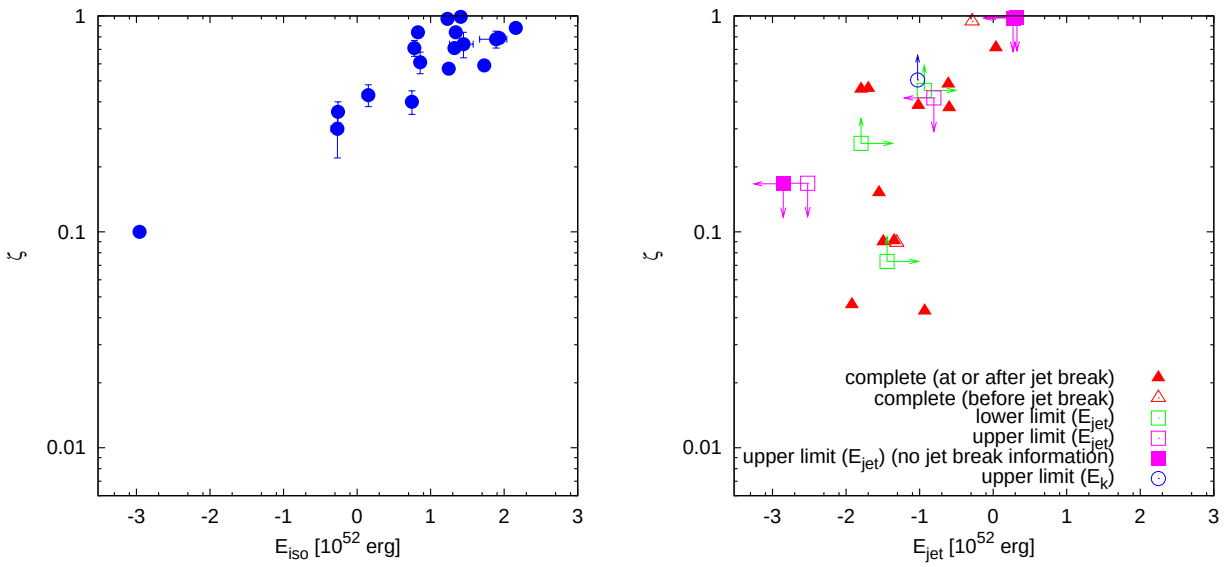

Figure 6.5: Left: Isotropic total energy $E_{\rm iso}$ and energy conversion efficiency in prompt emission. The result of X-ray afterglow (Lloyd-Ronning and Zhang, 2004). Right: Jet corrected total energy of prompt emission $E_{\rm jet}$ and energy conversion efficiency in prompt emission. The result of optical afterglow (this work).

If energy injection at late time occurs, the luminosity of the afterglow becomes higher and the estimated kinetic energy becomes larger than the kinetic energy of the relativistic shell just after the prompt emission. This may be the explanation for the low efficiency.

Efficiency and internal shock model

The efficiencies derived from both X-ray afterglows and optical afterglows are distributed around 10–100%. In the internal shock scenario, it is not straightforward to achieve such a high efficiency. The efficiency of energy conversion ϵ is derived from energy and momentum conservation for the inelastic collision of relativistic shells (Piran, 1999). For internal shocks, we assume that the Lorentz factor of fast and slow shells (Γ_f and Γ_s) satisfy $\Gamma_f \gtrsim \Gamma_s \gg 1$. In this case the maximum efficiency is given by

$$\epsilon = 1 - \frac{(m_f + m_s)\Gamma_m}{m_f\Gamma_f + m_s\Gamma_s}\,, \tag{6.3}$$

where m_f and m_s are the mass of the fast and slow shells, respectively, and Γ_m is the Lorentz factor of merged shell, which may be written as

$$\Gamma_m = \sqrt{\frac{m_f\Gamma_f + m_s\Gamma_s}{m_f/\Gamma_f + m_s/\Gamma_s}}\,. \tag{6.4}$$

Figure 6.7 shows an example of the energy conversion efficiency as a function of the ratio of Lorentz factor of fast and slow shells. The following conditions are needed for high efficiency:

1. the slow shell is ejected earlier than the fast shell,
2. the Lorentz factor of the fast shell is much larger than that of the slow shell ($\Gamma_f \gg \Gamma_s$),
3. the masses of two shells are similar.

These conditions present severe constraints on the mechanism of relativistic jet production.

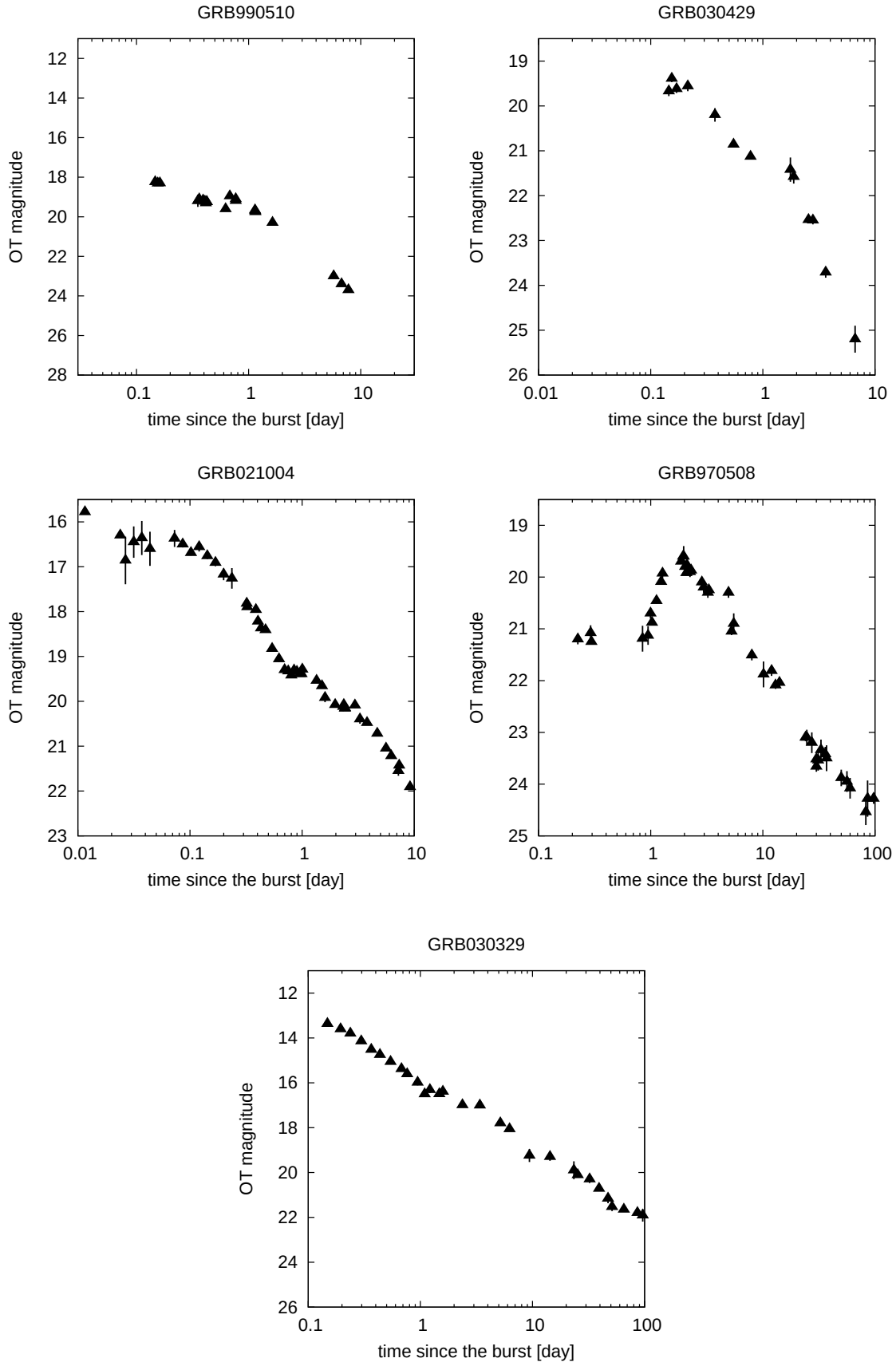

Figure 6.6: The indications of refreshed shock. The R-band light curves of afterglows which exhibit re-brightening or plateau; GRB990510(left top), GRB030429(right top), GRB021004(left middle), GRB970508(right middle) and GRB030329(bottom).

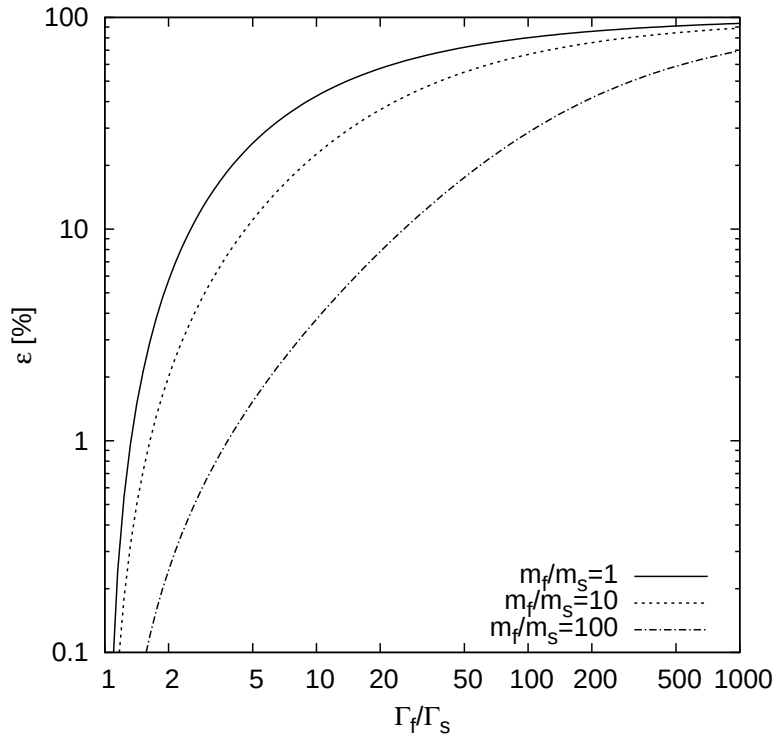

Figure 6.7: Efficiency of energy conversion for inelastic collision of relativistic shells. The horizontal axis is the ratio of Lorentz factor of fast and slow shells. The vertical axis is the percentage of the energy conversion efficiency. The energy conversion efficiency depends on the ratio of the mass of fast shell m_f to the mass of slow shell m_s.

Chapter 7

Conclusions

Based on the study of correlation between prompt emission and optical afterglows of 51 GRBs, we obtained the following results.

- There is persuasive evidence for a correlation between prompt fluence and magnitude of OTs especially at epochs earlier than 0.1 day after the burst. The null hypothesis probability for lack of correlation is as small $\sim 1\%$ for the most significant time interval.
- There is a good correlation between radiated total energy in prompt emission under the assumption of isotropic emission $E_{\rm iso}$ and luminosity of optical transient $L_{\rm ot}$. The probability for lack of correlation is as small as $\sim 0.1\%$ for the most significant time interval.
- For the correlation between properties in the source frame ($E_{\rm iso}$ vs. $L_{\rm ot}$, jet corrected total energy $E_{\rm jet}$ vs. $L_{\rm ot}$, and spectral peaking energy in the source frame $E^{\rm src}_{\rm peak}$ vs. $L_{\rm ot}$), the probability of null hypothesis is lowest at the time interval of 0.1 – 10 days. This is partly because the number of samples is largest at this time interval.

The study of relation between $L_{\rm ot}$ and $E_{\rm jet}$ reveals the possible existence of a non-linear relation. However, this may due to the selection effects, and confirmation with a large sample containing more faint OTs is required.

From the luminosity of the optical afterglow at the time interval of 1–10 days, we calculated the kinetic energy of the relativistic shell $E_{\rm kinetic}$ based on the fireball model. We find that $E_{\rm kinetic}$ and $E_{\rm jet}$ are comparable.

The efficiency of energy conversion $\zeta \equiv E_{\rm jet}/(E_{\rm kinetic} + E_{\rm jet})$ is typically above 10%. Such high efficiencies require special conditions in the internal shock scenario.

The bursts with $\zeta < 10\%$ exhibit re-brightening or a plateau in the light curves of their optical afterglows. This result can be understood as a effect of refreshed shock, which rebrightens the optical afterglow.

Appendix A

Statistical analysis of data containing upper limits

Our data of optical afterglow usually contain upper limits. In order to deal with these data, we use statistical method.

From the statistical point of view, these problems are studied as "survival analysis" since 1980's. Data which have only limits are called "censored data".

In this chapter, we introduce statistical method used for our analysis. More detailed explanations are provided by Isobe et al. (1986) or Schmitt (1985).

A.1 General notations for statistics and survival analysis

left censored and right censored

Data with upper limits are called right censored data, and data with lower limits are called left censored data. Various procedure dealing with censored data are developed to handle right censored data. On the other hand, the astronomical data generally contain upper limits due to the detection limit. For these data, it is convenient to convert left censored data to right censored data by subtraction. For example, using some constant M, the left censored data Y_i^L can be converted into right censored data Y_i^R as

$$Y_i^R = M - Y_i^L \,. \tag{A.1}$$

However, according to the definition of "magnitude" of optical data, they are already converted into right censored form. Thus we can use the upper limit of the magnitude as it is.

probability density function, distribution function, survival function and hazard function

In our analysis, we expect more or less linear relation between two values; i.e. $Y_i = a + bX_i$. We define residual z_i by

$$z_i = \frac{1}{\sigma}\left[Y_i - (a + bX_i)\right] \,, \tag{A.2}$$

where σ is an appropriately defined dispersion. If $f(z_i)$ is the probability density function of z_i, the distribution function is

$$F(z_i) = \Pr(Z \leq z_i) = \int_{-\infty}^{z_i} f(t)\, dt \,, \tag{A.3}$$

where Pr means "probability of," and we assume that measurements are continuous. This is the probability that the object detected at or before z_i.

The survival function $S(z_i)$ is defined as

$$S(z_i) = \Pr(Z \geq z_i) = 1 - F(z_i)\,, \tag{A.4}$$

and it means the probability that the object is not detected until z_i.

Another important function is the hazard function $\lambda(z_i)$ defined as

$$\begin{aligned} \lambda(z_i) &= \lim_{\Delta z \to 0} \frac{1}{\Delta z} \left[\Pr(z_i \leq Z \leq z_i + \Delta z | Z \geq z_i)\right] && \text{(A.5)} \\ &= \frac{f(z_i)}{S(z_i)}\,, && \text{(A.6)} \end{aligned}$$

and it is the instantaneous rate of detection at z_i, given that the object is not detected before z_i.

risk set

The risk set $R(z_i)$ is the data set containing all data points which are have not been detected before z_i. The risk set of censored values are not used.

A.2 Cox's proportional hazard model

Cox's proportional hazard model is one of the nonparametric method (Cox, 1972). Cox assumes that the hazard function can be expressed in the form,

$$\lambda(\boldsymbol{Y}_i;\, \boldsymbol{X}_i) = \lambda_0(\boldsymbol{Y}_i) e^{\boldsymbol{\beta}\cdot\boldsymbol{X}_i} \tag{A.7}$$

where $\boldsymbol{Y}_i$ is the dependent variable, $\boldsymbol{X}_i$ is the independent variable (the vector permits many covariants), and $\boldsymbol{\beta}$ is a vector of regression coefficients.

To derive a likelihood for the data set and and estimate of the regression coefficient $\boldsymbol{\beta}$, let us first order the $\boldsymbol{Y}$'s; $\boldsymbol{Y}_1 < \boldsymbol{Y}_2 < \cdots < \boldsymbol{Y}_n$. For convenience, assume no ties. Since $\lambda(\boldsymbol{Y}_i;\, \boldsymbol{X}_i)$ is the instantaneous detection rate, integration in the range $[\boldsymbol{Y}_i,\, \boldsymbol{Y}_i + \boldsymbol{\Delta Y}]$, gives

$$\begin{aligned} \Pr[\text{ a detection in } (\boldsymbol{Y}_\mathrm{i},\, \boldsymbol{Y}_\mathrm{i} + \boldsymbol{\Delta Y}) | \mathrm{R}(\boldsymbol{Y}_\mathrm{i})] &= \sum_{j \in R(\boldsymbol{Y}_i)} \int_{\boldsymbol{Y}_i}^{\boldsymbol{Y}_i + \boldsymbol{\Delta Y}} \lambda_0(t) e^{\boldsymbol{\beta}\cdot\boldsymbol{X}_j}\, dt && \text{(A.8)} \\ &\approx \sum_{j \in R(\boldsymbol{Y}_i)} \lambda_0(\boldsymbol{Y}_i) e^{\boldsymbol{\beta}\cdot\boldsymbol{X}_j} \boldsymbol{\Delta Y}\,. && \text{(A.9)} \end{aligned}$$

Therefore the "conditional probability" that the i th data point is detected at $\boldsymbol{Y}_i$, under the condition that a detection in $R(\boldsymbol{Y}_i)$ occurs at $\boldsymbol{Y}_i$, is

$$P_i = \lambda_0(\boldsymbol{Y}_i;\, \boldsymbol{X}_i) / \sum_{j \in R(\boldsymbol{Y}_i)} \lambda_0(\boldsymbol{Y}_i;\, \boldsymbol{X}_j) \tag{A.10}$$

or

$$\begin{aligned} P_i &= \lambda_0(\boldsymbol{Y}_i) e^{\boldsymbol{\beta}\cdot\boldsymbol{X}_i} \boldsymbol{\Delta Y} / \sum_{j \in R(\boldsymbol{Y}_i)} \lambda_0(\boldsymbol{Y}_i) e^{\boldsymbol{\beta}\cdot\boldsymbol{X}_j} \boldsymbol{\Delta Y} && \text{(A.11)} \\ &= e^{\boldsymbol{\beta}\cdot\boldsymbol{X}_i} / \sum_{j \in R(\boldsymbol{Y}_i)} e^{\boldsymbol{\beta}\cdot\boldsymbol{X}_j}\,. && \text{(A.12)} \end{aligned}$$

Note that this probability does not depend on the baseline hazard function, but depends on the Y values only in determining the censored status. Taking a product of those conditional probabilities, we get Cox's so-called conditional likelihood

$$L = \prod_{\boldsymbol{D}_i} \left[e^{\boldsymbol{\beta}\cdot\boldsymbol{X}_i} / \sum_{j \in R(\boldsymbol{Y}_i)} e^{\boldsymbol{\beta}\cdot\boldsymbol{X}_j} \right] , \tag{A.13}$$

where $\boldsymbol{D}_i$ denote the detected points.

To test for the existence of a correlation, Cox suggests a Rao-type asymptotic form for

$$\chi^2_r = \boldsymbol{S}' \boldsymbol{I}^{-1} \boldsymbol{S} \tag{A.14}$$

with

$$\boldsymbol{S} = \frac{\partial}{\partial \boldsymbol{\beta}} \log L(\boldsymbol{\beta}) , \tag{A.15}$$

$$\boldsymbol{I} = -\frac{\partial^2}{\partial \boldsymbol{\beta}^2} \log L(\boldsymbol{\beta}) , \tag{A.16}$$

where r denotes the degree of freedom given by the number of covariates and the prime denotes transpose of the vector.

Specifically, we will use the formula under the condition $r = 1$ and $\boldsymbol{\beta} = b = 0$

$$\boldsymbol{S}(\boldsymbol{\beta} = 0) = \sum_{D_i}^{m} \left\{ X_i \left[1 / \sum_{j \in R(\boldsymbol{Y}_i)} 1 \right] \sum_{j \in R(\boldsymbol{Y}_i)} X_j \right\} , \tag{A.17}$$

$$\boldsymbol{I}(\boldsymbol{\beta} = 0) = \sum_{D_i}^{m} \left[- \left\{ \left(\sum_{j \in R(\boldsymbol{Y}_i)} X_j \right)^2 / \left(\sum_{j \in R(\boldsymbol{Y}_i)} 1 \right)^2 \right\} + \left\{ \sum_{j \in R(\boldsymbol{Y}_i)} X_j^2 / \left(\sum_{j \in R(\boldsymbol{Y}_i)} 1 \right) \right\} \right] \tag{A.18}$$

where m is the number of detected points. The significance level of χ^2 can be found from standard tables.

A.3 BHK method

Brown et al. suggested another method that can consider the samples of upper limits. First we have to determine the matrix of $(m+n) \times (m+n)$, where m is a number of detected data and n is a number of limit data. For the X, we determine a_{ij} as the following:

$$a_{ij} = \begin{cases} -1 & (X_i < X_j) \\ 0 & (X_i = X_j \text{ or unknown}) \\ 1 & (X_i > X_j) \end{cases} . \tag{A.19}$$

In the case of $X_i > X_j$, if both are detected, $a_{ij} = 1$. If X_i is upper limit, a_{ij} should be 0. If X_j is upper limit, a_{ij} is then 1. For the Y we determine b_{ij} in the same way. Then we calculate

$$S = \sum_{i}^{N} \sum_{j}^{N} a_{ij} b_{ij} \tag{A.20}$$

where $N = m + n$ and

$$\begin{aligned} Var(S) &= C_1 \left(\sum_i^N \sum_j^N \sum_k^N a_{ij} a_{ik} - \sum_i^N \sum_j^N a_{ij} a_{ij} \right) \left(\sum_i^N \sum_j^N \sum_k^N b_{ij} b_{ik} - \sum_i^N \sum_j^N b_{ij} b_{ij} \right) \\ &\quad + C_2 \left(\sum_i^N \sum_j^N a_{ij} a_{ij} \right) \left(\sum_i^N \sum_j^N b_{ij} b_{ij} \right), \end{aligned} \tag{A.21}$$

where $C_1 = \frac{4}{N(N-1)(N-2)}$ and $C_2 = \frac{2}{N(N-1)}$. A standard normal score z is given by $S/[Var(S)]^{1/2}$. Then null hypothesis probability is found from a table of the integrated Gaussian distribution.

Appendix B

The study of Localization accuracy using XRBs in 2002

B.1 Introduction

The Wide-field X-ray Monitor (WXM) on board HETE-2 is the primary instrument for determining the position of celestial events and has ~ 60 deg $\times$ 60 deg field of view (Shirasaki et al., 2000).

The HETE-2 satellite generally points toward anti-solar direction. Therefore X-ray sources which lie in the Galactic center region come into the WXM field of view in May and go out in September Sakamoto et al. (2003). During the Summer of 2002 WXM has detected more than 300 X-ray events and localized 208 of them. Because the positions of XRB sources are well known, these events could be used for verifying the localization accuracy of WXM.

B.2 Results

Among all the candidate of XRB events, 208 were localized to known X-ray burst sources. The summary of these events is shown in table 1.

Using these events, we studied localization accuracy of WXM. To evaluate localization accuracy, we define $\Delta\theta$ as angular distance from localized position to the position in a catalog.

Figure 1 show the localization accuracy for events with large (> 20 deg) and small (< 20 deg) distances (r) from the center of the field of view of WXM.

Because WXM adopts the coded mask cross correlation method for localization, we usually use "image SN", which is the signal to noise ratio of cross correlation maximum, for evaluating goodness of localization. The other parameter for evaluating goodness of localization is "light curve SN", which is signal to noise ratio of the integrated counts in the burst light curve.

WXM is composed of two sets of one-dimensional position-sensitive detector in X-direction and Y-direction, therefore, image SN or light curve SN are calculated for X and Y individually. Here, we use RMS of X and Y values. Image SN and light curve SN are reported in GCN notice as WXM_IMAGE_SN and WXM_LC_SN, because these values can be important indicator of localization reliability.

Figure 2, 3, 4 show the relation between image SN or light curve SN and localization accuracy. (See figure captions.)

We can conclude that the WXM can localize blight event within about 0.2deg accuracy.

Table B.1: The summary of the number of the XRB events.

XRB sources	**Number of events**
GS1826-238	109
NGC6712	28
NGC6624	18
X1728-34	16
X1916-053	8
TERZAN5	7
NGC6652	6
X1812-121	6
X1730-333	3
X1724-307	2
X1755-338	2
X1608-522	1
X1702-429	1
NGC6441	1
Total	**202**

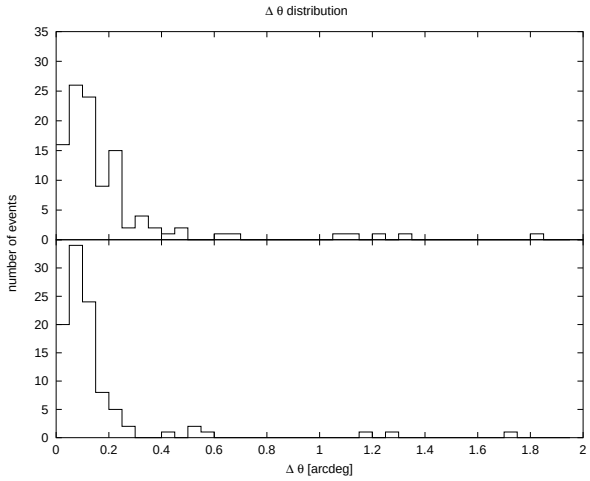

Figure B.1: The localization accuracy for events with large ($> 20\,\mathrm{deg}$) and small ($< 20\,\mathrm{deg}$) distances (r) from the center of the field of view of WXM are plotted. The horizontal axis is the difference from the position in the catalog ($\Delta\theta$). The vertical axis is the number of events. The upper panel is the case of $r > 20\,\mathrm{deg}$ and the lower is $r < 20\,\mathrm{deg}$.

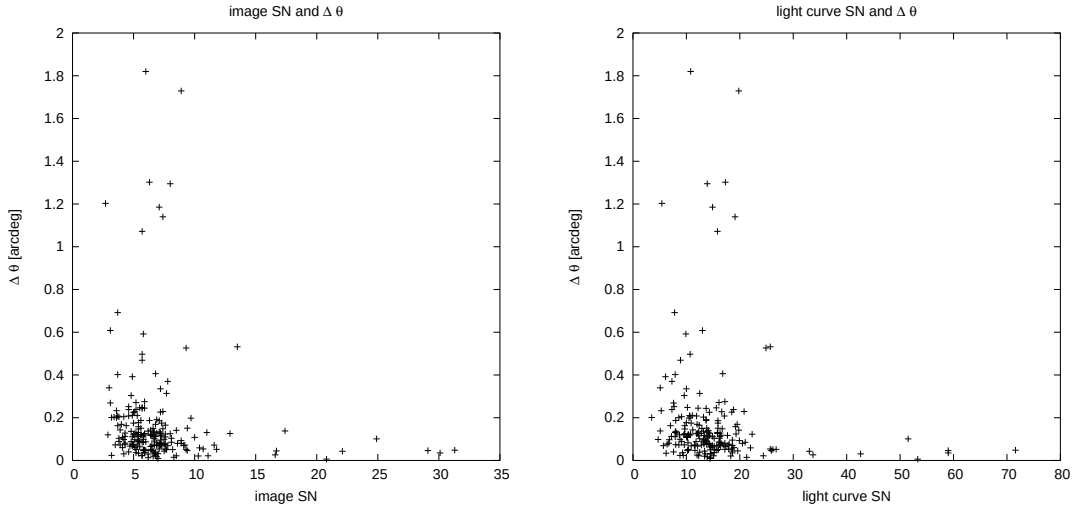

Figure B.2: Image SN (left) or light curve SN (right) and $\Delta\theta$ are plotted. The events with high image SN or high light curve SN are well localized.

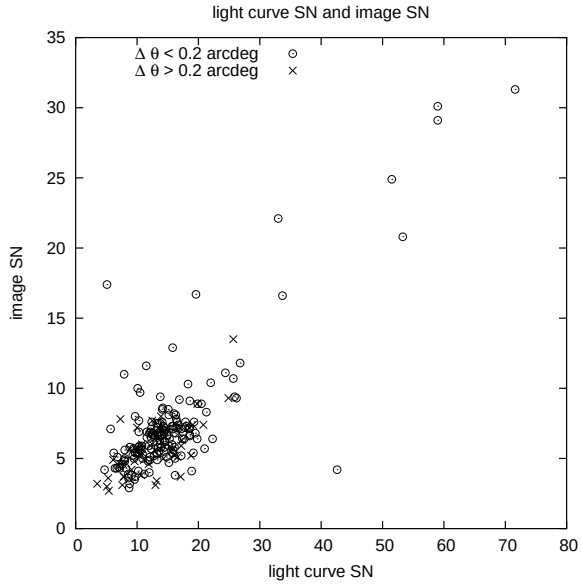

Figure B.3: Light curve SN and image SN for well localized ($\Delta\theta < 0.2\,\mathrm{deg}$) or not well localized ($\Delta\theta > 0.2\,\mathrm{deg}$) events are plotted. From this figure, we can see the events with high image SN are well localized even if light curve SN is relatively low.

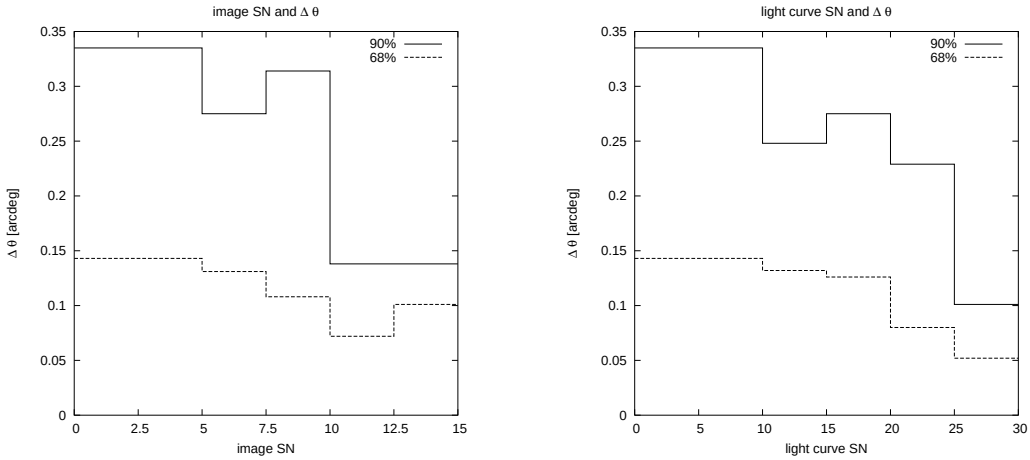

Figure B.4: Distribution of $\Delta\theta$ is shown using 90 percentile and 68 percentile value against image SN (left) and light curve SN (right). 90% (68%) of the events with the given SN lie below the solid (dashed) line. This figure shows the events with image SN > 10 or light curve SN > 25 can be well localized. From this figure, we can conclude 90% of these events are localized with difference within 0.35deg. We note that all of these events are localized to known XRB sources. There are a large number ($\sim 30\%$) of events with small SN which could not be localized. These dim events are localized to random position in the field of view. Taking account of these events, $\delta\theta$ in low SN should be raised.

Appendix C

How to calculate durations

C.1 temporal analysis

The main purpose of temporal analysis is to examine how long the burst activities last. There are at least two way to express the length of burst activity. One is called "duration" and the other is "emission time". The definition of duration T_{50} and emission time τ_{50} are shown schematically in Figure C.1.

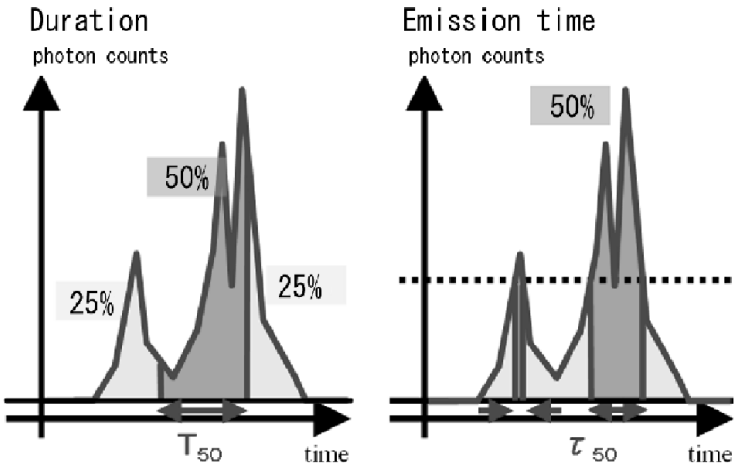

Figure C.1: Schematic picture of definitions of duration T_{50} (left) and emission time τ_{50} (right).

C.1.1 duration T_{50} and T_{90}

definition

Duration T_{50} (T_{90}) is the time during which the burst integrated counts increases from 25% (5%) to 75% (95%) of total counts $C_{\rm tot}$ (Kouveliotou et al., 1993; Fishman et al., 1994).

To calculate T_{50} or T_{90}, we adopt the following procedure.

1. fit background region
2. subtract background counts
3. sum background subtracted counts

4. select base region before and after the burst
5. calculate base levels (l_1 and l_2)
6. calculate total counts of the burst $C_{\rm tot} \equiv l_2 - l_1$
7. calculate duration and its errors

We define the time of the r% of the total count as

$$t_r = t\left(l_1 + \frac{r}{100} \times C_{\rm tot}\right). \tag{C.1}$$

how to define background region

We select background region by eye. Then fit background region and produce background subtracted data. Next, we produce time sequence of integrated counts and plot it. At last, we examine the plot whether the plot have the part of stable counts before and after the burst (base region) or not. If we cannot see such a stable part, we re-define background region and repeat the same procedure to find base regions.

statistical errors of T_{50} and T_{90}

There are two kind of errors to consider. One comes from an error of 50% (or 90%) region and the other comes from background fluctuation.

The former is defined with the total count of the burst $C_{\rm tot}$ as

$$\sigma_{c_{50}} = \sqrt{C_{\rm tot} \times 0.25 \times 0.75} \tag{C.2}$$

for $\rm T_{50}$ and

$$\sigma_{c_{90}} = \sqrt{C_{\rm tot} \times 0.05 \times 0.95} \tag{C.3}$$

for $\rm T_{90}$.

The latter is defined with the standard deviation of the count sum s_i in base region [t_1, t_2] and [t_3, t_4], i.e.

$$\sigma_B = \sqrt{\frac{\sum_{i=I+1}^{I+p}(s_i - l_0)^2 + \sum_{i=F+1}^{F+q}(s_i - l_{100})^2}{p+q}}. \tag{C.4}$$

The total error of counts is

$$\sigma_{c_{50,B}} = \sqrt{\sigma_{c_{50}}^2 + \sigma_B^2} \tag{C.5}$$

for $\rm T_{50}$ and

$$\sigma_{c_{90,B}} = \sqrt{\sigma_{c_{90}}^2 + \sigma_B^2} \tag{C.6}$$

for $\rm T_{90}$.

Then we calculate error region $[t_{rl}, t_{ru}]$ as

$$t_{rl} = t\left(l_1 + \frac{r}{100} \times C_{\rm tot} - \sigma_{c_{d,B}}\right) \tag{C.7}$$

$$t_{ru} = t\left(l_1 + \frac{r}{100} \times C_{\rm tot} + \sigma_{c_{d,B}}\right) \tag{C.8}$$

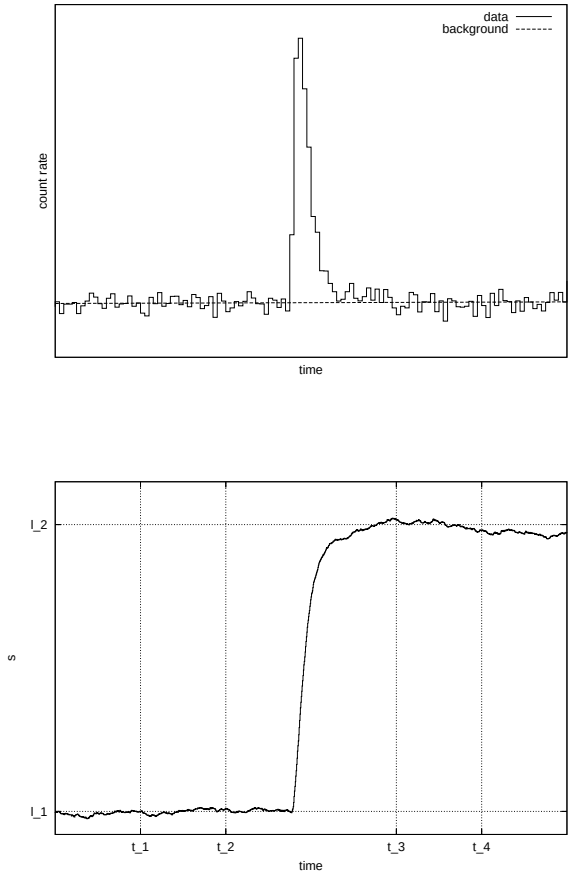

Figure C.2: Schematic picture of the background fitting (left) and integrated counts of background subtracted data (right).

where the suffix d is replaced with 50 or 90. Finally, we define the error of duration as

$$\sigma_d = \sqrt{\sum_r \Delta t_r^2} \tag{C.9}$$

$$\Delta t_r^2 = (t_r - t_{rl})^2 + (t_r - t_{ru})^2 \tag{C.10}$$

where r will be 25 and 75 for T_{50} and 5 and 95 for T_{90}.

Appendix D

Scatter plots

This chapter includes the scatter plots of the combination of properties of prompt emissions and properties of afterglows for which we investigate the significance of correlation in chapter 5.

D.1 Properties of observer frame

The first section contains the scatter plots of the properties in the observer frame, that is the following combination:

- OT magnitude vs. $E_{\rm peak}$,
- OT magnitude vs. $S_{\rm total}$,
- OT magnitude vs. $S_{\rm X}$,
- OT magnitude vs. S_{γ} .

Each combination has 23 plots (4 pages) which correspond to 23 time intervals of OT observation. The plots are aligned in order of earliness of the time interval from the top left to the bottom right. Open triangles in the plots are data of detected OTs and open circles with arrows are U.L. of OT.

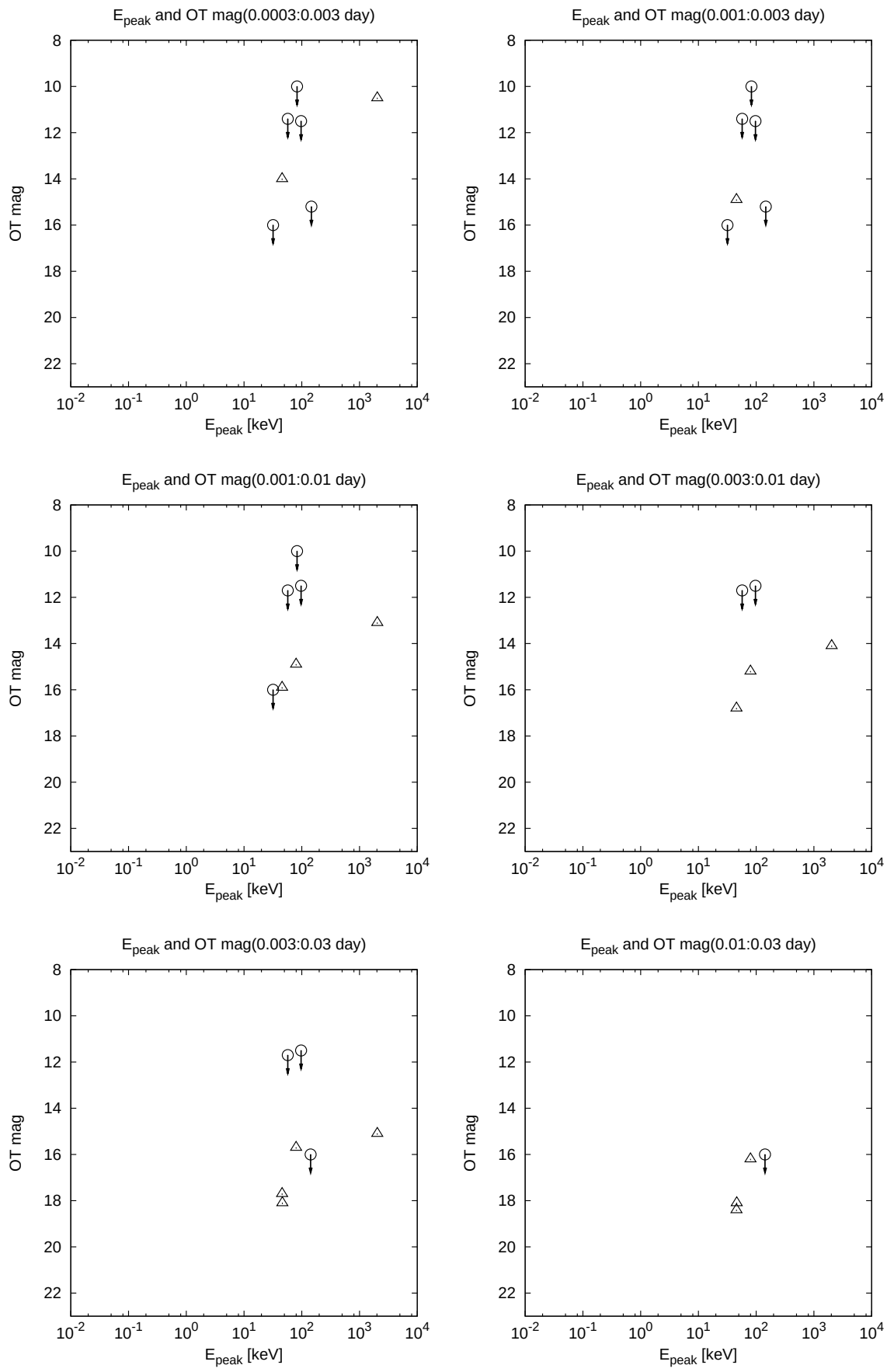

Figure D.1: Magnitude of OT vs. $E_{\rm peak}$ (0.0003:0.003 – 0.01:0.03 day)

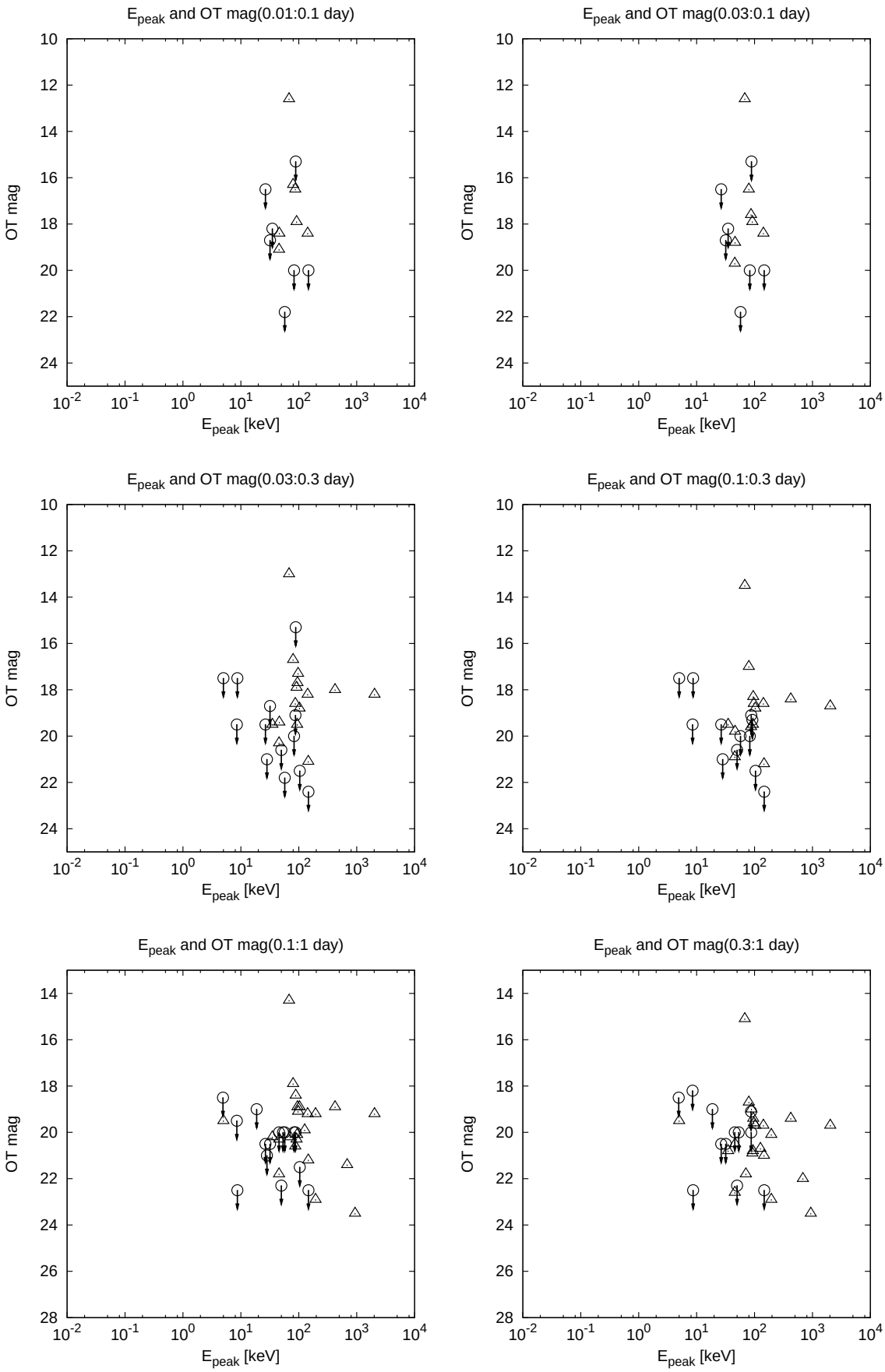

Figure D.2: Magnitude of OT vs. $E_{\rm peak}$ (0.01:0.1 – 0.3:1 day)

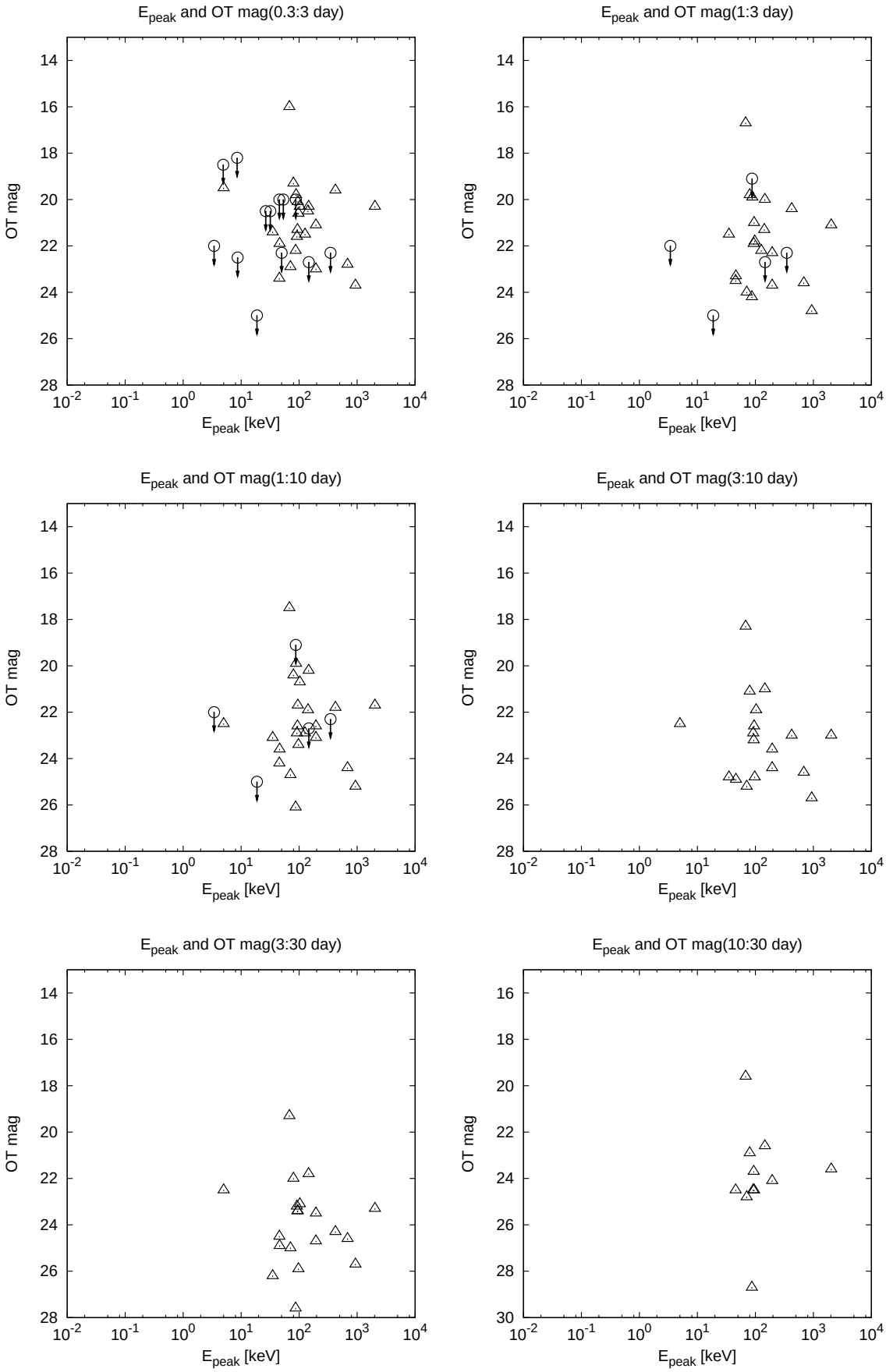

Figure D.3: Magnitude of OT vs. $E_{\rm peak}$ (0.3:3 – 10:30 day)

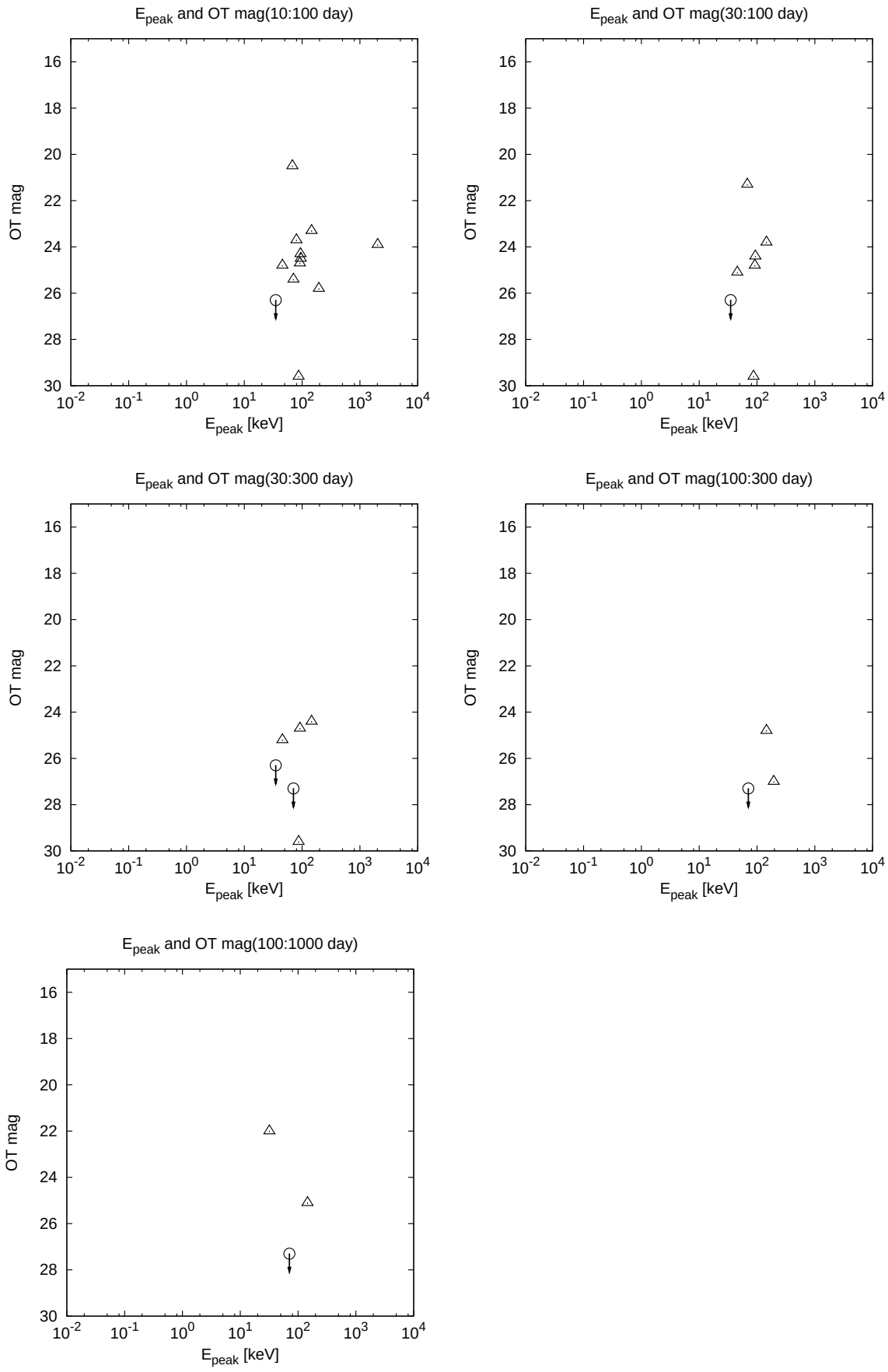

Figure D.4: Magnitude of OT vs. $E_{\rm peak}$ (10:100 – 100:1000 day)

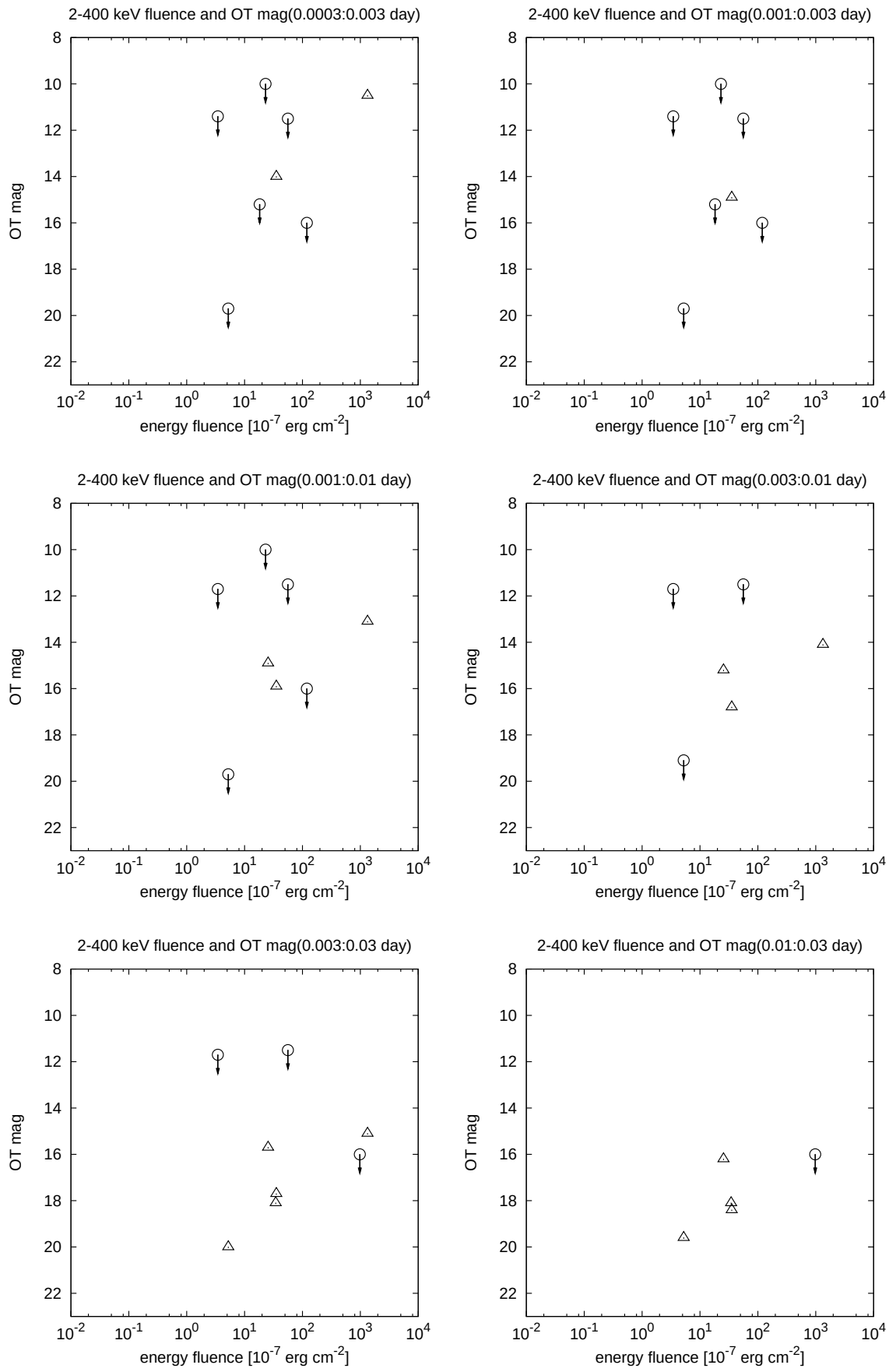

Figure D.5: Magnitude of OT vs. $S_{\rm total}$ (0.0003:0.003 – 0.01:0.03 day)

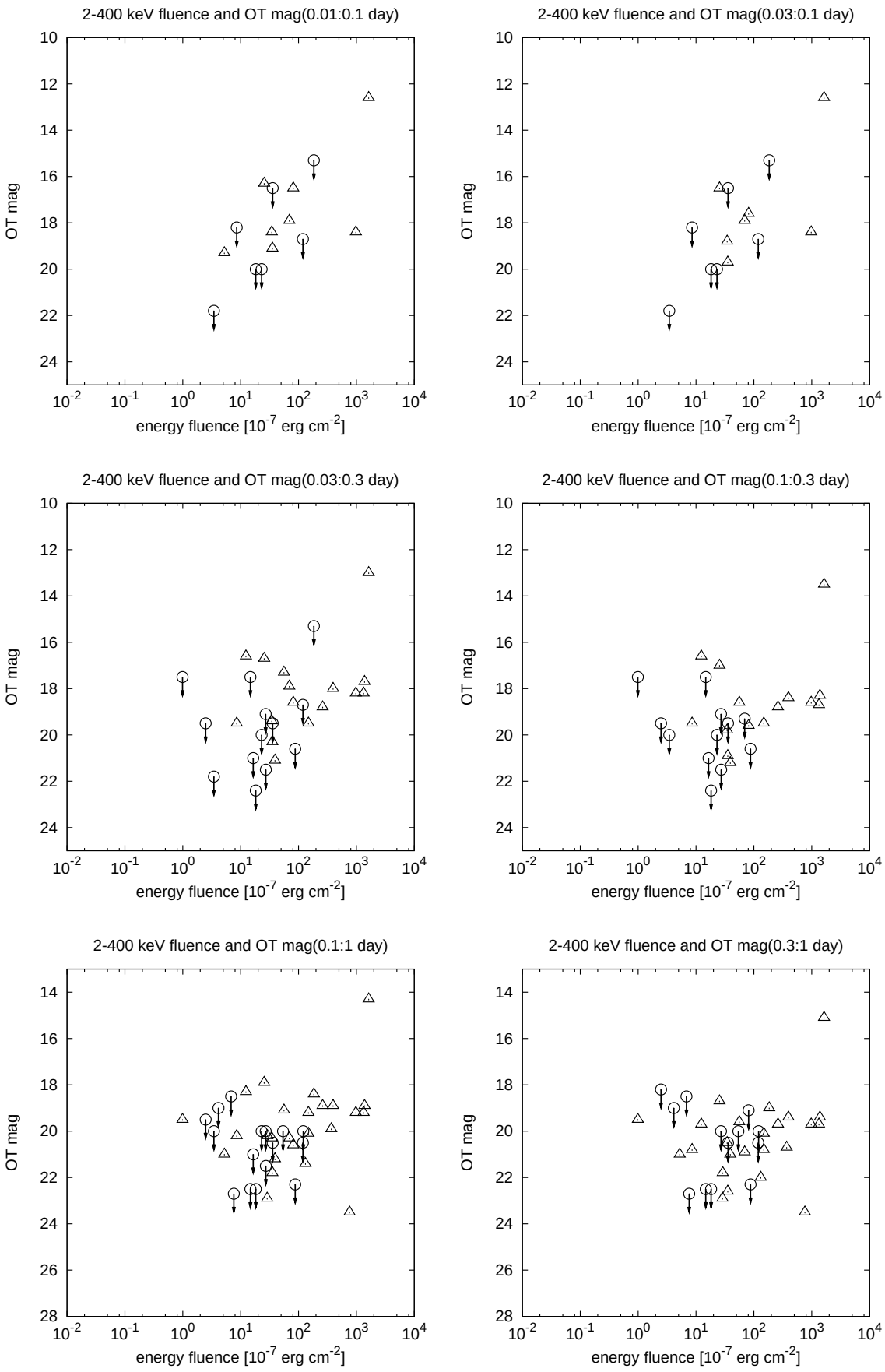

Figure D.6: Magnitude of OT vs. $S_{\rm total}$ (0.01:0.1 – 0.3:1 day)

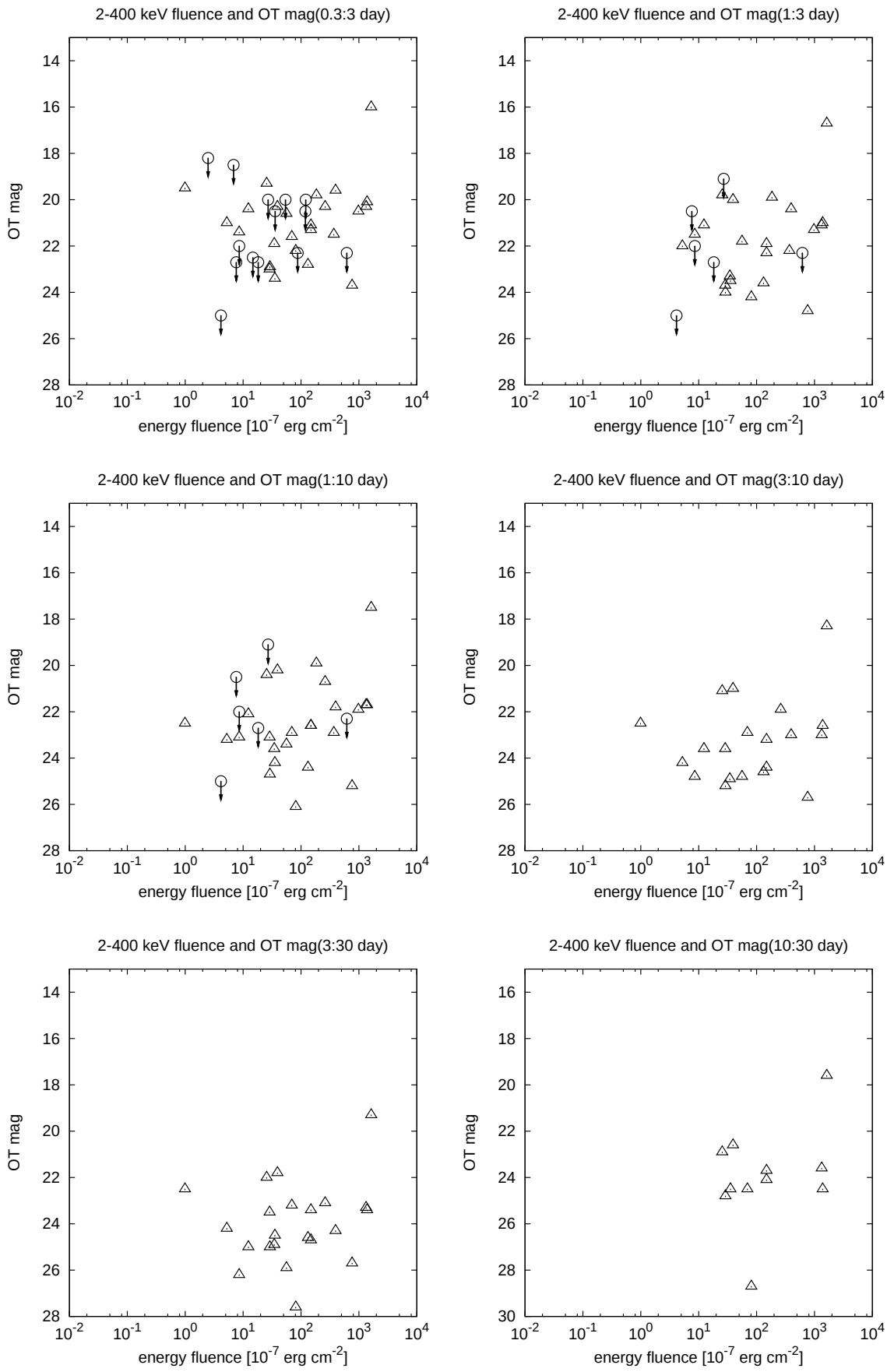

Figure D.7: Magnitude of OT vs. $S_{\rm total}$ (0.3:3 – 10:30 day)

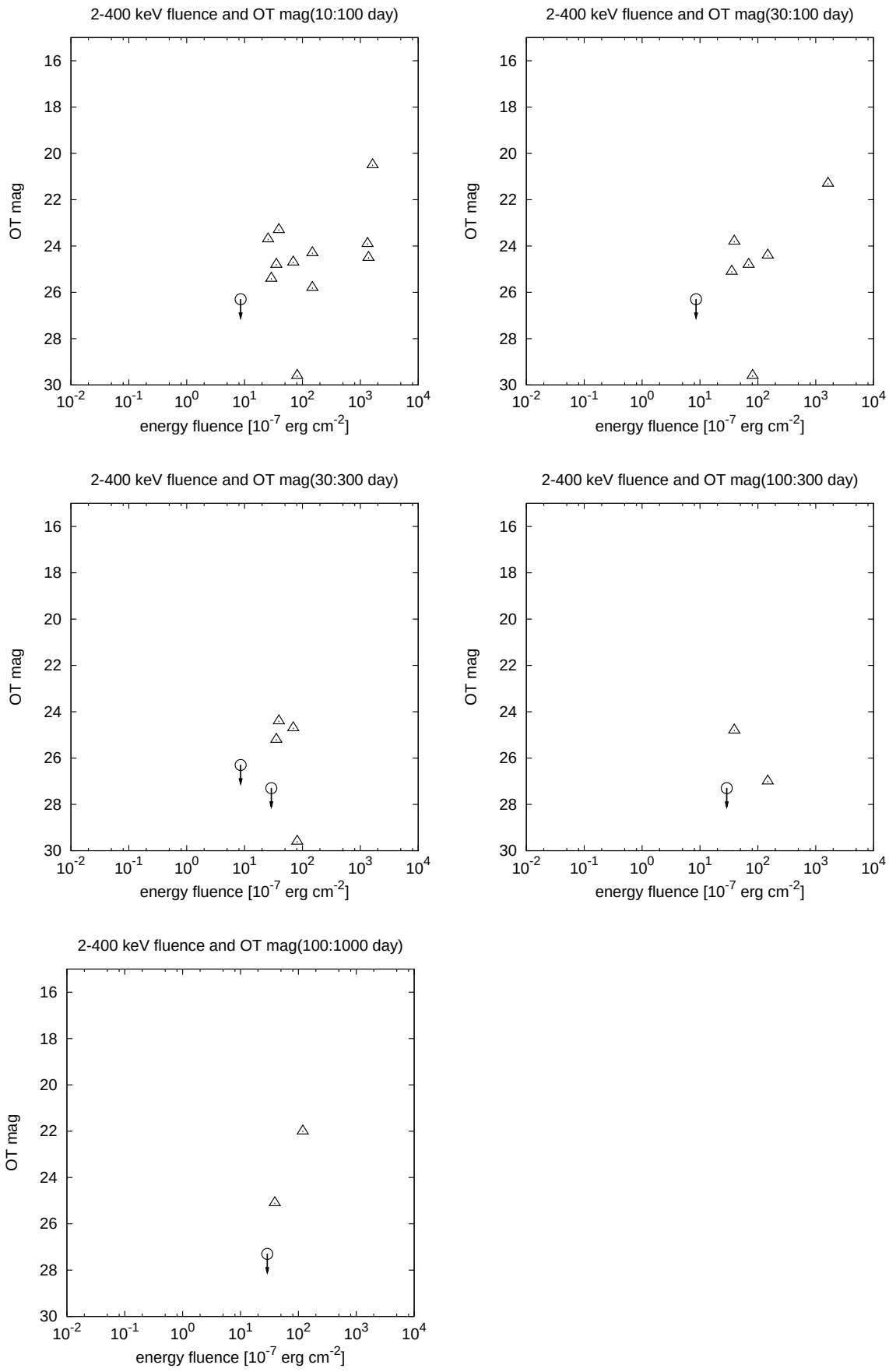

Figure D.8: Magnitude of OT vs. $S_{\rm total}$ (10:100 – 100:1000 day)

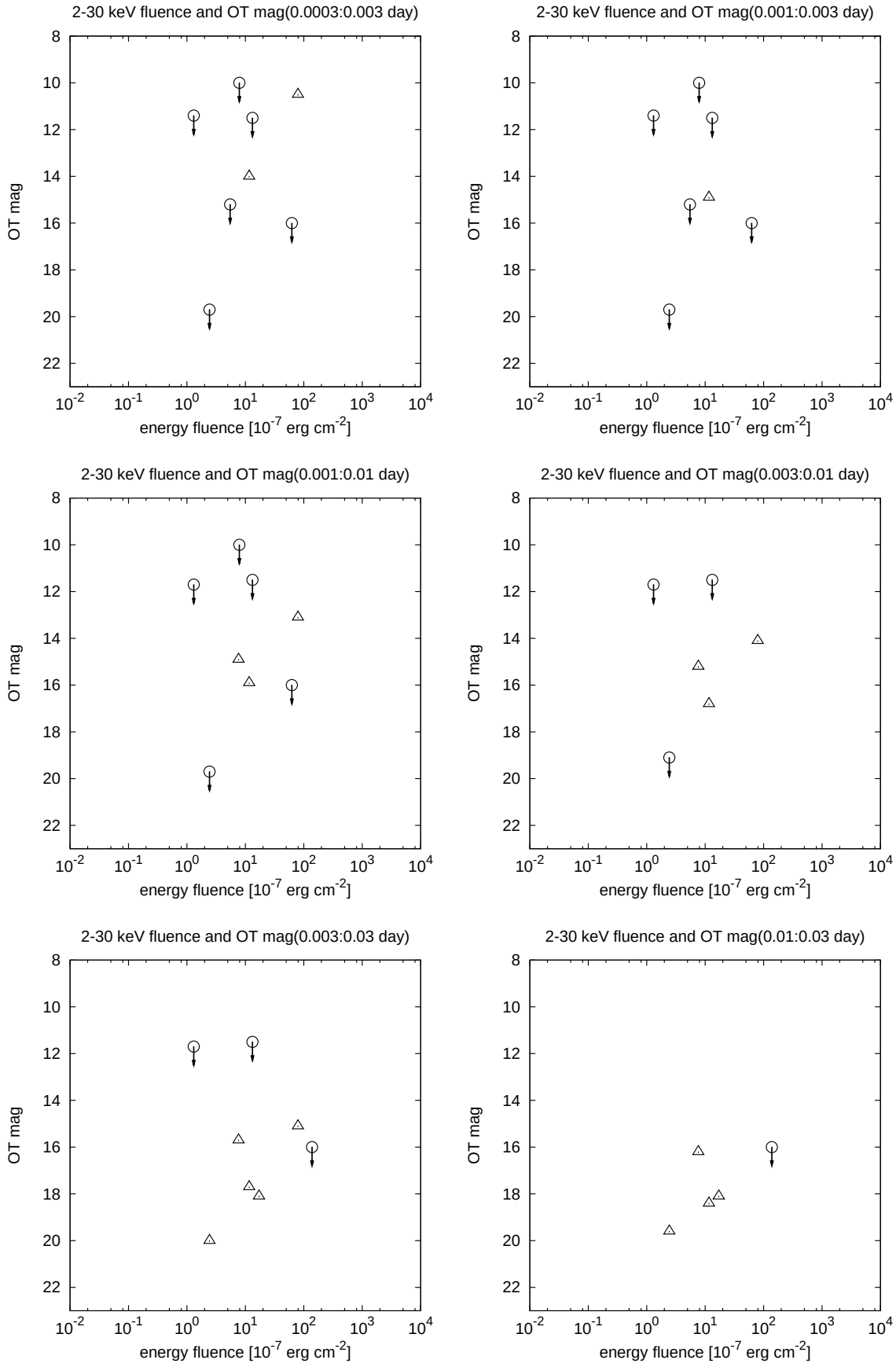

Figure D.9: Magnitude of OT vs. $S_{\rm X}$ (0.0003:0.003 – 0.01:0.03 day)

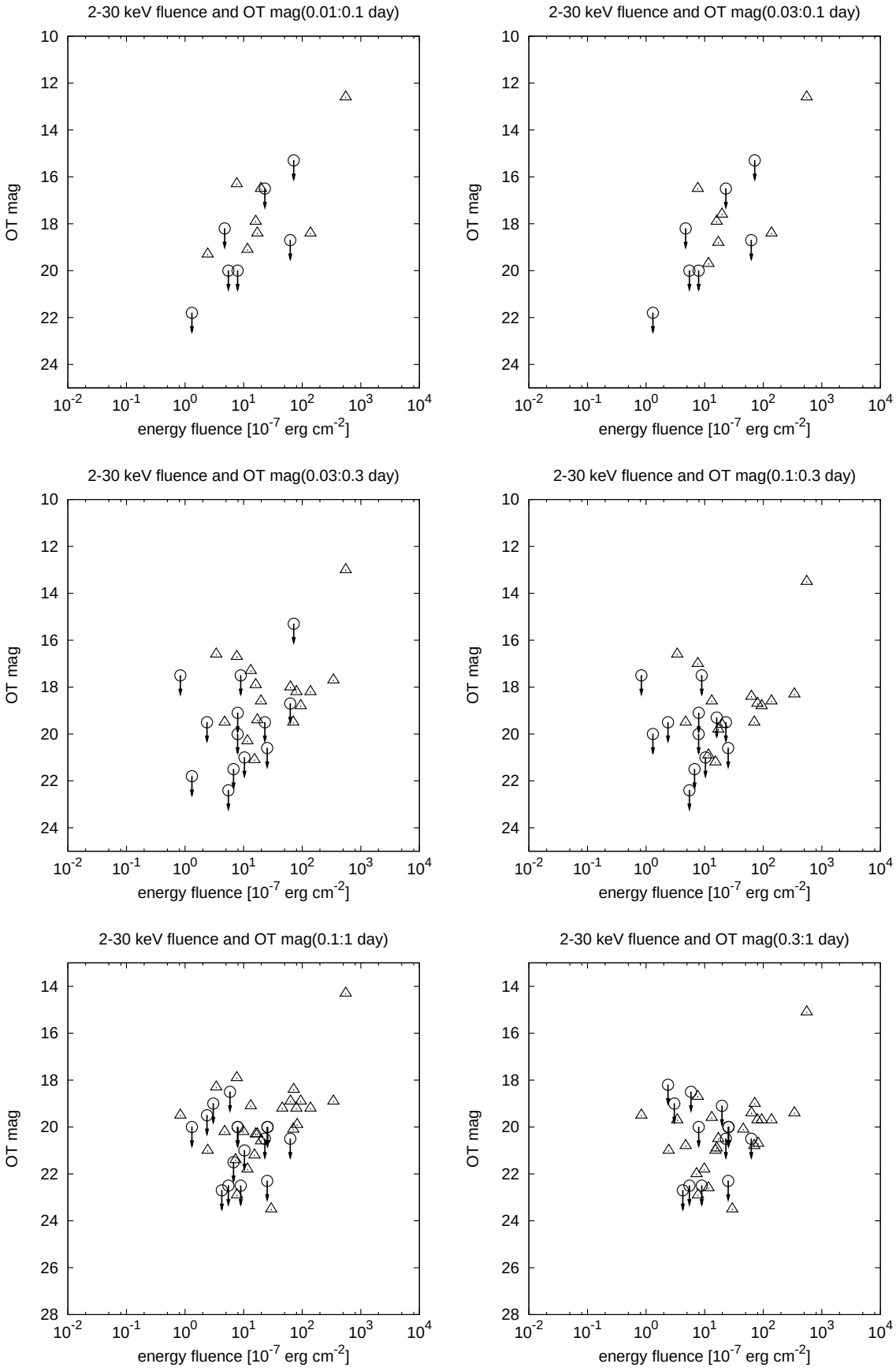

Figure D.10: Magnitude of OT vs. $S_{\rm X}$ (0.01:0.1 – 0.3:1 day)

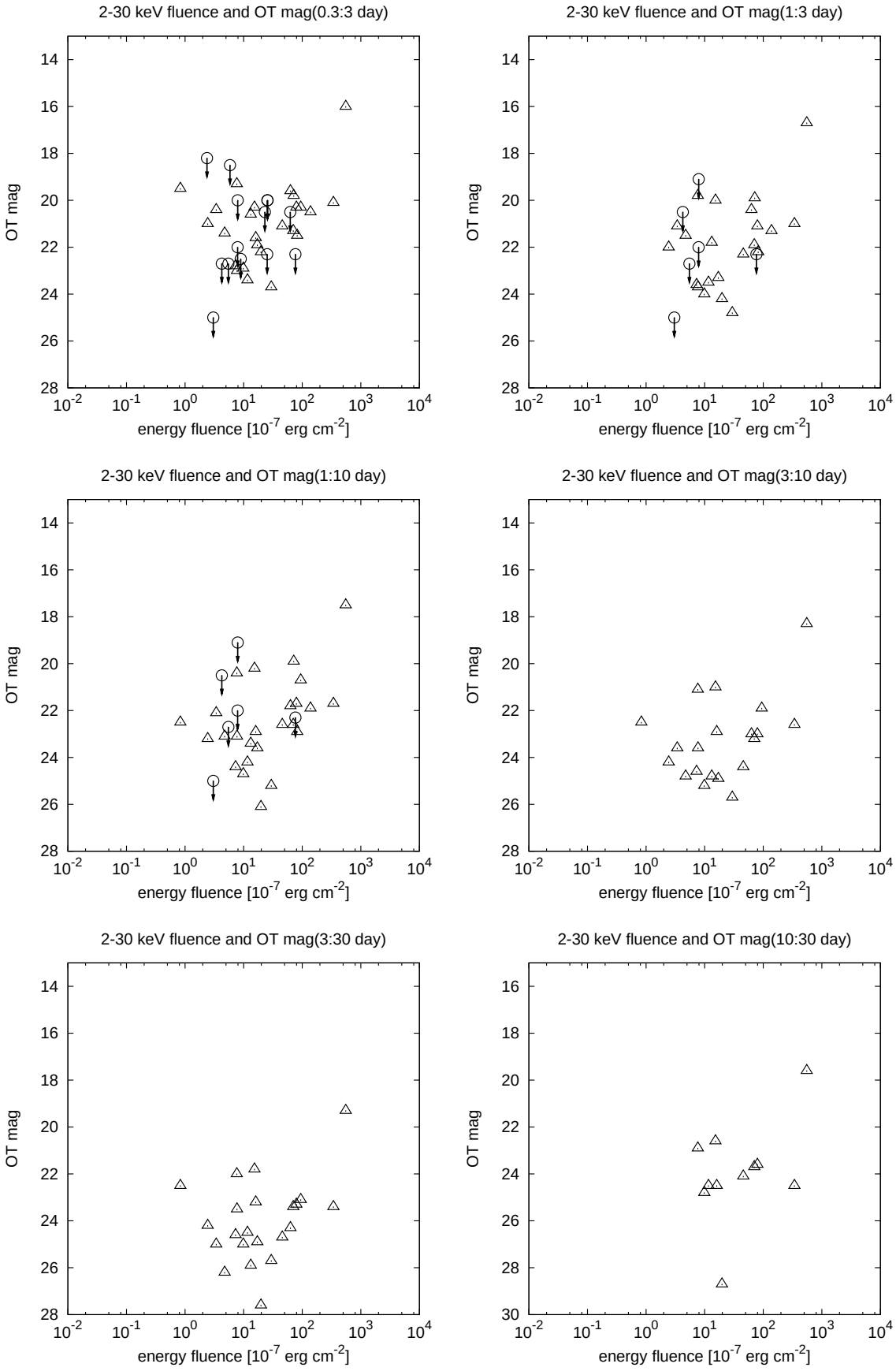

Figure D.11: Magnitude of OT vs. $S_{\rm X}$ (0.3:3 – 10:30 day)

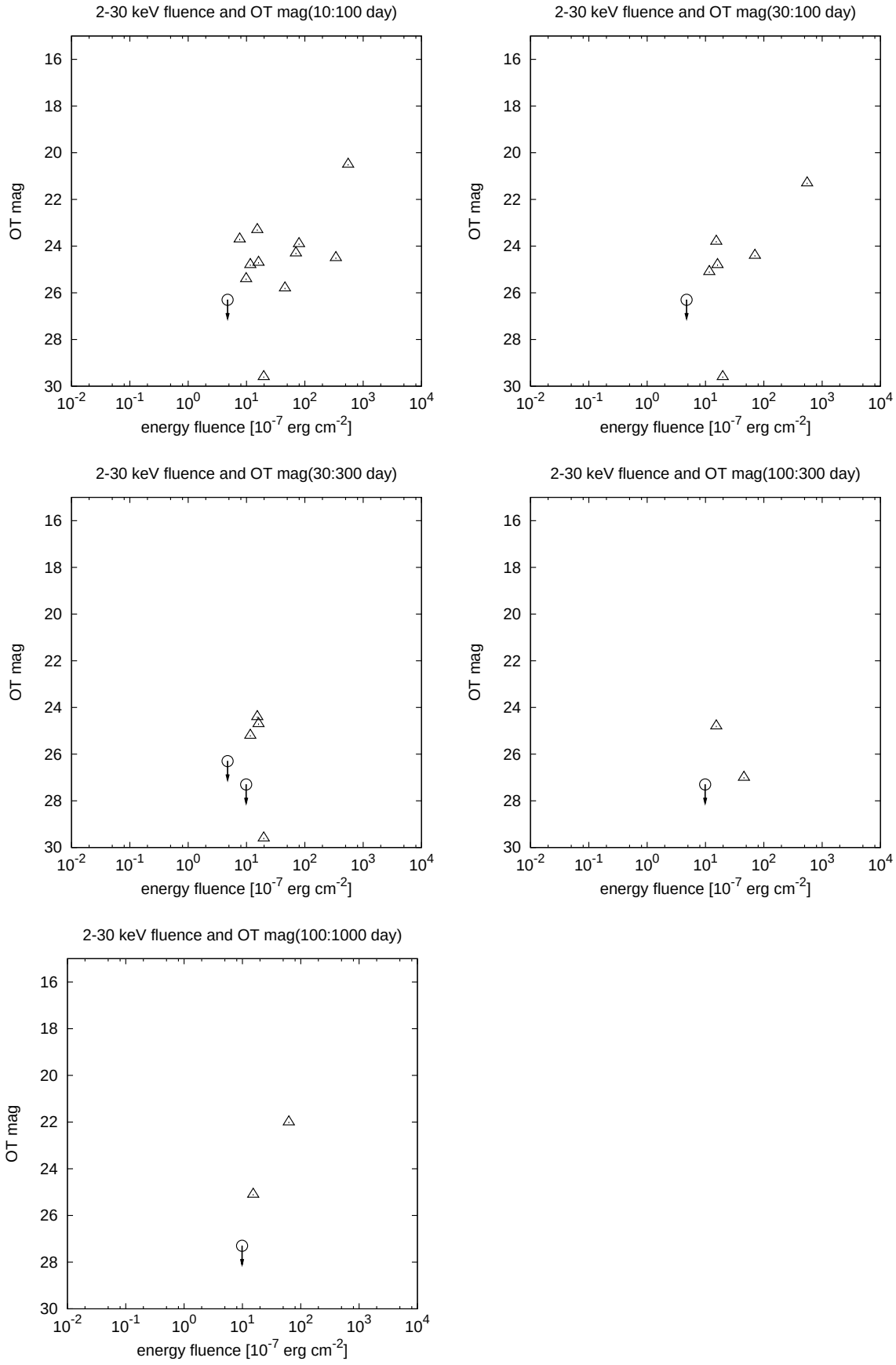

Figure D.12: Magnitude of OT vs. $S_{\rm X}$ (10:100 – 100:1000 day)

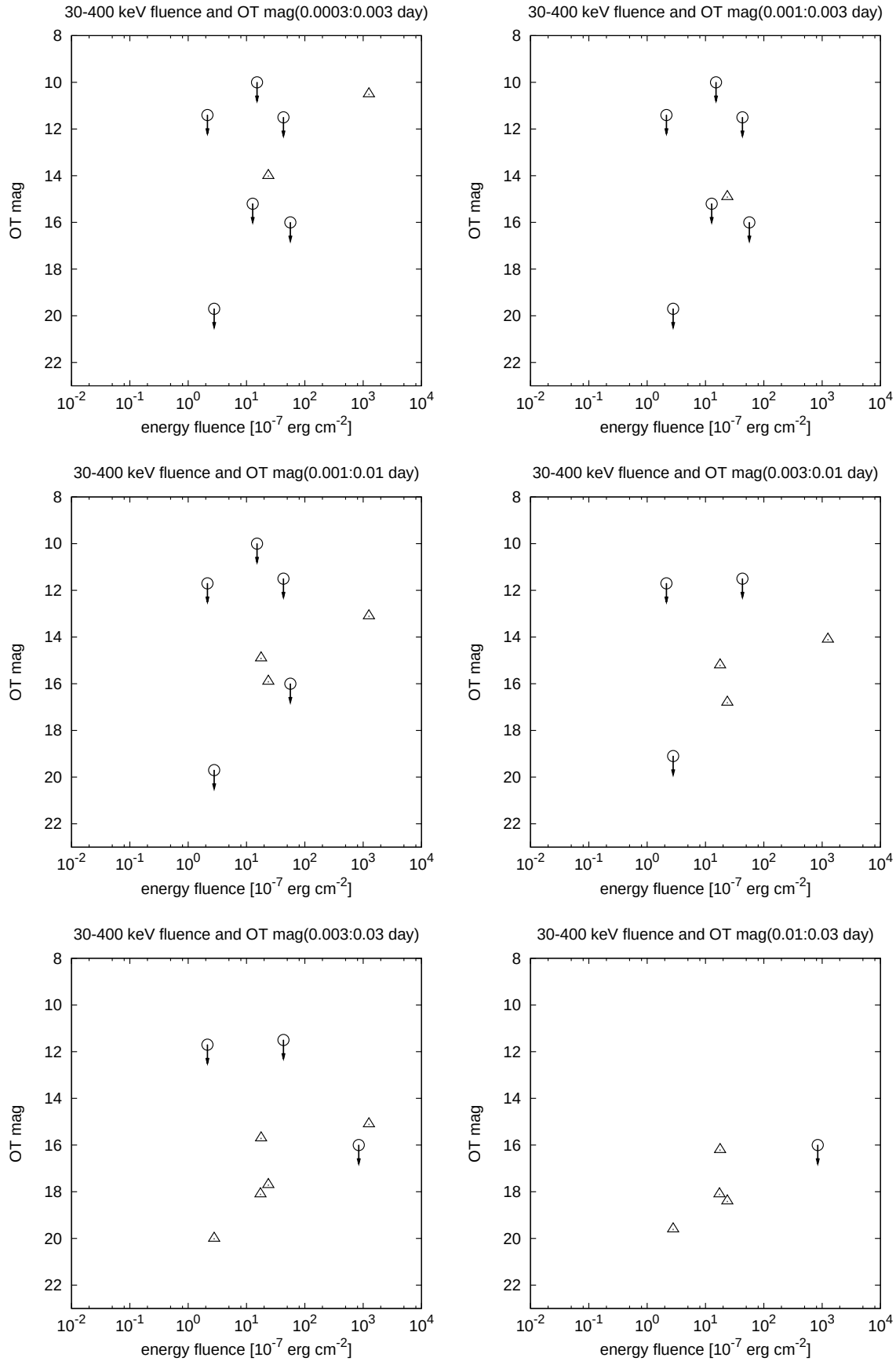

Figure D.13: Magnitude of OT vs. S_γ (0.0003:0.003 – 0.01:0.03 day)

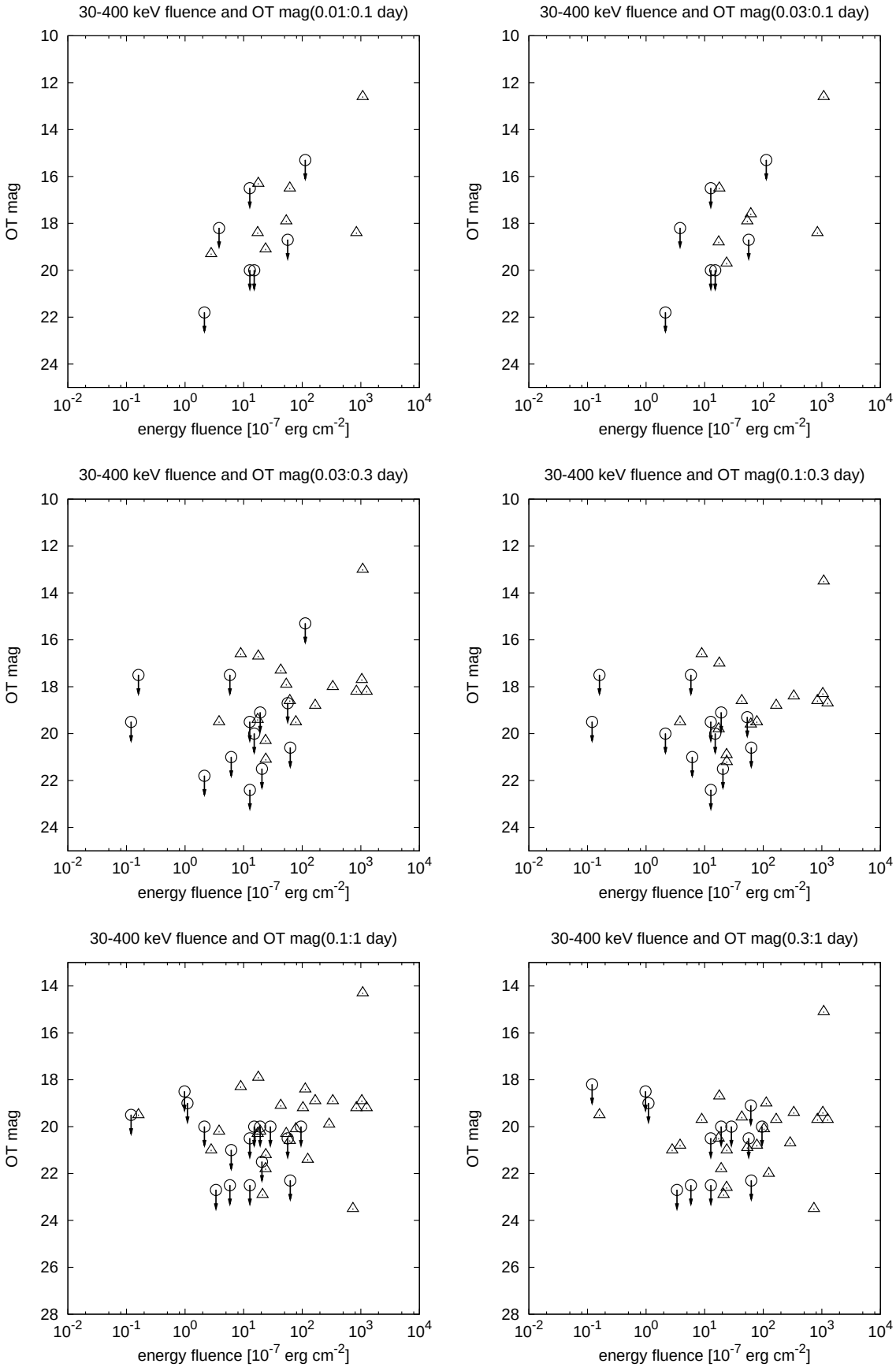

Figure D.14: Magnitude of OT vs. S_γ (0.01:0.1 – 0.3:1 day)

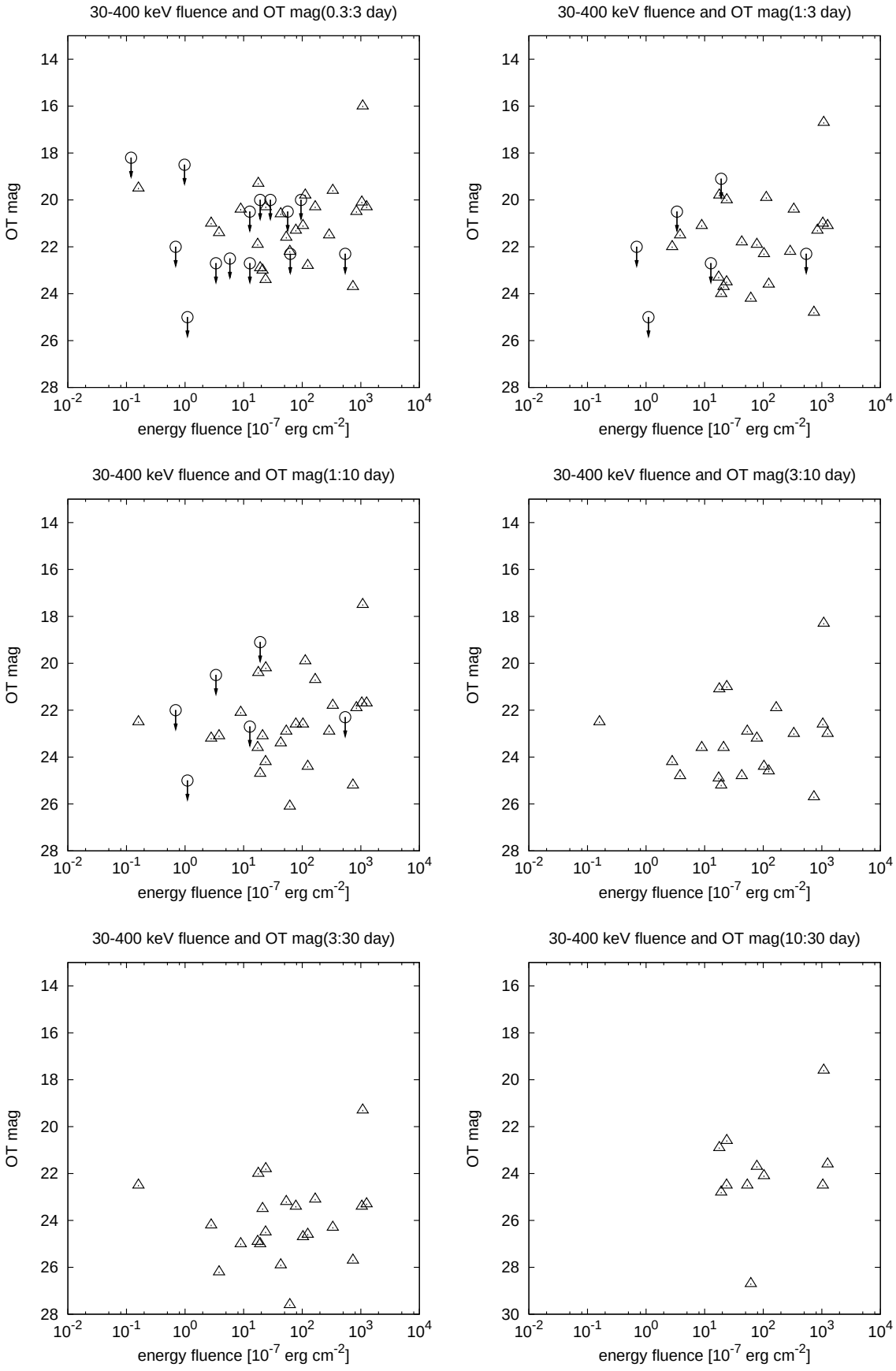

Figure D.15: Magnitude of OT vs. S_γ (0.3:3 – 10:30 day)

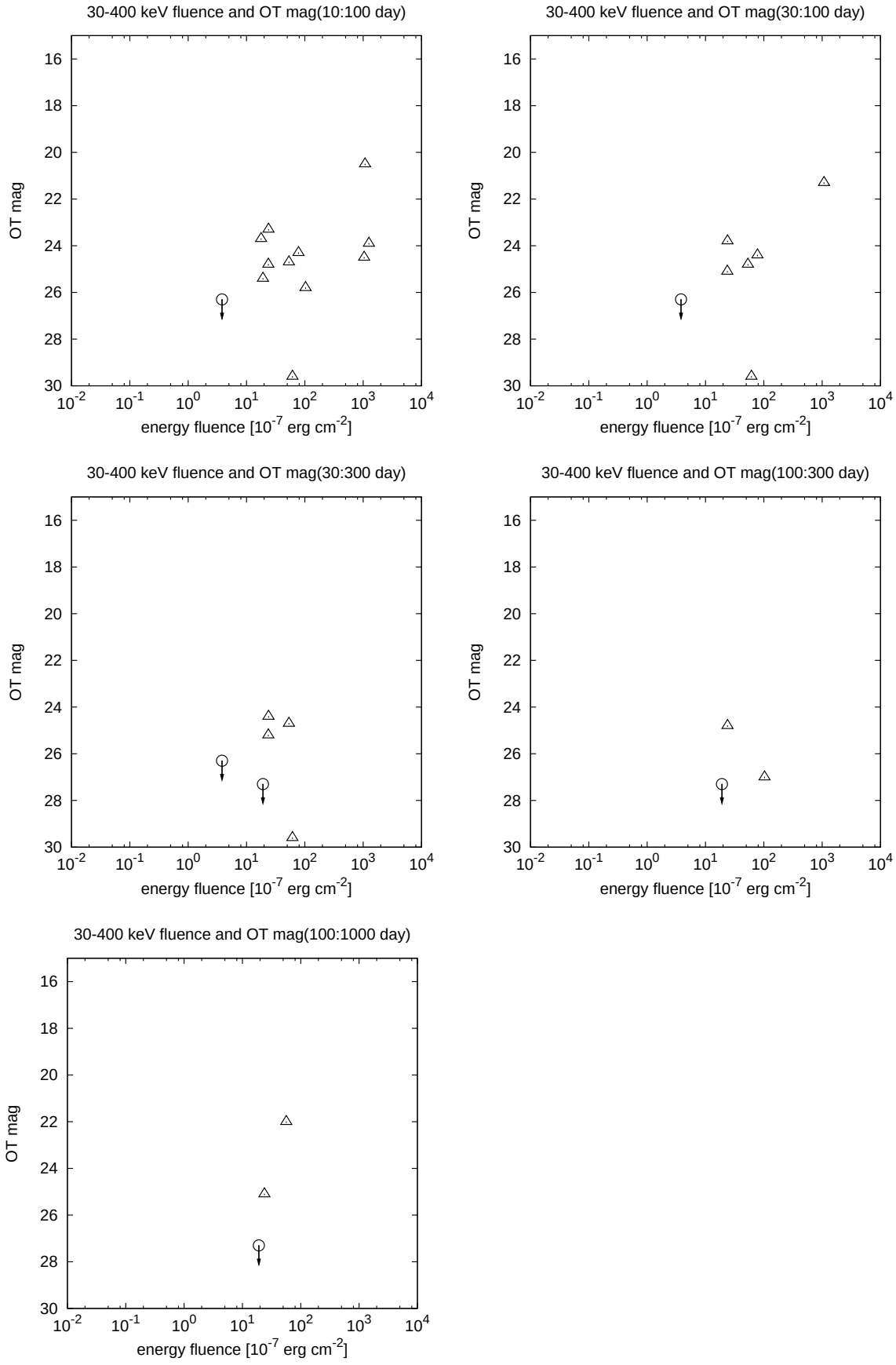

Figure D.16: Magnitude of OT vs. S_γ (10:100 – 100:1000 day)

D.2 Properties of source frame

This section contains the scatter plots of the properties in the source frame, that is the following combination:

- $L_{\rm ot}$ vs. $E^{\rm src}_{\rm peak}$,
- $L_{\rm ot}$ vs. $E_{\rm iso}$,
- $L_{\rm ot}$ vs. $E_{\rm jet}$,
- $L_{\rm ot,jet}$ vs. $E_{\rm jet}$.

The order of plots and symbols are the same as the previous section.

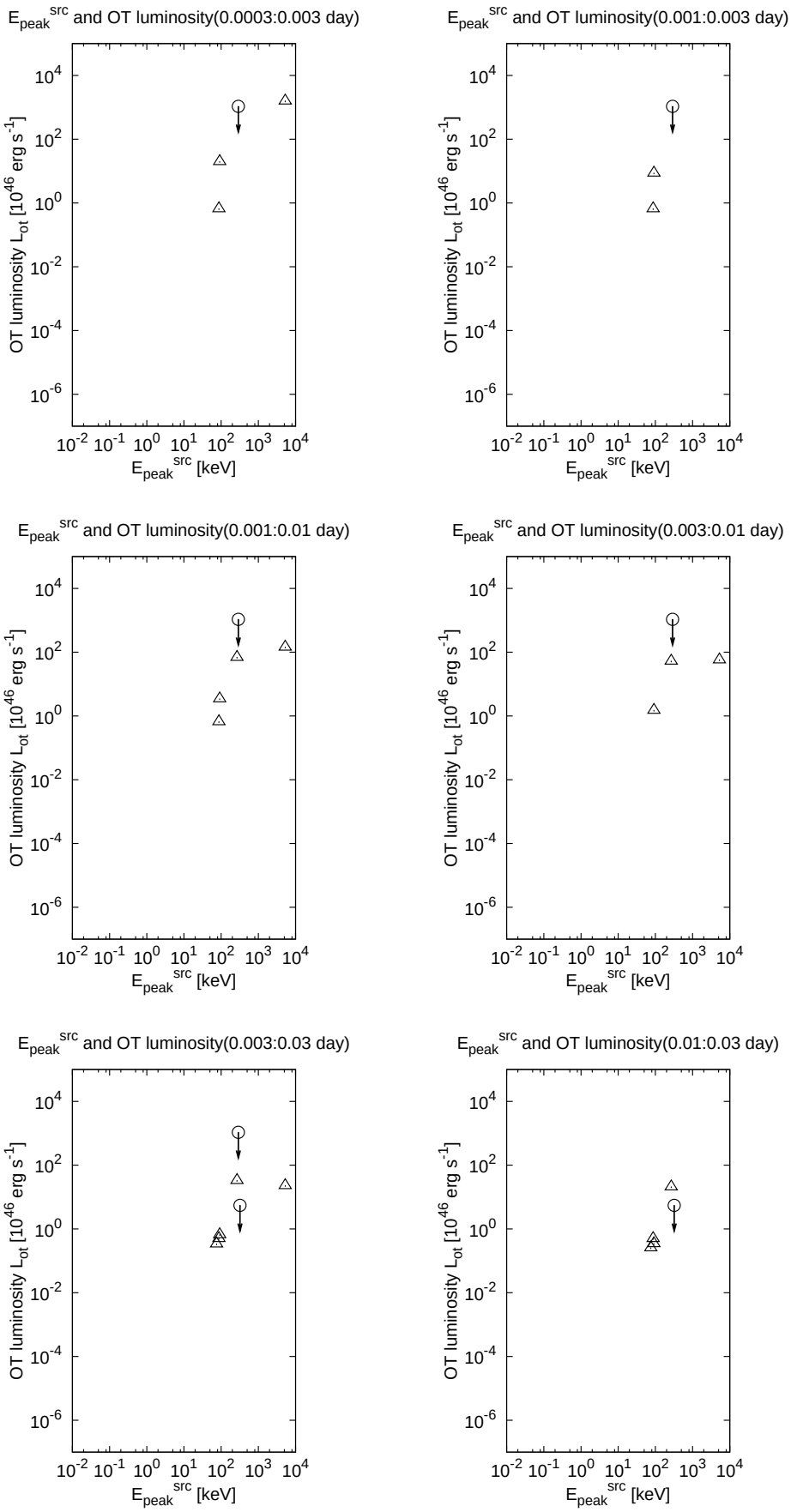

Figure D.17: $L_{\rm ot}$ vs. $E^{\rm src}_{\rm peak}$ (0.0003:0.003 – 0.01:0.03 day)

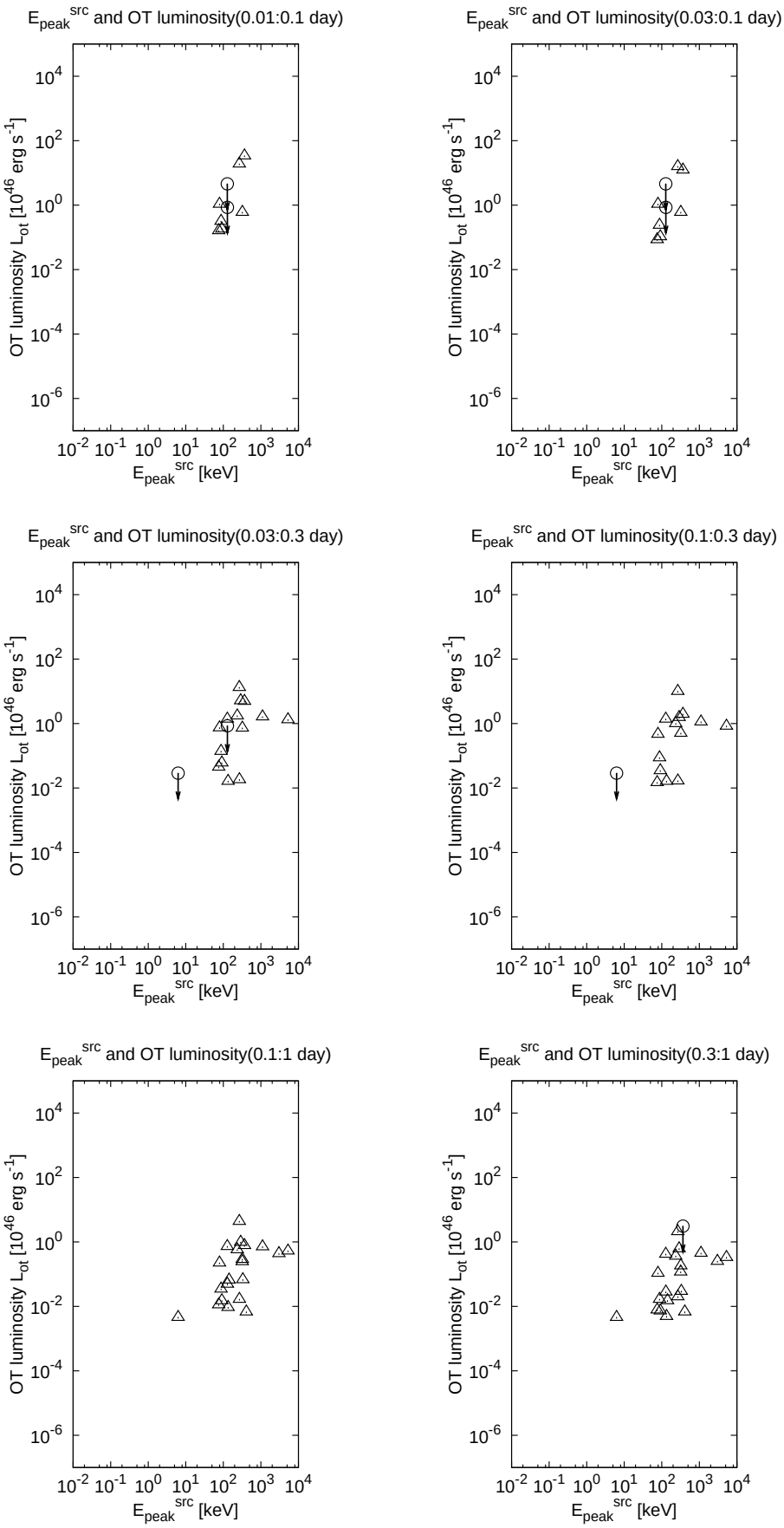

Figure D.18: $L_{\rm ot}$ vs. $E_{\rm peak}^{\rm src}$ (0.01:0.1 – 0.3:1 day)

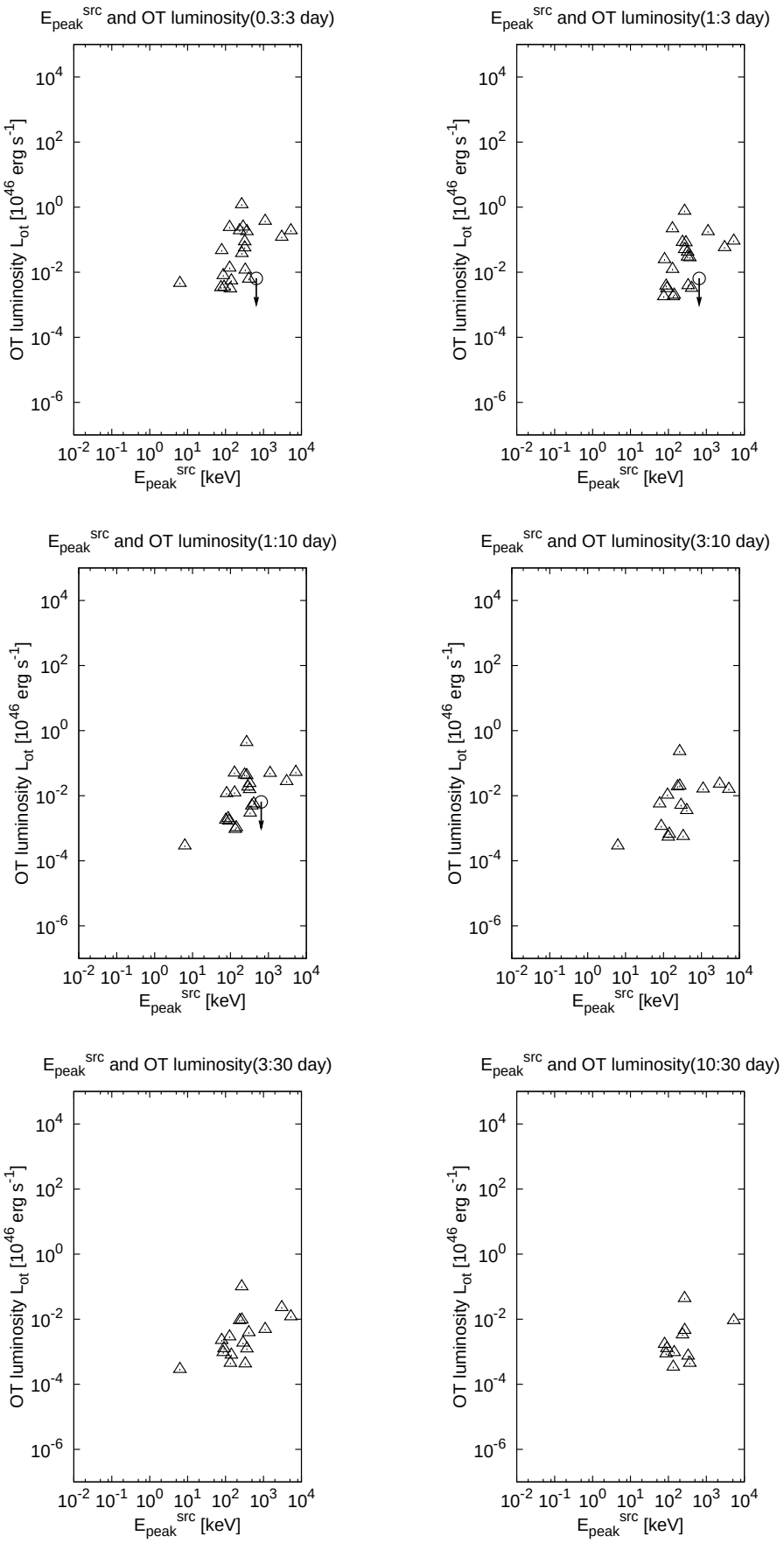

Figure D.19: $L_{\rm ot}$ vs. $E_{\rm peak}^{\rm src}$ (0.3:3 – 10:30 day)

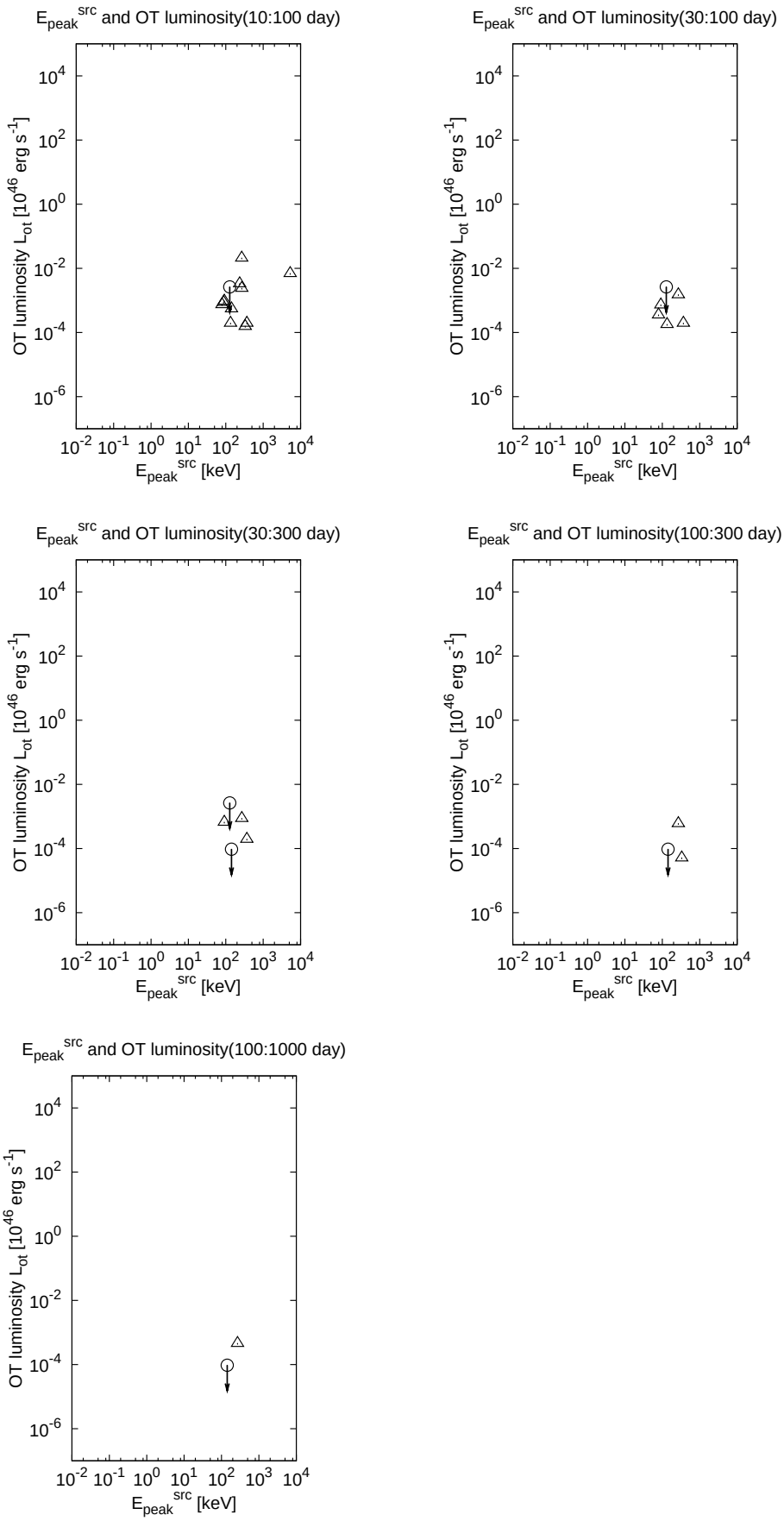

Figure D.20: $L_{\rm ot}$ vs. $E_{\rm peak}^{\rm src}$ (10:100 – 100:1000 day)

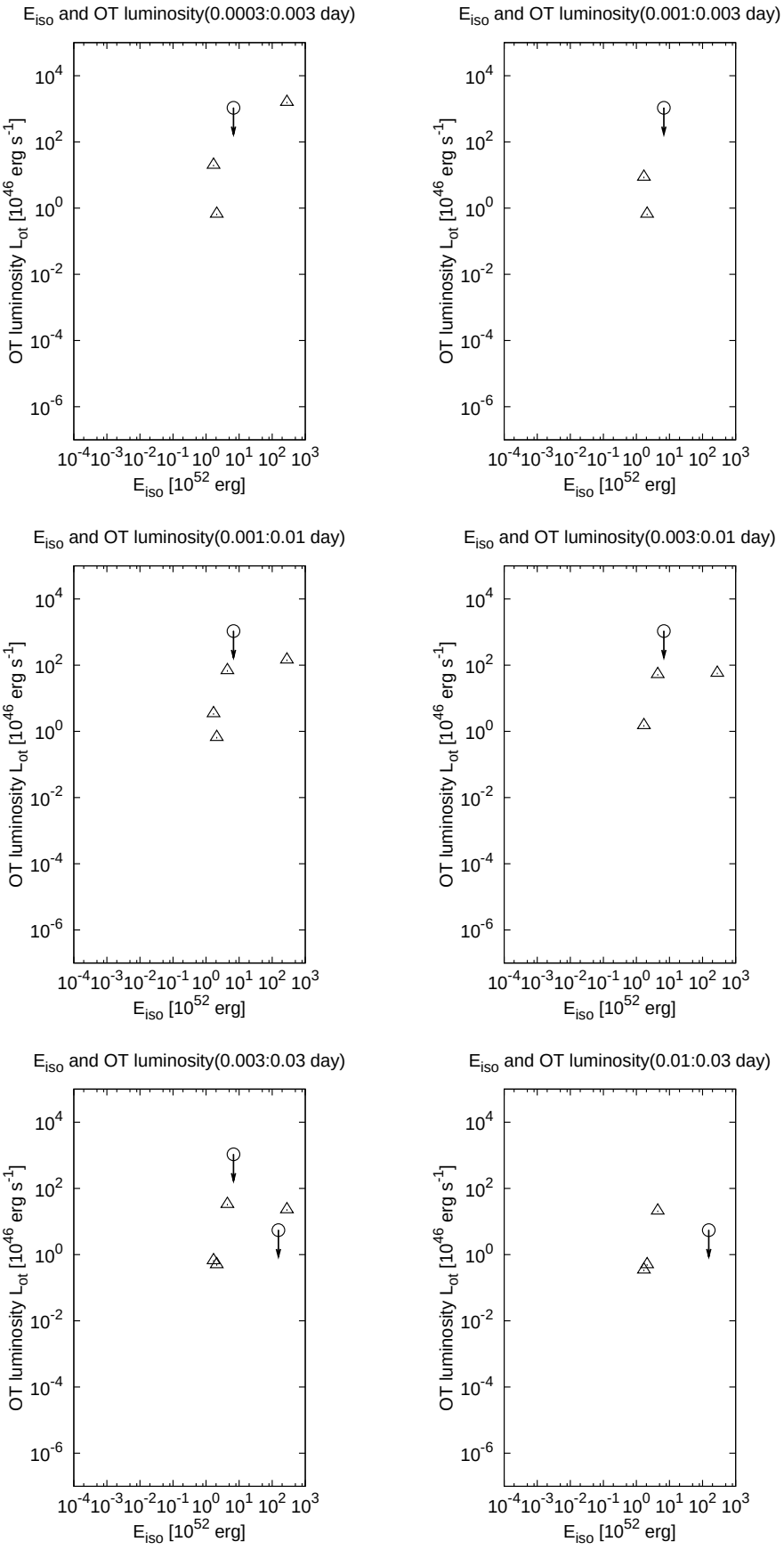

Figure D.21: $L_{\rm ot}$ vs. $E_{\rm iso}$ (0.0003:0.003 – 0.01:0.03 day)

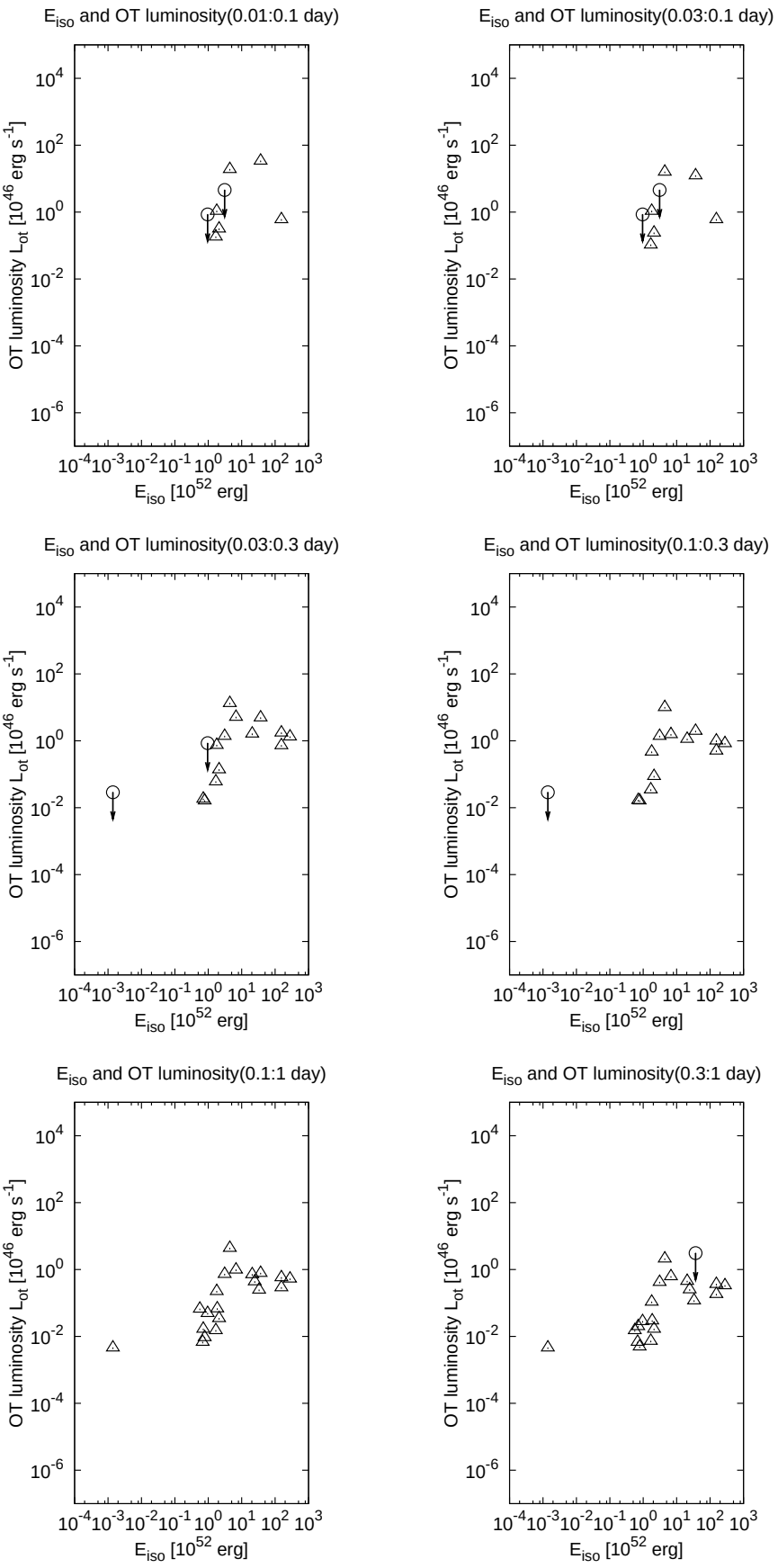

Figure D.22: $L_{\rm ot}$ vs. $E_{\rm iso}$ (0.01:0.1 – 0.3:1 day)

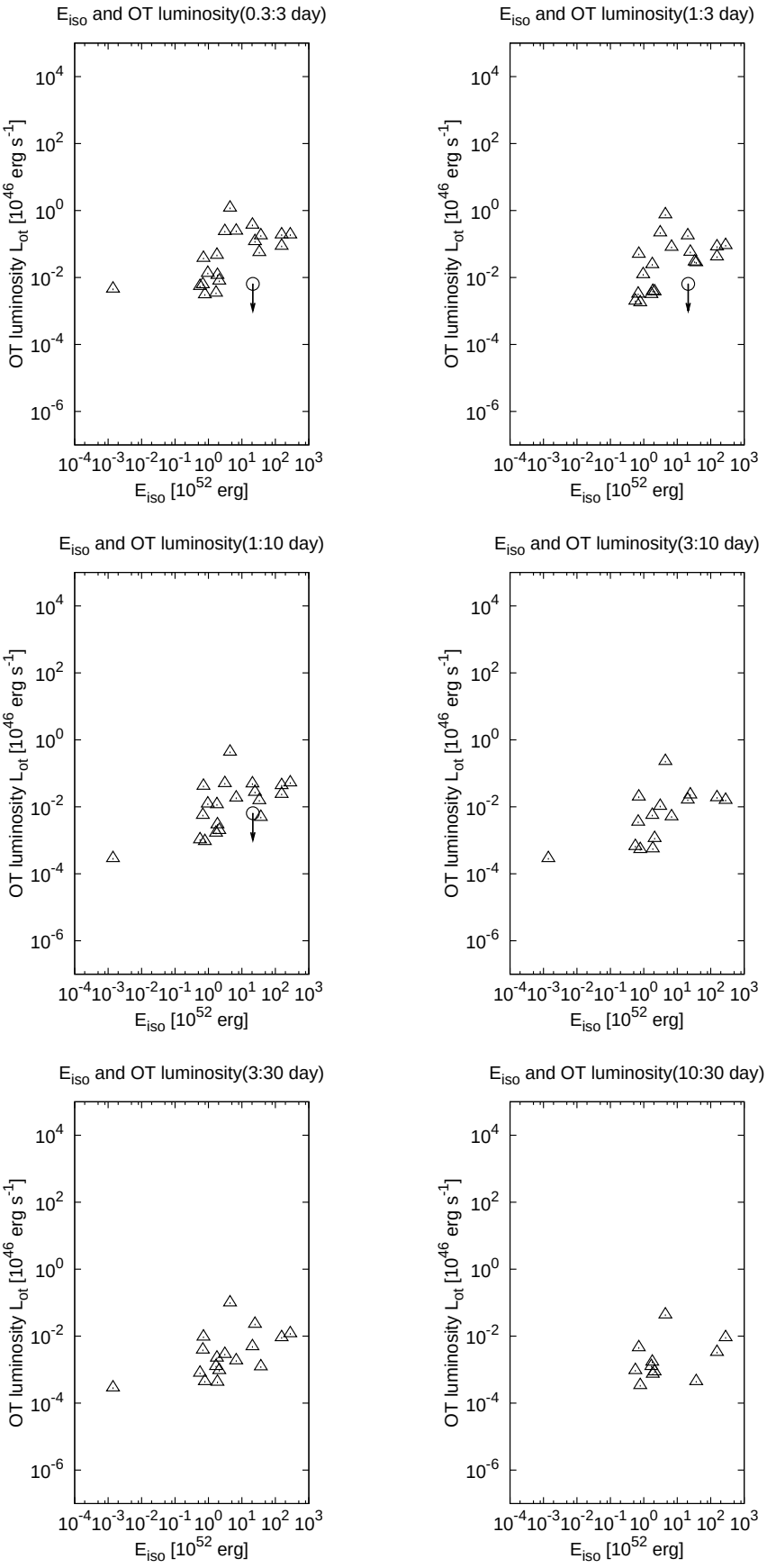

Figure D.23: $L_{\rm ot}$ vs. $E_{\rm iso}$ (0.3:3 – 10:30 day)

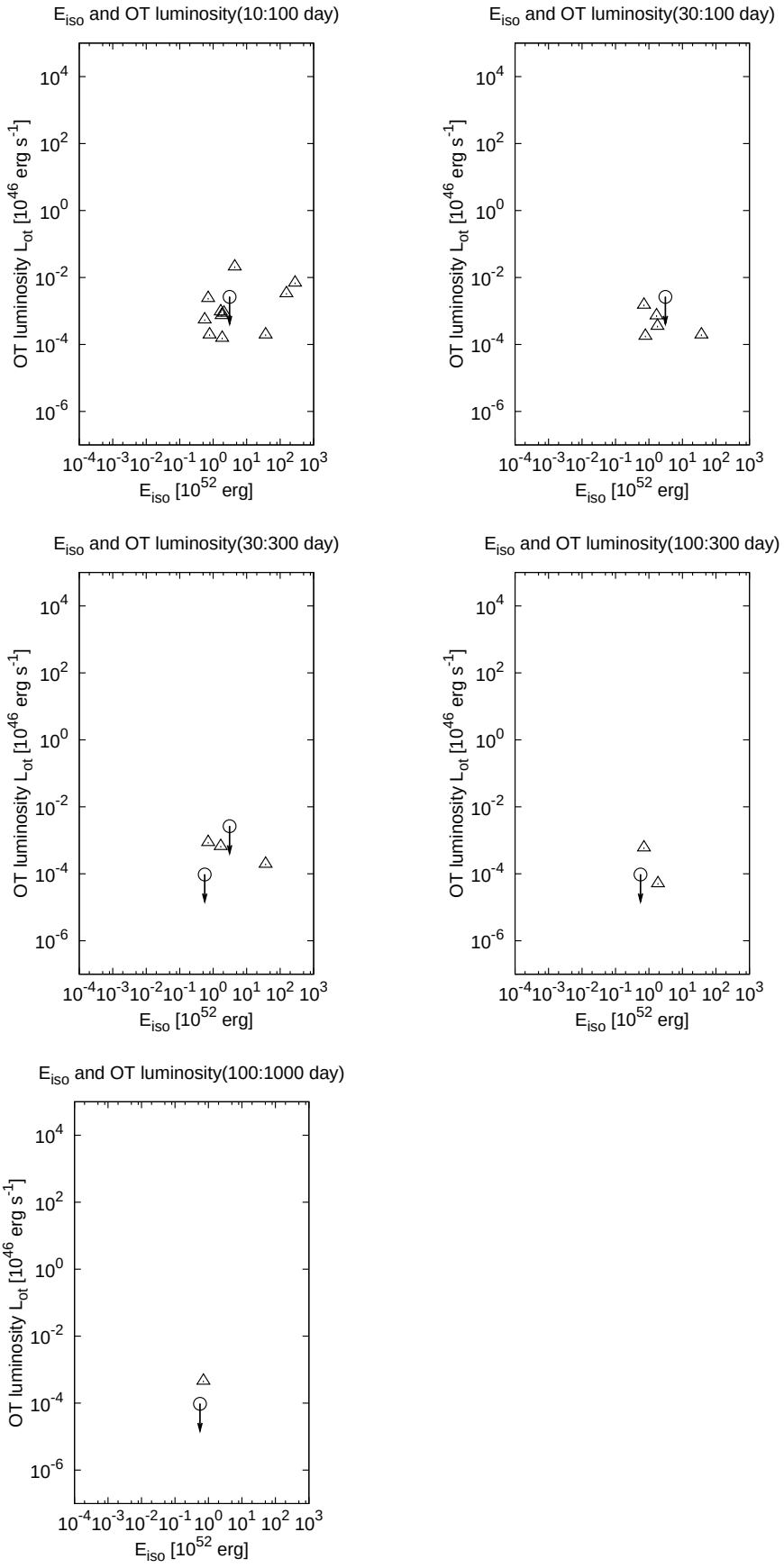

Figure D.24: $L_{\rm ot}$ vs. $E_{\rm iso}$ (10:100 – 100:1000 day)

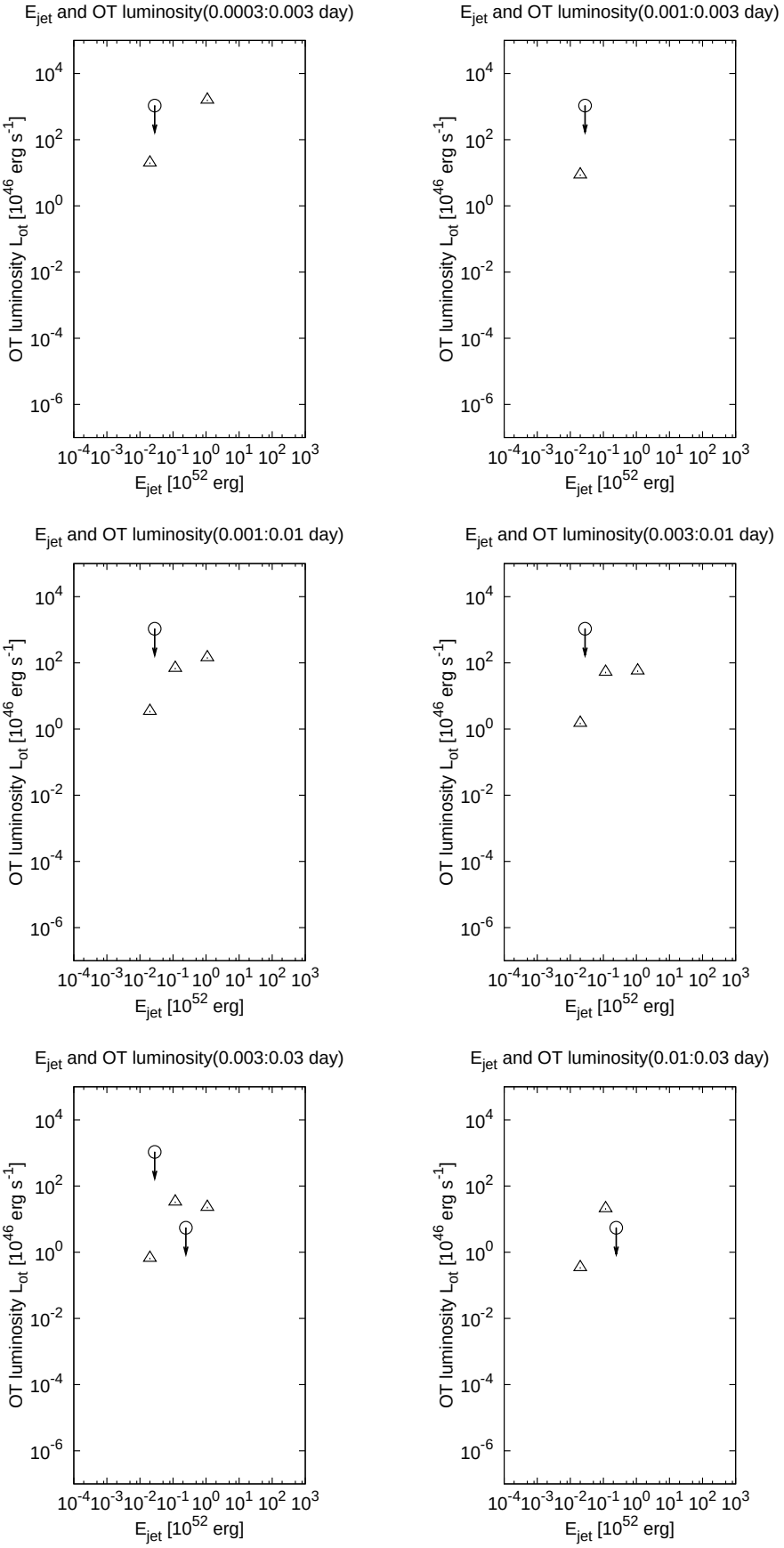

Figure D.25: $L_{\rm ot}$ vs. $E_{\rm jet}$ (0.0003:0.003 – 0.01:0.03 day)

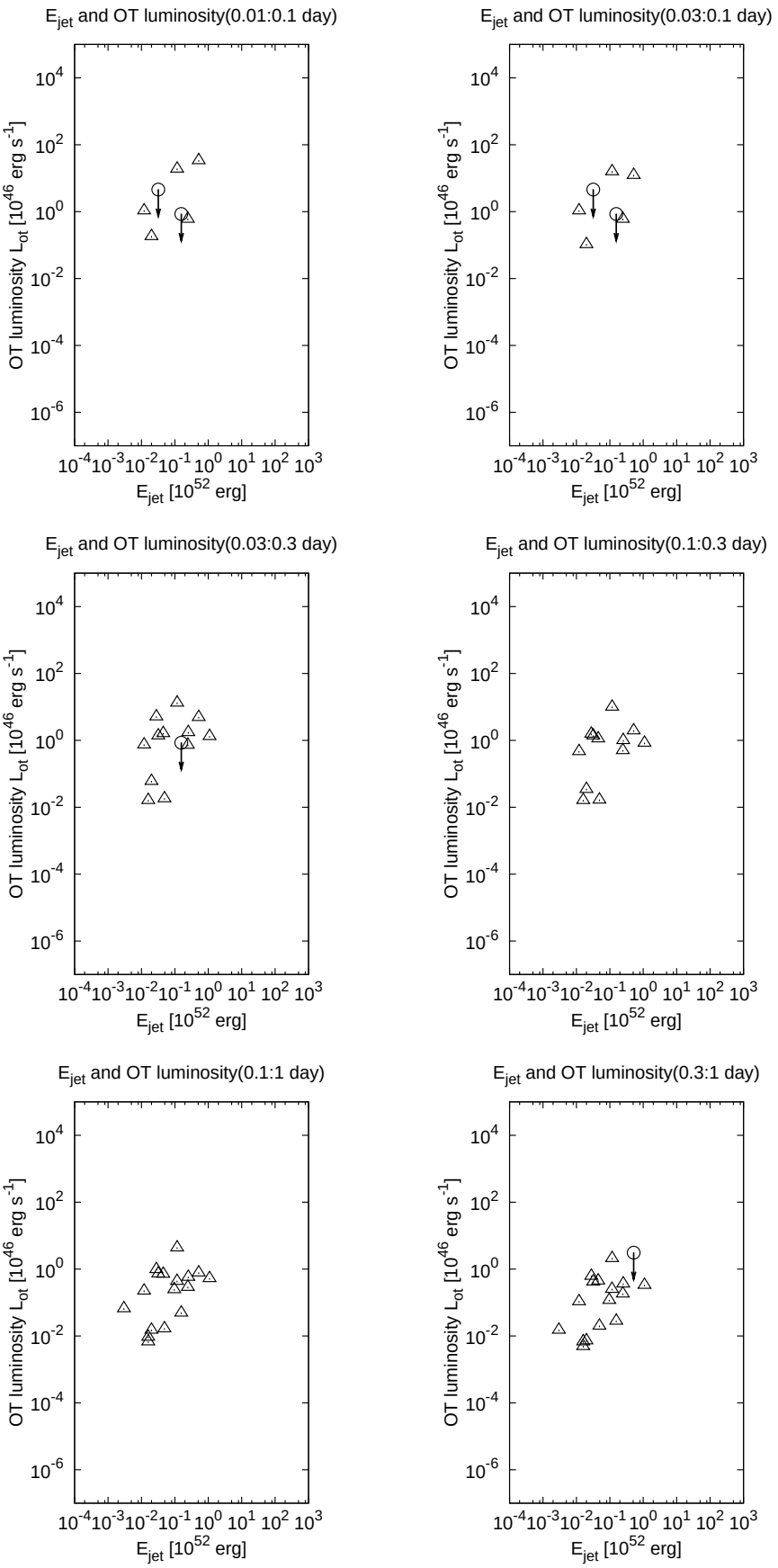

Figure D.26: $L_{\rm ot}$ vs. $E_{\rm jet}$ (0.01:0.1 – 0.3:1 day)

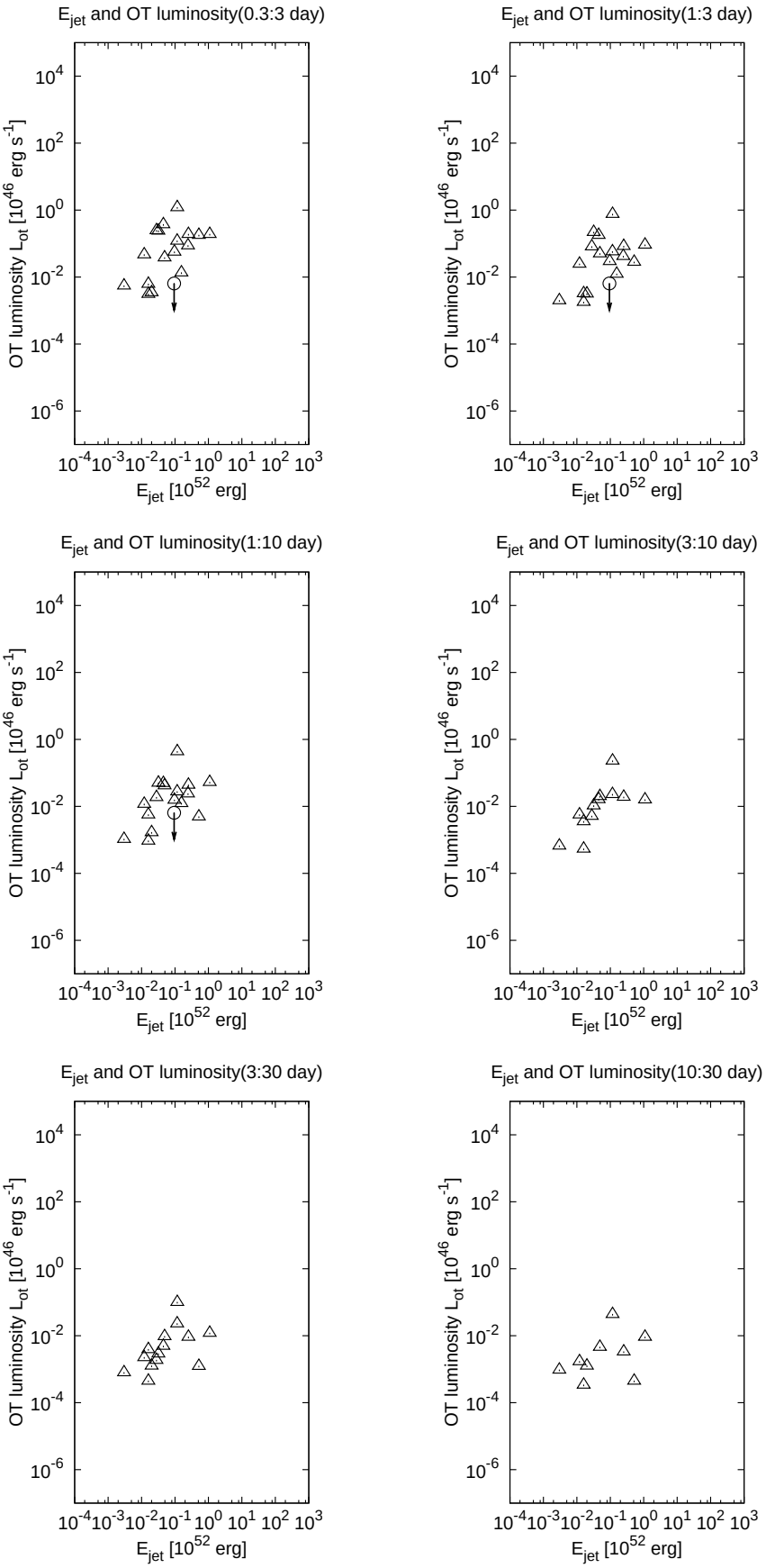

Figure D.27: $L_{\rm ot}$ vs. $E_{\rm jet}$ (0.3:3 – 10:30 day)

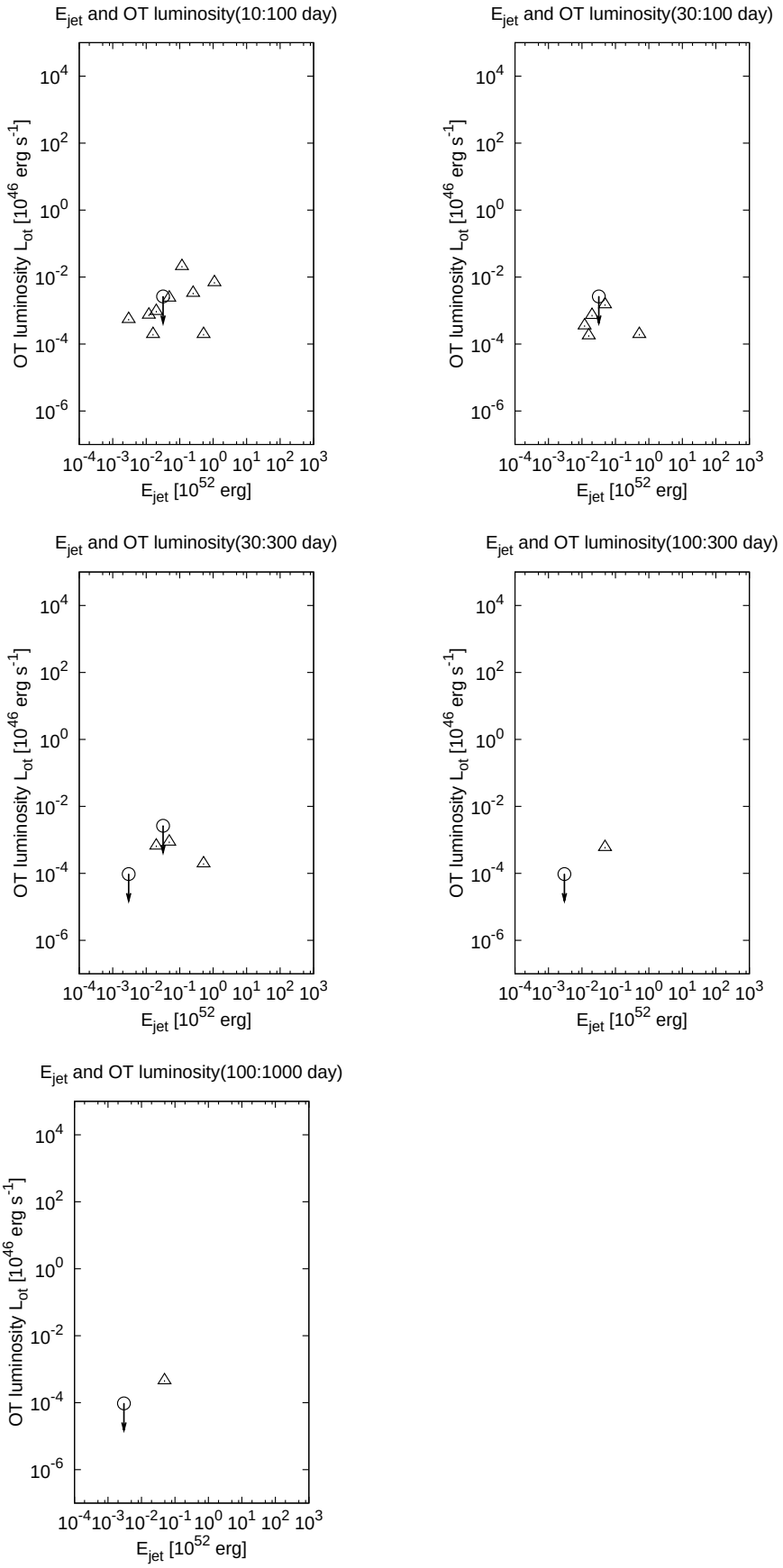

Figure D.28: $L_{\rm ot}$ vs. $E_{\rm jet}$ (10:100 – 100:1000 day)

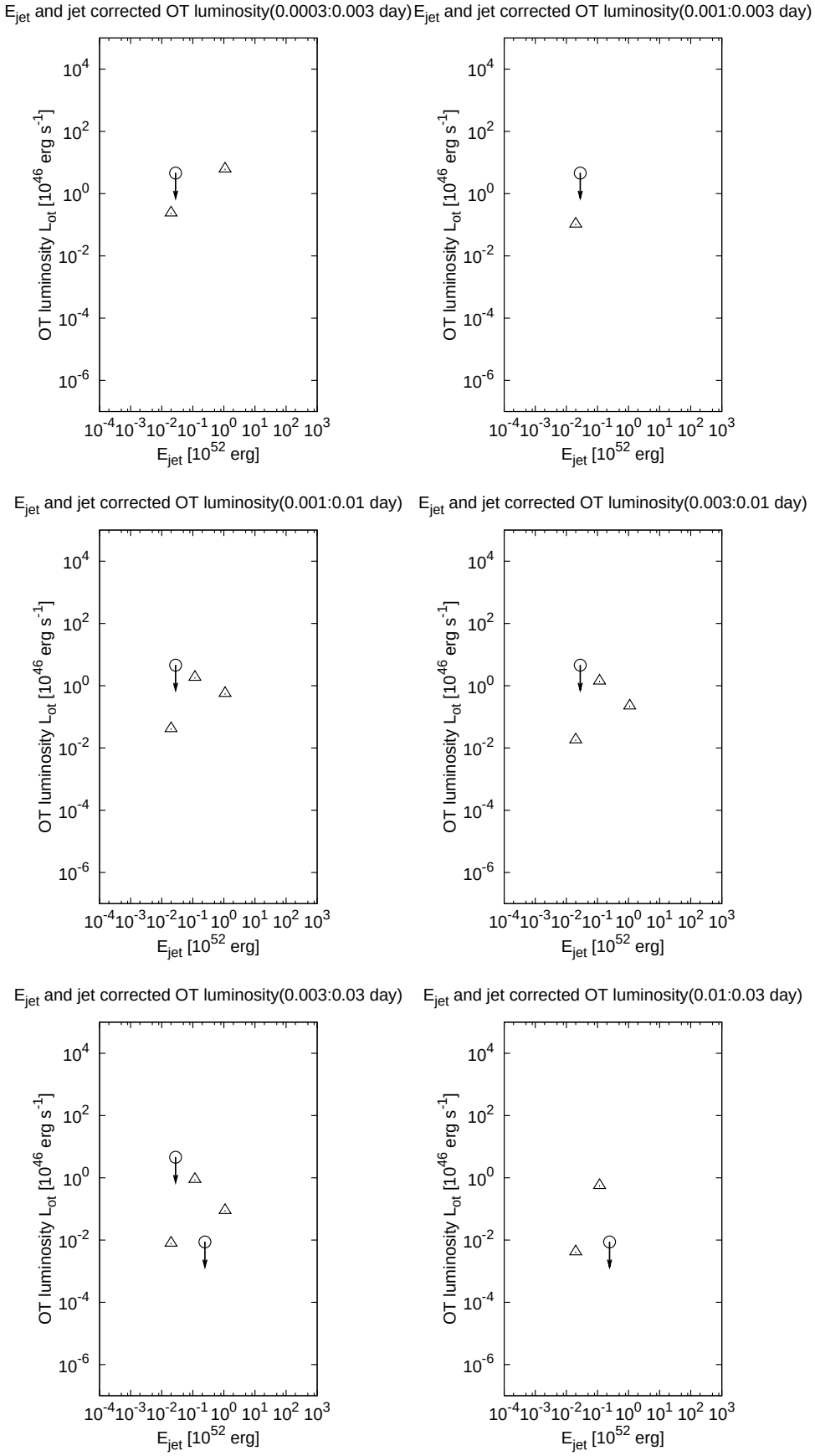

Figure D.29: $L_{\rm ot,jet}$ vs. $E_{\rm jet}$ (0.0003:0.003 – 0.01:0.03 day)

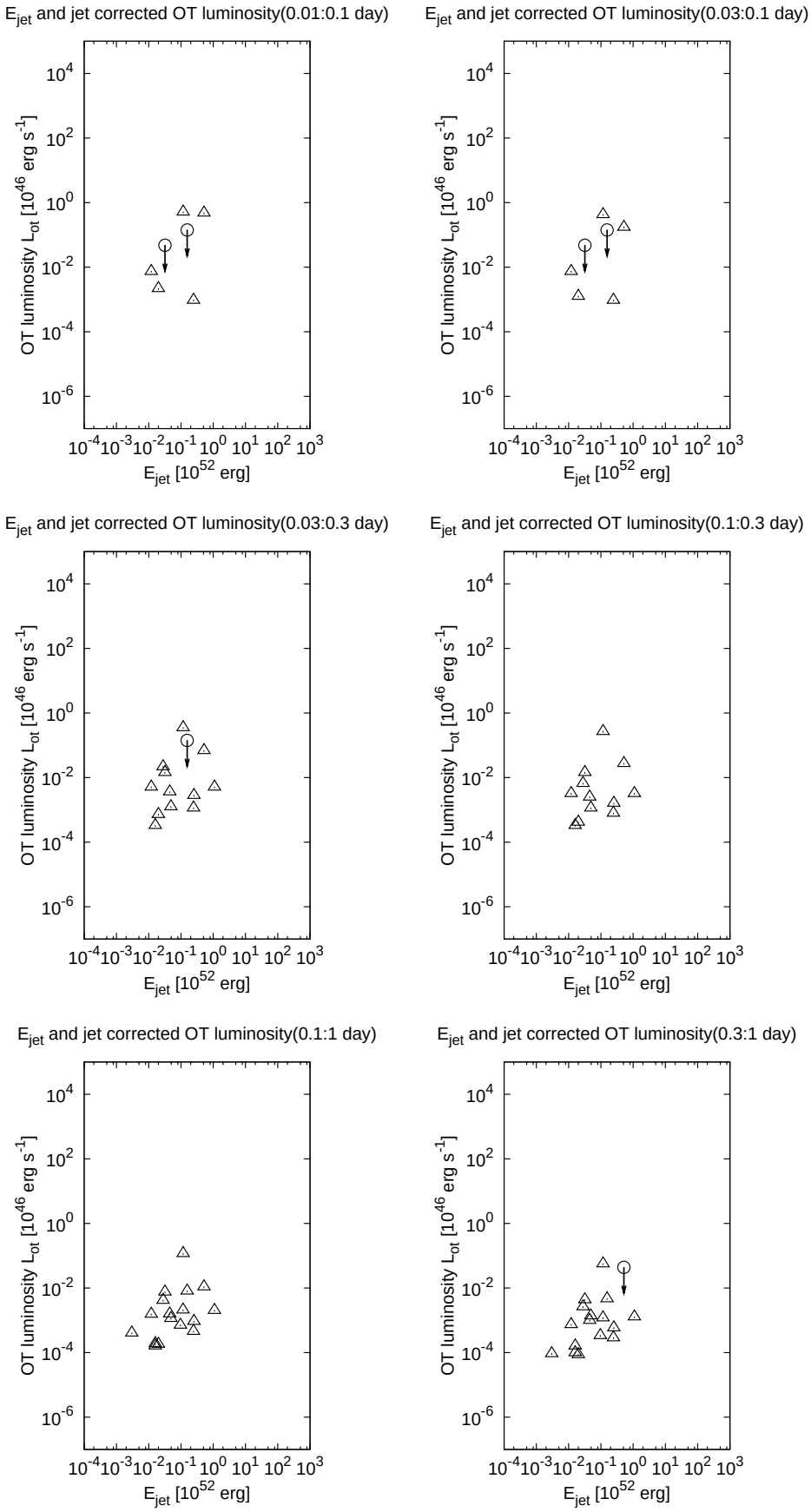

Figure D.30: $L_{\rm ot,jet}$ vs. $E_{\rm jet}$ (0.01:0.1 – 0.3:1 day)

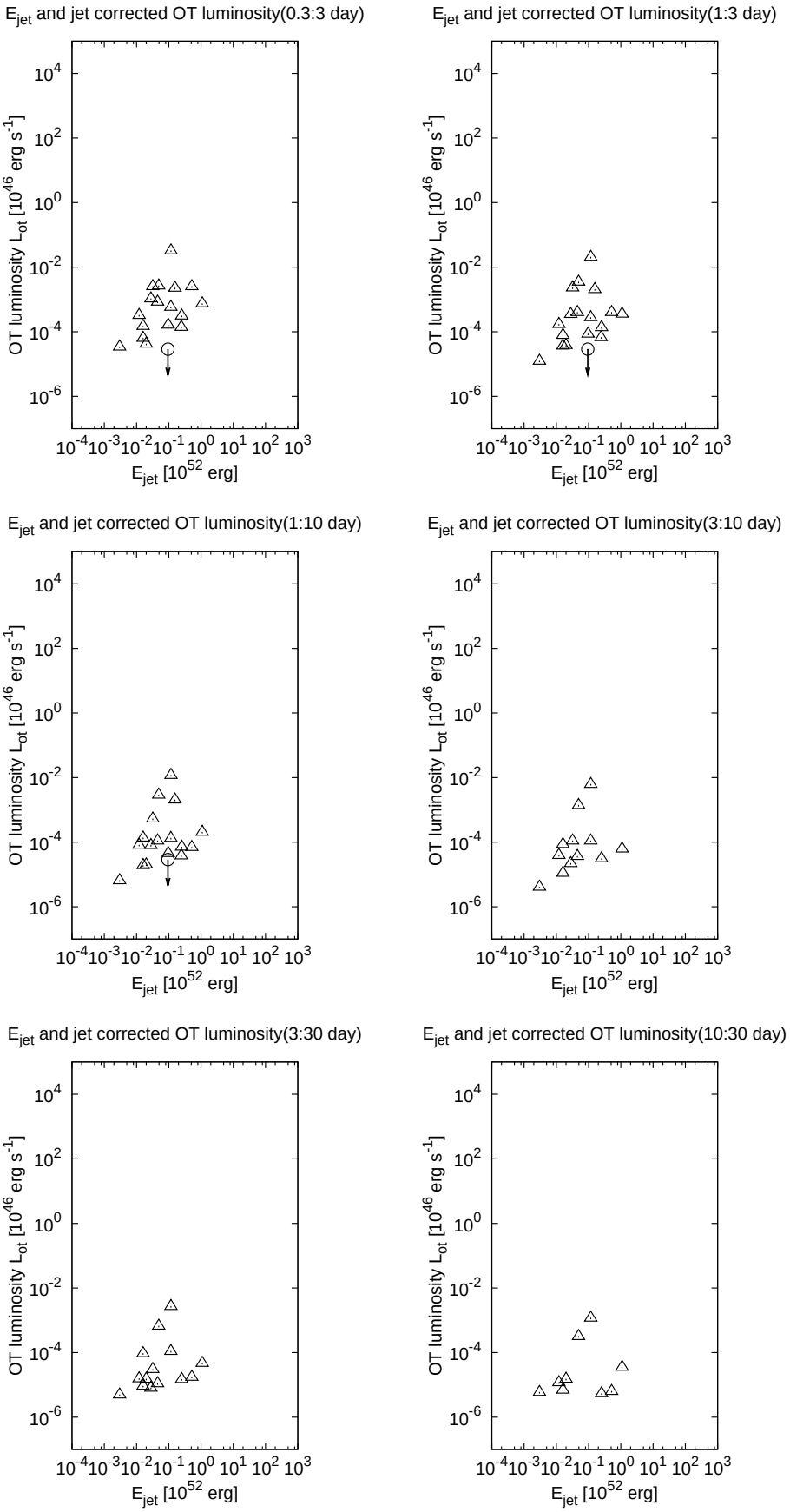

Figure D.31: $L_{\rm ot,jet}$ vs. $E_{\rm jet}$ (0.3:3 – 10:30 day)

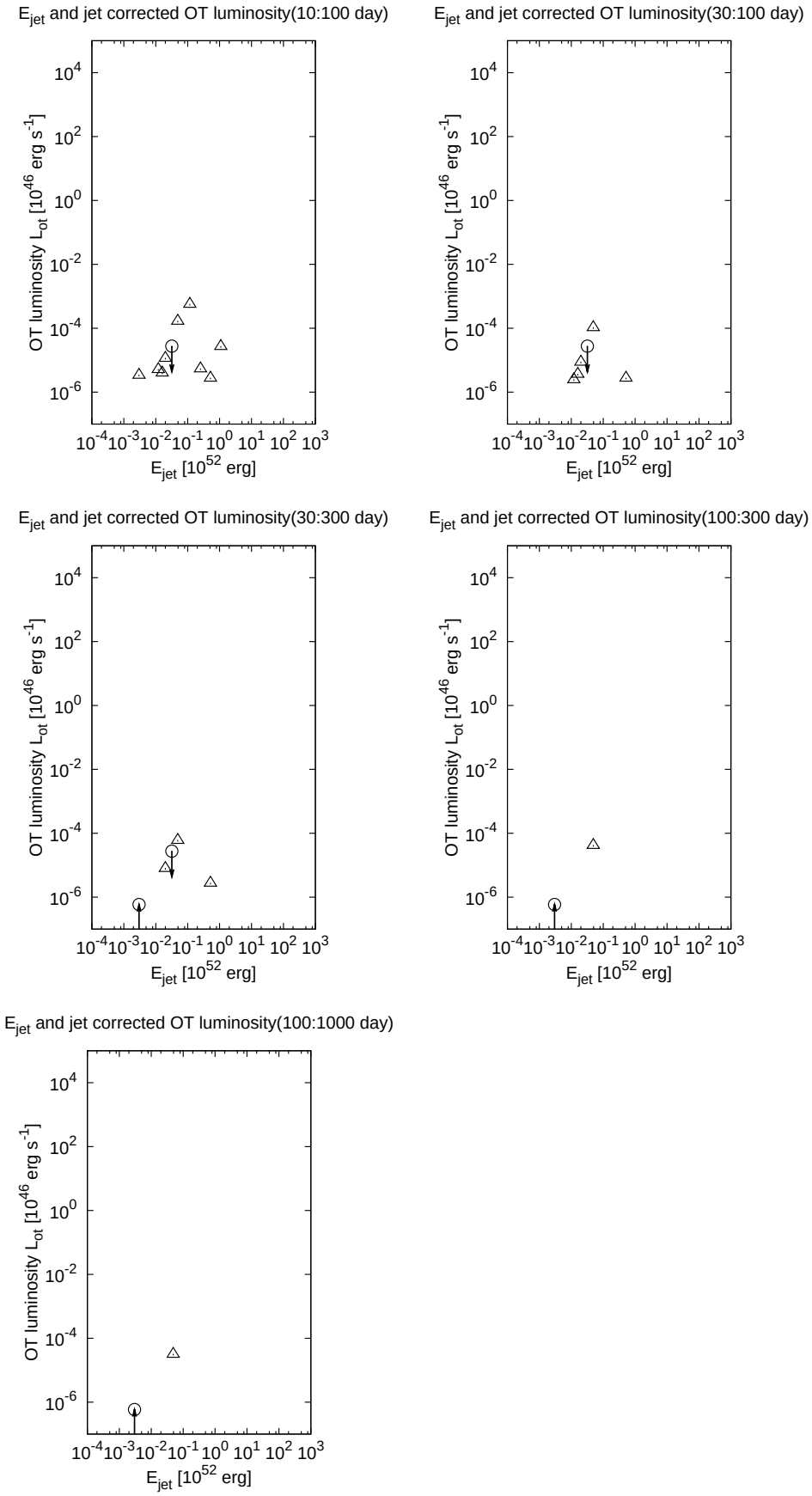

Figure D.32: $L_{\rm ot,jet}$ vs. $E_{\rm jet}$ (10:100 – 100:1000 day)

Appendix E

Data and references of optical afterglow

This chapter contains all the data we plotted in the section 4.3 and their references.

GRB970228

data#	time (start:end)	band	mag/flux density	reference
1	0.69	R	20.5 ± 0.5 [mag]	B
2	0.87	R	20.9 ± 0.14 [mag]	B
3	2.98	R	22.3 ± 0.9 [mag]	B
4	6.20	R	24.8 ± 1.2 [mag]	B
5	9.78	R	24.8 ± 1.2 [mag]	B
6	12.88	R	25.6 ± 2.6 [mag]	B
7	26.30	R	25.17 ± 0.13 [mag]	B
8	28.11	R	25.50 ± 0.13 [mag]	B
9	188.58	R	27.00 ± 0.35 [mag]	C
	0.876	V	<19 [mag]	E
	0.854(0.829:0.879)	5GHz	<0.7 [mJy]	A
	1.2(1.0:1.5)	5GHz	<0.7 [mJy]	A
	2.2(2.0:2.5)	5GHz	<0.7 [mJy]	A
	6.876	86.4GHz	<1.2 [mJy]	D

Table E.1: Data of GRB970228

ID	reference
A	Galama et al. (1997) IAUC 6574
B	Galama et al. (1997) Nature, 387, 479
C	Garcia et al. (1998) ApJL, 500, 105, Fruchter et al. (1997) IAUC 6747
D	Smith et al. (1997) IAUC 6577
E	Groot et al. (1997) IAUC 6574

Table E.2: References of GRB970228

GRB970508

data#	time (start:end)	band	mag/flux density	reference
1	0.224	R	21.20 ± 0.1 [mag]	A
2	0.291	R	21.08 ± 0.15 [mag]	A
3	0.296	R	21.25 ± 0.05 [mag]	A
4	0.846	R	21.19 ± 0.25 [mag]	A
5	0.946	R	21.13 ± 0.18 [mag]	A
6	0.995	R	20.7 ± 0.1 [mag]	A
7	1.026	R	20.88 ± 0.05 [mag]	A
8	1.126	R	20.46 ± 0.05 [mag]	A
9	1.238	R	20.09 ± 0.02 [mag]	A
10	1.274	R	19.93 ± 0.09 [mag]	A
11	1.866	R	19.70 ± 0.03 [mag]	A
12	1.946	R	19.6 ± 0.1 [mag]	A
13	1.968	R	19.6 ± 0.2 [mag]	A
14	2.026	R	19.80 ± 0.03 [mag]	A
15	2.076	R	19.92 ± 0.05 [mag]	A
16	2.106	R	19.77 ± 0.07 [mag]	A
17	2.240	R	19.9 ± 0.1 [mag]	A
18	2.294	R	19.87 ± 0.10 [mag]	A
19	2.856	R	20.10 ± 0.03 [mag]	A
20	2.964	R	20.2 ± 0.1 [mag]	A
21	3.235	R	20.3 ± 0.1 [mag]	A
22	3.299	R	20.25 ± 0.02 [mag]	A
23	4.946	R	20.3 ± 0.1 [mag]	A
24	5.263	R	21.05 ± 0.07 [mag]	A
25	5.496	R	20.9 ± 0.2 [mag]	A
26	7.980	R	21.51 ± 0.10 [mag]	A
27	10.147	R	21.88 ± 0.25 [mag]	A
28	11.971	R	21.81 ± 0.10 [mag]	A
29	12.988	R	22.09 ± 0.07 [mag]	A
30	14.066	R	22.04 ± 0.07 [mag]	A
31	24.008	R	23.10 ± 0.07 [mag]	A
32	24.686	R	23.1 ± 0.15 [mag]	A
33	27.356	R	23.2 ± 0.20 [mag]	A
34	29.975	R	23.52 ± 0.10 [mag]	A

Table E.3: Data of GRB970508

data#	time (start:end)	band	mag/flux density	reference
35	30.013	R	23.66 ± 0.10 [mag]	A
36	31.087	R	23.54 ± 0.20 [mag]	A
37	33.024	R	23.34 ± 0.20 [mag]	A
38	36.062	R	23.42 ± 0.14 [mag]	A
39	37.022	R	23.50 ± 0.25 [mag]	A
40	49.989	R	23.88 ± 0.16 [mag]	A
41	56.286	R	23.95 ± 0.20 [mag]	A
42	60.042	R	24.08 ± 0.20 [mag]	A
43	82.939	R	24.54 ± 0.25 [mag]	A
44	85.903	R	24.28 ± 0.35 [mag]	A
45	97.276	R	24.28 ± 0.10 [mag]	A
46	109.996	R	24.57 ± 0.07 [mag]	A
47	154.036	R	24.30 ± 0.20 [mag]	A
48	185.136	R	24.70 ± 0.15 [mag]	A
49	201.066	R	24.70 ± 0.14 [mag]	A
50	204.096	R	25.09 ± 0.14 [mag]	A
51	260.966	R	24.96 ± 0.17 [mag]	A
52	289.496	R	25.29 ± 0.16 [mag]	A
53	376.596	R	25.20 ± 0.25 [mag]	A

Table E.4: Data of GRB970508 (continued)

ID	reference
A	Garcia et al. (1998) ApJL, 500, 105

Table E.5: References of GRB970508

GRB971214

data#	time (start:end)	band	mag/flux density	reference
1	0.533(0.481:0.586)	R	21.67 ± 0.10 [mag]	F
2	0.537	R	22.06 ± 0.06 [mag]	H
3	1.557	R	23.36 ± 0.13 [mag]	H
4	2.527	R	24.08 ± 0.16 [mag]	H
5	2.537	R	24.4 ± 0.5 [mag]	G
6	3.527	R	24.61 ± 0.22 [mag]	H
	0.827	R	>21 [mag]	A
	0.497	I	21.2 ± 0.3 [mag]	B
	1.497	I	22.6 [mag]	B
	2.485(2.397:2.577)	I	22.9 ± 0.4 [mag]	C
	0.467	J	$20.47\ ^{+0.21}_{-0.19}$ [mag]	I
	1.477	J	$21.46\ ^{+0.34}_{-0.26}$ [mag]	I
	0.697	8.46GHz	<50 [μJy]	D
	1.367	8.46GHz	<17 [μJy]	D
	1.027	850 micron	<5 [mJy]	E
	2.027	850 micron	<1.4 [mJy]	E
	4.027	850 micron	<1.9 [mJy]	E
	7.027	850 micron	<1.3 [mJy]	E

Table E.6: Data of GRB971214

ID	reference
A	Itoh et al. (1997) IAUC 6788
B	Halpern et al. (1997) IAUC 6788
C	Rhoads et al. (1997) IAUC 6793
D	Frail et al. (1997) GCN3 message
E	Smith et al. (1997) GCN3 message
F	Henden et al. (1997) GCN3 massage
G	Castander et al. (1997) GCN3 message
H	Diercks et al. (1998) ApJL, 503, 105

Table E.7: References of GRB971214

GRB980326

data#	time (start:end)	band	mag/flux density	reference
1	0.422	R	21.04 [mag]	A
2	0.462	R	21.25 ± 0.03 [mag]	B
3	0.532	R	21.7 [mag]	C
4	1.122	R	22.9 [mag]	D
5	1.152	R	23.3 [mag]	D
6	1.282	R	23.4 [mag]	C
7	1.362	R	23.54 [mag]	A
8	1.362	R	23.58 ± 0.07 [mag]	B
9	2.382	R	24.45 ± 0.3 [mag]	B
10	3.312	R	24.5 [mag]	E
11	3.352	R	24.80 ± 0.15 [mag]	B
12	21.362	R	25.34 ± 0.33 [mag]	B
13	27.362	R	24.9 ± 0.3 [mag]	B
14	266.612	R	> 27.3 [mag]	B
	11.262	R	> 24.3 [mag]	F

Table E.8: Data of GRB980326

ID	reference
A	Eichelberger et al. (1998) GCN3 notice 33
B	Bloom et al. (1999) Nature, 401, 453
C	Groot et al. (1998) IAUC 6852
D	Groot et al. (1998) GCN3 notice 32
E	Grossan et al. (1998) GCN3 notice 34
F	Valdes et al. (1998) GCN3 notice 56

Table E.9: References of GRB980326

GRB980329

data#	time (start:end)	band	mag/flux density	reference
1	0.834	R	23.5 ± 0.2 [mag]	A
2	2.617(1.768:3.875)	R	24.8 ± 0.5 [mag]	B
3	3.844	R	25.7 ± 0.3 [mag]	C
	0.634	R	>22 [mag]	D
	0.654	R	>21 [mag]	E
	0.674	R	>20 [mag]	F
	0.744	R	>22 [mag]	D
	0.834	R	>21 [mag]	E
	1.384	R	>24 [mag]	A
	1.654	R	>22 [mag]	D
	1.754	R	>22 [mag]	D
	2.794	R	>22 [mag]	D
	2.854	R	>24 [mag]	A
	3.014	R	>24.2 [mag]	G
	4.944	R	>23.9 [mag]	G
	0.834	V	>23 [mag]	A
	1.834	V	>23 [mag]	A
	2.854	V	>23 [mag]	A
	0.737(0.644:0.844)	I	20.8 ± 0.3 [mag]	H
	0.694(0.684:0.704)	J	$19.27\ ^{+0.8}_{-0.5}$ [mag]	I
	3.066(3.011:3.121)	J	>20.9 [mag]	J
	4	K	20.7 ± 0.2 [mag]	K
	5	K	20.9 ± 0.2 [mag]	K
	8.114	K	21.4 ± 0.2 [mag]	L
	10.124	K	21.9 ± 0.4 [mag]	L
	7.044	850 micron	5 ± 1.5 [mJy]	M
	8.044	850 micron	4 ± 1.2 [mJy]	M
	9.044	850 micron	2 ± 0.8 [mJy]	M
	1.044	8.4GHz	166 ± 50 [μJy]	N
	2.944	8.4GHz	248 ± 16 [μJy]	N
	3.944	8.4GHz	65 ± 25 [μJy]	N
	— host	R	28.2 ± 0.3 [mag]	O

Table E.10: Data of GRB980329

ID	reference
A	Palazzi et al. (1998) GCN notice #48
B	Pedersen et al. (1998) GCN notice #52
C	Djorgovski et al. (1998) GCN notice #41
D	Guarnieri et al. (1998) IAUC 6855
E	Cappellaro et al. (1998) GCN notice #48
F	Brocato et al. (1998) GCN notice #48
G	Bradley (1998) GCN notice #45
H	Rhoads et al. (1998) GCN notice #157
K	Mannucci et al. (1998) GCN notice #46
J	Cole et al. (1998) GCN notice #47
K	Larkin et al. (1998) GCN notice #51
L	Metzger (1998) GCN notice #55
M	Smith et al. (1998) IAUC 6868
N	Taylor et al. (1998) GCN3 notice #40
O	Holland et al. (2000) GCN notice #778

Table E.11: References of GRB980329

GRB980613

data#	time (start:end)	band	mag/flux density	reference
1	0.6875	R	22.9 ± 0.2 [mag]	A
2	1.038	R	23.0 ± 0.1 [mag]	B
3	3.098	R	24.5 ± 0.5 [mag]	C
4	7.656	R	23.2 ± 0.1 [mag]	D
	0.736(0.678:0.798)	R	>20.5 [mag]	E
	2	R	>21 [mag]	F
	3	R	>21 [mag]	F
	4.7066	R	>24 [mag]	A
	0.998	I	22.5 ± 0.1 [mag]	B
	1.998	I	22.8 ± 0.2 [mag]	B
	0.688	I	>21.5 [mag]	G
	0.968	I	>22.3 [mag]	H
	1.968	I	>22.3 [mag]	H

Table E.12: Data of GRB980613

ID	reference
A	Hjorth et al. (1998) GCN notice #109
B	Halpern and Fesen (1998) GCN notice #134
C	Djorgovski et al. (1998) GCN notice #117
D	Sokolov et al. (1998) GCN notice #118
E	Castro-Tirado et al. (1998) GCN notice #102
F	Odewahn et al. (1998) GCN notice #105
G	Castro-Tirado et al. (1998) GCN notice #103
H	Halpern et al. (1998) GCN notice #106

Table E.13: References of GRB980613

GRB990123

data#	time (start:end)	band	mag/flux density	reference
1	0.0003	unfiltered	11.8 [mag]	A
2	0.0005	unfiltered	9.0 [mag]	A
3	0.0008	unfiltered	10.1 [mag]	A
4	0.0033	unfiltered	13.2 [mag]	A
5	0.0052	unfiltered	14.0 [mag]	A
6	0.0071	unfiltered	14.5 [mag]	A
7	0.157	R	18.2 [mag]	B
8	0.1600	R	18.7 $\pm$ 0.04 [mag]	C
9	0.1695	R	18.8 $\pm$ 0.04 [mag]	C
10	0.1778	R	18.8 $\pm$ 0.06 [mag]	C
11	0.348	R	19.2 $\pm$ 0.5 [mag]	D
12	0.668	R	19.9 $\pm$ 0.2 [mag]	E
13	0.681(0.654:0.709)	R	19.87 $\pm$ 0.2 [mag]	F
14	0.734	R	19.79 $\pm$ 0.1 [mag]	G
15	0.808	R	19.92 $\pm$ 0.1 [mag]	G
16	1.492	R	21.25 $\pm$ 0.1 [mag]	H
17	1.730	R	20.91 $\pm$ 0.1 [mag]	G
18	1.751	R	20.77 $\pm$ 0.1 [mag]	G
19	2.746	R	21.56 $\pm$ 0.1 [mag]	G

Table E.14: Data of GRB990123

data#	time (start:end)	band	mag/flux density	reference
20	7.112	R	23.01 ± 0.24 [mag]	I
21	11.132	R	23.55 ± 0.24 [mag]	J
22	14.192	R	23.44 ± 0.1 [mag]	K
23	16.192	R	23.41 ± 0.1 [mag]	L
24	22.092	R	23.77 ± 0.1 [mag]	J
	0.170	B	18.93 ± 0.03 [mag]	M
	0.550	B	20.16 ± 0.15 [mag]	N
	0.786	B	20.64 ± 0.07 [mag]	G
	1.492	B	21.25 ± 0.1 [mag]	H
	17.192	B	24.46 ± 0.15 [mag]	L
	0.756	V	19.97 ± 0.16 [mag]	G
	1.773	V	21.01 ± 0.20 [mag]	G
	1.795	V	20.93 ± 0.20 [mag]	G
	2.746	V	21.77 ± 0.16 [mag]	G
	16.192	V	24.05 ± 0.1 [mag]	L
	16	V	25.4 ± 0.1 [mag]	O
	59	V	27.7 ± 0.15 [mag]	O
	0.714	I	19.36 ± 0.2 [mag]	G
	1.410	i	21.0 ± 0.3 [mag]	P
	2.493	i	21.3 ± 0.3 [mag]	Q
	1.228	K	18.3 ± 0.03 [mag]	R
	1.752	K	>17.9 [mag]	S
	16	K	22 ± 0.7 [mag]	T
	1.812	J	>19.5 [mag]	U
	2.712	J	>19.3 [mag]	U
	1.242	8.46GHz	260 ± 32 [μJy]	V
	0.222	8.46GHz	<170 [μJy]	W
	3	8.46GHz	<78 [μJy]	X
	4	8.46GHz	<50 [μJy]	X
	5	8.46GHz	<50 [μJy]	X
	0.872	4.88GHz	<130 [μJy]	Y

Table E.15: Data of GRB990123 (continued)

ID	reference
A	Akerlof and McKay (1999) GCN notice #205
B	Odewahn et al. (1999) GCN notice #201
C	Gal et al. (1999) GCN notice #207
D	Zhu and Zhang (1999) GCN notice #204
E	Sokolov et al. (1999) GCN notice #209
F	Ofek and Leibowitz (1999) GCN notice #210
G	Masetti et al. (1999) GCN notice #233
H	Sagar et al. (1999) GCN notice #227
I	Yadigaroglu et al. (1999) GCN notice #242
J	Halpern et al. (1999) GCN notice #257
K	Veillet (1999) GCN notice #253
L	Veillet (1999) GCN notice #260
M	Bloom et al. (1999) GCN notice #206
N	Bloom et al. (1999) GCN notice #218
O	Fruchter et al. (2000) GCN notice #712
P	Zhu et al. (1999) GCN notice #217
Q	Zhu et al. (1999) GCN notice #226
R	Bloom et al. (1999) GCN notice #240
S	Antonelli et al. (1999) GCN notice #229
T	Djorgovski et al. (1999) GCN notice #256
U	Antonelli et al. (1999) GCN notice #232
V	Frail and Kulkarni (1999) GCN notice #211
W	Frail and Kulkarni (1999) GCN notice #200
X	Kulkarni and Frail (1999) GCN notice #239
Y	Galama et al. (1999) GCN notice #212

Table E.16: References of GRB990123

GRB990510

data#	time (start:end)	band	mag/flux density	reference
1	0.147	R	18.24 ± 0.02 [mag]	A
2	0.155	R	18.31 ± 0.02 [mag]	A
3	0.162	R	18.30 ± 0.02 [mag]	A
4	0.353	R	19.2 ± 0.3 [mag]	B
5	0.363	R	19.11 ± 0.02 [mag]	C
6	0.393	R	19.17 ± 0.02 [mag]	C
7	0.408	R	19.23 ± 0.07 [mag]	A
8	0.416	R	19.31 ± 0.07 [mag]	A
9	0.423	R	19.25 ± 0.02 [mag]	C
10	0.424	R	19.25 ± 0.04 [mag]	A
11	0.623	R	19.61 ± 0.01 [mag]	C
12	0.680	R	18.96 ± 0.02 [mag]	D
13	0.768	R	19.19 ± 0.02 [mag]	E
14	1.141	R	19.67 ± 0.07 [mag]	F
15	1.145	R	19.71 ± 0.06 [mag]	F
16	1.149	R	19.76 ± 0.09 [mag]	F
17	1.633	R	20.3 [mag]	G
18	5.743	R	23.0 ± 0.1 [mag]	H
19	6.740	R	23.4 ± 0.1 [mag]	I
20	7.764	R	23.7 ± 0.1 [mag]	I

Table E.17: Data of GRB990510

data#	time (start:end)	band	mag/flux density	reference
	0.994	B	20.47 ± 0.05 [mag]	J
	1.141	V	20.11 ± 0.09 [mag]	F
	1.145	V	20.01 ± 0.08 [mag]	F
	1.149	V	20.06 ± 0.07 [mag]	F
	2.033	V	21.2 [mag]	J
	3.001	V	21.86 ± 0.08 [mag]	K
	3.660	V	22.41 ± 0.06 [mag]	K
	3.862	V	22.46 ± 0.05 [mag]	K
	7.993	V	24.5 [mag]	L
	28.733	V	27.0 ± 0.2 [mag]	M
	38.533	V	27.8 ± 0.3 [mag]	M
	2.033	I	20.3 [mag]	J
	2.975	I	21.05 ± 0.13 [mag]	K
	3.631	I	21.17 ± 0.13 [mag]	K
	3.818	I	21.35 ± 0.07 [mag]	K

Table E.18: Data of GRB990510 (continued)

ID	reference
A	Axelrod et al. (1999) GCN notice #315
B	Vreeswijk et al. (1999) GCN notice #310
C	Galama et al. (1999) GCN notice #313
D	Covino et al. (1999) GCN notice #321
E	Lazzati et al. (1999) GCN notice #325
F	Bloom et al. (1999) GCN notice #323
G	Stanek et al. (1999) GCN notice #318
H	Marconi et al. (1999) GCN notice #329
I	Marconi et al. (1999) GCN notice #332
J	Pietrzynski et al. (1999) GCN notice #319
K	Pietrzynski et al. (1999) GCN notice #328
L	Beuermann et al. (1999) GCN notice #331
M	Fruchter et al. (1999) GCN notice #386

Table E.19: References of GRB990510

GRB990705

data#	time (start:end)	band	mag/flux density	reference
1	1.772	R	>22.0 [mag]	A
2	2.752	R	>22.3 [mag]	A
	0.227	H	16.57 ± 0.05 [mag]	B
	0.748	H	18.38 ± 0.05 [mag]	B
	1.287	H	>19.9 [mag]	B
	— host	V	22.8 ± 0.2 [mag]	C

Table E.20: Data of GRB990705

ID	reference
A	Halpern et al. (1999) GCN notice #381
B	Masetti et al. (2000) A&A, 354, 473
C	Holland et al. (2000) GCN notice #753

Table E.21: References of GRB990705

GRB990712

data#	time (start:end)	band	mag/flux density	reference
	0.176	R	19.35 ± 0.02 [mag]	A
1	0.176	R–host	19.5 ± 0.02 [mag]	A
	0.432	R	20.18 ± 0.01 [mag]	A
2	0.432	R–host	20.5 ± 0.01 [mag]	A
	0.454	R	20.18 ± 0.01 [mag]	A
3	0.454	R–host	20.5 ± 0.01 [mag]	A
	0.477	R	20.25 ± 0.09 [mag]	A
4	0.477	R–host	20.6 ± 0.09 [mag]	A
	0.631	R	20.47 ± 0.10 [mag]	A
5	0.631	R–host	20.9 ± 0.10 [mag]	A
	0.686	R	20.53 ± 0.02 [mag]	A
6	0.686	R–host	21.0 ± 0.02 [mag]	A
	0.698	R	20.46 ± 0.06 [mag]	A
7	0.698	R–host	20.9 ± 0.06 [mag]	A
	1.053	R	20.86 ± 0.09 [mag]	A
8	1.053	R–host	21.5 ± 0.09 [mag]	A
	1.430	R	20.97 ± 0.03 [mag]	A
9	1.430	R–host	21.7 ± 0.03 [mag]	A
	1.590	R	20.99 ± 0.04 [mag]	A
10	1.590	R–host	21.7 ± 0.04 [mag]	A
	1.986	R	21.49 ± 0.27 [mag]	A
11	1.986	R–host	23.2 ± 0.27 [mag]	A
	2.063	R	21.20 ± 0.12 [mag]	A
12	2.063	R–host	22.2 ± 0.12 [mag]	A
	3.706	R	21.42 ± 0.05 [mag]	A
13	3.706	R–host	21.42 ± 0.05 [mag]	A
	7.724	R	21.55 ± 0.05 [mag]	A
14	7.724	R–host	23.5 ± 0.05 [mag]	A

Table E.22: Data of GRB990712

data#	time (start:end)	band	mag/flux density	reference
	20.836	R	21.58 ± 0.04 [mag]	A
15	20.836	R–host	23.7 ± 0.04 [mag]	A
	30.535	R	21.65 ± 0.03 [mag]	A
16	30.535	R–host	24.3 ± 0.03 [mag]	A
	34.623	R	21.75 ± 0.06 [mag]	A
	34.748	R	21.78 ± 0.04 [mag]	A
17	48	R–host	24.35 ± 0.15 [mag]	B
	0.459	V	20.52 ± 0.01 [mag]	C
	0.459	V–host	20.7 ± 0.01 [mag]	C
	0.461	V	20.50 ± 0.01 [mag]	C
	0.461	V–host	20.7 ± 0.01 [mag]	C
	0.708	V	20.83 ± 0.03 [mag]	C
	0.708	V–host	21.2 ± 0.03 [mag]	C
	0.709	V	20.83 ± 0.03 [mag]	C
	0.709	V–host	21.2 ± 0.03 [mag]	C
	1.460	V	21.24 ± 0.04 [mag]	C
	1.460	V–host	21.8 ± 0.04 [mag]	C
	1.595	V	21.34 ± 0.08 [mag]	C
	1.595	V–host	21.9 ± 0.08 [mag]	C
	1.601	V	21.32 ± 0.08 [mag]	C
	1.601	V–host	21.9 ± 0.08 [mag]	C
	2.090	V	21.80 ± 0.09 [mag]	C
	2.090	V–host	22.9 ± 0.09 [mag]	C
	7.736	V	22.07 ± 0.10 [mag]	C
	7.736	V–host	23.8 ± 0.10 [mag]	C
	20.814	V	22.14 ± 0.04 [mag]	C
	20.814	V–host	24.3 ± 0.04 [mag]	C
	34.774	V	22.30 ± 0.05 [mag]	C
	47.706	V–host	25.3 ± 0.2 [mag]	C
	1.077	I	20.27 ± 0.08 [mag]	A
	1.077	I–host	20.8 ± 0.08 [mag]	A
	1.574	I	20.60 ± 0.08 [mag]	A
	1.574	I–host	21.4 ± 0.08 [mag]	A
	2.113	I	20.99 ± 0.26 [mag]	A
	2.113	I–host	22.2 ± 0.26 [mag]	A
	7.742	I	20.95 ± 0.10 [mag]	A
	7.742	I–host	22.2 ± 0.10 [mag]	A
	20.857	I	21.16 ± 0.17 [mag]	A
	20.857	I–host	23.1 ± 0.17 [mag]	A
	34.717	I	21.42 ± 0.10 [mag]	A
	— host	R	21.95 ± 0.15 [mag]	B
	— host	V	22.3 ± 0.05 [mag]	A
	— host	I	21.35 ± 0.05 [mag]	A

Table E.23: Data of GRB990712 (continued)

ID	reference
A	Sahu et al. (2000) ApJ, 540, 74
B	Fruchter et al. (2000) GCN notice #752
C	Björnsson et al. (2001) ApJ, 522, L121

Table E.24: References of GRB990712

GRB000210

data#	time (start:end)	band	mag/flux density	reference
1	0.250(0.234:0.268)	R	>18.0 [mag]	A
2	0.686	R	>23.3 [mag]	B
	0.616	radio	<0.26 [mJy]	C
	4.601(4.536:4.666)	8.46GHz	<55 [μJy]	D
	— host	R	23.5 $\pm$ 0.2 [mag]	E

Table E.25: Data of GRB000210

ID	reference
A	Bhargavi et al. (2000) GCN notice #554
B	Gorosabel et al. (2000) GCN notice #547
C	Berger and Frail (2000) GCN notice #546
C	McConnell et al. (2000) GCN notice #560
E	Gorosabel et al. (2000) GCN notice #783

Table E.26: References of GRB000210

GRB000214

data#	time (start:end)	band	mag/flux density	reference
	1.350	K'	>18.15 [mag]	A
	3.368	K'	>19.1 [mag]	A
	3.878	4.8GHz,8.6GHz	<235 [μJy]	B

Table E.27: Data of GRB000214

ID	reference
A	Rhoads et al. (2000) GCN notice #564
B	Subrahmanyan et al. (2000) GCN notice #562

Table E.28: References of GRB000214

GRB010213

data#	time (start:end)	band	mag/flux density	reference
	1.554	R	>17 [mag]	A
	1.565	R	>20.5 [mag]	B
1	1.975	R	>22 [mag]	C

Table E.29: Data of GRB010213

ID	reference
A	Boer et al. (2001) GCN notice #936
B	Hudec et al. (2001) GCN notice #941
C	Zhu (2001) GCN notice #946

Table E.30: References of GRB010213

GRB010222

data#	time (start:end)	band	mag/flux density	reference
1	0.157	R	18.18 ± 0.02 [mag]	A
2	0.166	R	18.21 ± 0.02 [mag]	A
3	0.178	R	18.36 ± 0.06 [mag]	B
4	0.2000	R	18.4 ± 0.1 [mag]	C
5	0.207	R	18.36 ± 0.02 [mag]	A
6	0.2156	R	18.67 ± 0.06 [mag]	D
7	0.225	R	18.67 ± 0.06 [mag]	B
8	0.2305	R	18.66 ± 0.06 [mag]	D
9	0.3340	R	18.9 ± 0.1 [mag]	C
10	0.642	R	19.62 ± 0.12 [mag]	E
11	0.702(0.700:0.704)	R	19.56 ± 0.03 [mag]	F
12	0.7091	R	19.71 ± 0.01 [mag]	D
13	0.713(0.712:0.715)	R	19.56 ± 0.03 [mag]	F
14	0.7548	R	19.92 ± 0.17 [mag]	G
15	0.7764	R	19.83 ± 0.01 [mag]	D
16	0.838(0.837:0.840)	R	19.76 ± 0.03 [mag]	F
17	0.858(0.857:0.859)	R	19.79 ± 0.05 [mag]	F
18	0.953	R	19.95 ± 0.06 [mag]	H
19	0.9778	R	20.13 ± 0.02 [mag]	D
20	1.7621	R	20.95 ± 0.02 [mag]	D
21	1.833	R	21.05 ± 0.03 [mag]	D
22	1.867	R	21.04 ± 0.03 [mag]	D
23	1.9280	R	20.88 ± 0.03 [mag]	I
24	2.1552	R	21.23 ± 0.06 [mag]	D
25	2.6844	R	21.41 ± 0.17 [mag]	J
26	2.7499	R	21.43 ± 0.06 [mag]	D
27	2.9455	R	21.64 ± 0.04 [mag]	D
28	3.1305	R	21.48 ± 0.08 [mag]	K
29	3.6875	R	21.99 ± 0.13 [mag]	J
30	6.345	R	22.73 ± 0.10 [mag]	L
31	7.320	R	22.96 ± 0.10 [mag]	L
32	8.3330	R	23.10 ± 0.10 [mag]	M
33	24	R	24.53 ± 0.25 [mag]	N
	1.821(1.777:1.866)	R	>21 [mag]	f
	6.5934	R	>22.1 [mag]	J
	6.6177	R	>22.1 [mag]	J
	7.6239	R	>22.9 [mag]	J
	0.1823	B	18.46 ± 0.02 [mag]	e
	0.5147	B	19.84 ± 0.31 [mag]	G
	0.866	B	19.64 ± 0.07 [mag]	d
	1.0135	B	20.25 ± 0.10 [mag]	e

Table E.31: Data of GRB010222

data#	time (start:end)	band	mag/flux density	reference
	0.6107	V	19.70 ± 0.13 [mag]	G
	0.7054	V	19.92 ± 0.14 [mag]	G
	0.8359	V	20.29 ± 0.21 [mag]	G
	2.6690	I	20.8 ± 0.2 [mag]	J
	3.6736	I	21.42 ± 0.18 [mag]	J
	0.712(0.700:0.725)	J	18.7 ± 0.1 [mag]	c
	0.775(0.760:0.791)	K	17.4 ± 0.3 [mag]	c
	0.2358	350GHz	4.2 ± 1.2 [mJy]	g
	1.15	350GHz	3.6 ± 0.9 [mJy]	g
	2.37	350GHz	4.2 ± 1.3 [mJy]	g
	0.312	22GHz	0.70 ± 0.15 [mJy]	a
	0.327(0.236:0.453)	850micron	4.2 ± 1.2 [mJy]	b
	8.379(8.313:8.445)	850micron	0.7 ± 1.1 [mJy]	h

Table E.32: Data of GRB010222 (continued)

ID	reference
A	Stanek et al. (2001) GCN notice #970
B	Henden and Vrba (2001) GCN notice #967
C	Watanabe et al. (2001) GCN notice #993
D	Holland et al. (2001) GCN notice #1002
E	Price et al. (2001) GCN notice #973
F	Fynbo et al. (2001) GCN notice #975
G	Oksanen et al. (2001) GCN notice #990
H	Orosz (2001) GCN notice #976
I	Masetti et al. (2001) GCN notice #985
J	Cowsik and Bhargavi (2001) GCN notice #1051
K	Stanek and Falco (2001) GCN notice #991
L	Veillet (2001) GCN notice #1000
M	Veillet (2001) GCN notice #1003
N	Garnavich et al. (2001) GCN notice #1009
a	Berger and Frail (2001) GCN notice #968
b	Fich et al. (2001) GCN notice #971
c	Paola et al. (2001) GCN notice #977
d	Bartolini et al. (2001) GCN notice #982
e	Stanek et al. (2001) GCN notice #983
f	Valentini et al. (2001) GCN notice #986
g	Kulkarni et al. (2001) GCN notice #996
h	Ivison et al. (2001) GCN notice #1004

Table E.33: References of GRB010222

GRB010629B

data#	time (start:end)	band	mag/flux density	reference
1	0.720	R	>20 [mag]	A
	1.018	I	>20.5 [mag]	B
	1.124	I	>20.5 [mag]	B
	1.32	I	>19 [mag]	C

Table E.34: Data of GRB010629B

ID	reference
A	Halpern Mirabal (2001) GCN notice #1079
B	Andersen et al. (2001) GCN notice #1080
C	Henden (2001) GCN notice #1077

Table E.35: References of GRB010629B

GRB010921

data#	time (start:end)	band	mag/flux density	reference
1	0.037	clear	>15.3 [mag]	A
2	0.889	r'	19.6 ± 0.3 [mag]	B
3	0.909	R	19.4 ± 0.2 [mag]	C
4	1.048	R	19.9 ± 0.2 [mag]	C
	1.909	R	>21.2 [mag]	C
	2.050	R	>21.2 [mag]	C
	0.037	V	>14.2 [mag]	A
	1.652	I	18.93 ± 0.03 [mag]	D

Table E.36: Data of GRB010921

ID	reference
A	Park et al. (2001) GCN notice #1114
B	Lamb et al. (2001) GCN notice #1125
C	Park et al. (2001) GCN notice #1131
D	Klose and Stecklum (2001) GCN notice #1113

Table E.37: References of GRB010921

GRB011019

data#	time (start:end)	band	mag/flux density	reference
	0.554	R	>15.5 [mag]	A
1	0.734	R	>19 [mag]	B
	1.027	R	>19.5 [mag]	C
2	1.057	R	>25 [mag]	D
	2.21	R	>19.5 [mag]	E

Table E.38: Data of GRB011019

ID	reference
A	Bondar et al. (2001) GCN notice #1130
B	Akerlof et al. (2001) GCN notice #1115
C	Price et al. (2001) GCN notice #1112
D	Komiyama et al. (2001) GCN notice #1128
E	Fox et al. (2001) GCN notice #1116

Table E.39: References of GRB011019

GRB011030

data#	time (start:end)	band	mag/flux density	reference
1	0.2999	R	> 21 [mag]	A
2	2	R	> 23.61 [mag]	B
3	4	R	> 23.28 [mag]	B
	10	R	> 22.9 [mag]	C
	1.461(1.456:1.466)	unfiltered	> 19.5 [mag]	D
	9.960	I	22.5 [mag]	E
	0.940	I	> 20.5 [mag]	F
	1.951	I	> 20.5 [mag]	F
	0.552(0.491:0.621)	J	> 19.8 [mag]	G
	1.829(1.810:1.849)	z	> 22.5 [mag]	H
	0.524(0.503:0.545)	K'	> 19.5 [mag]	I
	0.552(0.491:0.621)	K	> 18.0 [mag]	G
	0.841	K	> 18 [mag]	J
	1.931	K	> 18 [mag]	J
	11.63(11.58:11.68)	K	> 20.1 [mag]	K
	0.6159	15GHz	<0.4 [mJy]	L
	9.530	8.47GHz	181 ± 18 [μJy]	M

Table E.40: Data of GRB011030

ID	reference
A	Mohan et al. (2001) GCN notice #1120
B	Rhoads et al. (2001) GCN notice #1140
C	Bloom et al. (2001) GCN notice #1137
D	Hudec et al. (2001) GCN notice #1144
E	Halpern et al. (2001) GCN notice #1139
F	Halpern et al. (2001) GCN notice #1127
G	Mannucci et al. (2001) GCN notice #1145
H	Brown et al. (2001) GCN notice #1141
I	Klose et al. (2001) GCN notice #1142
J	Hammell et al. (2001) GCN notice #1126
K	Antonelli et al. (2001) GCN notice #1146
L	Pooley (2001) GCN notice #1121
M	Taylor et al. (2001) GCN notice #1136

Table E.41: References of GRB011030

GRB011121

data#	time (start:end)	band	mag/flux density	reference
1	0.4387	R	19.11 ± 0.03 [mag]	A
2	0.4915	R	19.25 ± 0.05 [mag]	B
3	0.5228	R	19.44 ± 0.03 [mag]	A
4	0.5714	R	19.60 ± 0.03 [mag]	A
5	1.4297	R	21.15 ± 0.07 [mag]	A
6	1.5311	R	21.1 ± 0.1 [mag]	C
7	2.5415	R	21.97 ± 0.07 [mag]	A
	0.5637	U	20.7 ± 0.2 [mag]	B
	1.5498	U	22.4 ± 0.1 [mag]	C
	0.5082	B	20.86 ± 0.05 [mag]	B
	1.5401	B	22.6 ± 0.1 [mag]	C
	0.5158	V	20.00 ± 0.05 [mag]	B
	0.5005	I	18.66 ± 0.05 [mag]	B
	0.5616	I	20.3 ± 0.1 [mag]	C
	0.5732	J	17.85 ± 0.05 [mag]	D
	0.5772	J	17.80 ± 0.04 [mag]	D
	0.5813	J	17.79 ± 0.04 [mag]	D
	0.9349	J	18.35 ± 0.10 [mag]	D
	1.5365	J	19.46 ± 0.07 [mag]	D
	6.7172	J	21.29 ± 0.28 [mag]	D
	7.517	J	>21.9 [mag]	E
	0.5350	K	15.96 ± 0.05 [mag]	D
	0.5416	K	15.96 ± 0.04 [mag]	D
	0.5501	K	16.05 ± 0.04 [mag]	D
	0.5626	K	16.03 ± 0.04 [mag]	D
	0.6943	K	16.42 ± 0.04 [mag]	D
	0.7126	K	16.54 ± 0.04 [mag]	D
	0.7298	K	16.50 ± 0.04 [mag]	D
	0.8238	K	16.61 ± 0.06 [mag]	D
	0.8569	K	16.78 ± 0.04 [mag]	D
	0.8994	K	17.04 ± 0.08 [mag]	D
	0.9444	K	17.01 ± 0.05 [mag]	D
	1.5508	K	17.92 ± 0.05 [mag]	D
	6.9264	K	19.35 ± 0.23 [mag]	D
	0.8839	3cm	0.2 [mJy]	F

Table E.42: Data of GRB011121

ID	reference
A	Stanek and Wyrzykowski (2001) GCN notice #1160
B	Olsen et al. (2001) GCN notice #1157
C	Brown et al. (2001) GCN notice #1158
D	Price et al. (2002) ApJ, 572, L51
E	Phillips et al. (2001) GCN notice #1164
F	Subrahmanyan et al. (2001) GCN notice #1156

Table E.43: References of GRB011121

GRB011130

data#	time (start:end)	band	mag/flux density	reference
1	0.684	R	> 18.5 [mag]	A
	0.976	R	> 18.5 [mag]	B

Table E.44: Data of GRB011130

ID	reference
A	Greiner et al. (2001) GCN notice #1171
B	Fox et al. (2001) GCN notice #1170

Table E.45: References of GRB011130

GRB011211

data#	time (start:end)	band	mag/flux density	reference
	0.402	R	19 [mag]	A
1	0.422	R	20.07 ± 0.15 [mag]	B
2	0.4488	R	20.10 ± 0.08 [mag]	C
3	0.452	R	20.28 ± 0.02 [mag]	D
4	0.4548	R	20.41 ± 0.04 [mag]	C
5	0.4758	R	20.43 ± 0.05 [mag]	C
6	0.482	R	20.12 ± 0.15 [mag]	B
7	0.4928	R	20.35 ± 0.03 [mag]	C
8	0.5208	R	20.40 ± 0.04 [mag]	C
9	0.542	R	20.58 ± 0.02 [mag]	D
10	1.0740	R	20.91 ± 0.13 [mag]	E
11	1.102	R	20.77 ± 0.06 [mag]	F
12	1.1620	R	21.04 ± 0.07 [mag]	E
13	1.200	R	21.12 ± 0.08 [mag]	F
14	1.4398	R	21.48 ± 0.11 [mag]	C
15	1.512	R	21.46 ± 0.04 [mag]	D
16	1.5418	R	21.52 ± 0.07 [mag]	C
17	4.5089	R	23.32 ± 0.25 [mag]	E
18	5.5049	R	23.69 ± 0.25 [mag]	E
19	6.5062	R	24.22 ± 0.40 [mag]	E
20	9.5098	R	25.27 ± 0.16 [mag]	E
21	9.992	R	24.8 ± 0.3 [mag]	G
22	14.0208	R	26.71 ± 0.16 [mag]	E
23	25.9738	R	26.45 ± 0.21 [mag]	E
24	31.9138	R	28.40 ± 0.48 [mag]	E
	2.702	R	>22.4 [mag]	H
	1.4485	U	21.5 ± 0.3 [mag]	E
	0.482	B	21.41 ± 0.15 [mag]	B
	1.1837	B	21.91 ± 0.11 [mag]	E
	1.184	B	22.07 ± 0.09 [mag]	F
	1.4298	B	22.24 ± 0.08 [mag]	E
	1.5400	B	22.29 ± 0.07 [mag]	E
	2.1568	B	23.06 ± 0.27 [mag]	E
	0.492	V	21.14 ± 0.15 [mag]	B
	0.5048	V	20.79 ± 0.05 [mag]	C
	0.562	V	21.21 ± 0.15 [mag]	B
	1.142	V	21.59 ± 0.06 [mag]	F
	1.4658	V	21.71 ± 0.09 [mag]	C
	1.472	V	21.7 [mag]	I
	1.492	V	21.81 ± 0.06 [mag]	J
	1.5062	V	21.76 ± 0.09 [mag]	E
	2.1198	V	21.82 ± 0.22 [mag]	E
	8.5105	V	25.00 ± 0.22 [mag]	E
	2.702	V	>22.3 [mag]	H

Table E.46: Data of GRB011211

data#	time (start:end)	band	mag/flux density	reference
	0.4648	I	19.95 ± 0.06 [mag]	C
	0.4848	I	19.92 ± 0.07 [mag]	C
	0.5128	I	19.96 ± 0.05 [mag]	C
	0.5288	I	20.10 ± 0.06 [mag]	C
	1.1897	I	20.92 ± 0.21 [mag]	E
	1.4161	I	20.99 ± 0.23 [mag]	E
	1.4548	I	20.80 ± 0.11 [mag]	C
	1.5255	I	20.86 ± 0.15 [mag]	E
	1.5518	I	20.94 ± 0.12 [mag]	C
	3.5087	I	22.75 ± 0.25 [mag]	E
	2.702	I	>21.0 [mag]	H
	9.2350	I	>23.2 [mag]	E
	0.5634	J	19.34 ± 0.05 [mag]	E
	2.5488	J	21.04 ± 0.05 [mag]	E
	0.5754	K	18.02 ± 0.07 [mag]	E

Table E.47: Data of GRB011211 (continued)

ID	reference
A	Grav et al. (2001) GCN notice #1191
B	Jensen et al. (2001) GCN notice #1195
C	Soszynski et al. (2001) GCN notice #1199
D	Gladders et al. (2001) GCN notice #1209
E	Jakobsson et al. (2003) A&A, 408, 941
F	Bhargavi and Cowsik (2001) GCN notice #1202
G	Burud et al. (2001) GCN notice #1213
H	Holland et al. (2001) GCN notice #1204
I	Fiore et al. (2001) GCN notice #1203
J	Covino et al. (2001) GCN notice #1214

Table E.48: References of GRB011211

GRB011212

data#	time (start:end)	band	mag/flux density	reference
	0.681	R	>19.5 [mag]	A
	0.697(0.644:0.755)	R	>18.5 [mag]	B
	0.981	r	>21.0 [mag]	C
1	0.981	R	>22.7 [mag]	D
2	1.376	R	>20.5 [mag]	E
	1.153(1.125:1.182)	I	>21.6 [mag]	F
	2.075(2.038:2.112)	I	>21.6 [mag]	F

Table E.49: Data of GRB011212

ID	reference
A	Sergeev et al. (2001) GCN notice #1206
B	Henden (2001) GCN notice #1198
C	Fox et al. (2001) GCN notice #1196
D	Saracco et al. (2001) GCN notice #1210
E	Kinugasa et al. (2001) GCN notice #1205
F	Vrba et al. (2001) GCN notice #1216

Table E.50: References of GRB011212

GRB020124

data#	time (start:end)	band	mag/flux density	reference
1	0.067	R_M	17.92 ± 0.04 [mag]	A
2	0.0702	R	18.22 ± 0.05 [mag]	A
3	0.072	R_M	17.98 ± 0.04 [mag]	A
4	0.0744	R	18.37 ± 0.09 [mag]	A
5	0.076	R_M	18.11 ± 0.05 [mag]	A
6	0.0787	R	18.38 ± 0.08 [mag]	A
	0.085	R	18.5 [mag]	B
7	0.107	R	$18.5\ ^{+0.4}_{-0.3}$ [mag]	C
8	0.113	R_M	18.68 ± 0.05 [mag]	A
9	0.117	R_M	18.87 ± 0.04 [mag]	A
10	0.122	R_M	18.84 ± 0.04 [mag]	A
11	1.610(1.590:1.631)	R	23.84 ± 0.17 [mag]	D
12	1.8960	R	24.40 ± 0.23 [mag]	A
13	17.645	Clear	$28.68\ ^{+0.25}_{-0.20}$ [mag]	A
14	24.855	Clear	$29.35\ ^{+0.60}_{-0.39}$ [mag]	A
15	32.265	Clear	$29.56\ ^{+0.76}_{-0.44}$ [mag]	A
	0.072(0.055:0.095)	unfiltered	>17.8 [mag]	E
	0.249(0.235:0.363)	unfiltered	>18.6 [mag]	E
	0.283(0.263:0.305)	unfiltered	>18.8 [mag]	E
16	0.325(0.305:0.346)	unfiltered	>19.1 [mag]	E
	0.475	R	>18.5 [mag]	F
	0.495	R	>16.3 [mag]	G
	0.510(0.469:0.554)	unfiltered	>15.0 [mag]	H
	0.067	B_M	18.63 ± 0.06 [mag]	A
	0.072	B_M	18.73 ± 0.06 [mag]	A
	0.076	B_M	18.84 ± 0.07 [mag]	A
	0.113	B_M	19.66 ± 0.09 [mag]	A
	0.117	B_M	19.58 ± 0.05 [mag]	A
	0.122	B_M	19.71 ± 0.05 [mag]	A

Table E.51: Data of GRB020124

ID	reference
A	Berger et al. (2002) ApJ, 581, 981
B	Price et al. (2002) GCN notice #1221
C	Torii et al. (2002) GCN notice #1378
D	Gorosabel et al. (2002) GCN notice #1224
E	Kawai et al. (2002) GCN notice #1343
F	Pavlenko et al. (2002) GCN notice #1226
G	Bondar' et al. (2002) GCN notice #1228
H	Jelinek et al. (2002) GCN notice #1236

Table E.52: References of GRB020124

GRB020127

data#	time (start:end)	band	mag/flux density	reference
	0.113	R	>14.1 [mag]	A
	0.131	R	>21.5 [mag]	B
	0.165	R	>13.7 [mag]	A
1	0.195	R	>19.5 [mag]	C
	0.235	R	>13.5 [mag]	A
	0.847	2.3GHz	<0.62 [mJy]	D

Table E.53: Data of GRB020127

ID	reference
A	Bondar' et al. (2002) GCN notice #1235
B	Castro Cerón et al. (2002) GCN notice #1234
C	Lamb et al. (2002) GCN notice #1230
D	Rol et al. (2002) GCN notice #1246

Table E.54: References of GRB020127

GRB020305

data#	time (start:end)	band	mag/flux density	reference
1	0.833	r*	20.1 ± 0.5 [mag]	A
2	7.103	R	22.6 [mag]	B
3	38.3(38.2:38.4)	Clear	24.69 ± 0.01 [mag]	C
4	103.0(102.9:103.0)	Clear	26.20 ± 0.03 [mag]	C
	0.436	R	>14.5 [mag]	D
	0.521	R	>14.5 [mag]	D
	0.617	R	>14.5 [mag]	D
	0.667	R	>18 [mag]	E
	3.843	R	>21.5 [mag]	F
	0.667	V	>17 [mag]	E
	7.103	I	22.1 [mag]	B
	7.933	K'	19.7 [mag]	G
	8.893	K'	19.8 [mag]	G

Table E.55: Data of GRB020305

ID	reference
A	Lee et al. (2002) GCN notice #1275
B	Ohyama et al. (2002) GCN notice #1271
C	Gorosabel et al. (2002) GCN notice #1542
D	Jelinek et al. (2002) GCN notice #1265
E	Moran et al. (2002) GCN notice #1264
F	Price et al. (2002) GCN notice #1267
G	Burud et al. (2002) GCN notice #1283

Table E.56: References of GRB020305

GRB020331

data#	time (start:end)	band	mag/flux density	reference
1	0.031	R	$17.9\ ^{+0.8}_{-0.4}$ [mag]	A
2	0.531	R	21 ± 0.11 [mag]	B
3	0.711	R	21 [mag]	C
4	8.371	R	22.9 ± 0.14 [mag]	D
5	23.211	Clear	24.54 ± 0.07 [mag]	E
6	35.911	Clear	24.86 ± 0.10 [mag]	E
7	42.011	Clear	25.01 ± 0.09 [mag]	E
8	48.611	Clear	24.76 ± 0.11 [mag]	E
	0.085(0.071:0.101)	unfiltered	>14.9 [mag]	F
9	0.101	R	>19.3 [mag]	G
	0.340(0.311:0.371)	K'	17.1 ± 1 [mag]	H

Table E.57: Data of GRB020331

ID	reference
A	Kato et al. (2002) GCN notice #1363
B	Monnelly et al. (2002) GCN notice #1339
C	Fox et al. (2002) GCN notice #1334
D	Dullighan et al. (2002) GCN notice #1364
E	Soderberg et al. (2002) GCN notice #1459
F	Kawai et al. (2002) GCN notice #1344
G	Price et al. (2002) GCN notice #1316
H	Klose et al. (2002) GCN notice #1317

Table E.58: References of GRB020331

GRB020405

data#	time (start:end)	band	mag/flux density	reference
1	0.723	R_M	19.6 ± 0.10 [mag]	A
2	0.732	R_M	19.6 ± 0.11 [mag]	A
3	0.748	R_M	19.6 ± 0.09 [mag]	A
4	0.907	R	19.8 ± 0.17 [mag]	A
5	1.401	R_M	20.5 ± 0.08 [mag]	A
6	4.405	R_M	21.9 ± 0.46 [mag]	A
7	6.665	R	23.2 ± 0.46 [mag]	A
	0.713	B	20.1 ± 0.72 [mag]	A
	0.723	B_M	20.3 ± 0.13 [mag]	A
	0.732	B_M	20.3 ± 0.09 [mag]	A
	0.748	B_M	20.3 ± 0.09 [mag]	A
	0.752	B_M	20.4 ± 0.09 [mag]	A
	1.401	B_M	21.3 ± 0.19 [mag]	A
	1.506	B	21.7 ± 0.13 [mag]	A
	1.713	B	22.1 ± 0.14 [mag]	A
	2.338	B	22.4 ± 0.25 [mag]	A
	2.605	B	22.7 ± 0.41 [mag]	A
	4.405	B_M	22.8 ± 0.53 [mag]	A
	1.036	V	20.2 ± 0.3 [mag]	B
	2.111	V	21.45 ± 0.1 [mag]	C
	3.135	V	22.0 ± 0.1 [mag]	C
	1.541	I	20.3 ± 0.04 [mag]	A
	1.721	I	20.5 ± 0.04 [mag]	A
	2.349	I	21.1 ± 0.06 [mag]	A
	2.610	I	21.7 ± 0.81 [mag]	A
	1.191	8.46GHz	490 [μJy]	D

Table E.59: Data of GRB020405

ID	reference
A	Price et al. (2003) ApJ, 589, 838
B	Palazzi et al. (2002) GCN notice #1328
C	Covino et al. (2002) GCN notice #1337
D	Berger et al. (2002) GCN notice #1331

Table E.60: References of GRB020405

GRB020625

data#	time (start:end)	band	mag/flux density	reference
1	0.170	R	>19.5 [mag]	A
2	0.472(0.438:0.510)	R	>18.2 [mag]	B
	0.692(0.678:0.706)	R	>20.5 [mag]	C
	1.679(1.676:0.683)	R	>21.0 [mag]	C
	3.523(3.515:3.531)	R	>21.0 [mag]	C

Table E.61: Data of GRB020625

ID	reference
A	Price et al. (2002) GCN notice #1441
B	Burnashev et al. (2002) GCN notice #1444
C	Castro-Tirado et al. (2002) GCN notice #1445

Table E.62: References of GRB020625

GRB020801

data#	time (start:end)	band	mag/flux density	reference
1	0.8422	unfiltered	>20 [mag]	A

Table E.63: Data of GRB020801

ID	reference
A	Kilmartin and Gilmore (2002) GCN notice #1462

Table E.64: References of GRB020801

GRB020812

data#	time (start:end)	band	mag/flux density	reference
	0.119(0.019:0.117)	R	>18 [mag]	A
	0.1850	R	>17 [mag]	B
1	0.503(0.401:0.631)	R	>20 [mag]	C
	0.119(0.019:0.117)	unfiltered	>16.5 [mag]	D
2	0.147(0.138:0.157)	unfiltered	>19.1 [mag]	E
	0.167(0.159:0.176)	unfiltered	>19.1 [mag]	E
3	1.200(0.192:0.207)	unfiltered	>19.1 [mag]	E

Table E.65: Data of GRB020812

ID	reference
A	Ohashi et al. (2002) GCN notice #1469
B	Kawabata et al. (2002) GCN notice #1489
C	Piccioni et al. (2002) GCN notice #1486
D	Pozanenko et al. (2002) GCN notice #1479
E	Kawabata et al. (2002) GCN notice #1493

Table E.66: References of GRB020812

GRB020813

data#	time (start:end)	band	mag/flux density	reference
1	0.074	R	18.38 ± 0.38 [mag]	A
2	0.165	R	18.49 ± 0.05 [mag]	B
3	0.185	R	18.58 ± 0.05 [mag]	B
4	0.199	R	18.65 ± 0.05 [mag]	B
5	0.393(0.374:0.414)	R	19.14 ± 0.13 [mag]	C
6	0.747	R	20.2 ± 0.2 [mag]	D
7	0.938	R	20.42 ± 0.05 [mag]	B
	0.072	unfiltered	17.75 [mag]	E
	0.074	unfiltered	17.77 [mag]	E
	0.084	unfiltered	17.82 [mag]	E
	0.134	unfiltered	18.10 [mag]	E
	0.201	unfiltered	18.42 [mag]	E
	0.234	unfiltered	18.55 ± 0.05 [mag]	F
8	1.077	unfiltered	20.55 ± 0.25 [mag]	F
9	1.175	unfiltered	21.08 ± 0.30 [mag]	F
10	0.013	unfiltered	>16.0 [mag]	G

Table E.67: Data of GRB020813

ID	reference
A	Williams et al. (2002) GCN notice #1492
B	Gladders and Hall (2002) GCN notice #1513
C	Kawabata et al. (2002) GCN notice #1501
D	Kiziloglu et al. (2002) GCN notice #1488
E	Li et al. (2002) GCN notice #1473
F	Li et al. (2002) GCN notice #1491
G	Rykoff et al. (2002) GCN notice #1480

Table E.68: References of GRB020813

GRB020819

data#	time (start:end)	band	mag/flux density	reference
	0.1237	R	>19 [mag]	A
	0.131	R	>20.5 [mag]	B
1	0.1409	R	>20.6 [mag]	C
	0.3047	R	>20 [mag]	D
	0.3576	R	>22.15 [mag]	E
2	0.4597	R	>22.30 [mag]	E
	0.471(0.369:0.600)	R	>22 [mag]	F
	0.5879	R	>21.75 [mag]	E
	0.7167	R	>21.5 [mag]	G
	0.370(0.343:0.400)	K'	>20.0 [mag]	H
	1.380(1.343:0.418)	K'	>20.5 [mag]	I
	1.7467	8.46GHz	315 [μJy]	J
	— host	R	19.8 [mag]	K

Table E.69: Data of GRB020819

ID	reference
A	Urata et al. (2002) GCN notice #1516
B	Price and McNaught (2002) GCN notice #1506
C	Kawabata and Urata (2002) GCN notice #1523
D	Piccioni et al. (2002) GCN notice #1509
E	Levan et al. (2002) GCN notice #1517
F	Rol et al. (2002) GCN notice #1512
G	Price et al. (2002) GCN notice #1511
H	Henden et al. (2002) GCN notice #1510
I	Klose et al. (2002) GCN notice #1520
J	Frail et al. (2003) GCN notice #1842
K	Levan et al. (2003) GCN notice #1844

Table E.70: References of GRB020819

GRB020903

data#	time (start:end)	band	mag/flux density	reference
1	0.9	R	19.5 [mag]	A
2	6.9	R	22.5 [mag]	A
3	0.174	R	>17.5 [mag]	B
	0.500	R	>17.4 [mag]	C
	0.999	R	>19.8 [mag]	D

Table E.71: Data of GRB020903

ID	reference
A	Soderberg et al. (2004) ApJ, 606, 994
B	Umemura et al. (2002) GCN notice #1537
C	Pavlenko et al. (2002) GCN notice #1535
D	Price et al. (2002) GCN notice #1533

Table E.72: References of GRB020903

GRB021004

data#	time (start:end)	band	mag/flux density	reference
1	0.0066	unfiltered	15.34 [mag]	A
2	0.0084	unfiltered	15.49 [mag]	A
3	0.0119	unfiltered	15.78 [mag]	A
4	0.0242	unfiltered	16.3 [mag]	B
5	0.0266	unfiltered	16.86 ± 0.53 [mag]	C
6	0.0314	unfiltered	16.45 ± 0.35 [mag]	C
7	0.0372	unfiltered	16.36 ± 0.38 [mag]	C
8	0.0440	unfiltered	16.60 ± 0.38 [mag]	C
9	0.0728	unfiltered	16.37 ± 0.19 [mag]	C
10	0.0862	unfiltered	16.50 ± 0.07 [mag]	C
11	0.1019	unfiltered	16.69 ± 0.06 [mag]	C
12	0.1206	unfiltered	16.56 ± 0.10 [mag]	C
13	0.1427	unfiltered	16.76 ± 0.07 [mag]	C
14	0.1688	unfiltered	16.91 ± 0.08 [mag]	C
15	0.1997	unfiltered	17.17 ± 0.13 [mag]	C
16	0.2362	unfiltered	17.26 ± 0.23 [mag]	C
17	0.3211	R	17.82 ± 0.03 [mag]	D
18	0.3245	R	17.90 [mag]	E
19	0.3877	R	17.96 [mag]	E
20	0.4043	R	18.22 [mag]	E
21	0.4300	R	18.37 [mag]	E
22	0.4724	R	18.41 [mag]	E
23	0.5404	R	18.83 [mag]	E
24	0.6221	R	19.06 ± 0.06 [mag]	F
25	0.6978	R	19.30 ± 0.04 [mag]	F
26	0.7520	R	19.33 ± 0.03 [mag]	F
27	0.8006	R	19.42 ± 0.03 [mag]	F
28	0.8485	R	19.31 ± 0.03 [mag]	F
29	0.8992	R	19.34 ± 0.03 [mag]	F
30	0.9568	R	19.39 ± 0.03 [mag]	F
31	0.9888	R	19.39 ± 0.04 [mag]	F
32	1.0036	R	19.29 ± 0.05 [mag]	G
33	1.3467	R	19.54 ± 0.04 [mag]	H
34	1.5034	R	19.66 ± 0.04 [mag]	H
35	1.6002	R	19.92 ± 0.10 [mag]	G
36	1.9717	R	20.08 ± 0.05 [mag]	I
37	2.3273	R	20.12 ± 0.10 [mag]	J
38	2.3553	R	20.08 ± 0.01 [mag]	J
39	2.4103	R	20.16 ± 0.03 [mag]	J
40	2.4183	R	20.15 ± 0.03 [mag]	J
41	2.9606	R	20.09 ± 0.06 [mag]	I
42	3.2772	R	20.4 ± 0.1 [mag]	K

Table E.73: Data of GRB021004

data#	time (start:end)	band	mag/flux density	reference
43	3.7911	R	20.48 ± 0.03 [mag]	L
44	4.6772	R	20.72 ± 0.04 [mag]	L
45	5.6010	R	21.05 ± 0.05 [mag]	M
46	6.22895	R	21.22 ± 0.03 [mag]	N
47	7.21822	R	21.55 ± 0.11 [mag]	N
48	7.34267	R	21.43 ± 0.03 [mag]	N
49	9.17161	R	21.91 ± 0.05 [mag]	N
50	10.1557	R	21.87 ± 0.11 [mag]	N
51	11.3436	R	22.22 ± 0.07 [mag]	N
52	12.1847	R	22.46 ± 0.15 [mag]	N
53	14.5582	R	22.70 ± 0.16 [mag]	O
54	21.746	R	23.39 ± 0.12 [mag]	P
55	23.493	R	23.22 ± 0.08 [mag]	O
56	30.5118	R	23.54 ± 0.11 [mag]	O

Table E.74: Data of GRB021004 (continued)

ID	reference
A	Fox (2002) GCN notice #1564
B	Uemura et al. (2002) GCN notice #1566
C	Uemura et al. (2003) PASJ, 55, L31
D	Balman et al. (2002) GCN notice #1580
E	Oksanen et al. (2002) GCN notice #1591
F	Halpern et al. (2002) GCN notice #1578
G	Bersier et al. (2002) GCN notice #1586
H	Holland et al. (2002) GCN notice #1585
I	Stanek et al. (2002) GCN notice #1598
J	Holland et al. (2002) GCN notice #1597
K	Masetti et al. (2002) GCN notice #1603
L	Mirabal et al. (2002) GCN notice #1618
M	Stefanon et al. (2002) GCN notice #1623
N	Pandey et al. (2003b) Bull. Astr. Soc. India, 31, 19
O	Holland et al. (2003) AJ, 125, 2291
P	Garnavich and Quinn (2002) GCN notice #1661

Table E.75: References of GRB021004

GRB021104

data#	time (start:end)	band	mag/flux density	reference
1	0.1236	unfiltered	>21 [mag]	A
	0.1636	R	>20 [mag]	B

Table E.76: Data of GRB021104

ID	reference
A	Fox and Price (2002) GCN notice #1671
B	Bradshaw et al. (2002) GCN notice #1677

Table E.77: References of GRB021104

GRB021112

data#	time (start:end)	band	mag/flux density	reference
1	0.0012	unfiltered	>11.4 [mag]	A
2	0.0032	unfiltered	>11.7 [mag]	A
	0.0565	unfiltered	>14.6 [mag]	A
3	0.075	R	>21.8 [mag]	B
4	0.229(0.183:0.286)	r'	>20 [mag]	C

Table E.78: Data of GRB021112

ID	reference
A	Wren et al. (2002) GCN notice #1689
B	Schaefer et al. (2002) GCN notice #1776
C	Newman et al. (2002) GCN notice #1695

Table E.79: References of GRB021112

GRB021113

data#	time (start:end)	band	mag/flux density	reference
1	0.1083	R	>22.1 [mag]	A
	0.1730	R	>20 [mag]	B
	0.218(0.190:0.250)	R	>17.6 [mag]	C
	0.3098	R	>19.8 [mag]	C
	0.3304	R	>19.8 [mag]	D
2	0.3914	R	>20.3 [mag]	D
	0.3827	V	>18.0 [mag]	E

Table E.80: Data of GRB021113

ID	reference
A	Nysewander et al. (2002) GCN notice #1699
B	Levan et al. (2002) GCN notice #1688
C	Kawabata et al. (2002) GCN notice #1700
D	Ishiguro et al. (2002) GCN notice #1694
E	Rumyantsev et al. (2002) GCN notice #1690

Table E.81: References of GRB021113

GRB021211

data#	time (start:end)	band	mag/flux density	reference
1	0.0015	R	14.67 ± 0.01 [mag]	A
2	0.0020	R	15.14 ± 0.01 [mag]	A
3	0.0026	R	15.54 ± 0.01 [mag]	A
4	0.0031	R	15.94 ± 0.02 [mag]	A
5	0.0034	R	16.04 ± 0.02 [mag]	A
6	0.0036	R	16.12 ± 0.02 [mag]	A
7	0.0040	R	16.35 ± 0.03 [mag]	A
8	0.0043	R	16.45 ± 0.02 [mag]	A
9	0.0045	R	16.55 ± 0.05 [mag]	A
10	0.0050	R	16.71 ± 0.03 [mag]	A
11	0.0052	R	16.79 ± 0.03 [mag]	A
12	0.0055	R	16.93 ± 0.04 [mag]	A
13	0.0059	R	16.95 ± 0.03 [mag]	A
14	0.0062	R	16.99 ± 0.03 [mag]	A
15	0.0064	R	17.07 ± 0.05 [mag]	A
16	0.0069	R	17.15 ± 0.05 [mag]	A
17	0.0071	R	17.23 ± 0.04 [mag]	A
18	0.0073	R	17.25 ± 0.04 [mag]	A
19	0.0081	R	17.35 ± 0.02 [mag]	A
20	0.0090	R	17.56 ± 0.02 [mag]	A
21	0.0106	R	17.76 ± 0.02 [mag]	A
22	0.0138	R	18.08 ± 0.02 [mag]	A
23	0.0144	R	18.29 ± 0.02 [mag]	B
24	0.0187	R	18.46 ± 0.03 [mag]	A
25	0.0251	R	18.83 ± 0.18 [mag]	A
26	0.0252	R	18.81 ± 0.05 [mag]	B
27	0.0287	R	19.09 ± 0.06 [mag]	B
28	0.0354	R	19.34 ± 0.07 [mag]	B
29	0.0410	R	19.29 ± 0.07 [mag]	B
30	0.0429	R	19.48 ± 0.08 [mag]	B
31	0.0508	R	19.53 ± 0.08 [mag]	B
32	0.0541	R	19.60 ± 0.09 [mag]	B
33	0.0560	R	19.76 ± 0.10 [mag]	B
34	0.0622	R	19.95 ± 0.11 [mag]	B
35	0.0689	R	20.09 ± 0.13 [mag]	B
36	0.0921	R	20.19 ± 0.32 [mag]	A
37	0.0985	R	20.20 ± 0.20 [mag]	A
38	0.1004	R	20.09 ± 0.25 [mag]	A
39	0.1037	R	20.18 ± 0.17 [mag]	A
40	0.2370	R	21.10 ± 0.13 [mag]	B

Table E.82: Data of GRB021211

data#	time (start:end)	band	mag/flux density	reference
41	0.2839	R	21.90 ± 0.21 [mag]	C
42	0.3082	R	21.90 ± 0.16 [mag]	C
43	0.3930	R	22.10 ± 0.18 [mag]	C
44	0.4020	R	22.10 ± 0.18 [mag]	C
45	0.4112	R	22.10 ± 0.14 [mag]	C
46	0.4204	R	22.40 ± 0.24 [mag]	C
47	0.4283	R	22.50 ± 0.21 [mag]	C
48	0.4608	R	22.20 ± 0.18 [mag]	C
49	0.8288	R	23.20 ± 0.18 [mag]	D
50	1.0370	r'	23.42 ± 0.07 [mag]	B
51	1.803(1.786:1.820)	R	23.1 [mag]	E
52	29.229	R	24.48 ± 0.18 [mag]	F
53	34.859	R	25.07 ± 0.15 [mag]	F
54	78.549	R	25.13 ± 0.12 [mag]	F
55	87.539	R	25.35 ± 0.17 [mag]	F
	0.501(0.487:0.515)	R	>22.7 [mag]	G
	0.798(0.789:0.806)	I	22.5 [mag]	E
	0.3318	I	>21.4 [mag]	C
	0.501(0.487:0.515)	I	>20.7 [mag]	G
	0.9170	i*	>23 [mag]	H
	0.7088	J	21.76 ± 0.11 [mag]	I
	1.034(1.019:1.049)	347GHz	<7.5 [mJy]	J
	0.8988	8.46GHz	<70 [μJy]	K
	1	4.9GHz	<0.17 [mJy]	L
	6	4.9GHz	<0.12 [mJy]	L

Table E.83: Data of GRB021211 (continued)

ID	reference
A	Li et al. (2003) ApJ, 586, L9
B	Fox et al. (2003a) ApJ, 586, L5
C	Pandey et al. (2003a) A&A, 408, L21
D	McLeod et al. (2002) GCN notice #1750
E	Levan et al. (2002) GCN notice #1758
F	Della Valle et al. (2003) A&A, 408, L21
G	Klose et al. (2002) GCN notice #1739
H	Lamb et al. (2002) GCN notice #1744
I	Bersier et al. (2002) GCN notice #1751
J	Hoge et al. (2002) GCN notice #1742
K	Berger and Frail (2002) GCN notice #1745
L	Rol and Strom (2002) GCN notice #1777

Table E.84: References of GRB021211

GRB030115

data#	time (start:end)	band	mag/flux density	reference
1	0.0001(0.00001:0.0016)	unfiltered	>10 [mag]	A
2	0.0793	R	>20 [mag]	B
	0.0850	R	>20 [mag]	C
	0.1336	R	>19.8 [mag]	D
3	0.1517	r'	>20 [mag]	E
	0.0503	B	>19.1 [mag]	F
	0.0892	V	>19 [mag]	G
	0.8593	J	20.2 ± 0.3 [mag]	H
	1.9593	J	21.5 ± 0.5 [mag]	I
	0.8593	H	19.9 ± 0.3 [mag]	H
	1.9593	H	20.4 ± 0.4 [mag]	I
	0.8593	Ks	18.4 ± 0.3 [mag]	H
	1.9593	Ks	19.1 ± 0.2 [mag]	I
	3.314(3.269:3.359)	347GHz	6 [mJy]	J
	0.939	250GHz	<3 [mJy]	K
	3.169	250GHz	<5 [mJy]	K
	2.279	8.46GHz	94 ± 22 [μJy]	L
	1.977(1.740:1.246)	4.9GHz	24 ± 21 [μJy]	M
	5.973(5.729:6.228)	4.9GHz	89 ± 24 [μJy]	M
	11.96(11.71:12.21)	4.9GHz	72 ± 26 [μJy]	M

Table E.85: Data of GRB030115

ID	reference
A	Castro-Tirado et al. (2003) GCN notice #1826
B	Castro-Tirado et al. (2003) GCN notice #1807
C	Masetti et al. (2003) GCN notice #1811
D	Flaccomio et al. (2003) GCN notice #1806
E	Blake et al. (2003) GCN notice #1808
F	Atteia et al. (2003) GCN notice #1810
G	Bourban et al. (2003) GCN notice #1820
H	Kato et al. (2003) GCN notice #1825
I	Kato et al. (2003) GCN notice #1830
J	Hoge et al. (2003) GCN notice #1832
K	Bertoldi et al. (2003) GCN notice #1835
L	Frail et al. (2003) GCN notice #1827
M	Rol and Wijers (2003) GCN notice #1867

Table E.86: References of GRB030115

GRB030226

data#	time (start:end)	band	mag/flux density	reference
1	— (:0.0069)	unfiltered	>11.5 [mag]	A
2	0.13	R	17.8 [mag]	B
3	0.14	R	18.0 [mag]	C
4	0.148	R	18.44 ± 0.05 [mag]	E
5	0.2007	R	18.87 ± 0.03 [mag]	D
6	0.493	R	19.0 ± 0.2 [mag]	F
7	0.6444	R	19.90 ± 0.05 [mag]	D
8	0.7795	R	20.22 ± 0.03 [mag]	D
9	0.8726	R	20.44 ± 0.03 [mag]	D
10	0.898	R	19.0 ± 0.2 [mag]	G
11	0.9274	R	20.57 ± 0.03 [mag]	D
12	0.9837	R	20.63 ± 0.04 [mag]	D
13	1.0541	R	20.64 ± 0.05 [mag]	D
14	1.0545	R	20.76 ± 0.05 [mag]	D
15	1.0701	R	20.70 ± 0.03 [mag]	D
16	1.0729	R	20.68 ± 0.03 [mag]	D
17	1.0750	R	20.84 ± 0.04 [mag]	D
18	1.1026	R	20.79 ± 0.05 [mag]	D
19	1.1989	R	20.99 ± 0.02 [mag]	D
20	1.9851	R	21.89 ± 0.13 [mag]	D
21	4.0937	R	24.22 ± 0.08 [mag]	D
22	7.0500	R	25.26 ± 0.15 [mag]	D
	0.8104	U	20.81 ± 0.03 [mag]	D
	0.8795	U	20.84 ± 0.02 [mag]	D
	0.9587	U	21.04 ± 0.04 [mag]	D
	1.0621	U	21.25 ± 0.05 [mag]	D
	1.1156	U	21.33 ± 0.06 [mag]	D
	1.8434	U	22.43 ± 0.14 [mag]	D
	2.0246	U	23.02 ± 0.08 [mag]	D
	0.2139	B	19.76 ± 0.03 [mag]	D
	0.6746	B	20.56 ± 0.07 [mag]	D
	0.8035	B	21.04 ± 0.03 [mag]	D
	1.0153	B	21.33 ± 0.11 [mag]	D
	1.0580	B	21.36 ± 0.03 [mag]	D
	1.0618	B	21.37 ± 0.03 [mag]	D
	1.0653	B	21.48 ± 0.04 [mag]	D
	1.1885	B	21.73 ± 0.03 [mag]	D
	4.0607	B	24.88 ± 0.06 [mag]	D

Table E.87: Data of GRB030226

data#	time (start:end)	band	mag/flux density	reference
	0.1882	V	19.09 ± 0.03 [mag]	D
	0.2062	V	19.27 ± 0.05 [mag]	D
	0.6604	V	20.19 ± 0.06 [mag]	D
	0.8076	V	20.67 ± 0.02 [mag]	D
	0.8298	V	20.73 ± 0.02 [mag]	D
	0.9521	V	20.88 ± 0.02 [mag]	D
	0.9993	V	21.03 ± 0.06 [mag]	D
	1.0555	V	21.11 ± 0.02 [mag]	D
	1.8368	V	22.50 ± 0.07 [mag]	D
	4.0798	V	24.66 ± 0.09 [mag]	D
	5.0753	V	24.64 ± 0.10 [mag]	D
	0.6194	I	19.37 ± 0.07 [mag]	D
	0.8437	I	20.01 ± 0.08 [mag]	D
	0.9153	I	19.92 ± 0.08 [mag]	D
	0.9201	I	20.21 ± 0.03 [mag]	D
	0.9677	I	20.30 ± 0.14 [mag]	D
	0.9785	I	20.46 ± 0.24 [mag]	D
	1.1997	I	20.52 ± 0.10 [mag]	D
	4.1083	I	23.95 ± 0.12 [mag]	D
	0.2024	Js	17.56 ± 0.10 [mag]	D
	0.2666	J	17.91 ± 0.10 [mag]	D
	0.3621	J	18.16 ± 0.10 [mag]	D
	0.2180	H	17.02 ± 0.10 [mag]	D
	0.2746	H	17.29 ± 0.10 [mag]	D
	0.3698	H	17.42 ± 0.10 [mag]	D
	0.1868	Ks	15.95 ± 0.05 [mag]	D
	0.2569	K	16.39 ± 0.05 [mag]	D
	0.3545	K	16.69 ± 0.05 [mag]	D
	1.2597	K	18.40 ± 0.05 [mag]	D
	1.3962	K	18.69 ± 0.05 [mag]	D
	2.3559	K	19.95 ± 0.08 [mag]	D
	4.1472	K	21.32 ± 0.21 [mag]	D

Table E.88: Data of GRB030226 (continued)

ID	reference
A	Castro-Tirado et al. (2003) GCN notice #1887
B	Ando et al. (2003) GCN notice #1882
C	von Braun et al. (2003) GCN notice #1881
D	Klose et al. (2004) AJ, 128, 1942
E	Garnavich et al. (2003) GCN notice #1885
F	Ando et al. (2003) GCN notice #1884
G	Guarnieri et al. (2003) GCN notice #1892

Table E.89: References of GRB030226

GRB030323

data#	time (start:end)	band	mag/flux density	reference
1	0.335	unfiltered	18.4 ± 0.1 [mag]	A
2	0.355	unfiltered	$18.8\ ^{+0.09}_{-0.08}$ [mag]	B
3	0.413	R	18.69 ± 0.06 [mag]	C
4	0.521	unfiltered	19.56 ± 0.4 [mag]	C
5	0.594	unfiltered	19.72 ± 0.4 [mag]	C
6	0.654	unfiltered	19.96 ± 0.4 [mag]	C
7	0.699	unfiltered	20.42 ± 0.4 [mag]	C
8	1.085	R	20.38 [mag]	D
9	1.125	R	20.62 [mag]	D
10	1.215	R	20.59 [mag]	D
11	1.331(1.271:1.392)	R	20.6 ± 0.1 [mag]	E
12	2.123	R	21.3 ± 0.2 [mag]	F
13	3.120	R	21.6 ± 0.2 [mag]	F
14	3.261(3.251:3.271)	R	22.27 ± 0.04 [mag]	G
15	4.242	R	22.8 ± 0.2 [mag]	F
16	0.275	unfiltered	>16.6 [mag]	B
	0.315	unfiltered	>16.3 [mag]	B

Table E.90: Data of GRB030323

ID	reference
A	Smith et al. (2003) GCN notice #1952
B	Wood-Vasey et al. (2003) GCN notice #1968
C	Gilmore et al. (2003) GCN notice #1949
D	Masi et al. (2003) GCN notice #1960
E	Lindsay et al. (2003) GCN notice #1966
F	Masi et al. (2003) GCN notice #1973
G	Castro Cern et al. (2003) GCN notice #2006

Table E.91: References of GRB030323

GRB030324

data#	time (start:end)	band	mag/flux density	reference
1	0.0005(0.0003:0.0007)	R	>14.8 [mag]	A
2	0.0009(0.0003:0.0029)	R	>15.2 [mag]	A
	0.0494	R	>19.6 [mag]	B
3	0.0616	R	>20 [mag]	C
4	0.1334	R	>22.4 [mag]	D
5	0.308	R	>22.5 [mag]	D
	0.389	R	>21.4 [mag]	E
	0.593	R	>21.0 [mag]	E
	0.713	R	>20.0 [mag]	F
	0.850	R	>21.9 [mag]	G
	1.540	R	>21.4 [mag]	E
	1.851	R	>21.4 [mag]	G
6	2.194	R	>22.7 [mag]	D
	0.259	i*	23.48 ± 0.21 [mag]	H
	12	i*	>19.5 [mag]	I

Table E.92: Data of GRB030324

ID	reference
A	Klotz et al. (2003) GCN notice #1961
B	Rykoff and Smith (2003) GCN notice #1958
C	Guzyi et al. (2003) GCN notice #1945
D	Luhman et al. (2003) GCN notice #2032
E	Price and McNaught (2003) GCN notice #1959
F	Rumyantsev et al. (2003) GCN notice #1964
G	Piccioni et al. (2003) GCN notice #1963
H	Lamb et al. (2003) GCN notice #2239
I	Lamb et al. (2003) GCN notice #2139

Table E.93: References of GRB030324

GRB030328

data#	time (start:end)	band	mag/flux density	reference
1	0.4351	R	20.5 [mag]	A
2	0.4660	R	20.45 [mag]	B
3	0.479	R	20.35 [mag]	C
4	0.5341	R	20.59 ± 0.07 [mag]	D
5	0.6341	R	20.79 ± 0.08 [mag]	D
6	0.6511	R	20.91 ± 0.09 [mag]	E
7	0.6761	R	21.00 ± 0.09 [mag]	E
8	0.7041	R	21.00 ± 0.07 [mag]	E
9	0.7081	R	20.8 [mag]	F
10	0.8511	R	21.36 ± 0.11 [mag]	E
11	1.3104	R	22.10 ± 0.28 [mag]	G
12	1.57	R	21.93 ± 0.06 [mag]	H
	0.389(0.308:0.490)	unfiltered	20.9 ± 0.2 [mag]	I
	1.2771	B	22.77 ± 0.43 [mag]	G

Table E.94: Data of GRB030328

ID	reference
A	Gal-Yam et al. (2003) GCN notice #1984
B	Bartolini et al. (2003) GCN notice #2008
C	Burenin et al. (2003) GCN notice #1990
D	Fugazza et al. (2003) GCN notice #1982
E	Andersen et al. (2003) GCN notice #1993
F	Martini et al. (2003) GCN notice #1979
G	Ibrahimov et al. (2003) GCN notice #2192
H	Garnavich et al. (2003) GCN notice #2192
I	Rumyantsev et al. (2003) GCN notice #1991

Table E.95: References of GRB030328

GRB030329

data#	time (start:end)	band	mag/flux density	reference
1	0.0620	unfiltered	12.55 ± 0.02 [mag]	A
2	0.1484	unfiltered	13.37 ± 0.03 [mag]	A
3	0.1943	unfiltered	13.60 ± 0.03 [mag]	A
4	0.2373	unfiltered	13.80 ± 0.04 [mag]	A
5	0.2970	unfiltered	14.15 ± 0.07 [mag]	A
6	0.365	R	14.52 [mag]	B
7	0.435	R	14.75 [mag]	B
8	0.542	R	15.06 [mag]	B
9	0.679	R	15.38 ± 0.02 [mag]	C
10	0.762	R	15.61 ± 0.02 [mag]	C
11	0.9457	unfiltered	15.99 ± 0.13 [mag]	A
12	1.0936	unfiltered	16.50 ± 0.13 [mag]	A
13	1.2172	unfiltered	16.32 ± 0.14 [mag]	A
14	1.477	R	16.5 [mag]	D
15	1.589	R	16.39 [mag]	D
16	2.38	R	16.99 [mag]	E
17	3.393	R	17.01 ± 0.02 [mag]	F
18	5.165	R	17.80 ± 0.05 [mag]	G
19	6.246	R	18.6 ± 0.03 [mag]	H
20	9.875	R	19.24 ± 0.29 [mag]	I
21	14.36	R	19.30 ± 0.18 [mag]	J
22	23.45	R	19.9 ± 0.4 [mag]	J
23	25.45	R	20.11 ± 0.07 [mag]	K
24	32.40	R	20.30 ± 0.17 [mag]	K
25	39.2	R	20.72 ± 0.09 [mag]	L
26	47.2	R	21.26 ± 0.21 [mag]	L
27	51.2	R	21.53 ± 0.19 [mag]	L
28	65.3	R	21.65 ± 0.07 [mag]	M
29	86.3	R	21.80 ± 0.10 [mag]	M
30	96.8	R	21.91 ± 0.28 [mag]	M

Table E.96: Data of GRB030329

ID	reference
A	Sato et al. (2003) GCN notice #2080
B	Burenin et al. (2003) GCN notice #2024
C	Zharikov et al. (2003) GCN notice #2022
D	Burenin et al. (2003) GCN notice #2046
E	Burenin et al. (2003) GCN notice #2054
F	Ibrahimov et al. (2003) GCN notice #2077
G	Ibrahimov et al. (2003) GCN notice #2084
H	Khamitov et al. (2003) GCN notice #2094
I	Kindt et al. (2003) GCN notice #2193
J	Klotz et al. (2003) GCN notice #2247
K	Klotz et al. (2003) GCN notice #2246
L	Ibrahimov et al. (2003) GCN notice #2288
M	Khamitov et al. (2003) GCN notice #2299

Table E.97: References of GRB030329

GRB030418

data#	time (start:end)	band	mag/flux density	reference
1	0.020(0.004:0.096)	R	17.4 – 18.7 [mag]	A
2	0.0517	R	18.8 [mag]	B
3	0.1517	R	19.8 [mag]	C
4	0.401(0.397:0.406)	R	20.5 ± 0.30 [mag]	D
5	2.60	R	23.3 ± 0.1 [mag]	E
	6.58	R	24.9 ± 0.4 [mag]	E
	6.60	V	25.1 ± 0.5 [mag]	E
	2.61	I	23.0 ± 0.1 [mag]	E
	6.59	I	>24 [mag]	E
	0.0479	J	13 [mag]	F

Table E.98: Data of GRB030418

ID	reference
A	Smith et al. (2003) GCN notice #2153
B	Price et al. (2003) GCN notice #2148
C	Price et al. (2003) GCN notice #2149
D	Ferrero et al. (2003) GCN notice #2284
E	Dullighan et al. (2003) GCN notice #2236
F	Mito et al. (2003) GCN notice #215

Table E.99: References of GRB030418

GRB030429

data#	time (start:end)	band	mag/flux density	reference
1	0.078	unfiltered	>18.2 [mag]	A
2	0.145	unfiltered	19.67 ± 0.11 [mag]	B
3	0.154	unfiltered	19.39 ± 0.08 [mag]	B
4	0.170	unfiltered	19.62 ± 0.09 [mag]	B
5	0.214	unfiltered	19.56 ± 0.11 [mag]	B
6	0.374	unfiltered	20.20 ± 0.15 [mag]	C
7	0.548	R	20.86 ± 0.04 [mag]	B
8	0.777	R	21.13 ± 0.04 [mag]	B
9	1.761	R	21.42 ± 0.27 [mag]	B
10	1.884	R	21.58 ± 0.15 [mag]	B
11	2.553	R	22.54 ± 0.06 [mag]	B
12	2.793	R	22.55 ± 0.09 [mag]	B
13	3.632	R	23.71 ± 0.12 [mag]	B
14	6.644	R	25.20 ± 0.30 [mag]	B
15	67.641	R	>26.3 [mag]	B
	1.747	B	22.24 ± 0.30 [mag]	B
	0.535	V	21.45 ± 0.03 [mag]	B
	0.764	V	21.79 ± 0.03 [mag]	B
	1.755	V	21.89 ± 0.32 [mag]	B
	2.541	V	23.18 ± 0.11 [mag]	B
	0.561	I	20.29 ± 0.05 [mag]	B
	0.790	I	20.63 ± 0.05 [mag]	B
	1.766	I	20.51 ± 0.37 [mag]	B
	2.566	I	21.72 ± 0.37 [mag]	B
	6.658	I	24.70 ± 0.30 [mag]	B
	0.281	J	18.8 ± 0.2 [mag]	D
	0.427	J	19.2 ± 0.2 [mag]	D
	0.538	J	19.25 ± 0.04 [mag]	B
	0.783	J	19.51 ± 0.04 [mag]	B
	1.322	J	19.0 ± 0.2 [mag]	D
	0.281	H	17.8 ± 0.2 [mag]	D
	0.427	H	18.3 ± 0.2 [mag]	D
	0.559	H	18.1 ± 0.2 [mag]	D
	1.322	H	18.4 ± 0.2 [mag]	D
	0.281	Ks	17.0 ± 0.2 [mag]	D
	0.427	Ks	17.5 ± 0.2 [mag]	D
	0.568	Ks	17.70 ± 0.06 [mag]	B
	0.783	Ks	18.01 ± 0.06 [mag]	B
	1.322	Ks	17.8 ± 0.2 [mag]	D

Table E.100: Data of GRB030429

ID	reference
A	Smith (2003) GCN notice #2178
B	Jakobsson et al. (2004) A&A, 427, 785
C	Rumyantsev et al. (2003) GCN notice #2218
D	Nishiyama et al. (2003) GCN notice #2195

Table E.101: References of GRB030429

GRB030528

data#	time (start:end)	band	mag/flux density	reference
	0.0017	unfiltered	>15.8 [mag]	A
1	0.0029	unfiltered	>16.0 [mag]	B
2	0.0985(0.0965:0.1006)	R	>18.7 [mag]	C
3	0.496	R	>20.5 [mag]	D
4	383.04	R	22.0 ± 0.2 [mag]	E
	6.5604	I	21.4 ± 0.3 [mag]	E
	32.595	I	21.2 ± 0.3 [mag]	E
	0.6684	J	20.6 ± 0.3 [mag]	E
	111.48	Js	21.0 ± 0.2 [mag]	E
	125.48	Js	20.7 ± 0.2 [mag]	E
	0.6809	H	20.3 ± 0.4 [mag]	E
	0.6920	Ks	18.6 ± 0.2 [mag]	E
	1.6993	Ks	18.9 ± 0.3 [mag]	E
	3.6486	Ks	19.6 ± 0.5 [mag]	E
	14.868	K	19.6 ± 0.1 [mag]	E

Table E.102: Data of GRB030528

ID	reference
A	Torii (2003) GCN notice #2253
B	Uemura et al. (2003) GCN notice #2252
C	Ayani and Yamaoka (2003) GCN notice #2257
D	Valentini et al. (2003) GCN notice #2258
E	Rau et al. (2004) A&A, 427, 815

Table E.103: References of GRB030528

GRB030723

data#	time (start:end)	band	mag/flux density	reference
1	0.0005	unfiltered	>19.0 [mag]	A
2	0.0022	unfiltered	>19.7 [mag]	A
3	0.0056	unfiltered	>19.1 [mag]	A
	0.0137	unfiltered	>19.5 [mag]	A
4	0.0217	unfiltered	19.5 ± 0.4 [mag]	A
5	0.0298	unfiltered	19.3 ± 0.4 [mag]	A
	0.320	R	>20 [mag]	C
	0.536	unfiltered	>20.0 [mag]	B
6	0.903	R	21.0 [mag]	D
7	1.040	R	21.13 ± 0.05 [mag]	E
8	1.230	R	21.3 [mag]	F
9	2.230	R	22.4 [mag]	F
10	5.115	R	24.2 ± 0.3 [mag]	G

Table E.104: Data of GRB030723

ID	reference
A	Smith et al. (2003) GCN notice #2338
B	Monard (2003) GCN notice #2312
C	de Ugarte et al. (2003) GCN notice #2314
D	Bond (2003) GCN notice #2339
E	Dullighan et al. (2003) GCN notice #2326
F	Fox et al. (2003) GCN notice #2323
E	Dullighan et al. (2003) GCN notice #2336

Table E.105: References of GRB030723

GRB030725

data#	time (start:end)	band	mag/flux density	reference
1	0.297	unfiltered	18.8 [mag]	A
2	0.357	unfiltered	19.0 [mag]	A
3	0.447	unfiltered	19.6 [mag]	A
4	3.889	R	21.2 ± 0.2 [mag]	B
5	6.814	r	22.25 ± 0.05 [mag]	C
6	7.675	r	22.55 ± 0.05 [mag]	C
	3.233	unfiltered	>21 [mag]	D

Table E.106: Data of GRB030725

ID	reference
A	Monard (2003) GCN notice #2322
B	Vinter et al. (2003) GCN notice #2335
C	Dullighan et al. (2003) GCN notice #2384
D	Monard (2003) GCN notice #2334

Table E.107: References of GRB030725

GRB030823

data#	time (start:end)	band	mag/flux density	reference
1	0.0768	unfiltered	>16.5 [mag]	A
	0.0957	unfiltered	>16.0 [mag]	B
	0.1470	R	>18.8 [mag]	C
2	0.2952	R	>19.5 [mag]	D
3	0.4106	R	>20.5 [mag]	D
	0.4432	R	>19.0 [mag]	D

Table E.108: Data of GRB030823

ID	reference
A	Suzuki et al. (2003) GCN notice #2362
B	Wren and Vestrand (2003) GCN notice #2361
C	Huang et al. (2003) GCN notice #2360
D	Ibrahimov et al. (2003) GCN notice #2366

Table E.109: References of GRB030823

GRB030824

data#	time (start:end)	band	mag/flux density	reference
1	0.1983(0.1684:0.2336)	R	>17.5 [mag]	A
2	0.5503	R	>22.5 [mag]	B

Table E.110: Data of GRB030824

ID	reference
A	Oksanen (2003) GCN notice #2379
B	Fox et al. (2003) GCN notice #2369

Table E.111: References of GRB030824

GRB031026

data#	time (start:end)	band	mag/flux density	reference
1	0.2448	R	>18 [mag]	A
2	0.3480(0.2482:0.4878)	R	>20.9 [mag]	B
	0.1629	I	>20.4 [mag]	C

Table E.112: Data of GRB031026

ID	reference
A	Budi et al. (2003) GCN notice #2427
B	Chen et al. (2003) GCN notice #2436
C	Nysewander et al. (2003) GCN notice #2433

Table E.113: References of GRB031026

GRB031111A

data#	time (start:end)	band	mag/flux density	reference
1	1.502	R	>18.5 [mag]	A
	0.156(0.139:0.176)	I	>13 [mag]	B
	2.822	4.9GHz	<77 [μJy]	C

Table E.114: Data of GRB031111A

ID	reference
A	Silvey et al. (2003) GCN notice #2447
B	Jelinek et al. (2003) GCN notice #2456
C	Soderberg and Frail (2003) GCN notice #2450

Table E.115: References of GRB031111A

GRB031111B

data#	time (start:end)	band	mag/flux density	reference
1	0.623	unfiltered	>17.2 [mag]	A

Table E.116: Data of GRB031111B

ID	reference
A	Uemura et al. (2003) GCN notice #2453

Table E.117: References of GRB031111B

GRB031220

data#	time (start:end)	band	mag/flux density	reference
1	0.079	unfiltered	>19.2 [mag]	A
2	0.2223	r'	>23 [mag]	B
	0.2618	r'	>22.5 [mag]	B
3	0.3466	R	>20.9 [mag]	C
4	1.0417	R	24.40 ± 0.18 [mag]	D
5	7.9125	R	>24 [mag]	D
	0.3264	I	>20 [mag]	E

Table E.118: Data of GRB031220

ID	reference
A	Rykoff et al. (2003) GCN notice #2495
B	Fox et al. (2003) GCN notice #2499
C	Yang et al. (2003) GCN notice #2494
D	Gorosabel et al. (2004) GCN notice #2513
E	Kosugi et al. (2003) GCN notice #2497

Table E.119: References of GRB031220

GRB040228B

data#	time (start:end)	band	mag/flux density	reference
1	0.060(0.052:0.069)	unfiltered	>10.5 [mag]	A
2	0.4983	R	>19.5 [mag]	B

Table E.120: Data of GRB040228B

ID	reference
A	Pedersen et al. (2004) GCN notice #2539
B	Sarugaku et al. (2004) GCN notice #2537

Table E.121: References of GRB040228B

GRB040511

data#	time (start:end)	band	mag/flux density	reference
1	0.0933	unfiltered	>17.5 [mag]	A
2	0.1150	unfiltered	>17.6 [mag]	A
	0.3022	R	>19.5 [mag]	B
	0.4140	R	>19.4 [mag]	C
3	0.463(0.448:0.479)	R	>21 [mag]	D
	0.5071	J	19.0 [mag]	E
	1.8071	J	20.9 [mag]	E
	0.5	J	>18.6 [mag]	F
	0.5	H	>18.2 [mag]	F
	0.5	Ks	>16.6 [mag]	F

Table E.122: Data of GRB040511

ID	reference
A	Smith et al. (2004) GCN notice #2595
B	Kumar et al. (2004) GCN notice #2590
C	Bourban et al. (2004) GCN notice #2589
D	Gorosabel et al. (2004) GCN notice #2592
E	Fox et al. (2004) GCN notice #2597
F	Testa et al. (2004) GCN notice #2600

Table E.123: References of GRB040511

GRB040916B

data#	time (start:end)	band	mag/flux density	reference
1	0.2309	R	22.3 ± 0.2 [mag]	A
2	0.3643	R	22.7 ± 0.3 [mag]	A
3	2.4893	R	24.8 ± 0.3 [mag]	A
4	4.4276	R	25 [mag]	B
	0.140(0.116:0.169)	R	>21 [mag]	C
5	0.0675(0.0121:0.3761)	unfiltered	>13.0 [mag]	D
	0.1098(0.0997:0.1209)	unfiltered	>19.4 [mag]	E
	0.3511	unfiltered	>20.5 [mag]	F
	0.1854	I	21.51 ± 0.23 [mag]	G
	0.203	V	22.12 ± 0.06 [mag]	H
	1.49	V	>21.5 [mag]	H
	23.22	8.46GHz	<99 [μJy]	I

Table E.124: Data of GRB040916B

ID	reference
A	Kosugi et al. (2004) GCN notice #2726
B	Kosugi et al. (2004) GCN notice #2730
C	de Ugarte Postigo et al. (2004) GCN notice #2717
D	Cwiok et al. (2004) GCN notice #2725
E	Klotz et al. (2004) GCN notice #2729
F	Kilmartin and Gilmore (2004) GCN notice #2715
G	Henden (2004) GCN notice #2727
H	Lamanna et al. (2004) GCN notice #2796
H	Frail and Soderberb (2004) GCN notice #2732

Table E.125: References of GRB040916B

GRB040924

data#	time (start:end)	band	mag/flux density	reference
1	0.0109	R	18.0 [mag]	A
2	0.0188	unfiltered	18.3 [mag]	B
3	0.0347	R	18.87 [mag]	A
4	0.0445	unfiltered	19.2 [mag]	B
5	0.2833	R	21.4 [mag]	C
6	0.3735	R	22.1 [mag]	D
7	0.7242	R	22.1 [mag]	E
8	1.556(1.495:1.620)	R	23.7 $\pm$ 0.2 [mag]	F
	0.0839	R	>19 [mag]	G
	0.2083	R	>19 [mag]	G
	0.482(0.469:0.496)	R	>21.0 [mag]	H
	0.101(0.097:0.105)	K	17.5 $\pm$ 0.1 [mag]	I
	1.147(1.135:1.159)	K	20.4 $\pm$ 0.2 [mag]	J
	0.651(0.523:0.812)	4.8GHz	<0.12 [mJy]	K
	5.785	8.46GHz	<147 [μJy]	L

Table E.126: Data of GRB040924

ID	reference
A	Fox (2004) GCN notice #2741
B	Li et al. (2004) GCN notice #2748
C	Hu et al. (2004) GCN notice #2743
D	Khamitov et al. (2004) GCN notice #2740
E	Fynbo et al. (2004) GCN notice #2747
F	Khamitov et al. (2004) GCN notice #2752
G	Perez-Ramirez et al. (2004) GCN notice #2739
H	Pavlenko et al. (2004) GCN notice #2753
I	Terada et al. (2004) GCN notice #2742
J	Terada et al. (2004) GCN notice #2750
K	van der Horst et al. (2004) GCN notice #2746
L	Frail and Soderberb (2004) GCN notice #2758

Table E.127: References of GRB040924

GRB041006

data#	time (start:end)	band	mag/flux density	reference
1	0.0027	unfiltered	16.8 [mag]	A
2	0.0113	unfiltered	17.1 ± 0.4 [mag]	B
3	0.0382	R	17 [mag]	C
4	0.0600	unfiltered	18.1 ± 0.4 [mag]	B
5	0.0774	R	18.5 [mag]	D
6	0.1464	R	18.7 ± 0.09 [mag]	E
7	0.1881	R	19.1 ± 0.10 [mag]	E
8	0.2637	R	19.81 ± 0.05 [mag]	F
9	0.3179	R	20.00 ± 0.05 [mag]	F
11	0.3646	R	20.18 ± 0.06 [mag]	F
12	0.4074	R	20.4 ± 0.1 [mag]	G
13	0.4674	R	20.6 ± 0.1 [mag]	G
14	0.557	R	20.76 ± 0.04 [mag]	H
15	1.5874	R	22.12 ± 0.08 [mag]	I
16	1.7384	R	22.31 ± 0.05 [mag]	J
17	4.6084	R	23.59 ± 0.06 [mag]	K
18	8.468(8.385:8.552)	R	23.8 ± 0.25 [mag]	L
19	12.41(12.31:12.51)	R	24.0 ± 0.2 [mag]	M
	0.3187	B	20.1 [mag]	N
	1.7384	B	23.09 ± 0.06 [mag]	J
	1.1507(1.1090:1.1939)	V	20.9 ± 0.2 [mag]	O
	0.3625	I	19.35 ± 0.3 [mag]	P
	0.7029	I	>19.1 [mag]	Q
	0.0985	J	16.5 [mag]	R
	0.0985	H	16.0 [mag]	R
	0.0985	Ks	14.0 [mag]	R
	0.0915	850 micron	2.93 ± 5.76 [mJy]	S
	1.0291	850 micron	<1.1 [mJy]	T
	0.7374	8.46GHz	<82 [μJy]	U
	0.7374	4.96GHz	<118 [μJy]	U

Table E.128: Data of GRB041006

ID	reference
A	Maeno et al. (2004) GCN notice #2772
B	Yost et al. (2004) GCN notice #2776
C	Fukushi et al. (2004) GCN notice #2767
D	Price et al. (2004) GCN notice #2771
E	Kahharov et al. (2004) GCN notice #2775
F	Misra and Pandey (2004) GCN notice #2794
G	Monfardini et al. (2004) GCN notice #2790
H	Fugazza et al. (2004) GCN notice #2782
I	D'Avanzo et al. (2004) GCN notice #2788
J	Garnavich et al. (2004) GCN notice #2792
K	Covino et al. (2004) GCN notice #2803
L	Balman et al. (2004) GCN notice #2821
M	Bikmaev et al. (2004) GCN notice #2826
N	Kinoshita et al. (2004) GCN notice #2784
O	Shaw et al. (2004) GCN notice #2799
P	Ferrero et al. (2004) GCN notice #2777
Q	Hoversten et al. (2004) GCN notice #2778
R	Kinugasa and Nishihara (2004) GCN notice #2814
S	Barnard et al. (2004) GCN notice #2774
T	Barnard et al. (2004) GCN notice #2786
U	Soderberg et al. (2004) GCN notice #2787

Table E.129: References of GRB041006

Bibliography

L. Amati, F. Frontera, M. Tavani, J. J. M. in't Zand, A. Antonelli, E. Costa, M. Feroci, C. Guidorzi, J. Heise, N. Masetti, E. Montanari, L. Nicastro, E. Palazzi, E. Pian, L. Piro, and P. Soffitta. Intrinsic spectra and energetics of BeppoSAX Gamma-Ray Bursts with known redshifts. *A&A*, 390:81–89, July 2002.

J.-L. Atteia, M. Boer, F. Cotin, J. Couteret, J.-P. Dezalay, M. Ehanno, J. Evrard, D. Lagrange, M. Niel, J.-F. Olive, G. Rouaix, P. Souleille, G. Vedrenne, K. Hurley, G. Ricker, R. Vanderspek, G. Crew, J. Doty, and N. Butler. In-Flight Performance and First Results of FREGATE. In *AIP Conf. Proc. 662: Gamma-Ray Burst and Afterglow Astronomy 2001: A Workshop Celebrating the First Year of the HETE Mission*, pages 17–24, Apr. 2003.

D. Band, J. Matteson, L. Ford, B. Schaefer, D. Palmer, B. Teegarden, T. Cline, M. Briggs, W. Paciesas, G. Pendleton, G. Fishman, C. Kouveliotou, C. Meegan, R. Wilson, and P. Lestrade. BATSE observations of gamma-ray burst spectra. I - Spectral diversity. *ApJ*, 413:281–292, Aug. 1993.

E. Berger, S. R. Kulkarni, J. S. Bloom, P. A. Price, D. W. Fox, D. A. Frail, T. S. Axelrod, R. A. Chevalier, E. Colbert, E. Costa, S. G. Djorgovski, F. Frontera, T. J. Galama, J. P. Halpern, F. A. Harrison, J. Holtzman, K. Hurley, R. A. Kimble, P. J. McCarthy, L. Piro, D. Reichart, G. R. Ricker, R. Sari, B. P. Schmidt, J. C. Wheeler, R. Vanderppek, and S. A. Yost. The Faint Optical Afterglow and Host Galaxy of GRB 020124: Implications for the Nature of Dark Gamma-Ray Bursts. *ApJ*, 581:981–987, Dec. 2002.

G. Björnsson, J. Hjorth, P. Jakobsson, L. Christensen, and S. Holland. The Jet and the Supernova in GRB 990712. *ApJ*, 552:L121–L124, May 2001.

J. S. Bloom, S. G. Djorgovski, and S. R. Kulkarni. The Redshift and the Ordinary Host Galaxy of GRB 970228. *ApJ*, 554:678–683, June 2001.

J. S. Bloom, S. G. Djorgovski, S. R. Kulkarni, and D. A. Frail. The Host Galaxy of GRB 970508. *ApJ*, 507:L25–L28, Nov. 1998.

J. S. Bloom, D. Fox, P. G. van Dokkum, S. R. Kulkarni, E. Berger, S. G. Djorgovski, and D. A. Frail. The First Two Host Galaxies of X-Ray Flashes: XRF 011030 and XRF 020427. *ApJ*, 599:957–963, Dec. 2003a.

J. S. Bloom, D. A. Frail, and S. R. Kulkarni. Gamma-Ray Burst Energetics and the Gamma-Ray Burst Hubble Diagram: Promises and Limitations. *ApJ*, 594:674–683, Sept. 2003b.

J. S. Bloom, S. R. Kulkarni, S. G. Djorgovski, A. C. Eichelberger, P. Cote, J. P. Blakeslee, S. C. Odewahn, F. A. Harrison, D. A. Frail, A. V. Filippenko, D. C. Leonard, A. G. Riess, H. Spinrad, D. Stern, A. Bunker, A. Dey, B. Grossan, S. Perlmutter, R. A. Knop, I. M.

Hook, and M. Feroci. The unusual afterglow of the gamma-ray burst of 26 March 1998 as evidence for a supernova connection. *Nature*, 401:453–456, 1999.

J. S. Bloom, S. R. Kulkarni, P. A. Price, D. Reichart, T. J. Galama, B. P. Schmidt, D. A. Frail, E. Berger, P. J. McCarthy, R. A. Chevalier, J. C. Wheeler, J. P. Halpern, D. W. Fox, S. G. Djorgovski, F. A. Harrison, R. Sari, T. S. Axelrod, R. A. Kimble, J. Holtzman, K. Hurley, F. Frontera, L. Piro, and E. Costa. Detection of a Supernova Signature Associated with GRB 011121. *ApJ*, 572:L45–L49, June 2002.

G. Boella, L. Chiappetti, G. Conti, G. Cusumano, S. del Sordo, G. La Rosa, M. C. Maccarone, T. Mineo, S. Molendi, S. Re, B. Sacco, and M. Tripiciano. The medium-energy concentrator spectrometer on board the BeppoSAX X-ray astronomy satellite. *A&AS*, 122:327–340, Apr. 1997.

L. Christensen, J. Hjorth, and J. Gorosabel. UV star-formation rates of GRB host galaxies. *A&A*, 425:913–926, Oct. 2004.

E. Costa, F. Frontera, J. Heise, M. Feroci, J. in 't Zand, F. Fiore, M. N. Cinti, D. dal Fiume, L. Nicastro, M. Orlandini, E. Palazzi, M. Rapisarda, G. Zavattini, R. Jager, A. Parmar, A. Owens, S. Molendi, G. Cusumano, M. C. Maccarone, S. Giarrusso, A. Coletta, L. A. Antonelli, P. Giommi, J. M. Muller, L. Piro, and R. C. Butler. Discovery of an X-ray afterglow associated with the gamma-ray burst of 28 February 1997. *Nature*, 387:783–785, 1997.

D. R. Cox. Regression models and life-tables (with discussion). *Journal of the Royal Statistical Society: Series B (Statistical Methodology)*, 34:187–220, Jan. 1972.

M. De Pasquale, L. Piro, R. Perna, E. Costa, M. Feroci, G. Gandolfi, J. i. Zand, L. Nicastro, F. Frontera, L. A. Antonelli, F. Fiore, and G. Stratta. A Comparative Study of the X-Ray Afterglow Properties of Optically Bright and Dark Gamma-Ray Bursts. *ApJ*, 592:1018–1024, Aug. 2003.

M. Della Valle, D. Malesani, S. Benetti, V. Testa, M. Hamuy, L. A. Antonelli, G. Chincarini, G. Cocozza, S. Covino, P. D'Avanzo, D. Fugazza, G. Ghisellini, R. Gilmozzi, D. Lazzati, E. Mason, P. Mazzali, and L. Stella. Evidence for supernova signatures in the spectrum of the late-time bump of the optical afterglow of GRB 021211. *A&A*, 406:L33–L37, July 2003.

A. H. Diercks, E. W. Deutsch, F. J. Castander, C. Corson, G. Gilmore, D. Q. Lamb, N. Tanvir, E. L. Turner, and R. Wyse. The Optical Afterglow of GRB 971214: R and J Photometry. *ApJ*, 503:L105+, Aug. 1998.

M. Feroci, F. Frontera, E. Costa, D. dal Fiume, L. Amati, L. Bruca, M. N. Cinti, A. Coletta, P. Collina, C. Guidorzi, L. Nicastro, M. Orlandini, E. Palazzi, M. Rapisarda, G. Zavattini, and R. C. Butler. In-flight performances of the BeppoSAX gamma-ray burst monitor. In *Proc. SPIE Vol. 3114, p. 186-197, EUV, X-Ray, and Gamma-Ray Instrumentation for Astronomy VIII, Oswald H. Siegmund; Mark A. Gummin; Eds.*, pages 186–197, Oct. 1997.

G. J. Fishman, C. A. Meegan, R. B. Wilson, M. N. Brock, J. M. Horack, C. Kouveliotou, S. Howard, W. S. Paciesas, M. S. Briggs, G. N. Pendleton, T. M. Koshut, R. S. Mallozzi, M. Stollberg, and J. P. Lestrade. The first BATSE gamma-ray burst catalog. *ApJS*, 92: 229–283, May 1994.

D. W. Fox, P. A. Price, A. M. Soderberg, E. Berger, S. R. Kulkarni, R. Sari, D. A. Frail, F. A. Harrison, S. A. Yost, K. Matthews, B. A. Peterson, I. Tanaka, J. Christiansen, and G. H. Moriarty-Schieven. Discovery of Early Optical Emission from GRB 021211. *ApJ*, 586:L5–L8, Mar. 2003a.

D. W. Fox, S. Yost, S. R. Kulkarni, K. Torii, T. Kato, H. Yamaoka, M. Sako, F. A. Harrison, R. Sari, P. A. Price, E. Berger, A. M. Soderberg, S. G. Djorgovski, A. J. Barth, S. H. Pravdo, D. A. Frail, A. Gal-Yam, Y. Lipkin, T. Mauch, C. Harrison, and H. Buttery. Early optical emission from the γ-ray burst of 4 October 2002. *Nature*, 422:284–286, Mar. 2003b.

D. A. Frail and S. R. Kulkarni. GRB 970508. *IAU Circ.*, 6662:1–+, May 1997.

D. A. Frail, S. R. Kulkarni, R. Sari, S. G. Djorgovski, J. S. Bloom, T. J. Galama, D. E. Reichart, E. Berger, F. A. Harrison, P. A. Price, S. A. Yost, A. Diercks, R. W. Goodrich, and F. Chaffee. Beaming in Gamma-Ray Bursts: Evidence for a Standard Energy Reservoir. *ApJ*, 562:L55–L58, Nov. 2001.

D. L. Freedman and E. Waxman. On the Energy of Gamma-Ray Bursts. *ApJ*, 547:922–928, Feb. 2001.

A. Fruchter, S. Pattel, C. Kouveliotou, J. Rhoads, S. Holland, I. Burud, and R. Wijers. XRF/GRB 011030: detection of the probable host galaxy. *GRB Circular Network*, 1268: 1–+, 2002.

A. S. Fruchter, E. Pian, S. E. Thorsett, L. E. Bergeron, R. A. González, M. Metzger, P. Goudfrooij, K. C. Sahu, H. Ferguson, M. Livio, M. Mutchler, L. Petro, F. Frontera, T. Galama, P. Groot, R. Hook, C. Kouveliotou, D. Macchetto, J. van Paradijs, E. Palazzi, H. Pedersen, W. Sparks, and M. Tavani. The Fading Optical Counterpart of GRB 970228, 6 Months and 1 Year Later. *ApJ*, 516:683–692, May 1999.

M. Fukugita, T. Ichikawa, J. E. Gunn, M. Doi, K. Shimasaku, and D. P. Schneider. The Sloan Digital Sky Survey Photometric System. *AJ*, 111:1748–+, Apr. 1996.

J. U. Fynbo, B. L. Jensen, J. Gorosabel, J. Hjorth, H. Pedersen, P. Møller, T. Abbott, A. J. Castro-Tirado, D. Delgado, J. Greiner, A. Henden, A. Magazzù, N. Masetti, S. Merlino, J. Masegosa, R. Østensen, E. Palazzi, E. Pian, H. E. Schwarz, T. Cline, C. Guidorzi, J. Goldsten, K. Hurley, E. Mazets, T. McClanahan, E. Montanari, R. Starr, and J. Trombka. Detection of the optical afterglow of GRB 000630: Implications for dark bursts. *A&A*, 369: 373–379, Apr. 2001.

T. Galama, P. J. Groot, J. Vanparadijs, C. Kouveliotou, C. R. Robinson, G. J. Fishman, C. A. Meegan, K. C. Sahu, M. Livio, L. Petro, F. D. Macchetto, J. Heise, J. Int Zand, R. G. Strom, J. Telting, R. G. M. Rutten, M. Pettini, N. Tanvir, and J. Bloom. The Decay of Optical Emission from the gamma-Ray Burst GRB970228. *Nature*, 387:479–+, May 1997.

T. J. Galama, N. Tanvir, P. M. Vreeswijk, R. A. M. J. Wijers, P. J. Groot, E. Rol, J. van Paradijs, C. Kouveliotou, A. S. Fruchter, N. Masetti, H. Pedersen, B. Margon, E. W. Deutsch, M. Metzger, L. Armus, S. Klose, and B. Stecklum. Evidence for a Supernova in Reanalyzed Optical and Near-Infrared Images of GRB 970228. *ApJ*, 536:185–194, June 2000.

M. R. Garcia, P. J. Callanan, D. Moraru, J. E. McClintock, E. Tollestrup, S. P. Willner, C. Hergenrother, C. R. Robinson, C. Kouveliotou, and J. van Paradijs. Power-Law Decays in the Optical Counterparts of GRB 970228 and GRB 970508. *ApJ*, 500:L105+, June 1998.

G. Ghirlanda, G. Ghisellini, and D. Lazzati. The collimation–corrected GRB energies correlate with the peak energy of their νF_ν spectrum. *ArXiv Astrophysics e-prints*, May 2004.

J. Greiner, M. Peimbert, C. Estaban, A. Kaufer, A. Jaunsen, J. Smoke, S. Klose, and O. Reimer. Redshift of GRB 030329. *GRB Circular Network*, 2020:1–+, 2003.

A. Guarnieri, C. Bartolini, N. Masetti, A. Piccioni, E. Costa, M. Feroci, F. Frontera, D. dal Fiume, L. Nicastro, E. Palazzi, A. J. Castro-Tirado, and J. Gorosabel. Early detection of the Optical Transient following the Gamma-Ray Burst GRB 970228. *A&A*, 328:L13–L16, Dec. 1997.

J. Heise, J. in't Zand, R. M. Kippen, and P. M. Woods. X-Ray Flashes and X-Ray Rich Gamma Ray Bursts. In *Gamma-ray Bursts in the Afterglow Era*, pages 16–+, 2001.

J. Hjorth, J. Sollerman, P. Møller, J. P. U. Fynbo, S. E. Woosley, C. Kouveliotou, N. R. Tanvir, J. Greiner, M. I. Andersen, A. J. Castro-Tirado, J. M. Castro Cerón, A. S. Fruchter, J. Gorosabel, P. Jakobsson, L. Kaper, S. Klose, N. Masetti, H. Pedersen, K. Pedersen, E. Pian, E. Palazzi, J. E. Rhoads, E. Rol, E. P. J. van den Heuvel, P. M. Vreeswijk, D. Watson, and R. A. M. J. Wijers. A very energetic supernova associated with the γ-ray burst of 29 March 2003. *Nature*, 423:847–850, June 2003.

S. T. Holland, M. Weidinger, J. P. U. Fynbo, J. Gorosabel, J. Hjorth, K. Pedersen, J. Méndez Alvarez, T. Augusteijn, J. M. Castro Cerón, A. Castro-Tirado, H. Dahle, M. P. Egholm, P. Jakobsson, B. L. Jensen, A. Levan, P. Møller, H. Pedersen, T. Pursimo, P. Ruiz-Lapuente, and B. Thomsen. Optical Photometry of GRB 021004: The First Month. *AJ*, 125:2291–2298, May 2003.

T. Isobe, E. D. Feigelson, and P. I. Nelson. Statistical methods for astronomical data with upper limits. II - Correlation and regression. *ApJ*, 306:490–507, July 1986.

P. Jakobsson, J. Hjorth, J. P. U. Fynbo, J. Gorosabel, K. Pedersen, I. Burud, A. Levan, C. Kouveliotou, N. Tanvir, A. Fruchter, J. Rhoads, T. Grav, M. W. Hansen, R. Michelsen, M. I. Andersen, B. L. Jensen, H. Pedersen, B. Thomsen, M. Weidinger, S. G. Bhargavi, R. Cowsik, and S. B. Pandey. The afterglow and the host galaxy of GRB 011211. *A&A*, 408: 941–947, Sept. 2003.

P. Jakobsson, J. Hjorth, J. P. U. Fynbo, M. Weidinger, J. Gorosabel, C. Ledoux, D. Watson, G. Björnsson, E. H. Gudmundsson, R. A. M. J. Wijers, P. Möller, K. Pedersen, J. Sollerman, A. A. Henden, B. L. Jensen, A. Gilmore, P. Kilmartin, A. Levan, J. M. Castro Cerón, A. J. Castro-Tirado, A. Fruchter, C. Kouveliotou, N. Masetti, and N. Tanvir. The line-of-sight towards GRB 030429 at z =2.66: Probing the matter at stellar, galactic and intergalactic scales. *A&A*, 427:785–794, Dec. 2004.

N. Kawai, A. Yoshida, M. Matsuoka, Y. Shirasaki, T. Tamagawa, K. Torii, T. Sakamoto, D. Takahashi, E. Fenimore, M. Galassi, T. Tavenner, D. Q. Lamb, C. Graziani, T. Donaghy, R. Vanderspek, M. Yamauchi, K. Takagishi, and I. Hatsukade. In-Orbit Performance of WXM (Wide-Field X-Ray Monitor). In *AIP Conf. Proc. 662: Gamma-Ray Burst and Afterglow Astronomy 2001: A Workshop Celebrating the First Year of the HETE Mission*, pages 25–32, Apr. 2003.

R. W. Klebesadel, I. B. Strong, and R. A. Olson. Observations of Gamma-Ray Bursts of Cosmic Origin. *ApJ*, 182:L85+, June 1973.

S. Klose, J. Greiner, A. Rau, A. A. Henden, D. H. Hartmann, A. Zeh, C. Ries, N. Masetti, D. Malesani, E. Guenther, J. Gorosabel, B. Stecklum, L. A. Antonelli, C. Brinkworth, J. M. C. Cerón, A. J. Castro-Tirado, S. Covino, A. Fruchter, J. P. U. Fynbo, G. Ghisellini, J. Hjorth, R. Hudec, M. Jelínek, L. Kaper, C. Kouveliotou, K. Lindsay, E. Maiorano, F. Mannucci, M. Nysewander, E. Palazzi, K. Pedersen, E. Pian, D. E. Reichart, J. Rhoads, E. Rol, I. Smail, N. R. Tanvir, A. de Ugarte Postigo, P. M. Vreeswijk, R. A. M. J. Wijers, and E. P. J. van den Heuvel. Probing a Gamma-Ray Burst Progenitor at a Redshift of z = 2: A Comprehensive Observing Campaign of the Afterglow of GRB 030226. *AJ*, 128:1942–1954, Nov. 2004.

C. Kouveliotou, C. A. Meegan, G. J. Fishman, N. P. Bhat, M. S. Briggs, T. M. Koshut, W. S. Paciesas, and G. N. Pendleton. Identification of two classes of gamma-ray bursts. *ApJ*, 413: L101–L104, Aug. 1993.

W. Li, A. V. Filippenko, R. Chornock, and S. Jha. The Early Light Curve of the Optical Afterglow of GRB 021211. *ApJ*, 586:L9–L12, Mar. 2003.

N. M. Lloyd-Ronning and B. Zhang. On the Kinetic Energy and Radiative Efficiency of Gamma-Ray Bursts. *ApJ*, 613:477–483, Sept. 2004.

G. Manzo, S. Giarrusso, A. Santangelo, F. Ciralli, G. Fazio, S. Piraino, and A. Segreto. The high pressure gas scintillation proportional counter on-board the BeppoSAX X-ray astronomy satellite. *A&AS*, 122:341–356, Apr. 1997.

N. Masetti, C. Bartolini, A. Guarnieri, and A. Piccioni. The optical light curve of GRB 970228 refined. *Nucl. Phys. B Proc. Suppl.*, 69:674–676, 1998.

N. Masetti, E. Palazzi, E. Pian, L. K. Hunt, M. Méndez, F. Frontera, L. Amati, P. M. Vreeswijk, E. Rol, T. J. Galama, J. van Paradijs, L. A. Antonelli, L. Nicastro, M. Feroci, G. Marconi, L. Piro, E. Costa, C. Kouveliotou, A. J. Castro-Tirado, R. Falomo, T. Augusteijn, H. Böhnhardt, C. Lidman, L. Vanzi, K. M. Merrill, C. D. Kaminsky, M. van der Klis, M. H. M. Heemskerk, F. van der Hooft, E. Kuulkers, H. Pedersen, and S. Benetti. Near-infrared detection and optical follow-up of the GRB990705 afterglow. *A&A*, 354:473–479, Feb. 2000.

M. R. Metzger, S. G. Djorgovski, S. R. Kulkarni, C. C. Steidel, K. L. Adelberger, D. A. Frail, E. Costa, and F. Frontera. Spectral constraints on the redshift of the optical counterpart to the gamma-ray burst of 8 May 1997. *Nature*, 387:879–+, 1997.

J. B. Oke and J. E. Gunn. Secondary standard stars for absolute spectrophotometry. *ApJ*, 266:713–717, Mar. 1983.

W. S. Paciesas, C. A. Meegan, G. N. Pendleton, M. S. Briggs, C. Kouveliotou, T. M. Koshut, J. P. Lestrade, M. L. McCollough, J. J. Brainerd, J. Hakkila, W. Henze, R. D. Preece, V. Connaughton, R. M. Kippen, R. S. Mallozzi, G. J. Fishman, G. A. Richardson, and M. Sahi. The Fourth BATSE Gamma-Ray Burst Catalog (Revised). *ApJS*, 122:465–495, June 1999.

A. Panaitescu and P. Kumar. Fundamental Physical Parameters of Collimated Gamma-Ray Burst Afterglows. *ApJ*, 560:L49–L53, Oct. 2001.

S. B. Pandey, G. C. Anupama, R. Sagar, D. Bhattacharya, A. J. Castro-Tirado, D. K. Sahu, P. Parihar, and T. P. Prabhu. The optical afterglow of the not so dark GRB 021211. *A&A*, 408:L21–L24, Sept. 2003a.

S. B. Pandey, D. K. Sahu, L. Resmi, R. Sagar, G. C. Anupama, D. Bhattacharya, V. Mohan, T. P. Prabhu, B. C. Bhatt, J. C. Pandey, P. Parihar, and A. J. Castro-Tirado. Optical observations of the bright long duration peculiar GRB 021004 afterglow. *Bulletin of the Astronomical Society of India*, 31:19–36, 2003b.

A. N. Parmar, D. D. E. Martin, M. Bavdaz, F. Favata, E. Kuulkers, G. Vacanti, U. Lammers, A. Peacock, and B. G. Taylor. The low-energy concentrator spectrometer on-board the BeppoSAX X-ray astronomy satellite. *A&AS*, 122:309–326, Apr. 1997.

H. Pedersen, A. O. Jaunsen, T. Grav, R. Ostensen, M. I. Andersen, M. Wold, H. Kristen, A. Broeils, M. Naeslund, C. Fransson, M. Lacy, A. J. Castro-Tirado, J. Gorosabel, J. M. Rodriguez Espinosa, A. M. Perez, C. Wolf, R. Fockenbrock, J. Hjorth, P. Muhli, P. Hakala, L. Piro, M. Feroci, E. Costa, L. Nicastro, E. Palazzi, F. Frontera, L. Monaldi, and J. Heise. Evidence for Diverse Optical Emission from Gamma-Ray Burst Sources. *ApJ*, 496:311–+, Mar. 1998.

T. Piran. Gamma-ray bursts and the fireball model. *Phys. Rep.*, 314:575–667, June 1999.

L. Piro, D. A. Frail, J. Gorosabel, G. Garmire, P. Soffitta, L. Amati, M. I. Andersen, L. A. Antonelli, E. Berger, F. Frontera, J. Fynbo, G. Gandolfi, M. R. Garcia, J. Hjorth, J. i. Zand, B. L. Jensen, N. Masetti, P. Møller, H. Pedersen, E. Pian, and M. H. Wieringa. The Bright Gamma-Ray Burst of 2000 February 10: A Case Study of an Optically Dark Gamma-Ray Burst. *ApJ*, 577:680–690, Oct. 2002.

R. D. Preece, M. S. Briggs, R. S. Mallozzi, G. N. Pendleton, W. S. Paciesas, and D. L. Band. The BATSE Gamma-Ray Burst Spectral Catalog. I. High Time Resolution Spectroscopy of Bright Bursts Using High Energy Resolution Data. *ApJS*, 126:19–36, Jan. 2000.

P. A. Price, E. Berger, D. E. Reichart, S. R. Kulkarni, S. A. Yost, R. Subrahmanyan, R. M. Wark, M. H. Wieringa, D. A. Frail, J. Bailey, B. Boyle, E. Corbett, K. Gunn, S. D. Ryder, N. Seymour, K. Koviak, P. McCarthy, M. Phillips, T. S. Axelrod, J. S. Bloom, S. G. Djorgovski, D. W. Fox, T. J. Galama, F. A. Harrison, K. Hurley, R. Sari, B. P. Schmidt, M. J. I. Brown, T. Cline, F. Frontera, C. Guidorzi, and E. Montanari. GRB 011121: A Massive Star Progenitor. *ApJ*, 572:L51–L55, June 2002.

P. A. Price, S. R. Kulkarni, E. Berger, D. W. Fox, J. S. Bloom, S. G. Djorgovski, D. A. Frail, T. J. Galama, F. A. Harrison, P. McCarthy, D. E. Reichart, R. Sari, S. A. Yost, H. Jerjen, K. Flint, A. Phillips, B. E. Warren, T. S. Axelrod, R. A. Chevalier, J. Holtzman, R. A. Kimble, B. P. Schmidt, J. C. Wheeler, F. Frontera, E. Costa, L. Piro, K. Hurley, T. Cline, C. Guidorzi, E. Montanari, E. Mazets, S. Golenetskii, I. Mitrofanov, D. Anfimov, A. Kozyrev, M. Litvak, A. Sanin, W. Boynton, C. Fellows, K. Harshman, C. Shinohara, A. Gal-Yam, E. Ofek, and Y. Lipkin. Discovery of GRB 020405 and Its Late Red Bump. *ApJ*, 589:838–843, June 2003.

A. Rau, J. Greiner, S. Klose, M. Salvato, J. M. Castro Cerón, D. H. Hartmann, A. Fruchter, A. Levan, N. R. Tanvir, J. Gorosabel, J. Hjorth, A. Zeh, A. Küpcü Yoldaş, J. P. Beaulieu, J. Donatowicz, C. Vinter, A. J. Castro-Tirado, J. P. U. Fynbo, D. A. Kann, C. Kouveliotou, N. Masetti, P. Møller, E. Palazzi, E. Pian, J. Rhoads, R. A. M. J. Wijers, and E. P. J. van den Heuvel. Discovery of the near-IR afterglow and of the host of GRB 030528. *A&A*, 427: 815–823, Dec. 2004.

M. J. Rees and P. Meszaros. Refreshed Shocks and Afterglow Longevity in Gamma-Ray Bursts. *ApJ*, 496:L1+, Mar. 1998.

G. R. Ricker, J.-L. Atteia, G. B. Crew, J. P. Doty, E. E. Fenimore, M. Galassi, C. Graziani, K. Hurley, J. G. Jernigan, N. Kawai, D. Q. Lamb, M. Matsuoka, G. Pizzichini, Y. Shirasaki, T. Tamagawa, R. Vanderspek, G. Vedrenne, J. Villasenor, S. E. Woosley, and A. Yoshida. The High Energy Transient Explorer (HETE): Mission and Science Overview. In *AIP Conf. Proc. 662: Gamma-Ray Burst and Afterglow Astronomy 2001: A Workshop Celebrating the First Year of the HETE Mission*, pages 3–16, Apr. 2003.

K. C. Sahu, M. Livio, L. Petro, F. D. Macchetto, J. van Paradijs, C. Kouveliotou, G. J. Fishman, C. A. Meegan, P. J. Groot, and T. Galama. The optical counterpart to gamma-ray burst GRB 970228 observed using the Hubble Space Telescope. *Nature*, 387:476–478, 1997.

K. C. Sahu, P. Vreeswijk, G. Bakos, J. W. Menzies, A. Bragaglia, F. Frontera, L. Piro, M. D. Albrow, I. A. Bond, R. Bower, J. A. R. Caldwell, A. J. Castro-Tirado, F. Courbin, M. Dominik, J. U. Fynbo, T. Galama, K. Glazebrook, J. Greenhill, J. Gorosabel, J. Hearnshaw, K. Hill, J. Hjorth, S. Kane, P. M. Kilmartin, C. Kouveliotou, R. Martin, N. Masetti, P. Maxted, D. Minniti, P. Møller, Y. Muraki, T. Nakamura, S. Noda, K. Ohnishi, E. Palazzi, J. van Paradijs, E. Pian, K. R. Pollard, N. J. Rattenbury, M. Reid, E. Rol, T. Saito, P. D. Sackett, P. Saizar, C. Tinney, P. Vermaak, R. Watson, A. Williams, P. Yock, and A. Dar. Discovery of the Optical Counterpart and Early Optical Observations of GRB 990712. *ApJ*, 540:74–80, Sept. 2000.

T. Sakamoto, D. Q. Lamb, C. Graziani, T. Q. Donaghy, M. Suzuki, G. Ricker, J. Atteia, N. Kawai, A. Yoshida, Y. Shirasaki, T. Tamagawa, K. Torii, M. Matsuoka, E. E. Fenimore, M. Galassi, J. Doty, R. Vanderspek, G. B. Crew, J. Villasenor, N. Butler, G. Prigozhin, J. G. Jernigan, C. Barraud, M. Boer, J. Dezalay, J. Olive, K. Hurley, A. Levine, G. Monnelly, F. Martel, E. Morgan, S. E. Woosley, T. Cline, J. Braga, R. Manchanda, G. Pizzichini, K. Takagishi, and M. Yamauchi. Global Characteristics of X-Ray Flashes and X-Ray-Rich GRBs Observed by HETE-2. *ArXiv Astrophysics e-prints*, Sept. 2004a.

T. Sakamoto, D. Q. Lamb, C. Graziani, T. Q. Donaghy, M. Suzuki, G. Ricker, J.-L. Atteia, N. Kawai, A. Yoshida, Y. Shirasaki, T. Tamagawa, K. Torii, M. Matsuoka, E. E. Fenimore, M. Galassi, T. Tavenner, J. Doty, R. Vanderspek, G. B. Crew, J. Villasenor, N. Butler, G. Prigozhin, J. G. Jernigan, C. Barraud, M. Boer, J.-P. Dezalay, J.-F. Olive, K. Hurley, A. Levine, G. Monnelly, F. Martel, E. Morgan, S. E. Woosley, T. Cline, J. Braga, R. Manchanda, G. Pizzichini, K. Takagishi, and M. Yamauchi. High Energy Transient Explorer 2 Observations of the Extremely Soft X-Ray Flash XRF 020903. *ApJ*, 602:875–885, Feb. 2004b.

T. Sakamoto, D. Takahashi, N. Kawai, A. Yoshida, Y. Shirasaki, T. Tamagawa, K. Torii, M. Matsuoka, E. Fenimore, M. Galassi, D. Q. Lamb, and C. Graziani. X-Ray Bursts Observed by the HETE-2 Satellite. In *AIP Conf. Proc. 662: Gamma-Ray Burst and Afterglow Astronomy 2001: A Workshop Celebrating the First Year of the HETE Mission*, pages 94–96, Apr. 2003.

R. Sari. Hydrodynamics of Gamma-Ray Burst Afterglow. *ApJ*, 489:L37+, Nov. 1997.

R. Sari and T. Piran. Variability in Gamma-Ray Bursts: A Clue. *ApJ*, 485:270–+, Aug. 1997.

R. Sari, T. Piran, and R. Narayan. Spectra and Light Curves of Gamma-Ray Burst Afterglows. *ApJ*, 497:L17+, Apr. 1998.

J. H. M. M. Schmitt. Statistical analysis of astronomical data containing upper bounds - General methods and examples drawn from X-ray astronomy. *ApJ*, 293:178–191, June 1985.

Y. Shirasaki, N. Kawai, A. Yoshida, M. Matsuoka, M. Namiki, I. Sakurai, M. Yamauchi, K. Takagishi, I. Hatsukade, E. E. Fenimore, and M. Galassi. Performance of the wide-field x-ray monitor on board the High-Energy Transient Explorer 2. In *Proc. SPIE Vol. 4012, p. 166-177, X-Ray Optics, Instruments, and Missions III, Joachim E. Truemper; Bernd Aschenbach; Eds.*, pages 166–177, July 2000.

A. M. Soderberg, S. R. Kulkarni, E. Berger, D. B. Fox, P. A. Price, S. A. Yost, M. P. Hunt, D. A. Frail, R. C. Walker, M. Hamuy, S. A. Shectman, J. P. Halpern, and N. Mirabal. A Redshift Determination for XRF 020903: First Spectroscopic Observations of an X-Ray Flash. *ApJ*, 606:994–999, May 2004.

B. E. Stern, Y. Tikhomirova, and R. Svensson. The Decline of the Source Population of Gamma-Ray Bursts and Their Luminosity Function. *ApJ*, 573:75–84, July 2002.

T. E. Strohmayer, E. E. Fenimore, T. Murakami, and A. Yoshida. X-Ray Spectral Characteristics of GINGA Gamma-Ray Bursts. *ApJ*, 500:873–+, June 1998.

M. Uemura, T. Kato, R. Ishioka, and H. Yamaoka. Discovery of a Short Plateau Phase in the Early Evolution of a Gamma-Ray Burst Afterglow. *PASJ*, 55:L31–L34, June 2003.

J. van Paradijs, P. J. Groot, T. Galama, C. Kouveliotou, R. G. Strom, J. Telting, R. G. M. Rutten, G. J. Fishman, C. A. Meegan, M. Pettini, N. Tanvir, J. Bloom, H. Pedersen, H. U. Nordgaard-Nielsen, M. Linden-Vornle, J. Melnick, G. van der Steene, M. Bremer, R. Naber, J. Heise, J. in 't Zand, E. Costa, M. Feroci, L. Piro, F. Frontera, G. Zavattini, L. Nicastro, E. Palazzi, K. Bennet, L. Hanlon, and A. Parmar. Transient optical emission from the error box of the gamma-ray burst of 28 February 1997. *Nature*, 386:686–689, 1997.

J. N. Villasenor, R. Dill, J. P. Doty, G. Monnelly, R. Vanderspek, S. Kissel, G. Prigozhin, G. B. Crew, and G. R. Ricker. An Overview of the HETE Soft X-ray Camera. In *AIP Conf. Proc. 662: Gamma-Ray Burst and Afterglow Astronomy 2001: A Workshop Celebrating the First Year of the HETE Mission*, pages 33–37, Apr. 2003.

R. A. M. J. Wijers, M. J. Rees, and P. Meszaros. Shocked by GRB 970228: the afterglow of a cosmological fireball. *MNRAS*, 288:L51–L56, July 1997.

Acknowledgments

First of all, I would like to thank Prof. N. Kawai for his great support for my three years Ph.D. program. I am flattered that he gave me an opportunity to work with *HETE*. I am grateful to Prof. D. Q. Lamb for his advice about this thesis.

My thanks also goes to WXM operation team members, especially Dr. T. Tamagawa and Dr. Y. Shirasaki, who instruct me about *HETE*, and Dr. T. Sakamoto, without his advice, this work could not be accomplished. I would like to express my gratitude to all *HETE* operation and science team members for helpful discussions about my research.

I wish, finally, to express my deep appreciation to all the staffs, the post doctorates, and the graduate students of Tokyo Institute of Technology.

This work was supported by a 21st Century COE Program at Tokyo Tech "Nanometer-Scale Quantum Physics" by the Ministry of Education, Culture, Sports, Science and Technology.